SOURCES OF AEROSOLS OVER THE SOUTH ATLANTIC OCEAN

Roulin Khondoker

Imperial College London

The Department of Earth Sciences and Engineering

Thesis submitted for the degree of Doctor of Philosophy (Ph.D.), 2014

Declaration of Originality

I declare that the comments of this thesis are completely my own, and that any work of others, published or otherwise, is fully and correctly acknowledged.

Roulin Khondoker

Copyright Declaration

Roulin Khondoker

Acknowledgements

My first thanks is for my supervisors Dominik Weiss, Tina van De Flierdt and Mark Rehkämper, for giving me the opportunity to do this project in their MAGIC group, and for supporting me throughout this PhD. All three have provided invaluable help.

Many thanks to Katharina Kreissig and Barry Cole for their advice, time and help in the lab.

A warm thanks to Stanislav Strekopytov, Emma Humphreys-Williams, Jen Najorka and Baruch Spiro for their vital technical and scientific support in the lab at the Natural History Museum.

I would like to greatly thank Dong Shuofei for his help with Pb chemistry, and his numerous advice. Many thanks as well to Myriam Lambelet for her irreplaceable help with Nd analysis of samples on the Triton and the many discussions we have had together were of invaluable help.

A warm thanks to all my colleagues from the MAGIC group and of the entire ESE Postgraduate Department.

Many thanks to Patricia Smichowski, Pedro Cid-Agüero, Simone Gioia, Marly Babinski, Remi Losno, Fabrice Monna, Aloys Bory, Vivianne Bout-Roumazeilles, and Will Homoky for providing sediment and aerosol samples from South America and South Africa (Chapters 2-4). Thanks as well to Rosie Chance and Alex Baker for collecting and providing the aerosol samples from the D357 and JC068 UK GEOTRACES cruises (Chapters 3 and 4).

Thanks as well to Gideon Henderson, Malcolm Woodward, the scientific party and the crew of the 40°S GEOTRACES cruise in 2011/2012 for warmly inviting me to participate in the cruise an experience life on board the RRS James Cook.

Lastly, I would like to thank all my close friends and family for providing generous hours of advice and stimulation and were there for me throughout the most challenging moments.

Abstract

The atmosphere is an important pathway of particulate matter and their associated trace elements to the ocean and can play vital roles in marine bio-geochemical cycles. Factors that control trace element inputs from the atmosphere (e.g. solubility, sources) are not well understood, in particular for the South Atlantic Ocean.

In this thesis, select major, trace and rare earth elements and the isotopes of two of the elements, lead (Pb) and neodymium (Nd), were investigated in potential sources of aerosols, and aerosol samples, from over the South Atlantic Ocean. Chapter 2 of this thesis presents new element concentration and isotopic compositions of potential source areas from South America and southern Africa, combined with previously published data to represent an up-to-date characterisation of natural and anthropogenic aerosol source areas in South America and southern Africa. Chapters 3 and 4 of this thesis present new element concentration and isotopic compositions of aerosol samples from across the 40°S transect of the South Atlantic Ocean (from the UK GEOTRACES GA10 transect). The results provide the first constraints on the elemental and isotopic composition of total and soluble fraction of aerosol samples across a zonal transect of the South Atlantic Ocean. By comparing the element and isotopic compositions of the aerosol samples to the potential source areas from South America we demonstrate that natural and anthropogenic sources from South America and southern Africa are major sources of atmospheric particulates, but of varied contribution, across the South Atlantic. Elemental and isotopic compositions of the aerosols suggest there is a strong impact of anthropogenic sources from South America on atmospheric particles delivered to the western South Atlantic and a strong influence of natural sources from South America on atmospheric particles delivered to the middle of the South Atlantic. We further demonstrate that there is an importance of anthropogenic southern African sources on aerosol composition over eastern South Atlantic as well as South American source inputs. In Chapter 4 we reveal that large ranges in trace element solubility (between <5 and >95%, generally above 40% across the ocean) in aerosols carried to the South Atlantic may be available for seawater dissolution and may have implications on marine biogeochemical cycles.

Overall the present thesis underlines the important role that anthropogenic source areas can play on atmospheric composition, and provide for the first time measurements of major, trace and rare earth element availability to the surface ocean of the South Atlantic. The thesis also highlights the key role that multi-element concentrations and Pb and Nd isotopic compositions can play in deciphering the provenance of aerosols and element seawater supply.

Table of Contents

		Page
	List of Figures	9
	List of Tables	11
Chapter 1	Introduction	14
	1.1. The importance of studying the atmosphere	15
	1.1.1. Aerosols	15
	1.1.2. Aerosols from source deposition	17
	1.1.3. The air-water exchange in elements from aerosols	17
	1.1.4. The importance of studying aerosols over the South Atlantic Ocean	18
	1.2. The GEOTRACES programme	19
	1.2.1. The International GEOTRACES Overview	19
	1.2.2. The UK GEOTRACES Overview	21
	1.3. Thesis aims and objectives	22
	1.4. Thesis outline	22
	1.5. Analytical methods	24
	1.5.1. Identifying mineralogy by X-ray diffraction	24
	1.5.2. Sample digestion	25
	1.5.3. Sample leaching	25
	1.5.4. Pb and Nd extraction from samples	26
	1.5.5. Determining element concentrations	28
	1.5.6. Determining Pb and Nd isotopic compositions	31
Chapter 2	Isotopic and element characterisation of atmospheric particulate sources from South America and southern Africa to the South Atlantic Ocean	34
	2.1. Introduction	35
	2.2. Methods	38
	2.2.1. Source characterisation and study area	38
	2.2.2. Sampling	39
	2.2.3. Mineralogical analyses	44
	2.3.4. Sample digestion	44

2.2.5. Elemental analysis 45
2.2.6. Lead and Nd isotope ratio analysis 45
2.2.7. Particle size separation 46
2.3. Results and Discussion 48
2.3.1. Mineralogy 48
2.3.2. Major element enrichment 49
2.3.3. Rare earth element enrichment and ratios 52
2.3.4. Trace element enrichment 55
2.3.5. Lead isotopic compositions of aerosol sources 78
2.3.6. Neodymium isotopic compositions of aerosol sources 80
2.3.7. Shelf sediments and their geochemical constrains on natural sources from Southern Africa 85
2.3.8. The effect of particle size on the geochemical constrain on natural and anthropogenic sources from South America and Southern Africa select elemental ratios 85
2.3.9. Provenance tracers of aerosol sources using element ratios 89
2.3.10. Provenance tracers of atmospheric particulate sources using elemental vs. isotopic signatures 95
2.4. Conclusions 96

Chapter 3 Spatial distribution and sources of major, trace and rare earth elements in aerosols along the GEOTRACES South Atlantic transect GA10 at 40°S 100

3.1. Introduction 101
3.2. Sampling and Methods 103
3.2.1. Aerosol sampling 103
3.2.2. Total digestion of aerosols and separation of lead and neodymium for isotopic analysis 105
3.2.3. Element and isotopic analysis 106
3.2.4. Determining filter blank of elements 106
3.2.5. Calculating atmospheric concentrations 107
3.2.6. Calculating enrichment factors 107
3.2.7. Correcting lead and neodymium isotope ratios in aerosols 108
3.3. Results 115
3.3.1. Air mass trajectories over the South Atlantic Ocean 115
3.3.2. Element enrichment composition in aerosol samples 118
3.3.3. Lead and neodymium isotopic compositions of aerosol 119

samples
3.4. Discussion 127
3.4.1. Trace metal sources in the aerosols collected in the western section of the South Atlantic 127
3.4.1.1. Zinc, Lead, Copper, Cadmium 127
3.4.1.2. Vanadium 128
3.4.1.3. Chromium, Nickel, Cobalt 128
3.4.2. Trace metal sources in the aerosols collected in the eastern section of the South Atlantic 130
3.4.2.1. Zinc, Lead, Copper, Vanadium 130
3.4.2.2. Chromium, Nickel, Cobalt, Cadmium 131
3.4.3. Major element sources 132
3.4.4. Mineral dust 132
3.4.5. Calculating source contributions of select elements to aerosols across the South Atlantic 135
3.4.6. Implications on temporal variation in sources of aerosols to the South Atlantic Ocean and air quality 136
3.5. Conclusions 138

Chapter 4 Major, trace and rare earth element solubility in aerosols across the South Atlantic GEOTRACES GA10 transect along 40°S 141

4.1. Introduction 142
4.2. Sampling and Methods 144
4.2.1. Aerosol sampling 144
4.2.2. Aerosol leaching procedure 144
4.2.3. Elemental and isotopic analysis 144
4.2.4. Filter blank corrections of elements in the soluble fraction of aerosols 145
4.2.5. Sea spray corrections of elements in the soluble fraction of aerosols 145
4.2.6. Solubility calculations 146
4.2.7. Correcting lead isotope ratios in the soluble fraction of aerosols 146
4.3. Results and Discussion 158
4.3.1. Uncertainties in aerosol solubility 158
4.3.2. Spatial variation in aerosol solubility to the South Atlantic 158

Ocean
4.3.3. Correlation of solubility and element enrichment factors with air mass back trajectories and the effect on element supply to the ocean 160
4.3.4. Lead isotopic composition of the soluble fraction of aerosols 161
4.3.5. Influence of element supply from aerosols to the ocean surface waters 165
4.4. Conclusions 166

Chapter 5 Conclusions 168

5.1. Major findings 169
5.1.1. Source characterisation by geochemical proxies 169
5.1.2. Geochemical characterisation of aerosols and sources of aerosols across the South Atlantic 170
5.1.3. Solubilty of aerosols over the South Atlnatic Ocean and Pb isotope composition of soluble fraction of aerosols 171
5.1.4 The use of provenance indicators for tracing aerosol sources 172
5.1.5. Air quality and temporal changes 172
5.1.6. Atmospheric transport 173
5.1.7. Implications of aerosol source impact on ocean chemistry and marine processes 173
5.2. Limitations and Further Work 175
5.2.1. Limitations and improvements in source characterisation 175
5.2.2. Limitations of isotope ratios 175
5.2.3. Aerosol collection method and improving the assessment of controls on aerosol solubility 176
5.2.4. Limitations in aerosol and ocean chemistry data and future work 177

References 178

Appendix 194

List of Figures

	Page
1.1. Systematic diagram of the atmospheric circulation patterns across the Earth	**16**
1.2. Atmospheric cycling of particular matter (taken from Pöschl, (2005)	**16**
1.3. Map showing the global ocean sections analysed by the GEOTRACES programme	**20**
1.4 Diagram of the extraction chromatographic procedure to separate the LREE, Th and U fractions using TRU.Spec resin and isolate Nd and Sm using the LN.Spec resin	**28**
1.5 Schematic diagram of the inductively coupled plasma atomic emission spectrometer (ICP-AES)	**29**
1.6 Schematic diagram of the inductively coupled plasma quadrupole mass spectrometer (ICP-QMS	**30**
1.7 Schematic diagram of the Nu Plasma MC-ICP-MS instrument, taken from Rekhämper et al., 2001	**31**
2.1. Location map of sampling sites from this study and from literature and basic geological boundaries in South America and Southern Africa	**41**
2.2. Enrichment Factor of select major elements with respect to upper continental crust for major bulk aerosol sources from South American and Southern African natural and anthropogenic sources	**75**
2.3. Enrichment Factor of REE with respect to upper continental crust for major bulk aerosol sources from South American and Southern African natural and anthropogenic sources	**76**
2.4. Enrichment Factor of select trace elements with respect to upper continental crust for major bulk aerosol sources from South American and Southern African natural and anthropogenic sources	**77**
2.5. Lead isotopic compositions of major bulk aerosol sources from South America and Southern Africa	**82**
2.6. $^{208}Pb/^{207}Pb$ vs. εNd compositions of major bulk aerosol sources from South America and Southern Africa	**83**
2.7. Geographical distribution of $^{208}Pb/^{207}Pb$ and εNd values of major bulk natural and anthropogenic aerosol sources from South America and Southern Africa	**84**
2.8. Element and isotopic characterisation of bulk shelf sediments	**87**
2.9. Element and isotopic compositions of fine fraction (<5 μm, circle symbols) and bulk fraction (square symbols) of sediments from South American rural and volcanic sources	**88**
2.10. Bivariate plots of: (A) Pb/Al×1000 versus Zn/Al×1000; (B) Pb/Al×1000 versus Cu/Al×1000; (C) Cd/Al×1000 versus Zn/Al×1000; (D) Pb/Al×1000 verses Cr/Al×1000; (E) and Pb/Al×1000 verses La/Cr in major aerosol sources from South America and Southern Africa	**92**
2.11. $^{208}Pb/^{207}Pb$ versus elemental ratios of: (A) Pb/Al×1000; (B) 1/[Pb]; (C) Cr/Al×1000; and εNd versus elemental ratios of (D) Pb/Al×1000; (E) 1/[Nd]; and (F) Cr/Al×1000 for all source areas	**93**
3.1. Aerosol sampling locations for cruises D357 (red symbols) and JC068 (green symbols) source samples from South America.	**103**

3.2. Examples of five-day air mass back-trajectories for aerosol samples for cruise D357 and JC068 **116**

3.3. Enrichment factors relative to the upper continental crust of select trace metals in aerosol samples from across the South Atlantic Ocean **120**

3.4. Enrichment factors relative to the upper continental crust of rare earth elements (La, Nd), Sc, Y and Th in aerosol samples across the South Atlantic Ocean **122**

3.5. Enrichment factors relative to the upper continental crust of major elements in aerosol samples across the South Atlantic Ocean **123**

3.6. Lead and neodymium isotopic composition in aerosol samples across the South Atlantic Ocean **124**

3.7. $^{208}Pb/^{207}Pb$ versus: (A) Pb/Al×1000, (B) 1/[Pb], (C) Zn/Al×1000, (D) Cd/Al×1000; and (E) La/Cr for aerosols (circle symbols) from across the South Atlantic Ocean **125**

3.8. εNd vs. (A) Pb/Al×1000 and (B) 1/[Nd] for aerosols (circle symbols) from across the South Atlantic Ocean **126**

3.9. Simplified diagrammatic of qualitative source contributions across the South Atlantic Ocean **136**

4.1. Solubility of trace elements and K and Mn from aerosols from cruise D357 and JC068 across the South Atlantic Ocean **152**

4.2. Solubility of Cr, Fe and Al from aerosols from cruise D357 and JC068 across the South Atlantic Ocean **154**

4.3. Solubility of rare earth elements and Sc, Y and Th from aerosols from cruise D357 and JC068 across the South Atlantic Ocean **155**

4.4. Solubility vs. enrichment factor relative to the continental crust in total bulk aerosols for select elements **156**

4.5. $^{206}Pb/^{207}Pb$ and $^{208}Pb/^{207}Pb$ isotopic ratios of soluble fraction of aerosols (circle symbols) and total aerosols (diamond symbols) across the South Atlantic Ocean **163**

List of Tables

Page

1.1. Ion exchange column procedure for separating Pb from sample matrix (taken from Weiss et al., 2004) **27**

2.1. Source classifications **39**

2.2. Sample location and source types of major atmospheric particulate sources from South America and southern Africa. **42**

2.3. Mineralogy for select aerosol sources from South America and southern Africa **59**

2.4. Major element concentrations of major aerosol sources from South America and Southern Africa **60**

2.5. Rare earth element, Cu, Pb, Cd, Zn, Cr, Ni, Co, Y, Th, V, and Sc concentrations of major aerosol sources from South America and Southern Africa (μg g^{-1}). **63**

2.6. Lead and neodymium isotope ratios and εNd values for major aerosol sources South America and Southern Africa **71**

2.7. Characteristic mineralogy, element and isotopic composition of major aerosols sources from South America and Southern Africa. **94**

3.1. Location of aerosol sample collection from UK GEOTRACES transect GA10 (D357 cruise; eastern South Atlantic). **104**

3.2. Location of aerosol sample collection from UK GEOTRACES transect GA10 (JC068 cruise; South Atlantic along 40°S). **105**

3.3. Major element composition of total aerosols collected across the South Atlantic **109**

3.4. Rare earth element composition of total aerosols collected across the South Atlantic **110**

3.5. Trace element Cu, Pb, Cd, Zn, Cr, Ni, Co, Y, Th, V, and Sc composition of total aerosols collected across the South Atlantic **111**

3.6. Lead and Nd isotope ratios and εNd values for total aerosols collected across the South Atlantic **112**

3.7. Element and isotopic composition of sources from Chapter 2 **114**

3.8. Examples of select element enrichment factors and lead and neodymium isotopic compositions of aerosols from literature **134**

3.9. Select anthropogenic source contributions of elements from South America over the South Atlantic Ocean **135**

4.1. Major and trace element composition in the soluble fraction of aerosols over the South Atlantic **147**

4.2. Rare earth element composition in the soluble fraction of aerosols over the South Atlantic from the D357 and JC068 cruise **148**

4.3. Solublity of major, trace and rare earth elements from aerosols over the South Atlantic Ocean from the D357 and JC068 cruise **149**

4.4. Lead isotope ratios in the soluble fraction of aerosols over the South Atlantic Ocean from **151**

the D357 and JC068 cruise
4.5. Examples of solubility of elements from aerosols over oceans and select natural and anthropogenic aerosols taken from literature **164**

CHAPTER 1

Introduction

This thesis focuses on the geochemical cycling of major, rare earth and trace elements, and lead (Pb) and neodymium (Nd) isotopes in the atmosphere over the South Atlantic Ocean, and is part of the international GEOTRACES programme. The introduction discusses the importance of studying the atmosphere, an overview of the GEOTRACES programme, and a background into the methods applied in this thesis.

1.1. The importance of studying the atmosphere

The Earth's atmosphere is an important pathway for the transport and deposition of aerosols and associated trace elements to the ocean surface waters (e.g. Duce et al., 1991; Galloway et al., 2004; Jickells et al., 2005). These atmospheric inputs can play a major role in marine biogeochemical processes such as regulating primary productivity and therefore atmospheric carbon dioxide concentrations and climate (Martin et al. 1990; Zhuang et al., 1992; Galloway et al., 2004; Jickells et al., 2005). Thus an understanding of the impacts that aerosols play on marine biogeochemical processes provides valuable knowledge on the environmental controls on climate change.

1.1.1. Aerosols

Aerosols are organic and inorganic solid particles or liquid droplets ranging from ~0.00 to 100 μm in size (Eby, 2004). Aerosols are divided into two types, primary and secondary. Primary aerosols are particulates that are emitted directly into the atmosphere, for instance, mineral dust, volcanic dust, sea-salt, smoke and soot, and some organics (Prospero, 1983). Secondary aerosols are particulates that form in the atmosphere by gas-to-particle conversion processes, for instance the interaction of solid particles with liquid droplets to form sulfates, nitrates, and some organics (Prospero, 1983). Anthropogenic aerosols are typically enriched in trace metals than natural dust (e.g. Chester, 2000; Pacyna and Pacyna, 2001). However volcanic emissions have been reported to contain high concentrations of trace metals (Carlson and Prospero, 1972; Jickells et al., 2005). Common anthropogenic sources of aerosols include emissions from fossil fuel burning, metal and mining processes, biomass burning, waste incineration, and traffic-related suspension of road or vehicle materials (Pacyna et al., 2001).

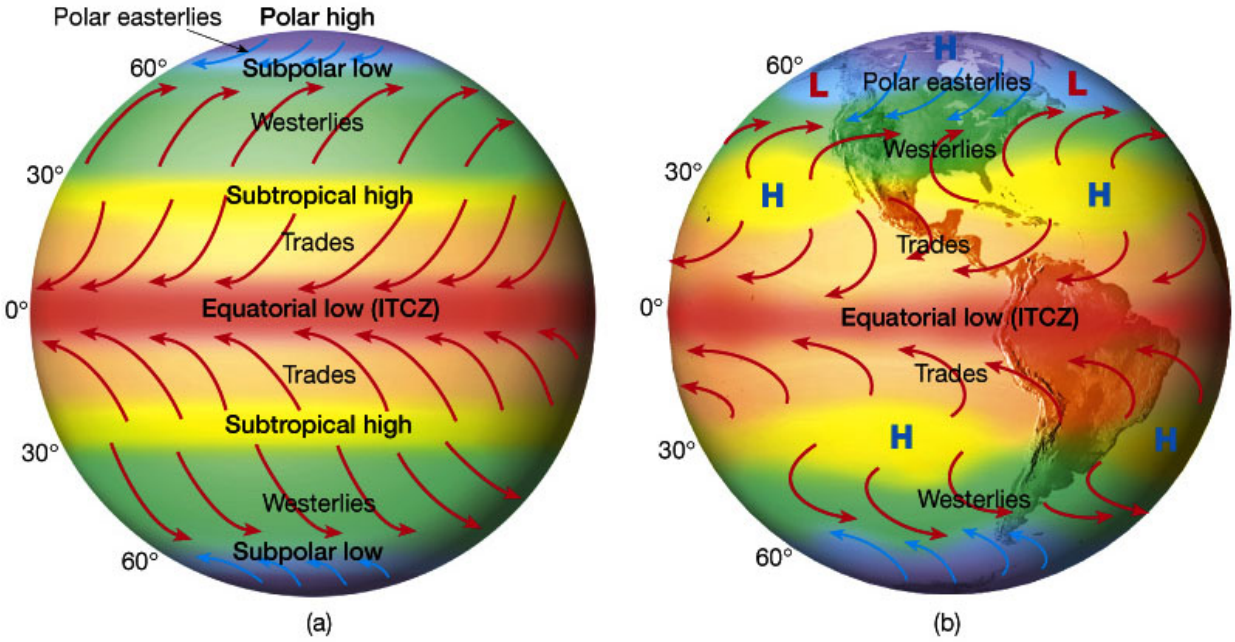

Figure 1.1. Systematic diagram of the atmospheric circulation patterns across the Earth (taken from Lutgens and Tarbuck, 1992).

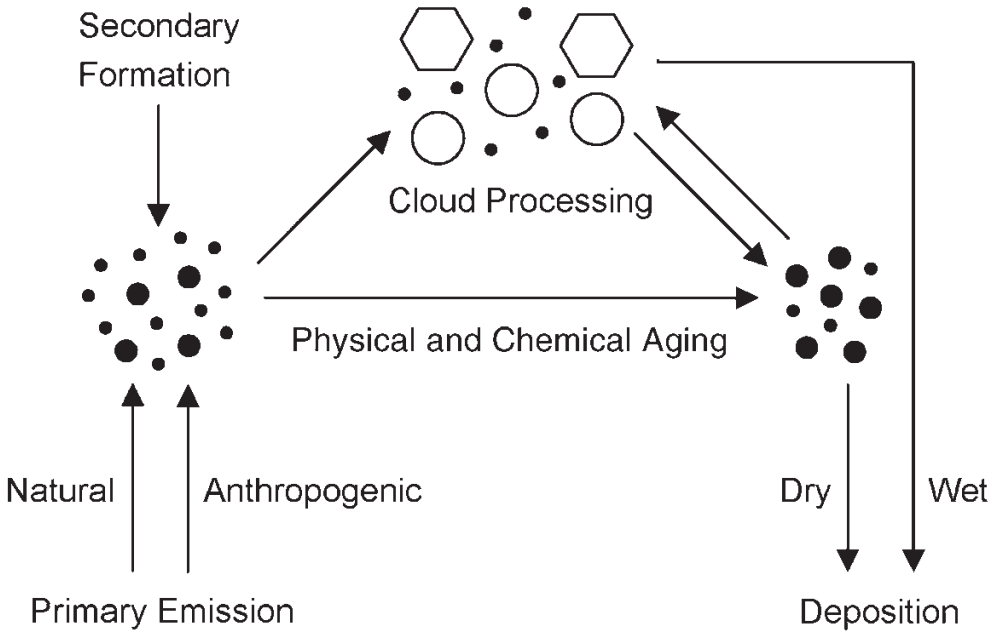

Figure 1.2. Atmospheric cycling of particular matter (taken from Pöschl, (2005)

1.1.2. Aerosols from source to deposition

Figures 1.1 and 1.2 describe the pathways that aerosols take from source to deposition and the large-scale atmospheric circulation patterns that control the movement of air mass and thus the aerosols carried by the air. As aerosols are uplifted from the Earth by wind, or are actively emitted from a source, they are transported through the atmosphere by mass transfer of air by prevailing winds (Berner and Berner, 1996). They may be transported in the troposphere between 0-14km above sea level where air packets rise and fall due to varying temperatures and pressures in the atmosphere (Goody and Walker, 1972). The top of this layer (tropopause) meets the stratosphere, which is up to 50km above sea level and is where air flows horizontally (Eby, 2004). Mass may transfer between the troposphere and stratosphere by diffusion or mass transfer at the tropopause (Eby, 2004).

Due to the rotation of the Earth, air mass movement is deflected as shown in Figure 1.1 (Barry and Chorley, 1987; Lutgens and Tarbuck, 1992). This effect is known as the Coriolis effect, which results in large-scale pockets of air movement across the Earth (Barry and Chorley, 1987; Lutgens and Tarbuck, 1992). As the Earth rotates, air moving over the surface of the Earth is deflected in a clockwise direction with respect to the direction of travel in the Northern Hemisphere and in a counter-clockwise direction in the Southern Hemisphere except at the equator where winds tend to flow to the right of this direction north of the equator and to the left of this direction south of it (Fig. 1.1, Lutgens and Tarbuck, 1992). Because of this, transfer of air mass between the Northern and Southern Hemisphere is negligible (Fig. 1.1, Lutgens and Tarbuck, 1992). In the Southern Hemisphere, air mass is transported west to east by the westerly winds between ~30-60ºS and southeast to northwest by the southeasterly trade winds between the equator and ~30ºS (Fig. 1.1, Lutgens and Tarbuck, 1992). The horizontal movement of air in the stratosphere and the large-scale atmospheric circulation patterns across the Earth are the key effects that can cause long-range transport (over kilometers) of aerosols through the atmosphere (Eby, 2004).

During the transportation of aerosols, they may undergo chemical modifications in cloud formations (Fig. 1.2, Pöschl, 2005). These reactions are known as cloud processing (Fig. 1.2) and occur due to interactions between water vapour from clouds and solids, liquids, and gases from aerosols. Gaseous acids include hydrochloric (HCl), nitric (HNO_3), sulfuric (H_2SO_4) and solutions with ammonia (NH_3) (Pöschl, 2005). Changes to the composition of an aerosol also occur due to particle fall out due to gravity (Pöschl, 2005). When gravity is greater than the uplifting or horizontal force maintaining an aerosol in the atmosphere, the aerosol falls from the atmosphere; this is known as dry deposition (Pöschl, 2005). Aerosols may also be deposited by wet deposition whereby the aerosol comes into contact with a wet surface such as rain or snow (Fig. 1.2, Pöschl, 2005). The components of the aerosol that are leached into the liquid are then deposited due to gravity (Pöschl, 2005).

1.1.3. The air-water exchange in elements from aerosols

For aerosols depositing over the oceans, elements from the aerosols may react with seawater, organics such as algae and photoplankton, and inorganics such as suspended materials from dust, river inputs, upwelled sediment, and result in dissolution, sedimentation or formation of colloids (Berner and Berner,

1996). Select elements are useful in the metabolic processes of organisms. Iron (Fe) is one of the key nutrients as it is essential for photosynthesis and thus primary production (Martin et al., 1990; Morel et al., 2003; Morel and Price, 2003; Boyd et al., 2007). Zinc (Zn) is an essential element required in the enzymes responsible for carbon uptake in phytoplankton (Chester and Jickells, 2012). Cadmium (Cd) can substitute for Zn in some enzyme systems (Morel and Price, 2003). Inorganic processes may result in the formation of calcium carbonates, locking carbon and depositing it to the bottom of the ocean (Eby, 2004). Respiratory processes release carbon in the form of carbon dioxide back into the atmosphere. These reactions occur immediately or over days to years (Eby, 2004).

In pristine natural settings, continental soil dust is the principal source via the atmosphere of dissolved elements, such as Fe, in seawater (e.g. Eby, 2004). Recent studies, however, have suggested that in areas downwind of major human activity, combustion aerosols become very important (e.g. ~80% solubility of Fe vs. 1-2% for soil dusts; Sholkovitz et al., 2009; ~43% solubility of Al, 100% in Ca and Mn in fly ash vs. 0.1% in Al, 8.1% in Ca and 6.1% in Mn in natural dusts; Desboeufs et al., 2001). These findings implied that human activity can profoundly affect marine element budgets and therefore biogeochemical cycles.

Depending on the reaction or multiple reactions that take place at the surface of the ocean, an element may remain in the surface waters for days to years, this is known as the residence time of an element in the ocean (Bruland and Lohan, 2003). For example, the residence time of Zn is 1000yrs, Pb is 9 yrs, Fe is 0.6yrs and Mn is 12yrs in the ocean (Bruland and Lohan, 2003). Surfae ocean circulation may transport the aerosol from the site of deposition to across the ocean for hundreds of years (Chester and Jickells, 2012). The currents responsible for ocean circulation are a result of prevailing winds, which are caused by uneven heating of the Earth's surface (Berner and Berner, 1996). The circulation patterns can be summarised as a number of current rings, also known as gyres (Berner and Berner, 1996). In the Northern Hemisphere gyres flow clockwise and in the Southern Hemisphere gyres flow counterclockwise due to the force conveyed by prevailing winds (Berner and Berner, 1996). The components of the aerosols, residence time and ocean circulation thus affect the element budget available for biogeochemical reactions in seawater before, straight after (within minutes to an hour) and a long time after (hours to years) aerosols come into contact with the seawater (Chester and Jickells, 2012).

1.1.4. The importance of studying aerosols over the South Atlantic Ocean

In the above-discussed ways, aerosols can provide elements to the Earth's oceans that may play a vital role in the marine micronutrient budget, marine primary productivity, and yield an indirect control on the removal of carbon dioxide from the global atmosphere and in turn affect climate change and global warming (Martin, 1990). Of particular interest is the southern region of the South Atlantic Ocean, along and south of ~40°S, which is thought to be depleted in micronutrients essential to biological activity (Prospero et al., 2002), probably due to low inputs of atmospheric particulates across the South Atlantic

(e.g. Li, 2008). However, approximately along 40°S across the South Atlantic Ocean, a region of high primary productivity and active sedimentation has been described (Mahowald et al., 2005) that suggests control by either major atmospheric deposition to this region or supply of nutrients by ocean currents. These conclusions have large uncertainties due to limited field measurements from this region of the South Atlantic Ocean. Understanding the source to ocean processes and element mobility and solubility within the atmosphere and ocean gives scientists a better understanding of the controls on climate systems. This will determine actions need to reduce negative effects to the climate to be able to maintain current life on Earth. Furthermore for the South Atlantic, understanding source to ocean processes of aerosols also improves the understanding on the effect element supply via the atmosphere has on the high primary productivity expected along 40°S. For these above reasons, the International GEOTRACES Programme was initiated.

1.2. The GEOTRACES programme

1.2.1. The International GEOTRACES Overview

Despite the recognised importance of trace elements and isotopes, our ability to exploit knowledge of their attributes is limited by uncertainties concerning their sources, sinks, internal cycling and chemical speciation within the ocean. For example, the marine biogeochemical cycles of micronutrients are known so poorly that their sensitivity to global change, and the impact of any resulting changes in elemental cycling on marine ecosystems and the ocean carbon cycle, cannot be predicted meaningfully. Similarly, sedimentary records reveal striking correlations between distributions of trace elements in sediments and independent indicators of climate variability; but our ability to use trace elements and their isotopes as reliable palaeoceanographic proxies is limited by incomplete characterisation of their current biogeochemistry. This limits the ability to test ocean models against past conditions, and therefore limits the ability to forecast future changes.

These concerns resulted in the international GEOTRACES programme, which set out to improve the understanding of biogeochemical cycles and large-scale distribution of trace elements and their isotopes in the marine environment. Figure 1.3 shows the sections of global oceans that will be analysed during the GEOTRACES programme.

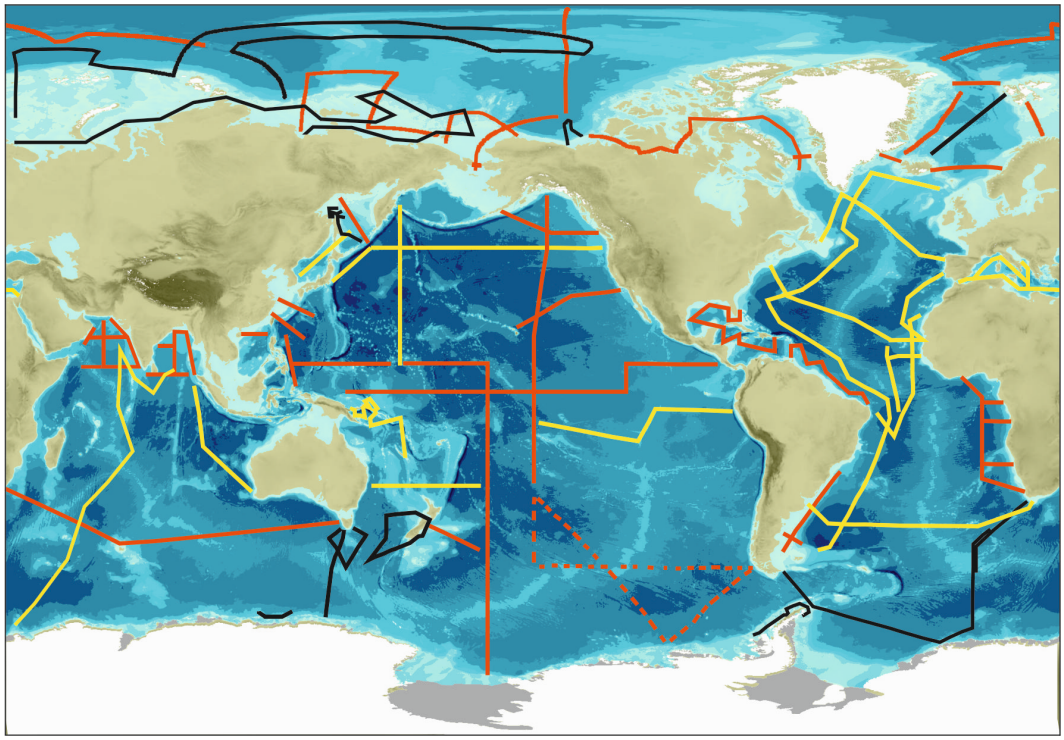

Figure 1.3. Map showing the global ocean sections analysed by the GEOTRACES programme. Sections in red denote planned sections, yellow denote completed and black denote completed as GEOTRACES contribution to the International Polar Year (IPY). GEOTRACES website (http://www.geotraces.org).

Three overriding goals support the GEOTRACES mission (SCOR, 2006, GEOTRACES Science Plan, p. 1):

1. To determine global ocean distributions of selected trace elements and isotopes – including their concentration, chemical speciation and physical form – and to evaluate the sources, sinks, and internal cycling of these species to characterise more completely the physical, chemical and biological processes regulating their distributions.

2. To understand the processes involved in oceanic trace-element cycles sufficiently well that the response of these cycles to global change can be predicted, and their impact on the carbon cycle and climate understood.

3. To understand the processes that control the concentrations of geochemical species used for proxies of the past environment, both in the water column and in the substrates that reflect the water column.

1.2.2. The UK GEOTRACES Overview

The UK GEOTRACES branch constitutes 11 UK institutions that aim to investigate the Atlantic Oceans. The UK GEOTRACES project set out since 2008 to develop a comprehensive understanding of the source, sinks and internal cycling of seven micronutrient elements in a productive region along 40°S in the Atlantic.

To address these International GEOTRACES questions with regard to the atmospheric to ocean systems for the South Atlantic, the following objectives are addressed within the consortium (SCOR, 2006, GEOTRACES Science Plan, p. 19):

i) Develop and refine chemical tracers in the surface ocean for quantification of atmospheric deposition (e.g., Nd and Pb). The geochemical behaviour of any trace element and isotopes is the result of a variety of competing processes of addition, removal and transformation, so the power of any tracer is limited by the knowledge and extent of these interactions.

ii) Use measurements of such tracers in surface waters and in the lower atmosphere (in collaboration with the International Convention for the Safety of Life at Sea – SOLAS) to provide global-scale ground-truthing of aerosol deposition models across the major ocean basins and through the major deposition gradients in those basins.

iii) Establish the range of fractional solubility of key atmospheric components and the processes that underlie that variability. This range in solubility is a master variable in the delivery of dissolved materials to the surface ocean.

iv) Provide a coarse-scale global database quantifying the addition of micronutrients and bioactive elements to the surface ocean (e.g., Fe, P, Co, Zn, Ni, Si, Ge and Cd) so that they can be used in biogeochemical and climate models.

v) Determine the speciation of trace elements added to the ocean by atmospheric deposition and therefore the bio- availability of these elements.

1.3. Thesis aims and objectives

The aim of this thesis was to characterise element cycling in the South Atlantic Ocean and test the hypothesis that anthropogenic sources play an important role to the element cycling from atmosphere to ocean. This was achieved by first identifying characteristic proxies (elemental ratios, enrichment factors, isotopic ratios) to identify specific source areas (Chapter 2), then to characterise aerosols and estimate source contributions over the South Atlantic (Chapter 3), and then characterise the bio-available fraction and discuss implications for atmosphere-ocean studies (Chapter 4).

1.4. Thesis outline

Chapter 2:

Sediment and aerosol samples representative of potential source areas were analysed for their major, trace and rare earth element concentrations and Pb and Nd isotopic composition to characterise potential sources of aerosols to the South Atlantic Ocean. Samples were collected from South America (southern Patagonia, north and south volcanic zones of the Andes, Buenos Aires and Sao Paulo) and South Africa (Johannesburg). The specific aims of the chapter are:

- To identify elemental and isotopic proxies that enable the identification of natural and anthropogenic source areas of aerosols to the South Atlantic
- To determine proxies useful for the provenance tracing of aerosols over the South Atlantic able to discriminate between i) South American and southern African source areas, ii) natural and anthropogenic source areas and iii) identify any particular variation within a source area.

Chapter 3:

Thirteen bulk aerosol samples were analysed for their major, trace and rare earth element concentrations and for Pb and Nd isotopic ratios. These samples were collected along 40°S across the South Atlantic during the UK GEOTRACES cruises D357 and JC068 during October 2010 and from December 2011 to January 2012, respectively. Additional sediments from Patagonia and the Andes and bulk shelf sediment SW off the coast of Cape Town, South Africa were characterised geochemically and the effect of size fractions tested. The specific aims of the chapter are:

- To characterise the elemental and isotopic composition of aerosols over the South Atlantic
- To supplement the characterised elemental and isotopic composition of potential source samples from South America and southern Africa from Chapter 2
- To quantify the contribution of natural vs. anthropogenic sources in the collected aerosols in particular for Zn, Cu, and Cd

Chapter 4:

In this chapter, the bio-available fraction of trace elements in the collected aerosols were characterised by leaching bulk aerosol samples with ammonium acetate. The specific aims of this chapter are:

- To characterise the elemental and isotopic ratios of the leachable fraction
- To determine the solubility of elements in aerosols in particular for Zn, Cu, and Cd
- To investigate the importance of anthropogenic sources of aerosols on solubility

Chapter 5:

This chapter summaries the major findings and conclusions that can be drawn from the studies in Chapter 2 to 4.

Appendix

The appendix lists the abstracts of conference posters and oral presentations during the period of this PhD study.

1.5. Analytical methods

Numerous chemical and physical methods are used to study aerosols in the environment, such as traditional filter sample methods, real-time online chemical analysis methods (e.g. aerosol time-of-flight mass spectrometry, Aerodyne aerosol mass spectrometry, and particle-into-liquid-sampler with ion chromatography), off-line chemical analysis (e.g. scanning and transmission electron microscopies, and proton nuclear magnetic resonance spectroscopy), and methods of measuring the physical and chemical properties of aerosols (e.g. density and refractive index, aerosol size distributions, and size-resolved aerosol compositions) (McMurry, 2000; Lee and Allen, 2012).

Stable isotope signatures have been very successful for source appointment and as tracers of aerosols, including non-radiogenic isotopes of the light elements carbon (C), nitrogen (N), and oxygen (O) (Wang et al., 2005; Wang et al., 2010; Kojima et al., 2011) and radiogenic isotopes of elements such as lead (Pb), and neodymium (Nd) (Grousset and Biscaye, 2005). Lead and Nd radiogenic isotopic systems are two tracer systems uniquely suited for unraveling the sources of natural and anthropogenic trace metals to the ocean. Lead isotopes provide a clear fingerprint of anthropogenic activity (e.g. Bollhofer and Rosman, 2000), while Nd isotopes are a reliable tracer for differentiating between continental source areas (e.g. Grousset, 2005).

Mineralogy, elemental composition and element ratios are widely used in provenance tracing studies of aerosols (e.g. Gallet et al., 1996; Gaiero et al., 2004; Monna et al., 2006; Ferrat et al., 2011; Fujiwara et al., 2011). For example, Ferrat et al. (2011) were able to discriminate between different Chinese deserts, Tibetan soils and Chinese loess plateau source areas using REE ratios such as La/Gd, La/Yb, Y/Tb and Nd/Er. This is because mineralogy is a control on the geochemical composition that is dependent on the type of geological formation the rock or loess derived.

Due to the importance that anthropogenic aerosol sources may have on element supply to the South Atlantic Ocean and potential use of geochemical data in provenance tracing of aerosols, aerosol samples were required (SCOR, 2006, GEOTRACES Science Plan). The following describes a background into the choices of physical and chemical analysis methods for this thesis.

1.5.1. Identifying mineralogy by X-ray diffraction

X-ray diffraction (XRD) is the primary tool for identifying and quantifying the mineralogy of crystalline compounds in rocks, soils and particulates (Reynolds and Moore, 1997). Every mineral or compound has a characteristic X-ray diffraction pattern, which can be matched against a database of over 250,000 recorded phases (Reynolds and Moore, 1997). A powdered sample of crystalline material is placed in a holder, and the sample is then illuminated with monochromatic X-rays of fixed wavelength (λ) at an angle (θ) and the intensity of the reflected radiation is recorded using a goniometer (Reynolds and Moore, 1997). The intensity of the reflected radiation differed by an integer (n) of wavelengths is expressed as the

inter-atomic spacing in the material that causes the intensity in radiation (d value in Angstrom units, 10^{-8} cm, Moore and Reynolds, 1997), using Bragg's Law (1).

$$n\lambda = 2d \sin\theta \quad (1)$$

Varying the angle results in different peak intensities of diffracted X-rays, and produces a characteristic pattern to the crystalline material (Reynolds and Moore, 1997). A database of known X-ray diffraction patterns for minerals is compared to the results to identify possible matches. When patterns are similar between minerals, identification becomes difficult and some knowledge of the expected mineralogy is required (Reynolds and Moore, 1997). This method requires tenths of a gram of material, which must be ground into a powder (Reynolds and Moore, 1997).

1.5.2. Sample digestion

Particulate samples must be completely dissolved as elemental and isotopic analysis methods only analyse liquids. Particulates are broken down or dissolved by acid treatment. Because most rocks are composed of a combination of many types of minerals, each having different chemical and physical properties, digestion is accomplished by using a combination of acids (e.g. Weiss et al., 2004; Dolgopolova et al., 2004; Mason et al., 2005; Jickells and Spokes, 2005; Ferrat et al., 2011). Most commonly used is a mixture of hydrofluoric, nitric, hydrochloric, and perchloric acids, which will decompose all but the most resistant minerals. The choice of extractants depends on the aim of the study, type of mineralogy, properties of the extractant, and experimental conditions (Twyman, 2005; Roundhill et al., 2009; Guveni and Akinci, 2011). Improper selection of extractants could cause partial dissolution of rock sample resulting in decreased element concentration levels in the sample (Hlavay et al., 2004; Twyman, 2005). Samples with silicate components are commonly digested in concentrated hydrofluoric acid (HF) and concentrated nitric acid (HNO_3) at a ratio of ~5:2 or ~4:1 (Mason et al., 2005; Ferrat et al., 2011). For sulphides free from silicate components, such as some mafic volcanic samples, these may be digested in HNO_3 and concentrated hydrochloric acid (HCl) at a ratio of ~4:1 (Mason et al., 2005). The acids are heated with the sample grains in Teflon containers on a hotplate. Teflon containers are resistant to temperatures up to ~260°C, pressures up to ~200bars and chemically inert against most substances (pH 0-14), are dielectric and anti-static, and are thus perfect for working with dissolving particulate materials (Plunkett, 1941).

1.5.3. Sample leaching

The different geochemical processes that aerosols may go through in their atmospheric lifetime, as discussed above, have led to studies choosing to analyse particular scenarios with regards to element supply to ocean surface waters. There are techniques that attempt to replicate seawater dissolution of

elements from aerosols by direct exposure of an aerosol sample to an aliquot of surface seawater (e.g. Bonnet et al., 2004; Thuroczy et al., 2009). Such experiments, although conceptionally simple, are extremely difficult in practice, requiring great skill to avoid potential contamination and to measure the tiny quantities of element (particularly Fe) released with sufficient accuracy (Buck et al., 2006; Wu et al., 2007). The low solubility of Fe from seawater dissolution has suggested that seawater dissolution conditions do not explain the levels of Fe delivered to the surface waters from the atmosphere (e.g. Baker et al., 2010). Lower pH conditions during wet deposition of aerosols deliver aerosols in a soluble form to the ocean surface which may enter straight into the microlayer on the surface of the seawater (Buck et al., 2006). A batch-leach method attempts to present the fractional solubility of elements that may be made available to the ocean surface waters by atmospheric dissolution during wet deposition (Bruland et al., 2001; Witt et al., 2006; 2010; Baker et al., 2006; 2010; 2013). The method uses an ammonium acetate (NH_4Ac) solution at pH 4.7 to represent acid conditions in polluted rainwater (Bruland et al., 2001; Baker et al., 2006a). Particulate samples are submerged in the ammonium acetate solution for ~1hr to represent the initial element dissolution from aerosols (Bruland et al., 2001; Baker, 2006a). However, this solution has too high an ionic strength and metal binding capacity to fully represent rainwater conditions (Bruland et al., 2001). Other acids that are typically found in gaseous condition in the atmosphere, such as HCl, HNO_3, and H_2SO_4 have been used to represent possible acidic conditions in clouds (e.g. Desbeoufs et al., 2001; Wu et al., 2007). A low pH of HCl, HNO_3, and H_2SO_4 may represent acidic conditions during cloud processing of aerosols (e.g. Wu, J. et al., 2007).

There are techniques that attempt to replicate seawater dissolution of elements from aerosols by direct exposure of an aerosol sample to an aliquot of surface seawater (e.g. Bonnet et al., 2004; Thuroczy et al., 2009). Such experiments, although conceptionally simple, are extremely difficult in practice, requiring great skill to avoid potential contamination and to measure the tiny quantities of element (particularly Fe) released with sufficient accuracy (Buck et al., 2006; Wu et al., 2007). The low solubilities of Fe from seawater dissolution has suggested that seawater dissolution conditions do not explain the levels of Fe delivered to the surface waters from the atmosphere. Lower pH conditions during wet deposition are thought to

The analysis of both atmospheric and seawater dissolution conditions present their uses but the diversity in experimental methods hinders efforts to make progress in the field of understanding element supply from the atmosphere to the ocean (Baker et al., 2010).

1.5.4. Pb and Nd extraction from samples

Lead purification by single-pass anion exchange resin using HCl or HNO_3 removes the major element matrix of almost all geological materials (Weiss, 2004; Kamber, 2009). The procedure is widely known as the “HCl method” (Kamber, 2009). Pb isotopes can then be analysed using multi-collector inductively coupled mass spectrometry (MC-ICP-MS, as discussed later in this chapter). It is suitable for Pb isotope

analysis as it is non-labour intense, easy to apply and the Pb separation by the HCl method is sufficient to obtain accurate and precise Pb isotope ratio measurements for a number of geo- and cosmogeochemical substances (Woodhead, 2002). The Pb separation procedure has been previously described (Weiss, 2004). After digestion, the sample solution is dried and the residues redissolved in 1.5 ml 2.4M HCl prior to the passage through the column. After conversion to the chloride form, Pb is separated using Pb selective extraction chromatographic Sr-resin from EiChrom using only HCl and one column passage. The column is first cleaned with 6M HCl and 18Ω MilliQ water, and then pre-conditioned with 2.4M HCl. The sample is then loaded onto the column and matrix removal using 2.4M HCl and then Pb extraction using 6M HCl is carried out (Table 1.1). The recovery of Pb from the column is quantitative from biological and silicate matrices (Weiss et al., 2004).

Table 1.1. Ion exchange column procedure for separating Pb from sample matrix (taken from Weiss et al., 2004)

Step	Molarity (of HCl) and volume used
1. Cleaning	6M (3 × 2-3ml)
	MQ (2-3ml)
2. Pre-conditioning	2.4M (1.5ml)
3. Sample Loading	2.4M (1.5ml)
4. Matrix Removal	2.4M (4ml)
5. Pb Extraction	6M (4ml)
6. Cleaning	6M (2 × 2-3ml)
	MQ (2-3ml)

Neodymium purification is achievable by a two-step element exchange resin procedure. The transuranic-element specific resin (TRU.Spec) provides a rapid and effective means to separate, on a single, small-sized column, the light rare earth elements (LREE), thorium, and uranium from most silicate samples (Pin and Zalduegui, 1996). The LREE fraction can then be stripped using dilute HNO_3, thereby permitting direct loading onto a second extraction chromatographic column for the isolation of individual lanthanides using lanthanide-element specific resin (LN.Spec) (Pin and Zalduegui, 1996). This column elution scheme enables the separation of neodymium and samarium be made in a single run from bulk rock solutions. Figure 1.4 illustrates the two-step procedure by Pin and Zalduegui (1996).

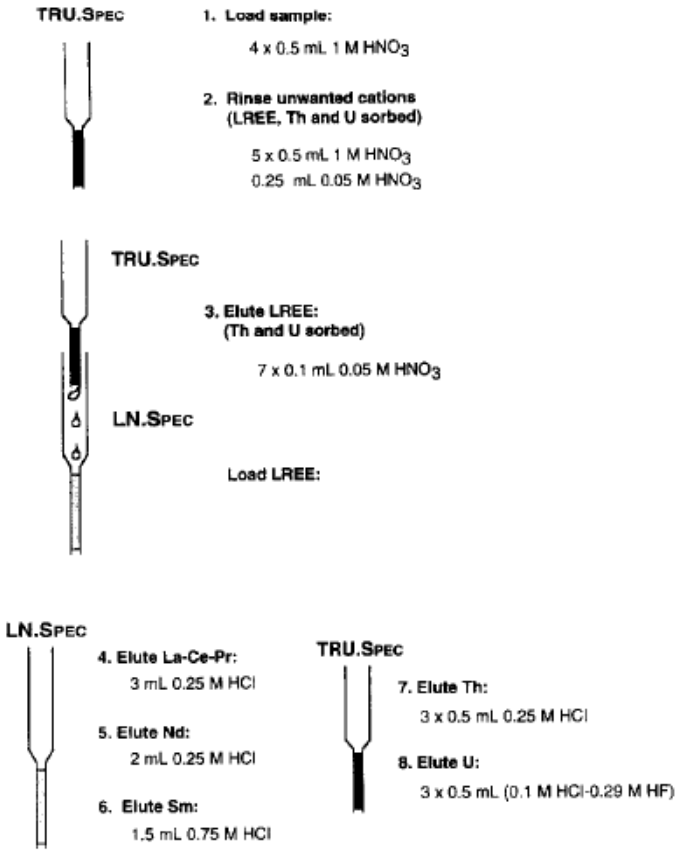

Figure 1.4 Diagram of the extraction chromatographic procedure to separate the LREE, Th and U fractions using TRU.Spec resin and isolate Nd and Sm using the LN.Spec resin (taken from Pin and Zalduegui, 1996).

The methods described by Pin and Zalduegui (1996) isolate the element of interest in a high degree of purity, as required for multi-collector inductively coupled mass spectrometry and thermal ionisation mass spectrometry analyses, with good yields and satisfactory blank levels. They use small amounts of solutions of dilute mineral acid, providing a clear environmental advantage over conventional methods that are based on anion or cation exchange resins that require the evaporation of large volumes of relatively more concentrated acids. Although residual amounts of elements that adhere to the resin after the REE separation step have been significantly reduced for Nd, they are still too large for Th and U, and require the use of new resin whenever low blank levels are necessary (Pin and Zalduegui, 1996).

1.5.5. Determining element concentrations

There are many fields in which the available sample volume and elemental concentration of a sample is the limiting factor for an elemental analysis. Over the last twenty years sample introduction systems used in plasma spectrometry (i.e. Inductively Coupled Plasma Atomic Emission Spectrometry, ICP-AES, and

Quadrupole Mass Spectrometry, ICP-QMS) have evolved in order to expand the field of applicability of these techniques to the analysis of micro and nano samples.

ICP-AES is an emission spectrophotometric technique (Figure 1.5). The sample introduction system on the ICP-AES consists of a peristaltic pump, Teflon tubing, a nebulizer, a spray chamber and plasma torch assembly (Fig. 1.5). The fluid is pumped into the nebulizer via the peristaltic pump. The nebulizer generates an aerosol mist and injects humidified Ar gas into the chamber along with the sample. This mist accumulates in the spray chamber where the largest mist particles settle out as waste and the finest particles are subsequently swept into the torch assembly into the plasma (Stefánsson et al., 2007). Radio frequency-generated and maintained Ar plasma, portions of which are as hot as 10,000K, excites the electrons (Stefánsson et al., 2007). When the electrons return to ground at a certain spatial position in the plasma, they emit energy at the specific wavelengths peculiar to the sample's elemental composition (Stefánsson et al., 2007). The light emitted is focused through a lens that passes through an entrance slit into the spectrometer (Stefánsson et al., 2007). Within the spectrometer is a diffraction grating and wavelength detectors (photomultiplier tubes) (Stefánsson et al., 2007). A computer control ensures that the detectors are synchronised with the grating so that the intensity at the detector at any given time correlates with the wavelength being diffracted by the grating (Fig. 1.5). The intensity of the energy emitted at the chosen wavelength is proportional to the amount (concentration) of that element in the analysed sample (Stefánsson et al., 2007). Thus, by determining which wavelengths are emitted by a sample and by determining their intensities, the element composition of the given sample relative to a reference standard can be quantified.

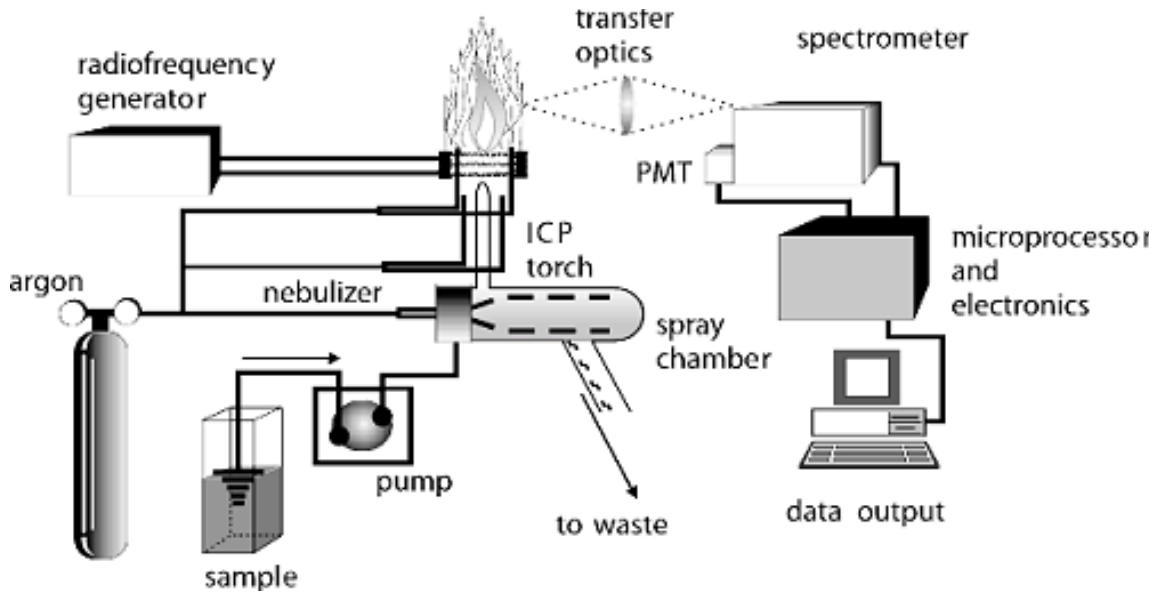

Figure 1.5 Schematic diagram of the inductively coupled plasma atomic emission spectrometer (ICP-AES), taken from Environmental Science, Baltic University, 2005.

Certain precautions are necessary to ensure accurate and precise determination of element concentration (Stefánsson et al., 2007). Differing viscosities in sample matrices may affect the amount of sample uptake and change the nature of the plasma, for instance matrices containing HF can attack the torch. The instrument reading can drift over a period of time due to physical changes in the optical system of the configuration of the plasma. Standards need to be run at the beginning and the end of each run of samples in order to estimate and correct for this drift. Internal standards are used to compensate for differing matrices from sample to sample. Accuracy and precision are limited to ppm levels due to ppm limits of detection using atomic emission spectrometry (Stefánsson et al., 2007).

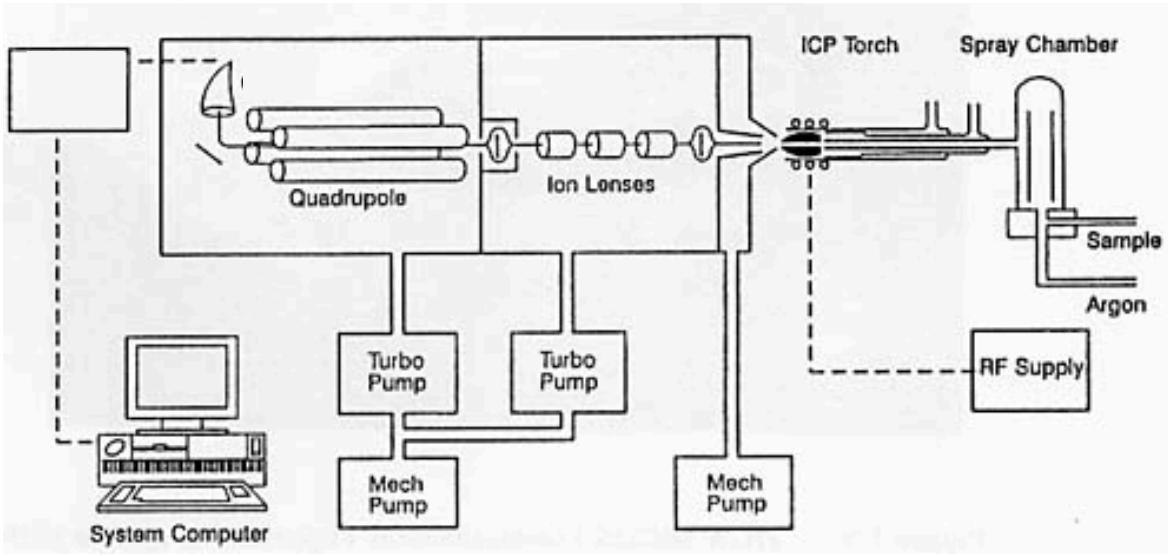

Figure 1.6 Schematic diagram of the inductively coupled plasma quadrupole mass spectrometer (ICP-QMS), taken from Lu and Sun, 2008.

ICP-QMS (Figure 1.6) has a higher sensitivity than AES, particularly for trace and REE, and the ability to handle both simple and complex matrix interferences due to the high-temperature of the ICP source (e.g. Wolf, 2005). As the name states, the ICP-QMS combines a high-temperature inductively coupled plasma source with a quadrupole mass spectrometer (Wolf, 2005). In the same way as the ICP-AES, the plasma converts the atoms of the elements in the sample to ions. The quadrupole mass analyser filters out elements not of interest, matrix and interfering ions, allowing only desired element ions of a single mass-to-charge ratio to be transmitted to an ion mass detector (Wolf, 2005). It is the accuracy of the mass spectrometer that provides the ability to detect element concentrations down to parts per billion (ppb) and parts per trillion (ppt) level (Wolf, 2005). In the same way as the ICP-AES, ICP-QMS accuracy and precision are optimum when matrix interferences are kept to a minimum. For this reason, once particulate samples are digested and evaporated to dryness, the residues are redissolved in dilute HNO_3 or HCl, which are non-corrosive to the ICP instruments (Wolf, 2005). The ICP-AES and ICP-QMS

instruments can provide extremely flexible, non-labour intense and rapid analysis of a number of elements without the need for element separation procedures (Wolf, 2005).

1.5.6. Determining Pb and Nd isotopic compositions

Since the importance of isotope ratios as tools to study the biogeochemistry of trace elements has been discovered, researchers have been developing mass spectrometric techniques to determine accurately and precisely isotopic ratios (Yang, 2009). Thermal ionisation mass spectrometry (TIMS) has been the technique of choice for metal isotopes (Balcaen et al., 2010) for a long time despite the disadvantages of extensive sample preparation requirement, limited ionisation efficient for elements with ionisation energy above 7.5eV, and long measurement time (Yang, 2009; Balcaen et al., 2010). The development of inductively coupled plasma mass spectrometry techniques coupled with multiple isotope collection in the 1990s (MC-ICP-MS) has brought a new dimension to metal isotope ratio analysis. The MC-ICP-MS overcame the limitations of the quadrupole ICP-MS with a magnetic mass filter, which creates flat top peaks and simultaneously measuring the intensity of several ion beams, which overcomes the instability of intensity that affect the precision of isotope ratio measurement (Abarède et al., 2004; Balcaen et al., 2010). The MC-ICP-MS technique provided accurate and precise determination of isotope ratios with precision up to 0.001%, which made it comparable to the TIMS technique (Albarède et al., 2004).

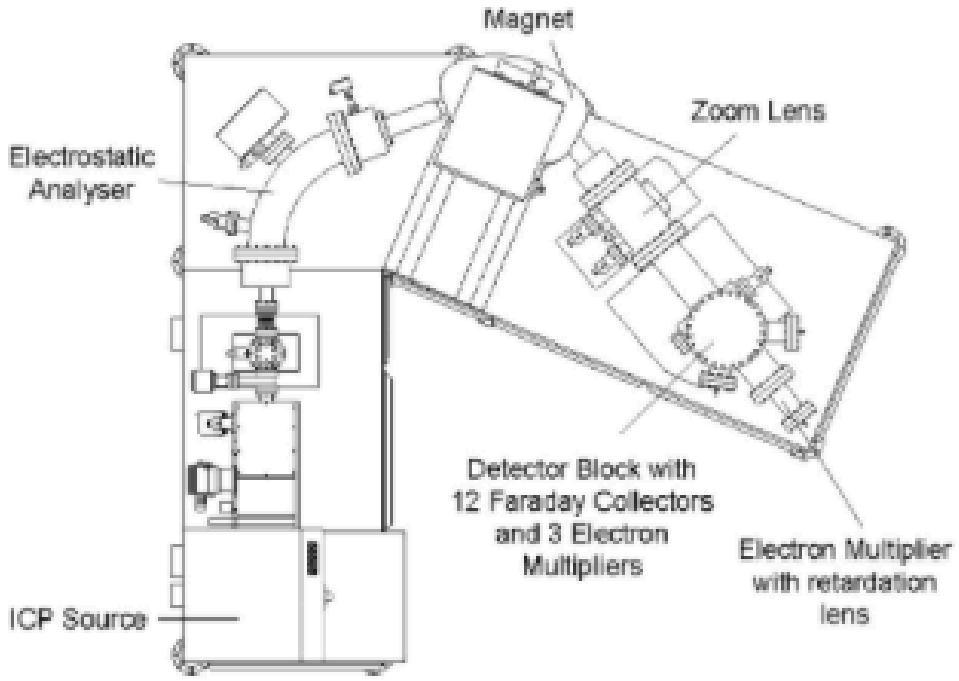

Figure 1.7 Schematic diagram of the Nu Plasma MC-ICP-MS instrument, taken from Rekhämper et al., 2001.

Since the first reported use of the MC-ICP-MS for Pb and Nd isotope ratio measurement (Walder et al., 1993), the isotope ratio of 46 elements have been reported by using the MC-ICP-MS technique (Yang et al., 2009). Throughout this PhD research, all isotope ratios of Pb and Nd were measured with a Nu Plasma MC-ICP-MS instrument (shown in Figure 1.7, Rekhämper et al., 2001) equipped with a Nu DSN-100 Desolvation Nebulizer System. The following describes the method, taken from Rekhämper et al. (2001). First an ion beam is generated in the plasma ion source. Then the ion beam is accelerated in the vacuum system of the mass spectrometer at high voltage and focused by a series of electrostatic lenses. A magnet separates the isotopes of the target element by virtue of their different masses. Finally an array of detectors collects the separated ion beams. The voltage ratios of the masses reflect the element isotope ratio. Essentially all elements introduced into the plasma are ionized including doubly charged species and oxides. Thus in order to achieve the highest accuracy and precision the sample solution needs to be chemically purified by such procedures as by column chemical separation described in Section 1.5.4.

Even though the multi-collector is static, high temperatures, pressures and high voltages cause interference with the plasma instability, which can limit precision and often require hours to days to regain instrument stability (e.g. Vervoort, 2012). Even though ionization efficiency of the plasma is near 100%, transmission of ions is lower than with the TIMS because the plasma-generated ion must be transferred from atmospheric pressure to the high vacuum of the mass spectrometer and many ions are lost during this difficult transfer (e.g. Vervoort, 2012). Mass bias may occur in the instrument and may occur during sampling of ions in the plasma and during formation of the aerosol from the nebulizer (Rekhämper et al., 2001). Mass bias is when a measured isotope for a target element does not correlate to the standard certified isotope for a target element due to isotope similarities between different elements (Rekhämper et al., 2001). The mass bias must be accounted for to determine the true isotope ratio for a target element, as discussed below (Rekhämper et al., 2001).

The isotope composition of Pb in environmental geochemistry is commonly expressed using the ratios of $^{206}Pb/^{207}Pb$ and $^{208}Pb/^{206}Pb$ because these isotopes are the most abundant and therefore can be determined more precisely than ratios involving the low abundance ^{204}Pb isotope (Komárek et al., 2008). However, the $^{206}Pb/^{204}Pb$ and $^{208}Pb/^{204}Pb$ ratio often yield the largest variability between samples due to the fact that the ^{238}U half-life is comparable with the age of the Earth and the ^{232}Th half-life is comparable with the age of the universe, whereas that for ^{235}U is much shorter, so that almost all primordial ^{235}U in the Earth has now decayed to ^{207}Pb (Dickin, 1995). Thus the abundance of ^{207}Pb has not changed in the last ~1Gyr compared to ^{206}Pb and ^{208}Pb.

To obtain accurate and precise Pb isotope ratios, a procedure described in Weiss et al. (2004) was used. A NIST SRM 981 Pb standard is used to calibrate the isotopic ratio of a Tl spike added to samples and then used for mass bias correction using the external normalisation process determined by Mason et al. (2004). A mass bias correction procedure was necessary to eliminate variation in Pb isotope ratios due to similar isotope ratios of other elements; Tl has two of such isotopic ratios, ^{203}Tl and ^{205}Tl. Mass bias

correction models used include the linear, power and exponential law (Albarède et al., 2004), but the exponential law is the most widely used (Yang et al., 2009) and is expressed as (2).

$$^{i/j}R_{true} = {}^{i/j}R_{measured}\,(m^i/m^j)^f \quad (2)$$

Here, R is the isotope ratio, m^i and m^j are absolute atomic masses of the isotopes of interest, and f is the mass bias correction factor.

After doping NBS SRM 981 Pb standard and unknown samples with the NIST SRM 997 Tl with the same Pb/Tl ratio and concentrations, the measurement of the raw Pb isotope ratio is conducted with the MC-ICP-MS. The mass 202 is measured simultaneously to correct for the isobaric interference on ^{204}Pb from ^{204}Hg. From the raw data, the Tl mass fractionation factor fTl is calculated using the exponential law (3). The ^{205}Tl/^{203}Tl ratio used to calculate the mass fractionation factor fTl is optimised each measurement session from repeated NIST SRM 981 Pb standard measurements dispersed between sample measurements.

$$f_{Tl} = \ln(^{205/203}Tl_{true}/^{205/203}Tl_{measured}) \,/\, \ln(m_{205}/m_{203}) \quad (3)$$

m_{205} and m_{203} represent the atomic masses of the two different Tl isotopes. The 'optimised' Tl mass correction factor fTl is then used to correct the measured Pb isotope ratios of the sample by (4).

$$^{i/j}Pb_{true} = {}^{i/j}Pb_{measured}(m_j/m_i)^{fTl} \quad (4)$$

m_i and m_j are the atomic masses of isotopes i and j, respectively (i.e.204, 206, 207, 208) and f_{Tl} is the mass fractionation coefficient derived from equation (3). The Tl ratio is then optimised using the ^{208}Pb/^{206}Pb value of Galer and Abouchami (1998), which is ^{208}Pb/^{206}Pb = 2.16771.

$$^{143/144}Nd_{true} = {}^{143/144}Nd_{measured} \times (^{143/144}JNd_{i\ true}/^{143/144}JNd_{i\ measured}) \quad (5)$$

The isotope ^{147}Sm decays to ^{143}Nd by a-emission, with a half-life of about 106Gy. Then the ^{143}Nd abundance in geological material varies according to time and its ^{147}Sm/^{144}Nd ratio.

To obtain accurate and precise Nd isotope ratios, a procedure as conducted in Tanaka et al. (2000) was used. Samples are analysed on the MC-ICP-MS with a Nd-standard. Tanaka et al. (2000) prepared a standard neodymium reference solution known as JNd_i. ^{143}Nd/^{144}Nd ratios are determined for samples and JNd_i and are corrected for mass fractionation by normalising to ^{146}Nd/^{144}Nd = 0.7219 (Tanaka et al., 2000). Samples are then normalised by the JNd_i value by equation (5) to take into account the offset from the recommended JNd_i value (Tanaka et al., 2000).

CHAPTER 2

Element and Pb and Nd isotopic characterisation of atmospheric particulate sources from South America and Southern Africa to the South Atlantic Ocean

2.1. Introduction

The atmosphere is a major pathway for delivering aerosols and their associated trace elements to the Earth's oceans (Duce et al., 1991). For regions of the South Atlantic, the atmosphere is thought to be the main pathway for delivering essential elements for primary production (in particular iron, Fe) to the ocean surface waters and therefore play a vital role in controlling carbon dioxide release into the atmosphere, and thus global climate (Mahowald et al., 2005). Thus, it is important to identify the sources of aerosols that reach the Earth's oceans to understand the controls on marine element budgets and climate.

Atmospheric dust modeling has determined that Patagonia is the main dust source from South America to reach the South Atlantic, followed by the Puno-west Argentinian region along the Andean Volcanic Belt (e.g. Prospero et al., 2002; Gaiero et al., 2003; Gasso et al., 2007). This is due to the arid conditions of these regions and prevailing westerly winds. Atmospheric modeling over Africa revealed that arid regions in Namibia and the Kalahari are the major natural dust sources (Chin et al., 2009) and suggested that anti-cyclonic wind patterns may transport dusts from Southern Africa to the South Atlantic Ocean (Piketh et al., 2002). Growing cities in the Southern Hemisphere may also impact aerosol composition from South America and Southern Africa. The global model GOCART was used to estimate the aerosol absorption by pollution, dust and smoke aerosols from 2000 to 2007 and revealed that sulfates and black carbon emission patterns indicated that pollution and biomass burning were major sources of aerosols from South America (north of ~45°S) and Southern Africa (Chin et al., 2009). These studies also revealed a seasonal pattern whereby black carbon emissions were most dominant during June-August (Chin et al., 2009).

The accuracy of determining the sources of aerosols that reach the South Atlantic may be improved by geochemical constrain of potential continental sources of aerosols. Mineralogy, which controls element composition, often varies between different natural sources consisting of different rock formations (e.g. Gaiero et al., 2003, 2004; Ferrat et al., 2011). Lead (Pb) isotopes are useful aerosol provenance indicators of both natural and anthropogenic aerosols (Bollhofer and Rosman, 2000; Gioia et al., 2010). Three of the four natural Pb isotopes, ^{204}Pb, ^{206}Pb, ^{207}Pb and ^{208}Pb are end-members of the ^{232}Th (^{208}Pb), ^{235}U (^{207}Pb) and ^{238}U (^{206}Pb) radioactive decay chains, and lead to the formation of different ore bodies showing different isotopic compositions according to their age and the initial Th and U content of the source rock. The higher the ^{208}Pb/^{207}Pb ratio in a rock, the younger the rock. Natural and anthropogenic sources (such as industrial or combustion processes) may be distinguishable from one another depending on the source of Pb (Bollhofer and Rosman, 2000). Another isotopic provenance tracer is neodymium (Nd), which is commonly used to differentiate between different aged rock formations due to the ^{143}Nd/^{144}Nd isotopic ratio. Neodymium has seven stable isotopes; of these ^{144}Nd is the most stable. ^{147}Sm decays to ^{143}Nd with a half-life of 1.53 x 10^{11} years. Variations in Nd isotopic compositions in ^{143}Nd/^{144}Nd are therefore a result of elemental fractionations occurring between ^{143}Nd and its parent ^{147}Sm

during radioactive decay and states that the higher the $^{143}Nd/^{144}Nd$ ratio in a rock, the older the rock (Jacobson and Wassenburg, 1980).

Due to the potential affect that particle size may have on chemical composition as a result of particle size control on mineralogy (Raes et al., 2000; Chang et al., 2000; Honda et al., 2004; Feng et al., 2010; Ferrat et al., 2011), it is important to assess loose material such as loess (terrestrial mineral dust deposits such as clays, silts, sands; <125 μm) and aerosols rather than rock deposits from potential sources. There are however limited studies that have geochemically characterised loess and aerosols from natural sources from South America and Southern Africa (Gaiero et al. 2003; 2004; 2007; Delmonte et al., 2004; Monna et al., 2006; Sugden et al., 2009; Gioia et al., 2010). Element compositions were found to be similar within loess and volcanic deposits from across Patagonia (Gaiero et al., 2003, 2004, 2007). Neodymium isotopic values reflected the young geological age (Mesozoic and younger) of rocks typically found across Patagonia (Delmonte et al., 2004; Gaiero et al., 2007; Sugden et al., 2009). Delmonte et al. (2004) also showed that Nd isotopic ratios in aerosols collected in rural areas in Southern Africa (Namib desert and the Kalahari) were less radiogenic than in South American sources (Patagonia) due to older rock formations (Archean to Neoproterozoic) in these Southern African regions. Meanwhile there are a number of studies that have geochemically characterised rock formations across Patagonia and the Andean Belt (GEOROC, 2003-2011), major urban areas in South America (e.g. Bertolo et al., 2011; de Campos, 2012; Guarino et al., 2012), and across Southern Africa (e.g. Condie and Hunter, 1976; Le Roex and Lanyon, 1998; Janney et al., 2002; Le Roex et al., 2003; Ewart et al., 2004). Although particle size may control mineralogy and thus chemical composition between finer and larger fractions, bulk rock data have shown similar chemical and isotopic composition to above mentioned loess data from the same source regions. Volcanic rock formations from Patagonia and the Andes (GEOROC, 2003-2011) revealed major and rare earth element (REE) compositions and Nd isotopic compositions in line with those from loess materials from Patagonia (Gaiero et al., 2003, 2004, 2007; Delmonte et al., 2004; Sugden et al., 2009).

There are a few studies that have characterised element and Pb isotopic compositions of anthropogenic sources from South America and Southern Africa (Bollhofer and Rosman, 2000; Monna et al., 2006; Gioia et al., 2010; Fujiwara et al., 2011). High trace element concentrations were determined in road dusts from across Buenos Aires (Fujiwara et al., 2011). Other studies assessed Pb isotopes in aerosols collected from major urban areas in the Southern Hemisphere and São Paulo, respectively, and found that different urban areas were characterised by different Pb signals dependent on the major anthropogenic Pb sources that were in use in these regions (Bollhofer and Rosman, 2000; and Gioia et al., 2010). These anthropogenic sources revealed less radiogenic Pb isotopic ratios than those from natural sources from Patagonia. The geochemical characteristics of aerosols from an urban area in Southern Africa were carried out (Monna et al., 2006). This study compared aerosols collected by lichens, on tree bark and samples of coal and gasoline in urban parts of the city as well as rural areas such as large parks to attempt to compare a natural from anthropogenic signal in Pb isotopes. Lichens are slow-growing

organisms which, over their lifespan, are expected to accumulate and retain high levels of mineral elements present in the atmosphere, but not from the host tree limb or rocks from which they are suspended (Getty et al., 1999; Loppi and Pirintos, 2003). Therefore, the Pb isotopic data from the lichen and bark samples are taken as being representative of the atmospheric aerosol composition of the local area (i.e. rural, urban or mine source areas from Johannesburg, Southern Africa).

It is clear that a key aspect to improving the accuracy of aerosol provenance tracing over the South Atlantic Ocean by geochemical constrain of continental sources is to determine geochemical proxies that can distinguish between i) natural and anthropogenic sources, ii) South American and Southern African sources, and iii) different source regions within sources. These were addressed by characterising the mineralogy, element and isotopic (such as Pb and Nd) compositions in potential major natural and anthropogenic aerosol sources from South America and Southern Africa. Where samples from natural sources were limited, shelf sediment off the coast of South Africa were geochemically characterised. Shelf sediment in a similar way to loess may represent a homogenised material from local source areas (e.g. Wildeman et al., 1965). They may contain a mixture of source materials such as atmospheric, riverine, upwelling, biogenic, and anthropogenic (e.g. Goldberg, 1963). However the lithogenic elements that arrive by river input and have not been influenced by other biogeochemical processes may maintain the chemical and isotopic characteristics and therefore be representative of the parent natural source areas from the local region (e.g. Wildeman et al., 1965). This study assesses the geochemical constrain of shelf sediment on natural sources from Southern Africa. Due to the potential affect that particle size may have on the geochemical constrain of sources, this study assesses the affect of particle size on select source samples. The above geochemical characteristics that showed differences between sources were identified using element enrichment factors relative to the upper continent crust and bivariate plots of element and isotopic ratios. This study presents new data for Patagonian deserts, the Andean Volcanic Belt, the urban areas of São Paulo, Buenos Aires and Johannesburg, and shelf sediment off the coast of Cape Town, and combines these results with published results for the same regions and other major source areas in South America and Southern Africa.

2.2. Methods

2.2.1. Source characterisation and study area

Sources are classified as natural and anthropogenic (Table 2.1). Natural sources are geogenic sources from areas outside of a major town or city and are sub-divided into rural (i.e. sand, glacier deposits, top soils, river bed sediment, dust) and volcanic (source samples dominantly consisting of volcanic deposits such as tephra and pyroclastic material, or volcanic rock). Anthropogenic sources are divided into samples collected from urban areas, and from major human activities in South America and Southern Africa such as oil and coal burning, and mining.

Figure 2.1 shows a simplified geology of South America and Southern Africa. The simplified geological boundaries in South America are based on de Almeida et al., 2000; and de Brito Neves et al., 2013, while geological boundaries in Southern Africa are based on Begg et al. (2009) and Tohver et al. (2006). South America can be simply divided into the Archean/Neoproterozoic shield area known as the South American Platform from central to the north (dark grey area, Fig. 2.1), and the Phanarezoic covers; Patagonia along the southeast margin (grey area in Fig. 2.1), and the Andean region along the west margin of the continent (light grey area in Fig. 2.1). Patagonia dominantly consists of volcanic rocks (basalts, andesites, rhyolites) and plutons, and continental sediment that overlies a basement of Mesozoic age essentially constituted by granites (de Almeida et al., 2000; Alkmim et al., 2001; Ducart, 2006; Rosello et al., 2008; Marfil and Maiza et al., 2012; de Brito Neves et al., 2013). The Andes can be subdivided into volcanic zones: the northern volcanic zone (NVZ; >10°S), central volcanic zone (CVZ; 10-34°S), southern volcanic zone (SVZ; 32-40°S) and austral volcanic zone (AVZ; 40-52°S). The Andes is composed of Cenozoic volcanism of silicic associations and intermediate to basic lava flows along a volcanic arc to the west and basaltic back arc lava flows across the east (Jakes and White, 1972; Dostal, 1977; Grunder, 1987; Rapela et al., 1988; Kay et al., 1993; Stern and Kilian, 1996; Giocada et al., 2014).

In Southern Africa, natural source areas include desert regions in Namibia, the Kalahari and rural areas close to and within Cape Town and Johannesburg. The natural source areas investigated in Southern Africa largely overlay Archean to Neoproterozoic shield composed of intermediate to basic volcanic and metamorphic formations (Condie and Hunter, 1976; Le Roex et al., 2003; Begg et a., 2009; dark grey area, Fig. 2.1). Phanerozoic covers (typically mafic, olivine basaltic, volcanic lava flows and sedimentary basins) lie south of the shield, across the southern coastline of South Africa and along the coastline of Namibia (Le Roex and Lanyon, 1998; Ewart et al., 2004; Janney et al., 2002; Begg et al., 2009).

In South America, the anthropogenic source areas include the major cities across the continent, which overlie all three main geological formations in South America. The South American Platform is composed of metamorphic amphibolite to granulite facies and igneous granitic complexes, and constrained by volcano-sedimentary formations along the eastern margin due to the Brasilia/Pan African extension (de Almeida et al., 2000; Bertolo et al., 2011; de Campos, 2012; Guarino et al., 2012; de Brito Neves et al., 2013). In Southern Africa anthropogenic source regions include cities such as Cape Town,

Johannesburg, Port Elizabeth and Windhoek and overlie a mixture of Archean/Neoproterozoic and sedimentary basin (Condie and Hunter, 1976; Le Roex et al., 2003; Tohver et al., 2006; Begg, et al., 2009).

Table 2.1. Source classification

Source		**Sample Type****
Natural	Rural	Topsoil Sand Glacier deposits Dust Riverbed Sediments
	Volcanic[+]	Tephra Volcanic Rock
Anthropogenic	Urban[*]	Road dust Aerosol
	Coal	Coal sample
	Gasoline	Fuel sample
	Mine	Mine dumps Aerosol

[+] Samples collected from rural areas and are mainly volcanic deposits or volcanic rock

[*] Samples collected from urban areas and may consist of anthropogenic and natural sources

2.2.2. Sampling

The locations of source samples from South America and Southern Africa from this study are listed in Table 2.2. These are shown in Figure 2.1 (green symbols) alongside the sources assessed from previous studies (different cross shaded areas). Samples outlined in red denote samples that have been analysed in previous element or isotope studies (Fig. 2.1).

Topsoil and riverbed sediment were collected in southern Patagonia in 2012 from Rio Santa Cruz, Bahia San Sebastian, Rio Gallegos, El Calafate and Punta Arenas National Parks (34-55°S, Bory and Bout-Roumazeilles, 2012). Volcanic tephra and clast deposits were collected from the volcanic slopes after the 2011 eruption of the Chaiten and Puyehue volcanoes in the southern volcanic zone (Cid-Agüero, 2011) and volcanic topsoil was obtained from Cotopaxi volcano slopes in the northern volcanic zone.

Size fraction samples (50-75µm, and 75-100µm) of road dusts were acquired from across Buenos Aires (Fujiwara et al., 2011). A dustpan and brush were used to collect dust at pavement edges that accumulated over a two-month period, covering an area of ~ 7 × 12 km^2 in the Summer 2010, and the samples were later sieved to remove large debris such as leaves and brick, dried at 100°C for 24 hours and then sieved (Fujiwara et al. 2011). Samples were collected from urban zones with different traffic

patterns and urban characteristics but samples were not collected adjacent to site-specific pollution sources (Fujiwara et al. 2011).

Aerosol samples (PM_{10}) were collected at the University of São Paulo over a two-day period and the collection method is described in detail by Gioia et al. (2010). The sampling area was located 500 m south of a beltway with intense traffic and staked filter units were used to collect aerosol on 47 mm diameter Teflon membranes sampling <10μm aerosol fraction with an airflow rate of ~ 16 L min^{-1}.

Lichens and tree bark collected in Johannesburg in May 2001 and June 2003 were used to characterise the aerosols originating from South Africa (Monna, et al., 2006). Five lichens were collected from urban areas, one lichen from a rural area and one tree bark sample adjacent to a mine dump site. The location and sampling method of these samples are described in detail by Monna et al. (2006). Lichens growing on trees were collected between 1 and 3 m above ground level by means of pre-cleaned plastic knives. In the lab, remaining leaf debris was removed and the samples dried at 80°C over a period of 2 days.

Seven bulk shelf sediment (top 1-3cm layer) were collected SW off the coast of Cape Town on the Cape Shelf (~18°E, 34°S, 236 m below sea level). These samples were collected during the D357 cruise using a Bowers Connelly megacorer deployed on a steel coring rope (Homoky, 2010).

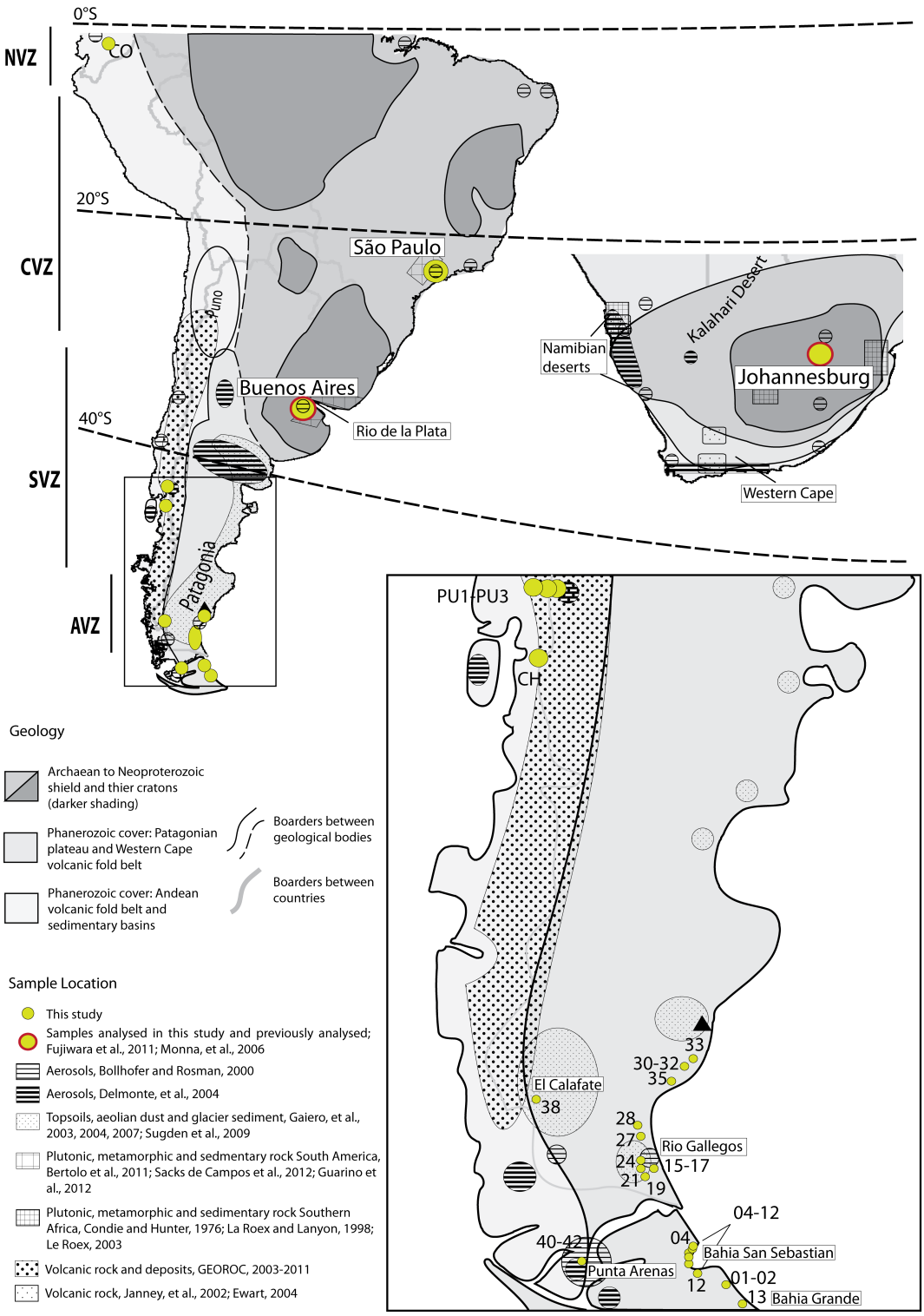

Figure 2.1. Location map of sampling sites from this study and from literature and basic geological boundaries in South America and Southern Africa (taken from de Almeida, et al., 2000; Begg, et al., 2009; Tohver et al., 2006).

Table 2.2. Sample location and source types of major aerosol sources from South America and Southern Africa.

Sample ID	Sample Location	Source Type	Longitude (°)	Latitude (°)
South America				
Argentina				
Rural – (bulk)				
4*	Bahia San Sebastian, Southern Patagonia	Topsoil	-68.39	-52.99
5	Bahia San Sebastian, Southern Patagonia	Topsoil	-68.39	-53.04
8	Bahia San Sebastian, Southern Patagonia	Topsoil	-68.50	-53.14
9	Bahia San Sebastian, Southern Patagonia	Topsoil	-68.57	-53.17
10	Bahia San Sebastian, Southern Patagonia	Topsoil	-68.57	-53.20
11	Bahia San Sebastian, Southern Patagonia	Topsoil	-68.57	-53.23
12	Bahia San Sebastian, Southern Patagonia	Topsoil	-68.52	-53.32
19	Rio Gallegos, Southern Patagonia	Topsoil	-69.53	-51.81
21	Rio Gallegos, Southern Patagonia	Topsoil	-69.60	-51.71
35	Rio Santa Cruz, Southern Patagonia	Topsoil	-68.94	-50.24
40	Punta Arenas, Southern Patagonia	Topsoil	-71.11	-53.29
42*	Punta Arenas, Southern Patagonia	Topsoil	-71.11	-53.29
1	Rio Grande, Southern Patagonia	Lagoon sediment	-68.07	-53.59
2	Rio Grande, Southern Patagonia	Lagoon sediment	-68.07	-53.59
13	Rio Grande, Southern Patagonia	Topsoil/Bed sediment	-67.80	-53.83
15	Rio Grande, Southern Patagonia	Topsoil/Bed sediment	-69.28	-51.73
17	Rio Grande, Southern Patagonia	Topsoil/Bed sediment	-69.28	-51.73
24	Rio Grande, Southern Patagonia	Topsoil/Bed sediment	-69.64	-51.63
27	Bahia Grande, Southern Patagonia	Topsoil/Bed sediment	-69.51	-51.16
28	Bahia Grande, Southern Patagonia	Topsoil/Bed sediment	-69.53	-51.09
30	Rio Santa Cruz, Southern Patagonia	Bed Sediment	-68.90	-49.97
32*	Rio Santa Cruz, Southern Patagonia	Bed Sediment	-68.90	-49.97
33	Rio Santa Cruz, Southern Patagonia	Bed Sediment	-68.56	-49.83
38	Argentino Lake, Southern Patagonia	Bed Sediment	-72.17	-50.31
Urban – 50-75µm				
3C	Urban Area, Buenos Aires	Road dust	-58.51	-34.60
9C	Urban Area, Buenos Aires	Road dust	-58.48	-34.59
110C	Urban Area, Buenos Aires	Road dust	-58.49	-34.65
112C	Urban Area, Buenos Aires	Road dust	-58.49	-34.65
Urban – 75-100µm				
3D	Urban Area, Buenos Aires	Road dust	-58.51	-34.60
9D	Urban Area, Buenos Aires	Road dust	-58.48	-34.59
110D	Urban Area, Buenos Aires	Road dust	-58.49	-34.65
112D	Urban Area, Buenos Aires	Road dust	-58.49	-34.65

*: denotes samples that were analysed for the <5 µm particle size assessment

Table 2.2. (*continued.*)

Sample ID	Sample Location	Source Type	Longitude (°)	Latitude (°)
Brazil				
Urban – <10µm				
631	Urban Area, São Paulo	Aerosol	-46.72	-23.56
648	Urban Area, São Paulo	Aerosol	-46.72	-23.56
649	Urban Area, São Paulo	Aerosol	-46.72	-23.56
650	Urban Area, São Paulo	Aerosol	-46.72	-23.56
660	Urban Area, São Paulo	Aerosol	-46.72	-23.56
665	Urban Area, São Paulo	Aerosol	-46.72	-23.56
Chile				
Volcanic – bulk				
CH*	Chaiten Volcano, Southern Volcanic Zone	Volcanic tephra	-71.03	-43.02
PU1	Puyehue Volcano, Southern Volcanic Zone	Volcanic tephra	-71.16	-40.62
PU2*	Puyehue Volcano, Southern Volcanic Zone	Volcanic tephra	-71.16	-41.06
PU3	Puyehue Volcano, lakeside near La Angostura	Volcanic clast deposits	-71.64	-40.76
Ecuador				
Volcanic – bulk				
CO	Cotopaxi Volcano, Northern Volcanic Zone	Volcanic topsoil	-78.44	-0.68
Southern Africa				
South Africa				
Rural – bulk				
PICA	Rural Area, Johannesburg	Aerosol	28.00	-26.00
ST0	African Margin, sea-shelf off Cape Town	Shelf sediment	17 58	-34 11
ST1	African Margin, sea-shelf off Cape Town	Shelf sediment	17 58	-34 11
ST3	African Margin, sea-shelf off Cape Town	Shelf sediment	17 58	-34 11
ST6	African Margin, sea-shelf off Cape Town	Shelf sediment	17 58	-34 11
ST8	African Margin, sea-shelf off Cape Town	Shelf sediment	17 58	-34 11
ST11	African Margin, sea-shelf off Cape Town	Shelf sediment	17 58	-34 11
ST13	African Margin, sea-shelf off Cape Town	Shelf sediment	17 58	-34 11
Urban – bulk				
RIVER	Urban Area, Johannesburg	Aerosol	28.06	-26.06
DELTA	Urban Area, Johannesburg	Aerosol	28.00	-26.00
CMG	Urban Area, Johannesburg	Aerosol	28.03	-26.20
EMMER	Urban Area, Johannesburg	Aerosol	28.01	-26.16
HUDD	Urban Area, Johannesburg	Aerosol	28.11	-26.11
BOT2	Urban Area, Johannesburg	Aerosol	27.99	-26.15
Mine – bulk				
DRD	Mine Dump Site, Johannesburg	Aerosol	27.88	-26.18

2.2.3. Mineralogical analyses

Minerals were identified in selected samples by X-ray diffraction at the Natural History Museum, London. The sample was ground in an agate mortar and loaded into a circular well mount (5mm diameter, 1mm depth). X-ray diffraction data were collected using an Enraf-Nonius PDS120 diffractometer equipped with a primary Germanium (1 1 1) monochromator and INEL 120° curved position sensitive detector (PSD). Operating conditions for the Co source were 40kV and 35mA. The samples were measured in a flat-plate asymmetric reflection geometry with a constant tilting angle between incident beam and sample surface of 3.5°. The sample was rotated during the measurements to improve particle-counting statistics. The angular linearity of the PSD was calibrated using the external standards silver behenate and silicon (NIST SRM 640).

The identification of the mineral phases in the samples were selected by matching the X-ray diffraction pattern for the sample with external mineral standards selected from reference materials of the mineral collection at the Natural History Museum, London and analysed under identical run conditions as the samples. Major mineral phases were classed as diffraction intensities equating to >10% (w/w), and minor phases were classified as presenting intensities <10% (w/w).

2.2.4. Sample digestion

Fifty milligrams of bulk top soils, riverbed sediments, volcanic, and shelf sediment samples were weighed into 14.7 ml screw top Savillex PTFE vessels and digested on a hotplate for 48 hours in a mixture of 1 ml concentrated HF (30 M) and 0.25 ml concentrated HNO_3 (15.6 M) at 120°C with daily ultrasonic according to the digestion method described by Yu et al. (2001). Samples were then evaporated to dryness and re-fluxed twice in 0.5 ml 15.6 M HNO_3 to dissolve any solid fluorides that may have form due to excess HF, as insoluble fluorides will affect REE recovery.

Aerosols from São Paulo (half a circular Teflon filter; 3 cm in diameter) were acid washed with 5 ml 15.6 M HNO_3 at 120°C for 24 hours in 14.7 ml screw top Savillex PTFE vessels to remove particulates from the filter. The sample was then digested by the same HF/HNO_3 digestion procedure as described above.

Fifty milligrams of lichens and tree bark from Johannesburg were weighed into 14.7 ml screw top Savillex PTFE vessels and treated with a mixture of 2 ml concentrated $HClO_4$ (11 M) and 1 ml 15.6 M HNO_3 on a hotplate for 1 to 3 hours at 90°C, then 1 hour each at 110°C, 140°C, 180°C and 220°C in order to remove organics. The Savillex vials were uncapped throughout this procedure. Following this initial step, samples were evaporated to dryness and then underwent the same HF/HNO_3 digestion procedure as described above.

After digestion, all samples were diluted to 4 ml ca. 0.8 M HNO_3. 1.5 ml for Pb and Nd isotope ratio determination, 1 ml for archive, and 1.5 ml was further diluted to 5 ml ca. 0.8 M HNO_3 for elemental concentration analysis.

2.2.5. Elemental analysis

Major (Ca, Mg, Na, K, Mn) and trace element (Cd, Co, Cr, Cu, Ni, Pb, V, Zn) concentrations were determined by inductively coupled plasma atomic emission spectroscopy using a Thermo iCap 6500 Duo at the Natural History Museum (NHM) in London. Scandium, Th, Y, and REE concentrations were determined by quadrupole inductively coupled plasma mass spectrometry using an Agilent 7700x located at the NHM. Detection limits for all elements were calculated after each run based on the signal intensity and standard deviation measurements of the calibration blank relative to a calibration standard and were at or below the ng ml^{-1} level for all trace elements studied. Procedural blank solutions were prepared with similar acid mixtures and under identical experimental conditions as the atmospheric particulate source samples and yielded concentrations for all elements of interest below detection limits.

Quantitative total dissolution was monitored with the certified reference material USGS G-2 granite (n=12). The estimated reproducibility (2σ relative standard deviation; n = 12) was better than 10% for major elements, better than 6% for REE and better than 2% for trace elements except Zn (< 8%). As the G-2 granite is characterised by abundant refractory phases, results are considered as a maximum uncertainty introduced during sample digestion.

Element concentrations were normalised relative to the upper continental crust (UCC, Taylor and McLennan, 1985) to alleviate variability due to grain size and mineralogical composition between the upper continental crust and the source samples (Bertine and Goldberg, 1977; Windom, 1989; Schropp et al., 1990; Loring, 1991; Hanson et al., 1993; Covelli and Fontolan, 1997). The element most used for aerosol normalisation is aluminium (Al) since it represents aluminosilicates, the main group of minerals generally found in fine sediment fractions from the continent, have negligible anthropogenic input, and behave as a conservative element in aerosols (Loring, 1991). This enables the distinction between aerosols that originate from the continental crust, by showing an enrichment factor of 1, and aerosols that have been influenced by non-crustal sources of an element or have undergone variations of weathering, erosion or hydrothermal alterations, by showing an enrichment factor greater or less than 1 (Loring, 1991). The following equation (1) was used to calculate the enrichment factors relative to the crust (EF_{crust}) of sources samples. The concentration ratio of the component relative to Al in the sample (X/Al_S) is divided by the component relative to Al in the upper continental crust (X/Al_{UCC}, values taken from Taylor and McLennan, 1985).

$$EF_{crust} = [X/Al]_S / [X/Al]_{UCC} \quad (1)$$

2.2.6. Lead and Nd isotope ratio analysis

Lead was isolated from the sample matrix by ion exchange chromatography using Eichrom Sr spec resin (Weiss et al. (2004). Neodymium was isolated using a two-step column procedure (Pin and Zalduegui, 1997). The REE fraction was separated from the sample matrix using Eichrom TRU spec resin, followed

by isolation of the Nd fraction from the other REE using Eichrom Ln spec resin on volumetrically calibrated Teflon columns. Lead and neodymium isotopic compositions were analysed on a Nu Plasma (Nu Instruments Limited, UK) multiple collector inductively coupled plasma mass spectrometer (MC-ICP-MS). The samples were introduced with a Nu DSN-100 Desolvation Nebulizer System and PTFE nebulizer.

For Pb isotope analysis, samples and NIST-SRM8 981 Pb standards were doped with NIST-SRM 997 Tl to yield Pb/Tl ratio of 3:1. The instrument mass bias was corrected for using the Tl as an external spike (Weiss et al. 2004). The precision and accuracy of Pb isotope ratio measurements was assessed using certified reference material USGS G-2 granite. Samples were measured over a five-month period. Repeat measurements yielded $^{206}Pb/^{204}Pb$ values = 18.399 ± 0.005, $^{207}Pb/^{204}Pb$ = 15.640 ± 0.006, and $^{208}Pb/^{204}Pb$ = 38.902 ± 0.021 (n = 22). Reported Pb isotope results for USGS G-2 granite are in agreement with published data (18.396 ± 0.023, 15.636 ± 0.005, 38.900 ± 0.019, respectively, Weis, et al., 2006).

For Nd isotope analysis, samples were analysed with Nd-standard JNd_i and $^{143}Nd/^{144}Nd$ ratios were corrected for mass fractionation by normalising to $^{146}Nd/^{144}Nd$ = 0.7219. Repeated analysis of Nd-standard JNd_i (certified value of 0.512115 ± 0.000007; Tanaka et al., 2000) yielded $^{143}Nd/^{144}Nd$ ratios of 0.512147 ± 0.000016 (n = 26), and all sample results were normalised to take into account the offset from the recommended JNd_i value. Repeat analysis of USGS G-2 granite (n = 22) yielded $^{143}Nd/^{144}Nd$ ratios of 0.512230 ± 0.000026 and are in agreement with reported Nd isotope results for USGS G-2 granite ($^{143}Nd/^{144}Nd$ ratios of 0.512230 ± 0.000013, Weis, et al., 2006). Neodymium isotope data are reported in epsilon units (εNd) where εNd describes the deviation of a samples $^{143}Nd/^{144}Nd$ ratio from the chondritic uniform reservoir value (CHUR = 0.512638) in parts per 10,000 (Jacobsen and Wasserburg, 1980).

2.2.7. Particle size separation

Different grain sizes from selected South American source areas were analysed. This includes three of the bulk top soils and riverbed sediments collected from Rio Gallegos, Bahia San Sebastian and Punta Arenas in southern Patagonia (Bory and Bout-Roumazeilles, 2012), and two bulk volcanic tephra from Chaiten and Puyehue volcanoes in the Andean volcanic belt within western Patagonia analysed in this study (Cid-Agüero, 2011). The specific samples are identified by an asterix by their sample ID in Table 2.2. The target was to separate the <5 µm fraction of these samples by applying Stoke's Law gravity sedimentation (e.g., Biscaye et al., 1965; Biscaye et al., 1997). This approximates a 5 µm diameter particle will fall in water at 20°C at 10 cm every 1.5 hrs, or 5 cm in 45 minutes.

Bulk samples were wet sieved with ultraclean (MQ) water through 60 µm nylon mesh into 90 ml Savillex beakers. The supernatant was siphoned off from the <60 µm fraction using acid cleaned pipettes. The <60 µm fraction was then transferred to 15 ml centrifuge tubes, 10 ml of MQ water was added, and samples were shaken with a vortex shaker and left to stand for 45 minutes. The top 5 ml containing the <5 µm fraction was subsequently siphoned out into a separate 15 ml centrifuge tube. The <60 µm fraction

was re-filled with MQ to 10 ml, shaken and left to stand for 45 minutes. This step was repeated 3 or 4 times until all the <5 μm fraction were removed from the <60 μm fraction. The <5 μm fraction was centrifuged for 45 minutes, the supernatant removed, and the fine fraction sediment left to dry in a laminar flow hood.

The <5 μm fractions were then digested and underwent the same element and isotopic analysis methods that were conducted on the bulk sediment from Patagonia and the Andes, as described in Section 2.2.4 and 2.2.5 to 2.2.6, respectively.

2.3. Results and Discussion

2.3.1. Mineralogy

The mineralogy was determined for South American rural sources (seven bulk Patagonian topsoil and riverbed sediment samples), one bulk volcanic sediment each from Cotopaxi (topsoil), Chaiten and Puyehue (tephra) volcanic areas, and South American urban sources (two road dusts of 50-75μm fraction from Buenos Aires, and three <10μm aerosol samples from São Paulo). Their identified major (>10%) and minor (≤10%) phase minerals are displayed in Table 2.3.

The rural sources from southern Patagonia were characteristic of chlorites and amphiboles (Table 2.3). Select samples south of Rio Gallegos contained bentonite (sample 42, Table 2.3), and aragonite and calcite (sample 4, Table 2.3). These minerals were typically identified across Patagonia (Rosello et al., 2008; Ducart et al., 2006; Marfil and Maiza et al., 2012) and were previously identified in loess samples from Patagonia (Gaiero et al., 2004). This is because these minerals are distinctive of weathered or hydrothermally altered silicic and mafic volcanic rock (e.g. Alkmim et al., 2001; Ducart, 2006), basement sediment, and marine sediment (de Almeida et al., 2000; de Brito Neves et al., 2013), which are found across Patagonia (de Almeida et al., 2000; deBrito Neves et al., 2013). A wider array of minerals have been classified in bedrock between the Negro River and Terra del Fuego which overlaps geographically with the samples analysed in this study and include alunite, dickite, pyrophyllite, pyrite, diaspora, rutile and barite (Rosello et al., 2008; Ducart et al., 2006; Marfil and Maiza et al., 2012). This suggested that alluminosilicates, carbonates and felsic minerals were the main materials weathered from bedrock in Patagonia.

The volcanic sample from Cotopaxi consisted of plagioclase minerals in the major phase (Table 2.3). In contrast, the volcanic deposits from Chaiten and Puyehue were characteristically amorphous-rich and contained trace to no plagioclase and quartz (Table 2.3). The mineralogy of the three volcanic areas analysed in this study did not account for the wide array of silicic to mafic volcanic rock found across the Andean volcanic belt. Select previous studies for example suggested that the Andean belt can consist typically of quartz and feldspars in the calc-alkaline volcanic regions in the CVZ (Jakes and White, 1972; Dostal, 1977), plagioclase, pyroxenes, magnetite and amphiboles in the silicic to mafic regions of the SVZ (Grunder, 1987), and adakites in the AVZ (Stern and Kilian, 1996). The mineralogy of the three volcanic areas however may have represented the mineralogy expected in fine particulate volcanic deposits rather than volcanic rock and thus were most likely representative of volcanic aerosol sources. The similar mineralogies identified in volcanic and rural aerosol sources in South America suggested that the volcanic sources were not well distinguished from the rural sources by mineralogy. The variations in mineralogy between the volcanic areas in South America assessed in this study and the previous studies implied that mineralogy was useful to discriminate between different volcanic areas due to variations in magma formation in each volcanic area.

The road dusts from Buenos Aires and the aerosols from São Paulo contained minerals that were not common to the sediment samples from Patagonia and the Andes (Table 2.3). These included muscovite in Buenos Aires, and gypsum, halite, lepidocrocite (iron oxide), and mohrite (sulfate) in São Paulo (Table 2.3). These minerals largely reflect the volcano-sedimentary geology exposed along the eastern section of the South American Platform due to the Brasilia/Pan African extension, which typically host chlorides, evaporites and ferric oxides within the surrounding silicic to mafic volcanic rock, basement sediment and marine sediment (e.g. de Almeida et al., 2000; de Brito Neves et al., 2013). The iron oxides may have also indicated rusting of metals, while calcite, clay minerals and sulfate minerals are typically used in construction materials. These minerals may therefore be indicative of South American anthropogenic sources. The major phases of salts in the urban sources were useful for discriminating the major South American urban sources from major South American rural and volcanic sources (Table 2.3).

The rural, urban and mine samples from Southern Africa were not sediments and thus were not measured for mineralogy. However, previously published data were assessed. The Archean/Neoproterozoic shield underlying geology of Johannesburg, and parts of Namibia and the Kalahari are formed of granitoids and greenschists, amphibolites, quartzites, lavas and dolomites. These formations consist of quartz, feldspars, amphiboles, calcium/magnesium carbonates, and mafic minerals such as chlorite, epidote, olivines, pyroxenes, and melilite (Condie and Hunter, 1976; Le Roex et al., 2003; Monna et al., 2006; Tohver et al., 2006; Begg, et al., 2009). The geology along the Cape Fold Belt constitute mafic to ultramafic volcanic rock consisting of minerals such as pyroxenes rich in Cr, Mn, Ni and Co (Janney et al., 2002) while meta-sedimentary covers along the west coast of Namibia and southern coast of South Africa consist primarily of clays, carbonates, quartz, and mafic to ultramafic minerals rich in Ca, Fe and Mg (Le Roex and Lanyon, 1998; Ewart et al., 2004; Tohver et al., 2006; Begg, et al., 2009). These studies implied that the characteristically more mafic mineralogy across Southern Africa than South America may be useful to distinguish the two source areas.

2.3.2. Major element enrichment

The major element concentrations are listed in Table 2.4 and illustrated as element enrichment relative to the upper continental crust in Figure 2.2.

The major South American rural sources (top soils and riverbed sediment samples from Patagonia) revealed enrichment factors generally ranging from 1 to 2 relative to the continental crust (Fig. 2.2A). Variations in major element enrichment were accountable by the sample mineralogy. Slight depletions in enrichment factor in CaO, K_2O and Na_2O relative to the continental crust (as low as 0.2, Fig. 2.2A) were in line with the absence of major Ca- or alkali-bearing minerals such as calcite, and alkali feldspars (Table 2.3). One sample (sample 4, Fig. 2.2A) showed enrichment in CaO, MgO and MnO relative to the crust of 20, 6 and 5, respectively (Fig. 2.2A) and were due to the major phases of Ca-

bearing calcite and aragonite, and clays (which are typically Mg- and Mn-bearing) in this sample (Table 2.3). These characteristic major element compositions were similar to previously analysed dust and top soils from Patagonia which revealed enrichment factors ranging from 0.5 to 2 relative to the crust for Fe_2O_3, K_2O, MgO and NaO, and 0.5 to 5 in CaO, and up to 20 in MnO (Gaiero et al., 2003; Fig. 2.2A). This suggested that major element enrichment composition reflected the mineralogy of the rural sources from Patagonia.

The South American volcanic samples (tephra and clast deposit samples along the Andes) revealed enrichment factors ranging from 0.2 to 4 relative to the continental crust (Fig. 2.2B). CaO, Fe_2O_3 and MgO were slightly depleted in the Chaiten volcanic area relative to the crust (enrichment factor ranging 0.2 to 0.4, Fig. 2.2B), and the Puyehue volcanic area was similarly depleted in CaO and MgO (Fig. 2.2.B). This reflected their glassy composition and absence of major phases of plagioclase feldspars or clays (Table 2.3). The Cotopaxi volcanic area was slightly depleted in K_2O (enrichment factor of 0.5) and slightly enriched in MgO (enrichment factor of 2) relative to the continental crust (Fig. 2.2B). This reflected the presence of major phases of plagioclase (which are Ca- and Na-bearing rather than alkali feldspars which are predominantly K-bearing) and presence of clays (Table 2.3). The differences in major element composition between the volcanic samples were in line with different volcanic sources (Fig. 2.2B). Similar to the sample from Cotopaxi, volcanic sources in the CVZ to SVZ revealed that these sources were also characteristic of depletion in K_2O as low as an enrichment factor of 0.08 and enrichment in MgO up to 5 relative to the crust (GEOROC et al., 2003-2011, Fig. 2.2B). Volcanic sources in the SVZ to AVZ were also in line with the volcanic samples exhibiting major enrichment factors between 0.08 and 2 (Gaiero et al., 2003; GEOROC et al., 2003-2011, Fig. 2.2B). These differences reflected the different mineralogy within these sources, as expressed in Section 2.3.1. Thus, major element enrichment patterns were useful for distinguishing volcanic areas from one another, but due to similar enrichment profile patterns and similar enrichment factors, were not useful for discriminating South American rural sources from volcanic sources.

The road dusts from Buenos Aires (50-100μm particle size, Fig. 2.2C) revealed slight enrichments in CaO, Fe_2O_3 and MgO (enrichment factor up to 2, 5 and 2, respectively) and reflected the presence of calcite and clays in these samples (Table 2.3). CaO enrichment factors ranged from 0.2 to 3 in aerosols from São Paulo (Fig. 2.2C). This was dependent on the presence or absence of Ca-bearing gypsum as a major or minor phase mineral in the samples from São Paulo (Table 2.3). Enrichments relative to the continental crust were up to 5 in Fe_2O_3, up to 3 in K_2O and MgO, up to 10 in MnO and up to 8 in NaO in the samples from São Paulo (Fig. 2.2C). Iron enrichments reflected the presence of major phase minerals iron oxides, and Fe-bearing mohrite and actinolite, in the samples from São Paulo (Table 2.3). NaO, K_2O, MgO and MnO enrichments were due to the presence of halite and clays (Table 2.3). Chin et al. (2009) proposed that biomass burning was a major aerosol source from South America (determined from atmospheric modeling using GOCART). Potassium is a tracer for biomass burning and despite this proposal, the non-enriched levels of K revealed that biomass burning was an unlikely main

anthropogenic contribution to aerosols emitted from South America. The Fe_2O_3, MgO and MnO element compositions in previously analysed road dusts from Buenos Aires ranging in grain size between >0 to 100μm were within the enrichment factor values of samples from São Paulo and Buenos Aires for Mg and Mn (enrichment factors between 0.7 and 10; Fujiwara et al., 2011, Fig. 2.2C). Additionally the major element enrichment patterns of the road dust and aerosols were in line with those of local rocks in and around Buenos Aires and São Paulo, in particular those with a lamprophyre geology (which showed major element enrichment factors between 0.2 and 5, soils and sandstones, Bertolo et al., 2011; diabases and lamprophyres, de Campos, 2012; diorites, carbonatite, magnetite, apatitite and lamprophyres, Guarino et al., 2012, Fig. 2.2C). This suggested that the major element enrichment patterns in road dusts and aerosols collected in these urban areas were accounted for by natural sources. These urban areas were therefore not well distinguished from one another or from the major rural or volcanic sources from South America by their major element composition.

Enrichment factors in Fe_2O_3 and K_2O in rural, urban and mine sources from Southern Africa (aerosols from Johannesburg) were similar to the composition of the continental crust (Fig. 2.2D). The rural, urban and mine sources were depleted in NaO relative to the continent crust (down to 0.07, Fig. 2.2D). The rural and mine sources exhibited similar enrichments in CaO and MgO (enrichment factor of ~50 and 2, respectively, Fig. 2.2D), which were higher than in the urban sources (enrichment factor of up to 9 and 1, respectively, Fig. 2.2D). MnO was higher in the mine source (enrichment of 80 relative to the crust, Fig. 2.2D) than the rural source (enrichment of 6 relative to the crust, Fig. 2.2D), and higher in both these sources than the urban sources (enrichment of ~2 relative to the crust, Fig. 2.2D). The rural, urban and mine sources from Southern Africa overlay major element compositions that were found in rocks of the Kaapvaal Craton formation and Archean/Neoproterozoic shield (~0.1-400, Fig. 2.2D), which includes the Barberton greenstone belt and the eastern granitic Kaapvaal Craton east of Johannesburg (Condie and Hunter, 1976), and kimberlitic formations in Kimberley, SW of Johannesburg (Le Roex et al., 2003). The Barberton Region and Kaapvaal Craton revealed a major element profile similar to the continental crust (Condie and Hunter, 1976, Fig. 2.2D). The kimberlites represent mafic and ultramafic bodies typical of the Archean/Neoproterozoic shield from Southern Africa (e.g. Janney et al., 2002; Tohver et al., 2006; Begg, et al., 2009). Kimberlites exhibited high CaO, MgO and MnO, and depleted levels of NaO relative to the crust (enrichment factors of ~20 to 40, ~90 to 400, ~10 to 50, and ~0.2 to 0.3, respectively, Le Roex, 2003, Fig. 2.2D), which reflect the mafic and NaO depleted nature of the Archean/Neoproterozoic shield (Tohver et al., 2006; Begg, et al., 2009). The major element enrichments of the rural, urban and mine samples from Johannesburg most likely reflected mineral dust derived from a mixture of rock formations from the Archean/Neoproterozoic shield as this could explain the similar composition to the crust with the exception of high MnO and depleted NaO in all the samples. Although not analysed in this study, rural sources from Namibia (lamprophyres and carbonatites from Damaraland, northern Namibia, Le Roex and Lanyon, 1998), and volcanic sources from Namibia (mafic lavas in Etendeka, northern Namibia, Ewart et al., 2004) and South Africa (mafic lavas and melilitites from Cape Province along

southern South Africa, Janney et al., 2002) were included in Fig. 2.2D. The rural sources from Namibia were in line with the rural sources from the Archean/Neoproterozoic shield (Condie and Hunter, 1976) except for enriched MnO levels similar to kimberlites (Le Roex et al., 2003). The volcanic sources from Namibia and South Africa suggested that these sources have a similar major element profile pattern to one another, which are enriched in CaO, Fe_2O_3, MgO, and MnO compared to the crust, except for higher enrichment in MgO in the Cape Province than the Etendeka (enrichment factor range of ~3 to 20 in the Cape Province, Janney et al., 2002; while ~2 to 3 in the Etendeka, Ewart et al., 2004, Fig. 2.2D). The absence in K_2O enrichment further indicated that biomass burning was not a main source of anthropogenic aerosols emitted from Southern Africa, as proposed by Chin et al. (2009). The different major element enrichment profiles shown in different rural and volcanic sources from Southern Africa (Fig. 2.2D) suggested that major element profiles were useful for distinguishing between select rural and volcanic sources in Southern Africa. Aside from the major element enrichment patterns of kimberlites, there were no significant differences between the rural and volcanic sources (this study, Condie and Hunter, 1976; Le Roex nd Lanyon, 1998; Janney et al., 2002; Le Roex et al., 2003; Ewart et al., 2004) and the urban sources from Johannesburg (Fig. 2.2D). This suggested that major element profiles were not useful to discriminate urban from all rural and volcanic sources from Southern Africa. The one sample from a rural and mine source however were not enough to represent the entire major element composition of aerosols from Johannesburg, nor Southern Africa, but they give some indication of aerosol composition from a rural and mine source from Johannesburg.

2.3.3. Rare earth element enrichment and ratios

The rare earth element concentrations are listed in Table 2.5 and illustrated as element enrichments relative to the continental crust in Figure 2.3.

The samples from major South American rural sources revealed a REE profile of a slight enrichment in HREE (La/Yb ratios between 7.5 and 18; Fig. 2.3A), positive Eu-anomalies (Eu* up to 1.47, Fig. 2.3A) and enrichment values ranging from 0.2 to 3 relative to the continental crust (Fig. 2.3A). This reflected LREE removal during weathering of source rocks (Gaiero et al., 2004), indicated by the presence of major phases of clays in these samples (Table 2.3). Positive Eu-anomalies were due to the presence of plagioclase, which were also a major phase in these samples (Table 2.3). The REE enrichment patterns revealed a wider range and higher Eu* values than previous REE enrichment of topsoils and dust from Patagonia (enrichment factor 0.5 to 0.6, positive Eu* of 1.16 to 1.68 and La/Yb ratio of 8.36 to 11.0; Gaiero et al., 2004, Fig. 2.3A). This suggested that the topsoils and riverbed samples from this study were more weathered than the previous analysis of Gaiero et al. (2004).

The REE profiles of three volcanic sources, Chaiten, Cotopaxi, and Puyehue, differed to each other (Fig. 2.3B). Volcanic tephra from Chaiten and Cotopaxi showed flat REE enrichment relative to the continental crust profiles and enrichment factors from 0.4 to 1, while samples from Puyehue revealed

enrichment in HREE (La/Yb ratios of 5.1 to 18.7) and enrichment factors between 1 and 3, relative to the crust (Fig. 2.3B). The sample from Cotopaxi showed a positive Eu-anomaly (Eu* = 1.09). Varying REE profile patterns indicated dissimilar differentiation of magmas during formation, which results in different mineralogies. This was in line with the different characteristic mineralogies identified in the volcanic source samples (Table 2.3). In particular, the positive Eu-anomaly was due to the large abundance of anorthite in the sample from Cotopaxi (Table 2.3). Variations in REE enrichment patterns were also found between other volcanic sources and were also due to variable mineralogies between sources (GEOROC, 2003-2011, Fig. 2.3B). The previously studied REE profiles in the central volcanic zone to SVZ (basaltic andesite to rhyolite lava and rhyolitic tuffs) showed enrichment factors between 0.4 and 2 relative to the crust, flat to enriched HREE with La/Yb ratios ranging from 7.1 to 14.6, and a range of negative to positive Eu-anomalies (Eu* = 0.49-1.65) reflecting relatively low to high plagioclase content (GEOROC, 2003-2011, Fig. 2.3B). The Southern volcanic zone to AVZ back-arc silicic lavas showed enrichment factors between 0.4 and 3, La/Yb ratios of 7.2 to 28.7 and a positive Eu-anomaly (Eu* = 1.42-3.22) reflecting the presence of plagioclase (GEOROC, 2003-2011, Fig. 2.3B). The varying REE enrichment profiles between different volcanic sources suggested that REE enrichment profiles were a useful tool for discriminating between different volcanic areas. The general range in REE enrichments however overlapped with the South American rural areas (Fig. 2.3A and B), which showed that REE enrichments were not useful for distinguishing between South American rural and volcanic sources.

The urban sources in South America revealed LREE-enrichment relative to HREE and slight enrichment relative to the continental crust particularly in the LREEs (Fig. 2.3C). This was particularly true for samples from São Paulo (La/Yb ratios between 94.7 and 112, enrichment factor of La between 5 and 10, Fig. 2.3C) and less pronounced in samples from Buenos Aires (La/Yb ratios between 16.0 to 29.1, enrichment factor of La between 1 and 3, Fig. 2.3C). This was most likely due to the underlying volcano meta-sedimentary geology at Buenos Aires and São Paulo, as LREE enrichment is typical of rock formations such as lamprophyres, and calk-alkaline formations that are associated with the orogenic activity which formed the Brasiliano/Pan African series (La Roex and Lanyon, 1998; Prevec, 2004). These REE enrichment patterns therefore showed some agreement with the mineralogy (calcite and kaolinite) identified in the samples (Table 2.3). Except for the La-Ce values from the aerosols from São Paulo, the REE enrichment factors were within the range of REE enrichment factors (between 0.8 and 4) of previously analysed rock formations from rural areas along southern Brazil, near Buenos Aires (de Campos, 2012), and near São Paulo (Guarino et al., 2012). The samples from Buenos Aires and São Paulo best fit the LREE enrichment (La/Yb = 10.8) and absence of a Eu-anomaly of the lamprophyre formations previously studied (Guarino et al., 2012, Fig. 2.3C). This suggested that mineral dust in Buenos Aires and São Paulo primarily derived from lamprophyre-rich formations. The elevated La-Ce in São Paulo indicated that there may have been anthropogenic enrichment. LREE rich emissions derive from components such as catalytic converters, ceramics, motor vehicles, glass, and polishing compounds (Humphries, 2013). These may relate to the iron-oxide phases in the aerosol samples from São Paulo

(Table 2.3). The different REE profile patterns in the urban sources from rural and volcanic sources were useful for distinguishing these sources by their REE enrichment profiles.

The Southern African urban sources displayed flat REE profile patterns and were similarly enriched to samples from Buenos Aires (enrichment factor 1.5 to 3; Fig. 2.3D). The rural and mine sources from Southern Africa showed a similar range in enrichment factor to one another and the samples from São Paulo, and exhibited LREE enrichment (La/Yb ratios of 31.4 and 27.2, respectively; Fig. 2.3D). This most likely reflected the similar underlying Archean/Neoproterozoic geology of the analysed urban sources in South America and Southern Africa (de Almeida et al., 2000; Britos Neves et al., 2013; grey shading (b) in Fig. 2.1). Previously analysed rural sources from the Kaapvaal Craton and Archean/Neoproterozoic shield include lamprophyre and calk-alkaline formations similarly found in Archean/Neoproterozoic shield formations in South America (Condie and Hunter et al., 1976; Le Roex and Lanyon, 1998; Le Roex et al., 2003). They showed a range in enrichment patterns from LREE enrichment (La/Yb = 9.1 to 206) and La enrichment up to ~200 relative to the continental crust, to an enrichment composition similar to the crust except for a positive Eu-anomaly (Eu* = 0.59 to 2.27) (Condie and Hunter, 1976; Le Roex et al., 2003; Fig. 2.3D). These studies suggested that the REE profiles of rural and mine samples from Johannesburg were in line with the REE profiles of different rock formations across the Archean/Neoproterozoic shield and suggested that the REE profile in the aerosols from Johannesburg are associated with mineral dust from a mixture of different rock formations from the Archean/Neoproterozoic shield. The flat REE profile in the urban samples implied that rural sources did not account for the REE composition in the aerosols from the urban source from Southern Africa. This may have been due to anthropogenic sources of aerosols, which were dissimilar to the anthropogenic sources that may account for the LREE enrichments exhibited in the South American urban sources.

Rare earth element enrichment relative to the continental crust for rural sources from Namibia (lamprophyres and carbonatites from Damaraland, northern Namibia, Le Roex and Lanyon, 1998) and volcanic sources from Namibia (mafic lavas in Etendeka, northern Namibia, Ewart et al., 2004) and South Africa (Cape Province along southern South Africa, Janney et al., 2002) were assessed in this study and are shown in Fig. 2.3D. They showed overlying ranges in enrichment factor relative to the continental crust and strong positive Eu-anomalies (Eu* = 1.26 to 8.43; Le Roex and Lanyon, 1998; Janney et al., 2002; Ewart et al., 2004), but suggested distinguishable REE enrichment profile patterns from one another (Fig. 2.3D). The rural sources from Namibia were characterised by a large range in enrichment factors (La enrichment factors between 1 and 200) and a slight LREE enrichment (La/Yb = 28.1 to 118) (Le Roex and Lanyon, 1998). The volcanic sources from Namibia were characterised by a range in enrichment factors between ~0.5 and 2 in La relative to the crust and HREE enrichment (La/Yb = 3.20 to 17.0) (Ewart et al., 2004). Lastly the volcanic sources from South Africa were distinguished by a range in enrichment factors of ~2 to 3 in La, LREE to HREE enrichment (La/Yb = 30.9 to 51.0), and a Lu composition similar to the crust or depleted (enrichment factors between ~0.5 and 1) (Janney et al., 2002). These previous studies of rural and volcanic sources in comparison to the rural, urban and mine sources

from this study suggested that the Southern African urban sources were distinguishable from the Southern African rural, volcanic and mine sources by REE enrichment patterns. They further revealed that select rural and volcanic sources within Southern Africa were distinguishable by REE enrichment patterns.

2.3.4. Trace element enrichments

The trace element concentrations are listed in Table 2.5 and illustrated as element enrichment patterns in Figure 2.4.

The major South American rural sources exhibited enrichment factors from 0.2 to 3 relative to the continental crust (Fig. 2.4A). This was within the range of previously published data for Patagonian soils and dust (enrichment factor between 0.08 and 20, Gaiero et al., 2003; Fig. 2.4A), and indicated that the trace element enrichment factors reflected the mineralogy in the samples.

Except for Cr and Ni, the enrichment factors of trace elements in volcanic sources from South America ranged from 0.01 to 3 (Fig. 2.4B). Samples from Puyehue and Chaiten (in the SVZ) showed depletion in Cr and Ni relative to the crust (enrichment factor of 0.01 to 0.06, Fig. 2.4B), while Cotopaxi (in the NVZ) showed enrichment in Cr and Ni (factor ranging 6 to 10, Fig. 2.4B). Similar variations in trace element enrichment factors in the volcanic sources were found in previously published data for the CVZ to AVZ (enrichment of 0.1 to 10; GEOROC, 2003-2011; Fig. 2.4B). In particular, Ni enrichment factors in the volcanic sources were similar to previously published data for volcanic rock from SVZ to the AVZ (enrichment factor between 0.7 and 7, GEOROC, 2003-2011). The differences in Cr and Ni composition between volcanic sources most likely reflected the different fractionation of magmas between silicic (Cr and Ni depleted) to mafic (Cr and Ni enriched) composition (GEOROC, 2003-2011). This was in line with the abundance of acid-rich glassy minerals and quartz in the samples from Puyehue and Chaiten, and Cr and Ni-enriched basic minerals in association with the plagioclase-rich deposit from Cotopaxi (Table 2.3). These elements were useful to distinguish between different volcanic sources, and distinguish select rural from volcanic sources from South America.

The South American urban sources were 10 to 1000 times enriched in Cu, Pb, Cd and Zn, and between 1 and 100 times in Cr and Ni relative to the South American natural sources and to the continental crust (Fig. 2.4C). Except for Cd, previously published data for Cu, Pb, Zn, Ni and Co from Buenos Aires (road dusts from >0 to 100 μm, Fujiwara et al., 2011) agreed well with the aerosols from São Paulo. This suggested that these two urban sources were not distinguishable by the enrichment factors of these trace elements (Fig. 2.4C). Fujiwara et al. (2011) showed depletion in Cd of 0.5 to 5 in road dusts for Buenos Aires (Fig. 2.4C) and implied that this study expanded the range of Cd enrichment factors exhibited in Buenos Aires source samples to 0.5 to 50 (Fig. 2.4C). This was lower than the Cd enrichment observed in the samples from São Paulo (1000 to 5000) and suggested that the urban sources were discriminated by Cd enrichment factors (Fig. 2.4C). Such a significant difference in enrichment factors between the urban sources and rural and volcanic sources from South America proposed that trace

elements Cu, Pb, Cd, Zn, Cr and Ni were useful for distinguishing these sources. Despite these differences, the trace element composition of the road dusts from Buenos Aires were in line with rural sources (diabase and lamprophyre-rich formations) from around Buenos Aires, which revealed that enrichment factors of Cu, Zn, V, Y were within 1 to 4, Cr within 0.7 to 10, Ni, Co within 1 and 10, and Th within 0.05 and 3 (Bertolo et al., 2011; de Campos et al., 2012, Fig. 2.4C). Although this implied that mineral dust accounted for the elevated enrichment in Cu, Pb, Cd, Zn and Cr relative to the crust, the minerals identified in the road dust from this study (primarily quartz, plagioclase and calcite, Table 2.3), aside from kaolinite and muscovite, were not typically enriched in mafic metals and therefore did not account for all the trace element contribution. Previously analysed rural sources (volcano meta-sediment formations) from around São Paulo were in line with the trace element composition of the aerosols from São Paulo, except for lower enrichment ranges in Zn and Cr, and higher enrichment ranges in V and Sc, in the rural sources (enrichment ranging from 3 to 40 in Zn, 2 to 20 in Cr, 3 to 400 in V, and 2 to 40 in Sc; Guarino et al., 2003, Fig. 2.4C). To the knowledge of this study, there were no previous data in Cd from studies of rural sources around Buenos Aires and São Paulo. Nonetheless the higher Zn and Cr, and possibly higher Cd enrichments in the aerosols from São Paulo than in the rural sources around São Paulo (as suggested from aerosols from São Paulo, this study) have suggested that rural sources did not contribute to the total Zn, Cr and Cd in aerosols from São Paulo. This was in line with the absence of mafic enriched mineralogy, except for Fe- and sulfate-rich minerals, identified in the aerosols from São Paulo (Table 2.3). Given the proximity to human activities, it was likely that the aerosols received an anthropogenic contribution of Zn, Cr and Cd in São Paulo, which were useful for distinguishing the São Paulo urban source from natural sources (from around São Paulo, Buenos Aires and Patagonia) and to a lesser extent from the Buenos Aires urban source (Cr and Cd only) (Fig. 2.4A-C). As these trace elements are typically coupled with other trace elements from anthropogenic sources, such as Cu and Pb are commonly correlated to Zn sources, and Ni and Co with Cr, and V with Cd (Pacyna et al., 2001), it could not be ruled out that other trace element compositions in samples from urban sources from South America may be, at least, partially controlled by anthropogenic sources of aerosols. Copper, Pb, Cd, Zn, Cr and Ni from South America were reported to derive from industrial processes, non-ferrous metal processing, smelting, waste incineration, biomass burning, coal burning, and oil combustion (e.g. Nriagu, 1988; Bollhofer and Rosman, 2000; Pacyna et al., 2001; Ulke and Andrade, 2001). Cadmium and V are predominantly from oil combustion (Pacyna et al., 2001), and the higher enrichment of Cd and V in São Paulo than Buenos Aires indicated that oil combustion played a larger role in aerosol emissions in São Paulo. Potentially higher Cr levels in São Paulo than Buenos Aires suggested higher metal and mining processing of chromite and mafic to ultramafic sediments (rich in Cr).

The rural, urban and mine sources in Southern Africa showed similar enrichment factors (ranging between 1 and 100) in trace element composition to Buenos Aires, except Cr which was 100 times more enriched in the Southern African sources relative to Buenos Aires (Fig. 2.4D). This was useful to discriminate South American urban sources from Southern African sources. The rural, urban and mine

sources from Southern Africa however were not well distinguished from one another by trace element profile patterns (Fig. 2.4D). This was reflected in previous studies of rural, urban, mine, and coal sites in Johannesburg; overlapping enrichment factors in trace elements with one another, Monna et al., 2006, and with aerosols from Johannesburg from this study, except in Cd (Fig. 2.4D). Cadmium in rural and urban source areas from published data were lower (factor of 0.1 to 1, Monna et al., 2006) than Cd enrichments measured in this study (factor of 10 to 100) and suggested that this study expands the range of Cd enrichments exhibited in rural and urban source areas from Southern Africa (Fig. 2.4D). The similar trace element enrichment factors in this and Monna's study most likely reflected the limited sample locations, which were all from Johannesburg, as previous studies of difference rural and volcanic sources across Southern Africa have shown different trace element profiles (Le Roex et al., 2003; Janney et al., 2002; Ewart et al., 2004; Le Roex and Lanyon, 1998). Previously published trace element data from rural areas of the Kaapvaal Craton and Archean/Neoproterozoic shield suggested that these regions have trace element profiles ranging from Pb, Sc, Y and Th enrichments similar to the crust with Cr enrichment of ~50 relative to the crust (regions near Johannesburg, Condie and Hunter, 1976, Fig. 2.4D), to enriched levels in Cu, Zn, V, Sc, Y and Th, and very enriched levels in Cr Ni and Co relative to the crust (regions in Kimberley, SW of Johannesburg, Le Roex et al., 2003, Fig. 2.4D). These profiles reflected the geology of the Archean/Neoproterozoic shield, which have been influenced by crustal mixing or reflect the mafic to ultramafic (heavy metal-rich) formations found across the shield, respectively (e.g. Condie and Hunter, 1976; Le Roex et al., 2003; Tohver et al., 2006; Begg, et al., 2009). The rural, urban and mine sources from this study were within the range of trace element compositions from these rural sources from Southern Africa (Fig. 2.4D). Similar to the major element enrichment profiles, it was most likely that the trace element enrichment profiles in the rural, urban and mine sources from Johannesburg reflected a mixture of mineral dust from different rock formations from the Archean/Neoproterozoic shield encompassing Johannesburg. These previous studies suggested that Pb composition was similar to the crust in the Kaapvaal Craton and Archean/Neoproterozoic shield (Condie and Hunter, 1976; Le Roex et al., 2003, Fig. 2.4D). They further implied that the enriched Pb (enrichment factor between 10 and 70) in the rural, urban and mine sources from this study and Monna's study (Pb enrichment factor between 10 and 300, Monna et al., 2006) were not accounted for by natural sources from Southern Africa. Due to the collecting date of these aerosols, before the lead-ban in South Africa, it is likely that the Pb in these aerosols primarily originated from anthropogenic sources such as leaded gasoline, as acknowledged by Bollhofer and Rosman, 2000 and Monna et al., 2006. Although Cr composition in the rural, urban and mine sources from this study may have derived from rural sources around Johannesburg, it could not be ruled out that aerosols within Johannesburg were influenced by emissions from Cr mining and metal processing in South Africa, as it is the largest producer of chrome in the world (Papp, 2007). These comparisons showed that Pb and Cr were useful to discriminate between natural and anthropogenic sources in Southern Africa.

Rural (Damaraland, Le Roex and Lanyon, 1998) and volcanic sources (Etendeka, Ewart et al., 2004) from Namibia, and volcanic sources from South Africa (Cape Province, Janney et al., 2002) showed similar ranges in trace element enrichment profiles (Fig. 2.4D). The trace element enrichment factors ranged in compositions similar to the crust except for a depletion in Pb, Ni and Sc (depletions as low as ~0.1, ~0.5 and ~0.2, respectively, Le Roex and Lanyon, 1998; Ewart et al., 2004, Fig. 2.4D), to enriched levels up to ~20 in Cu, Cr and Ni, up to ~5 in Co, V and Sc, and depleted as low as ~0.1 in Th, relative to the crust (Ewart et al., 2004; and similarly in the Cape Province, except there was no Cu data to compare, Janney et al., 2002). This assessment of previous natural sources suggested that, although different to the rural, urban and mine trace element profiles, the different volcanic sources from Southern Africa were not well distinguished by their trace element enrichment profiles, while select rural sources were.

Table 2.3. Mineralogy for select aerosol sources from South America and Southern Africa.

Sample ID	Source Location	Major Phases (>10%)	Minor Phases (<10%)
South America			
Rural – Topsoil, Bed sediment (bulk)			
4	Bahia San Sebastian, Southern Patagonia	Quartz – Aragonite – Calcite – Albite – Montmorillonite	
15	Rio Grande, Southern Patagonia	Quartz – Albite	Illite – Actinolite – Kaolinite – Clinoclore
17	Rio Grande, Southern Patagonia	Quartz	Albite – Clinoclore – Illite
19	Rio Gallegos, Southern Patagonia	Quartz – Montmorillonite	Albite – Illite
32	Rio Santa Cruz, El Calafate, Southern Patagonia	Quartz – Albite	Clinoclore – Anorthite – Actinolite
40	Punta Arenas, Southern Patagonia	Quartz – Albite – Montmorilonite	Clinoclore – Actinolite – Kaolinite
42	Punta Arenas, Southern Patagonia	Quartz – Albite – Montmorillonite (bentonite)	Anorthite – Clinoclore – Actonilite
Volcanic – Volcanic clasts and tephra (bulk)			
CO	Cotopaxi Volcano, Northern Volcanic Zone	Anorthite	Illite – Montmorillonite
CH	Chaiten Volcano, Southern Volcanic Zone	Amorphous/volcanic glass	Quartz – Opal – Albite
PU2	Puyehue Volcano, Southern Volcanic Zone	Amorphous/volcanic glass	Anorthoclase
Urban – Road dusts (50-100µm), Aerosols (<10µm)			
3C	Urban Area, Buenos Aires	Quartz – Anorthite	Calcite – Muscovite – Kaolinite
112C	Urban Area, Buenos Aires	Quartz – Anorthite	Calcite – Muscovite - Kaolinite
631	Urban Area, São Paulo	Halite – Gypsum	Illite – Kaolinite – Quartz – Lepidocrocite
660	Urban Area, São Paulo	Mohrite – Quartz - Illite	Illite – Kaolinite – Gypsum – Albite
665	Urban Area, São Paulo	Illite	Kaolinite – Montmorillonite – Gypsum – Actinolite

Table 2.4. Major element concentrations of major aerosol sources from South America and Southern Africa, in % (w/w).

Sample ID	Sample Location	Al_2O_3	CaO	Fe_2O_3	K_2O	MgO	MnO	Na_2O
South America								
Rural – Topsoil, Bed sediment (bulk)								
4	Bahia San Sebastian, Southern Patagonia	4.66	26.8	1.93	0.878	3.76	0.112	1.51
5	Bahia San Sebastian, Southern Patagonia	11.6	1.80	4.41	1.92	2.76	0.115	3.31
8	Bahia San Sebastian, Southern Patagonia	12.8	1.72	5.63	2.23	2.49	0.127	3.46
9	Bahia San Sebastian, Southern Patagonia	12.3	2.31	5.17	2.15	2.49	0.139	3.73
10	Bahia San Sebastian, Southern Patagonia	11.5	1.72	5.21	2.02	2.22	0.126	3.05
11	Bahia San Sebastian, Southern Patagonia	11.3	2.14	4.95	2.00	2.81	0.113	2.93
12	Bahia San Sebastian, Southern Patagonia	11.8	1.85	4.55	1.78	1.68	0.096	3.12
19	Rio Gallegos, Southern Patagonia	13.2	1.96	5.22	1.43	1.25	0.048	2.28
21	Rio Gallegos, Southern Patagonia	12.9	3.90	5.55	1.17	1.97	0.131	2.71
35	Rio Santa Cruz, Southern Patagonia	14.1	3.31	4.70	1.65	1.65	0.114	3.02
40	Punta Arenas, Southern Patagonia	14.5	3.84	4.96	0.883	2.85	0.081	2.43
42	Punta Arenas, Southern Patagonia	15.8	1.16	6.01	0.861	1.27	0.048	1.39
1	Rio Grande, Southern Patagonia	13.0	2.22	4.93	1.73	1.64	0.084	2.75
2	Rio Grande, Southern Patagonia	13.4	2.47	5.08	1.89	1.84	0.067	2.83
13	Rio Grande, Southern Patagonia	11.9	1.52	4.71	1.76	1.47	0.049	2.57
15	Rio Grande, Southern Patagonia	12.5	2.80	3.93	1.61	1.77	0.077	4.64
17	Rio Grande, Southern Patagonia	10.6	2.90	3.75	1.22	1.52	0.104	4.17
24	Rio Grande, Southern Patagonia	11.9	2.58	3.79	1.65	1.36	0.079	3.49
27	Bahia Grande, Southern Patagonia	9.68	2.54	3.01	1.13	1.26	0.072	2.55
28	Bahia Grande, Southern Patagonia	12.0	3.01	4.51	1.65	2.05	0.101	2.83
30	Rio Santa Cruz, El Calafate, Southern Patagonia	13.0	2.20	4.20	1.61	1.17	0.046	2.43
32	Rio Santa Cruz, El Calafate, Southern Patagonia	7.32	1.38	2.34	1.00	0.623	0.030	1.57
33	Rio Santa Cruz, El Calafate, Southern Patagonia	11.8	2.25	4.16	1.72	1.36	0.064	2.84
38	Argentino Lake, El Calafate, Southern Patagonia	11.6	2.52	4.73	1.37	1.35	0.087	1.82
Volcanic – Volcanic clasts and tephra (bulk)								
CH	Chaiten Volcano, Southern Volcanic Zone	13.5	1.44	1.43	3.07	0.289	0.225	4.05
PU1	Puyehue Volcano, Southern Volcanic Zone	13.8	2.03	4.42	2.83	0.584	0.454	5.99
PU2	Puyehue Volcano, Southern Volcanic Zone	13.3	1.99	4.15	2.82	0.568	0.442	5.66

Table 2.4. *continued.*

Sample ID	Sample Location	Al_2O_3	CaO	Fe_2O_3	K_2O	MgO	MnO	Na_2O
Volcanic – Volcanic clasts and tephra (bulk)								
PU3	Puyehue Volcano, lakeside near La Angostura	11.9	1.91	2.75	2.81	0.500	0.389	4.54
CO	Cotopaxi Volcano, Northern Volcanic Zone	18.2	7.00	8.64	1.52	5.116	0.125	4.63
Urban – Road dusts (50-100µm), Aerosols (<10µm)								
3C	Urban Area, Buenos Aires	11.3	3.28	4.10	2.17	1.16	0.073	2.37
9C	Urban Area, Buenos Aires	10.9	4.74	5.93	2.10	1.39	0.094	2.32
110C	Urban Area, Buenos Aires	10.2	4.51	5.97	1.86	1.10	0.086	2.15
112C	Urban Area, Buenos Aires	9.47	4.79	6.01	1.99	1.18	0.092	1.96
3D	Urban Area, Buenos Aires	9.95	3.23	4.13	2.28	1.20	0.066	2.02
9D	Urban Area, Buenos Aires	9.66	4.41	4.84	2.17	1.28	0.077	2.05
110D	Urban Area, Buenos Aires	8.53	4.16	6.04	1.75	1.01	0.085	1.79
112D	Urban Area, Buenos Aires	10.11	4.63	5.42	1.89	1.13	0.080	2.09
648	Urban Area, São Paulo	0.543	0.028	0.658	0.276	0.116	0.018	0.526
649	Urban Area, São Paulo	0.219	0.157	0.263	n.d.	n.d.	0.010	0.173
650	Urban Area, São Paulo	0.441	0.020	0.483	0.214	0.116	0.014	0.736
Southern Africa								
Rural – Aerosol, shelf sediment (bulk)								
PICA	Rural Area, Johannesburg	0.530	7.21	0.329	0.366	0.164	0.015	0.019
ST0	Sea-Shelf off Cape Town	4.21	11.7	15.4	7.42	3.78	0.004	0.790
ST1	Sea-Shelf off Cape Town	5.45	n.d.	2.33	1.22	1.06	0.047	1.94
ST3	Sea-Shelf off Cape Town	6.92	7.39	2.25	1.66	0.767	0.064	1.95
ST6	Sea-Shelf off Cape Town	13.3	5.32	5.54	2.66	2.18	0.372	3.74
ST8	Sea-Shelf off Cape Town	6.11	10.6	1.84	1.51	0.656	0.019	1.79
ST11	Sea-Shelf off Cape Town	14.9	1.12	6.33	2.86	2.52	0.348	4.44
ST13	Sea-Shelf off Cape Town	6.48	n.d.	2.24	1.53	0.973	0.027	2.15
Urban – Aerosols (bulk)								
RIVER	Urban Area, Johannesburg	1.08	0.600	0.526	0.759	0.173	0.013	0.040
DELTA	Urban Area, Johannesburg	1.34	2.98	0.706	0.851	0.206	0.019	0.040
CMG	Urban Area, Johannesburg	1.09	0.642	0.627	0.760	0.130	0.013	0.018
EMMER	Urban Area, Johannesburg	1.61	2.95	0.803	0.577	0.197	0.017	0.033
HUDD	Urban Area, Johannesburg	1.16	0.212	0.634	0.667	0.143	0.016	0.031
BOT2	Urban Area, Johannesburg	1.05	0.129	0.594	0.786	0.153	0.011	0.033
Mine – Aerosols (bulk)								
DRD	Mine Dump Site, Johannesburg	0.312	2.44	0.209	0.066	0.077	0.110	0.027

Table 2.4. *continued.*

South America – rural and volcanic sediment, <5 µm								
4	Bahia San Sebastian, Southern Patagonia	3.55	0.00	1.93	0.614	4.30	0.142	0.660
32	Rio Santa Cruz, El Calafate, Southern Patagonia	22.5	1.41	7.55	2.10	1.57	0.092	0.950
42	Punta Arenas, Southern Patagonia	22.9	0.15	9.07	0.823	1.30	0.053	0.475
CH	Chaiten Volcano, Southern Volcanic Zone	14.4	1.47	1.68	3.72	0.445	0.063	4.31
PU2	Puyehue Volcano, Southern Volcanic Zone	14.1	1.76	3.76	3.46	0.466	0.101	5.27
Reference Material								
USGS								
G-2	**This study (n=12)**	13.65	1.88	2.55	4.41	0.72	0.03	3.86
	RSD (2σ, %)	6.1	9.8	2.5	7.3	8.4	9.3	8.5
USGS								
G-2	**USGS**	15.39	1.96	2.66	4.48	0.75	0.03	4.08
	RSD (2σ, %)	0.3	0.08	0.17	0.13	0.03	0.01	0.13

Results for certified reference material USGS G-2 Granite are reported and compared to the recommended literature value (Gladney et al., 1992; Govindaraju, 1989, 1994). Measurement precision is given as the relative standard deviation (RSD) at the 2σ level (n = 12).

n.d. = not determined

Table 2.5. Rare earth element, Cu, Pb, Cd, Zn, Cr, Ni, Co, Y, Th, V, and Sc concentrations of major aerosol sources from South America and Southern Africa (μg g^{-1}).

Sample ID	Sample Location	La	Ce	Pr	Nd	Sm	Eu	Gd	Tb	Dy	Ho	Er	Tm	Yb	Lu
South America															
Rural – Topsoil, Bed sediment (bulk)															
4	Bahia San Sebastian, Southern Patagonia	7.72	17.8	2.00	8.01	1.66	0.427	1.58	0.248	1.52	0.311	0.898	0.137	0.86	0.133
5	Bahia San Sebastian, Southern Patagonia	20.1	45.2	5.21	21.0	4.52	1.06	4.14	0.653	3.92	0.814	2.29	0.338	2.14	0.329
8	Bahia San Sebastian, Southern Patagonia	22.2	49.9	5.72	23.0	4.96	1.13	4.56	0.715	4.37	0.881	2.59	0.383	2.48	0.374
9	Bahia San Sebastian, Southern Patagonia	21.5	48.3	5.58	22.4	4.74	1.14	4.43	0.705	4.32	0.874	2.54	0.378	2.41	0.368
10	Bahia San Sebastian, Southern Patagonia	21.0	47.0	5.36	21.6	4.55	1.06	4.29	0.669	4.10	0.826	2.34	0.360	2.29	0.356
11	Bahia San Sebastian, Southern Patagonia	20.7	46.5	5.35	21.6	4.60	1.07	4.26	0.666	4.05	0.820	2.38	0.358	2.30	0.350
12	Bahia San Sebastian, Southern Patagonia	21.9	49.1	5.63	22.5	4.86	1.13	4.37	0.689	4.16	0.839	2.43	0.359	2.31	0.353
19	Rio Gallegos, Southern Patagonia	13.3	27.3	2.84	10.5	2.07	0.635	1.66	0.269	1.68	0.357	1.11	0.178	1.21	0.196
21	Rio Gallegos, Southern Patagonia	18.6	40.4	4.62	18.5	3.84	1.09	3.46	0.530	3.18	0.642	1.82	0.275	1.77	0.267
35	Rio Santa Cruz, Southern Patagonia	19.4	43.3	4.81	19.3	4.07	1.10	3.99	0.627	3.90	0.809	2.34	0.359	2.35	0.366
40	Punta Arenas, Southern Patagonia	14.0	27.9	2.97	11.5	2.10	0.794	1.80	0.264	1.56	0.307	0.837	0.125	0.783	0.117
42	Punta Arenas, Southern Patagonia	7.72	16.7	1.87	7.49	1.59	0.398	1.44	0.239	1.51	0.322	0.943	0.153	1.03	0.162
1	Rio Grande, Southern Patagonia	20.1	44.7	5.20	21.0	4.48	1.10	4.21	0.663	4.08	0.824	2.42	0.359	2.29	0.349
2	Rio Grande, Southern Patagonia	20.9	46.3	5.37	21.6	4.64	1.10	4.42	0.700	4.30	0.876	2.52	0.380	2.46	0.376
13	Rio Grande, Southern Patagonia	22.0	47.8	5.67	22.9	4.87	1.14	4.52	0.699	4.27	0.859	2.51	0.374	2.41	0.375
15	Rio Grande, Southern Patagonia	20.0	44.2	5.15	20.8	4.36	1.10	4.18	0.656	3.98	0.810	2.29	0.347	2.22	0.338
17	Rio Grande, Southern Patagonia	20.3	45.5	5.36	21.7	4.53	1.07	4.32	0.675	4.05	0.814	2.28	0.348	2.17	0.323
24	Rio Grande, Southern Patagonia	17.5	37.9	4.40	17.7	3.68	0.991	3.50	0.543	3.29	0.672	1.94	0.287	1.86	0.285
27	Bahia Grande, Southern Patagonia	17.9	34.9	3.77	14.1	2.68	0.809	2.52	0.417	2.76	0.565	1.71	0.256	1.66	0.250
28	Bahia Grande, Southern Patagonia	17.0	36.6	4.17	16.6	3.56	0.930	3.30	0.519	3.17	0.649	1.91	0.286	1.83	0.293

Table 2.5. *continued*.

Sample ID	Sample Location	La	Ce	Pr	Nd	Sm	Eu	Gd	Tb	Dy	Ho	Er	Tm	Yb	Lu
30	Rio Santa Cruz, El Calafate, Southern Patagonia	25.6	53.5	6.42	25.4	5.21	1.29	4.67	0.722	4.33	0.873	2.58	0.382	2.44	0.375
32	Rio Santa Cruz, El Calafate, Southern Patagonia	21.9	44.3	5.58	22.4	4.56	1.26	4.52	0.704	4.29	0.867	2.45	0.371	2.38	0.363
33	Rio Santa Cruz, El Calafate, Southern Patagonia	17.8	37.9	4.47	18.0	3.76	0.948	3.57	0.564	3.43	0.697	1.99	0.302	1.95	0.297
38	Argentino Lake, El Calafate, Southern Patagonia	23.0	49.0	5.70	22.5	4.47	1.05	3.95	0.594	3.46	0.693	1.93	0.291	1.86	0.287
Volcanic – Volcanic clasts and tephra (bulk)															
CH	Chaiten Volcano, Southern Volcanic Zone	37.2	70.6	7.15	23.1	3.86	0.755	3.27	0.506	2.78	0.573	1.80	0.278	1.99	0.310
PU1	Puyehue Volcano, Southern Volcanic Zone	30.8	69.0	8.66	37.0	8.41	1.61	8.45	1.32	8.89	1.80	5.83	0.833	5.88	0.881
PU2	Puyehue Volcano, Southern Volcanic Zone	30.2	66.9	8.46	36.1	8.27	1.66	8.38	1.30	8.73	1.76	5.75	0.819	5.73	0.869
PU3	Puyehue Volcano, lakeside near La Angostura	24.9	52.8	6.75	29.2	6.77	1.36	7.07	1.09	7.37	1.48	4.79	0.689	4.93	0.739
CO	Cotopaxi Volcano, Northern Volcanic Zone	14.6	27.9	3.52	15.2	3.25	0.961	3.04	0.416	2.54	0.472	1.36	0.190	1.26	0.196
Urban – Road dusts (50-100µm)															
3C	Urban Area, Buenos Aires	34.1	64.1	7.74	28.7	5.10	1.10	4.18	0.625	3.73	0.731	2.15	0.331	2.13	0.319
9C	Urban Area, Buenos Aires	45.8	95.1	10.6	40.3	7.36	1.33	5.61	0.794	4.56	0.868	2.49	0.368	2.44	0.381
110C	Urban Area, Buenos Aires	39.2	77.8	8.76	33.8	6.03	1.18	4.71	0.687	3.96	0.787	2.26	0.341	2.34	0.366
112C	Urban Area, Buenos Aires	52.8	106	11.9	43.7	7.15	1.15	5.17	0.735	3.86	0.713	1.91	0.285	1.85	0.279
3D	Urban Area, Buenos Aires	45.9	106	10.1	37.9	6.12	1.16	4.29	0.602	3.42	0.651	1.88	0.280	1.78	0.279
9D	Urban Area, Buenos Aires	42.2	90.1	10.3	39.0	6.49	1.14	4.58	0.608	3.39	0.621	1.77	0.269	1.73	0.266
110D	Urban Area, Buenos Aires	47.9	91.5	10.8	39.6	6.47	1.02	4.31	0.586	3.27	0.597	1.70	0.247	1.64	0.240
112D	Urban Area, Buenos Aires	39.5	81.4	8.87	33.3	5.80	1.11	4.56	0.637	3.68	0.716	2.07	0.301	1.93	0.295

Table 2.5. *continued*.

Sample ID	Sample Location	La	Ce	Pr	Nd	Sm	Eu	Gd	Tb	Dy	Ho	Er	Tm	Yb	Lu
Urban – Aerosols (<10µm)															
648	Urban Area, São Paulo	5.00	6.42	0.572	1.94	0.299	0.065	0.209	0.027	0.130	0.021	0.068	0.007	0.053	0.006
649	Urban Area, São Paulo	4.13	4.88	0.518	1.31	n.d.	n.d.	n.d.	n.d.	n.d.	n.d.	n.d.	n.d.	n.d.	n.d.
650	Urban Area, São Paulo	9.95	9.53	0.871	2.62	0.399	0.100	0.286	0.038	0.219	0.036	0.089	0.011	0.089	0.013
Southern Africa															
Rural – Aerosols, shelf sediment (bulk)															
PICA	Rural Area, Johannesburg	5.56	10.6	0.93	3.13	0.492	0.122	0.413	0.061	0.355	0.069	0.191	0.028	0.177	0.027
ST0	Sea-shelf off Cape Town	57.4	93.8	13.3	55.7	11.5	2.51	13.6	1.83	10.1	2.15	6.16	0.751	4.38	0.625
ST1	Sea-shelf off Cape Town	14.4	24.6	3.54	13.6	2.74	0.583	2.76	0.421	2.42	0.522	1.59	0.222	1.47	0.213
ST3	Sea-shelf off Cape Town	22.8	46.2	6.44	25.6	5.63	1.23	5.60	0.819	4.51	0.915	2.68	0.355	2.36	0.343
ST6	Sea-shelf off Cape Town	24.1	67.2	6.36	24.0	5.08	1.11	4.80	0.741	4.10	0.817	2.42	0.338	2.28	0.336
ST8	Sea-shelf off Cape Town	14.0	29.9	3.76	14.6	3.10	0.754	3.10	0.457	2.54	0.532	1.61	0.220	1.47	0.212
ST11	Sea-shelf off Cape Town	27.4	78.2	7.06	26.9	5.67	1.22	5.34	0.811	4.53	0.911	2.69	0.378	2.52	0.363
ST13	Sea-shelf off Cape Town	17.1	33.9	4.33	16.5	3.37	0.695	3.35	0.506	2.77	0.580	1.74	0.246	1.66	0.244
Urban – Aerosols (bulk)															
RIVER	Urban Area, Johannesburg	3.41	7.34	0.75	2.69	0.509	0.096	0.453	0.073	0.467	0.091	0.260	0.040	0.261	0.042
DELTA	Urban Area, Johannesburg	5.55	12.0	1.19	4.31	0.809	0.153	0.705	0.111	0.689	0.139	0.385	0.060	0.391	0.061
CMG	Urban Area, Johannesburg	3.85	8.32	0.87	3.19	0.605	0.119	0.546	0.087	0.543	0.104	0.293	0.043	0.276	0.044
EMMER	Urban Area, Johannesburg	4.66	8.91	1.05	3.85	0.703	0.158	0.658	0.105	0.601	0.123	0.342	0.055	0.337	0.046
HUDD	Urban Area, Johannesburg	3.70	7.80	0.87	3.25	0.617	0.116	0.564	0.092	0.539	0.113	0.342	0.051	0.328	0.048
BOT2	Urban Area, Johannesburg	3.51	7.12	0.75	2.82	0.555	0.103	0.457	0.072	0.451	0.087	0.244	0.039	0.242	0.039
Mine – Aerosols (bulk)															
DRD	Mine Dump Site, Johannesburg	2.68	4.04	0.48	1.68	0.275	0.062	0.245	0.036	0.203	0.040	0.105	0.016	0.099	0.015

Table 2.5. *continued*.

Sample ID	Sample Location	La	Ce	Pr	Nd	Sm	Eu	Gd	Tb	Dy	Ho	Er	Tm	Yb	Lu
South America – rural and volcanic sediment, <5 µm															
4	Bahia San Sebastian, Southern Patagonia	5.89	14.2	1.64	6.38	1.35	0.307	1.28	0.191	1.07	0.220	0.646	0.089	0.585	0.090
32	Rio Santa Cruz, El Calafate, Southern Patagonia	32.4	100	9.91	41.3	9.42	2.16	9.53	1.45	7.96	1.57	4.72	0.636	4.26	0.609
42	Punta Arenas, Southern Patagonia	6.14	12.7	1.45	5.22	1.13	0.309	1.06	0.187	1.17	0.264	0.838	0.133	0.948	0.153
CH	Chaiten Volcano, Southern Volcanic Zone	24.6	48.4	5.25	17.5	2.96	0.529	2.44	0.377	2.09	0.428	1.38	0.210	1.48	0.230
PU2	Puyehue Volcano, Southern Volcanic Zone	29.7	71.6	8.94	36.9	8.39	1.58	8.74	1.44	8.66	1.85	5.89	0.880	6.16	0.924
Reference Material															
USGS G-2	**This study (n=12)**	87	158	16	52	7.2	1.3	4.0	0.46	2.2	0.35	0.85	0.1	0.7	0.1
	RSD (2σ, %)	1.3	1.2	3.1	2.1	2.5	3.5	4.3	4.0	5.4	4.9	3.8	5.5	4.1	4.4
USGS G-2	**USGS**	89	160	18	55	7.2	1.4	4.3	0.48	2.4	0.4	0.92	0.18	0.8	0.11
	RSD (2σ, %)	18	13	n.a.	22	19	17	n.a.	n.a.	25	n.a.	n.a.	n.a.	50	n.a.
UCC	**Tayor and McLennan (1985)**	30	64	7.1	26	4.5	0.88	3.8	0.64	3.5	0.8	2.3	0.33	2.2	0.32

Table 2.5. *continued*.

Sample ID	Sample Location	Cu	Pb	Cd	Zn	Cr	Ni	Th	Co	Y	V	Sc
South America												
Rural – Topsoil, Bed sediment (bulk)												
4	Bahia San Sebastian, Southern Patagonia	10.8	4.25	0.137	46.8	13.0	6.4	2.31	4.67	7.44	38.7	4.93
5	Bahia San Sebastian, Southern Patagonia	7.00	11.4	0.054	69.3	42.0	14.0	7.20	8.55	19.2	100	12.7
8	Bahia San Sebastian, Southern Patagonia	7.44	13.0	0.047	83.9	51.5	18.9	8.41	10.5	21.5	122	15.3
9	Bahia San Sebastian, Southern Patagonia	9.74	14.7	0.063	76.0	43.8	16.8	7.49	10.9	21.2	115	14.1
10	Bahia San Sebastian, Southern Patagonia	9.85	14.2	0.068	84.4	49.6	18.0	7.88	10.9	20.2	130	14.9
11	Bahia San Sebastian, Southern Patagonia	10.1	13.9	0.053	83.2	46.7	17.4	7.74	11.0	20.3	116	14.4
12	Bahia San Sebastian, Southern Patagonia	6.15	10.8	0.041	68.1	44.4	15.3	7.55	8.29	21.1	106	13.9
19	Rio Gallegos, Southern Patagonia	22.7	16.7	0.066	71.9	39.4	9.3	7.28	8.13	9.18	84.0	13.9
21	Rio Gallegos, Southern Patagonia	12.6	8.12	0.080	69.2	42.5	13.5	4.56	12.2	16.3	114	16.5
35	Rio Santa Cruz, Southern Patagonia	14.9	10.9	0.093	72.6	27.1	18.3	5.89	13.3	21.1	109	14.6
40	Punta Arenas, Southern Patagonia	22.3	9.86		55.4	30.5	22.0	3.90	18.8	7.72	105	12.2
42	Punta Arenas, Southern Patagonia	19.4	13.5	0.082	65.3	29.7	10.1	4.35	7.04	8.24	106	11.3
1	Rio Grande, Southern Patagonia	9.79	10.6	0.086	67.0	38.7	12.4	6.76	7.73	19.9	94.8	12.3
2	Rio Grande, Southern Patagonia	9.78	11.2	0.087	69.7	41.6	14.1	7.65	8.56	20.8	105	13.0
13	Rio Grande, Southern Patagonia	11.8	12.5	0.061	68.9	45.0	12.8	7.64	5.32	21.8	104	13.4
15	Rio Grande, Southern Patagonia	8.11	9.49	0.040	56.8	39.6	13.2	6.14	8.35	20.4	89.0	12.6
17	Rio Grande, Southern Patagonia	7.92	7.00	0.036	48.2	34.0	13.3	4.92	8.28	20.7	88.2	12.4
24	Rio Grande, Southern Patagonia	6.76	8.45	0.044	49.6	32.4	11.9	5.05	8.00	17.1	80.7	10.6
27	Bahia Grande, Southern Patagonia	3.71	6.27	0.034	39.0	66.9	10.5	4.83	7.43	14.5	66.7	10.1

Table 2.5. *(continued.)*

Sample ID	Sample Location	Cu	Pb	Cd	Zn	Cr	Ni	Th	Co	Y	V	Sc
Rural – Topsoil, Bed sediment (bulk)												
28	Bahia Grande, Southern Patagonia	16.7	10.5	0.078	64.9	54.0	19.9	5.95	11.0	17.1	102	13.8
30	Rio Santa Cruz, El Calafate, Southern Patagonia	10.5	12.9	0.047	56.8	38.4	10.8	8.24	8.83	22.6	76.4	12.5
32	Rio Santa Cruz, El Calafate, Southern Patagonia	8.12	11.8	0.047	55.3	28.5	11.2	6.90	7.39	21.9	76.8	11.5
33	Rio Santa Cruz, El Calafate, Southern Patagonia	10.3	10.5	0.082	56.2	13.7	11.7	5.92	8.39	18.4	78.5	10.7
38	Argentino Lake, El Calafate, Southern Patagonia	18.1	9.87	0.099	65.1	47.1	18.4	7.11	11.9	17.9	99.1	12.8
Volcanic – Volcanic clasts and tephra (bulk)												
CH	Chaiten Volcano, Southern Volcanic Zone	2.81	19.2	0.068	33.7	0.974	0.343	12.9	1.19	12.0	3.30	2.31
PU1	Puyehue Volcano, Southern Volcanic Zone	17.8	16.5	0.192	83.8	0.606	0.409	0.482	3.66	48.0	15.3	18.3
PU2	Puyehue Volcano, Southern Volcanic Zone	15.6	17.4	0.194	82.7	1.45	0.477	0.473	3.78	47.1	17.7	18.2
PU3	Puyehue Volcano, lakeside near La Angostura	13.6	18.8	0.140	80.8	0.329	0.268	0.346	2.25	41.8	6.4	15.2
CO	Cotopaxi Volcano, Northern Volcanic Zone	21.4	7.12	0.108	89.3	41.3	25.4	0.185	27.0	13.8	216	25.4
Urban – Road dusts (50-100µm)												
3C	Urban Area, Buenos Aires	234	244	0.999	519	66.2	23.3	8.52	7.71	17.9	52.8	6.70
9C	Urban Area, Buenos Aires	231	482	0.796	643	113	32.7	12.6	8.86	21.2	72.8	7.94
110C	Urban Area, Buenos Aires	794	489	1.73	1000	117	58.6	10.5	9.42	19.3	63.3	7.26
112C	Urban Area, Buenos Aires	944	569	1.79	1306	144	174	17.9	18.2	17.7	55.1	6.50
3D	Urban Area, Buenos Aires	298	269	0.819	422	79.0	19.2	12.6	7.25	16.3	46.3	5.60
9D	Urban Area, Buenos Aires	142	426	0.624	535	81.2	21.7	14.5	7.32	15.6	43.9	5.90
110D	Urban Area, Buenos Aires	1623	547	1.25	1199	116	46.0	12.7	9.35	15.0	52.4	5.44

Table 2.5. *continued*.

Sample ID	Sample Location	Cu	Pb	Cd	Zn	Cr	Ni	Th	Co	Y	V	Sc
Urban – Aerosols (<10µm)												
112D	Urban Area, Buenos Aires	627	407	1.75	993	96.5	44.3	11.2	8.70	17.4	58.7	6.87
648	Urban Area, São Paulo	93.7	97	4.50	584	146	25.2	0.619	2.08	40.4	40.4	0.437
649	Urban Area, São Paulo	42.2	133	5.54	990	n.d.	17.0	n.d.	2.02	6.90	14.6	n.d.
650	Urban Area, São Paulo	220	270	13.1	1357	278	53.2	0.716	9.48	34.5	34.5	0.705
Southern Africa												
Rural – Aerosols (bulk)												
PICA	Rural Area, Johannesburg	11.7	6.07	0.061	30.3	202	12.7	0.876	1.96	1.88	7.17	0.885
ST0	Sea-shelf off Cape Town	2.83	3.92	0.075	58.0	258	18.8	2.57	142	7.27	97.3	6.49
ST1	Sea-shelf off Cape Town	39.9	5.54	0.184	55.7	55.4	29.6	6.61	43.4	6.32	17.5	4.42
ST3	Sea-shelf off Cape Town	38.0	9.08	0.107	36.2	54.1	22.8	7.39	41.4	5.20	28.9	7.82
ST6	Sea-shelf off Cape Town	159	22.1	0.161	113	89.8	110	33.9	106	14.8	23.2	9.86
ST8	Sea-shelf off Cape Town	11.2	6.94	0.190	33.5	54.5	16.3	2.44	32.2	3.94	17.5	4.46
ST11	Sea-shelf off Cape Town	169	23.0	0.135	129	101	106	36.1	117	18.1	26.2	10.9
ST13	Sea-shelf off Cape Town	26.6	7.75	0.198	54.5	64.9	30.2	4.15	40.6	5.57	19.7	6.04
Urban – Aerosols (bulk)												
RIVER	Urban Area, Johannesburg	23.5	68.7	0.295	84.5	147	8.99	1.07	1.59	2.48	11.1	1.37
DELTA	Urban Area, Johannesburg	33.0	108	0.212	80.6	196	14.4	1.64	2.56	3.81	17.2	1.99
CMG	Urban Area, Johannesburg	20.6	71.0	0.322	121	91.8	10.9	1.21	2.34	2.81	11.6	1.54
EMMER	Urban Area, Johannesburg	44.1	93.7	0.292	80.5	119	12.3	1.41	2.67	3.09	13.6	1.71
HUDD	Urban Area, Johannesburg	20.1	46.9	0.149	94.3	116	10.4	1.33	1.69	2.76	11.0	1.46
BOT2	Urban Area, Johannesburg	18.5	52.5	0.158	72.8	156	10.8	1.15	1.75	2.22	11.2	1.27
Mine – Aerosols (bulk)												
DRD	Mine Dump Site, Johannesburg	6.92	9.53	0.121	31.6	26.4	7.14	0.373	5.72	1.11	3.36	0.459

Table 2.5. *continued*.

Sample ID	Sample Location	Cu	Pb	Cd	Zn	Cr	Ni	Th	Co	Y	V	Sc
South America – rural and volcanic sediment, <5 µm												
4	Bahia San Sebastian, Southern Patagonia	10.9	4.71	0.146	68.0	9.76	6.04	5.59	36.4	4.09	5.85	1.68
32	Rio Santa Cruz, El Calafate, Southern Patagonia	19.5	24.1	0.098	130	45.0	30.4	14.7	147	22.0	43.6	10.6
42	Punta Arenas, Southern Patagonia	28.8	18.8	0.082	96.7	45.4	13.0	9.09	159	12.6	6.60	5.85
CH	Chaiten Volcano, Southern Volcanic Zone	3.83	20.5	0.069	47.1	3.63	1.44	1.72	9.00	2.95	13.3	13.0
PU2	Puyehue Volcano, Southern Volcanic Zone	13.2	24.9	0.190	83.8	0.521	0.404	3.05	8.40	11.5	52.8	8.88
Reference Material												
USGS G-2	**This study (n=12)**	9.1	32	0.02	86	7.6	2.2	24	4.5	9.1	35	4.7
	RSD (2σ, %)	1.1	1.0	0.01	7.4	1.2	0.4	0.6	0.2	0.3	1.6	0.4
USGS G-2	**USGS**	11	30	n.a.	86	n.a.	n.a.	25	4.6	11	36	3.5
	RSD (2σ, %)	73	n.a.	n.a.	19	n.a.	n.a.	16	30	36	22	23
UCC	**Taylor and McLennan (1985)**	25	20	0.098	71	35	20	10.7	10	22	60	11

Results for certified reference material USGS G-2 Granite are reported and compared to the recommended literature value (Gladney et al., 1992; Govindaraju, 1989, 1994). Precision is given as the relative standard deviation (RSD) at the 2σ level (n = 12)

Blank spaces denotes below detection limit

n.d. = not determined. n.a. = not available.

Table 2.6. Lead and neodymium isotope ratios and εNd values for major aerosol sources from South America and Southern Africa

Sample ID	Sample Location	$^{206}Pb/^{207}Pb$	2SE	$^{208}Pb/^{207}Pb$	2SE	$^{206}Pb/^{204}Pb$	2SE	$^{207}Pb/^{204}Pb$	2SE	$^{208}Pb/^{204}Pb$	2SE	$^{144}Nd/^{143}Nd$	2SE	εNd
South America														
Rural – Topsoil, Bed sediment (bulk)														
4	Bahia San Sebastian, Southern Patagonia	1.1967	0.0001	2.4681	0.0001	18.696	0.001	15.623	0.002	38.560	0.005	0.512670	0.000029	0.1
5	Bahia San Sebastian, Southern Patagonia	1.2004	0.0002	2.4744	0.0004	18.781	0.007	15.645	0.009	38.713	0.028	0.512477	0.000014	-3.1
8	Bahia San Sebastian, Southern Patagonia	1.1902	0.0002	2.4641	0.0004	18.614	0.007	15.639	0.009	38.536	0.029	0.512463	0.000018	-3.4
9	Bahia San Sebastian, Southern Patagonia	1.1936	0.0003	2.4671	0.0005	18.668	0.008	15.640	0.010	38.586	0.033	0.512486	0.000018	-3.0
10	Bahia San Sebastian, Southern Patagonia	1.1988	0.0003	2.4726	0.0006	18.755	0.009	15.640	0.012	38.684	0.038	0.512505	0.000012	-2.6
11	Bahia San Sebastian, Southern Patagonia	1.1998	0.0001	2.4731	0.0001	18.771	0.002	15.645	0.003	38.691	0.007	0.512488	0.000011	-2.9
12	Bahia San Sebastian, Southern Patagonia	1.2000	0.0001	2.4740	0.0001	18.776	0.001	15.647	0.001	38.711	0.001	0.512477	0.000010	-3.1
19	Rio Gallegos, Southern Patagonia	1.1983	0.0002	2.4714	0.0004	18.725	0.004	15.626	0.006	38.620	0.021	0.512599	0.000017	-0.1
21	Rio Gallegos, Southern Patagonia	1.1978	0.0001	2.4717	0.0003	18.722	0.001	15.631	0.003	38.639	0.008	0.512623	0.000015	-0.3
35	Rio Santa Cruz, Southern Patagonia	1.1995	0.0001	2.4723	0.0001	18.757	0.003	15.637	0.003	38.663	0.009	0.512598	0.000014	-0.8
40	Punta Arenas, Southern Patagonia	1.1870	0.0001	2.4590	0.0003	18.534	0.001	15.615	0.003	38.397	0.008	0.512814	0.000026	3.4
42	Punta Arenas, Southern Patagonia	1.1960	0.0001	2.4695	0.0001	18.697	0.002	15.632	0.003	38.605	0.009	0.512561	0.000022	-1.5
1	Rio Grande, Southern Patagonia	1.1962	0.0003	2.4696	0.0006	18.707	0.010	15.639	0.012	38.622	0.038	0.512461	0.000035	-3.5
2	Rio Grande, Southern Patagonia	1.1978	0.0002	2.4713	0.0004	18.737	0.006	15.644	0.008	38.660	0.025	0.512448	0.000025	-3.7
13	Rio Grande, Southern Patagonia	1.2006	0.0001	2.4741	0.0002	18.772	0.002	15.636	0.003	38.686	0.005	0.512463	0.000010	-3.4
15	Rio Grande, Southern Patagonia	1.1968	0.0001	2.4695	0.0003	18.707	0.003	15.630	0.004	38.601	0.014	0.512540	0.000013	-1.9
17	Rio Grande, Southern Patagonia	1.1734	0.0001	2.4465	0.0001	18.327	0.002	15.618	0.002	38.212	0.008	0.512582	0.000020	-1.1
24	Rio Grande, Southern Patagonia	1.1967	0.0003	2.4707	0.0004	18.719	0.005	15.642	0.008	38.647	0.023	0.512559	0.000018	-1.6

Table 2.6. *continued*.

Sample ID	Sample Location	$^{206}Pb/^{207}Pb$	2SE	$^{208}Pb/^{207}Pb$	2SE	$^{206}Pb/^{204}Pb$	2SE	$^{207}Pb/^{204}Pb$	2SE	$^{208}Pb/^{204}Pb$	2SE	$^{144}Nd/^{143}Nd$	2SE	εNd
27	Bahia Grande, Southern Patagonia	1.1963	0.0001	2.4716	0.0003	18.701	0.001	15.632	0.008	38.636	0.008	0.512575	0.000021	-1.2
28	Bahia Grande, Southern Patagonia	1.1987	0.0001	2.4742	0.0003	18.748	0.005	15.640	0.005	38.698	0.018	0.512512	0.000021	-2.5
30	Rio Santa Cruz, El Calafate, Southern Patagonia	1.1967	0.0001	2.4739	0.0003	18.711	0.005	15.635	0.005	38.681	0.020	0.512576	0.000014	-1.2
32	Rio Santa Cruz, El Calafate, Southern Patagonia	1.1814	0.0001	2.4579	0.0002	18.461	0.002	15.627	0.002	38.410	0.008	0.512573	0.000017	-1.3
33	Rio Santa Cruz, El Calafate, Southern Patagonia	1.1969	0.0001	2.4746	0.0001	18.715	0.002	15.636	0.002	38.694	0.005	0.512570	0.000017	-1.3
38	Argentino Lake, El Calafate, Southern Patagonia	1.1967	0.0001	2.4745	0.0001	18.714	0.003	15.638	0.003	38.698	0.010	0.512544	0.000023	-1.8
Volcanic – Volcanic clasts and tephra (bulk)														
CH	Chaiten Volcano, Southern Volcanic Zone	1.2026	0.0001	2.4780	0.0003	18.812	0.006	15.643	0.006	38.763	0.020	0.512586	0.000008	-1.0
PU1	Puyehue Volcano, Southern Volcanic Zone	1.1908	0.0001	2.4670	0.0002	18.601	0.003	15.621	0.004	38.538	0.013	0.512829	0.000009	3.7
PU2	Puyehue Volcano, Southern Volcanic Zone	1.1907	0.0001	2.4664	0.0003	18.590	0.008	15.612	0.008	38.505	0.027	0.512841	0.000010	4.0
PU3	Puyehue Volcano, lakeside near La Angostura	1.1891	0.0001	2.4656	0.0001	18.570	0.002	15.617	0.002	38.506	0.004	0.512831	0.000009	3.8
CO	Cotopaxi Volcano, Northern Volcanic Zone	1.2002	0.0001	2.4703	0.0003	18.765	0.002	15.635	0.003	38.623	0.011	0.512816	0.000010	3.5
Urban – Road dusts (50-100µm)														
3C	Urban Area, Buenos Aires	1.1626	0.0001	2.4391	0.0001	18.158	0.001	15.619	0.001	38.094	0.003	0.511957	0.000010	-13.3
9C	Urban Area, Buenos Aires	1.1630	0.0001	2.4420	0.0001	18.165	0.003	15.618	0.003	38.128	0.046	0.511840	0.000009	-15.6
110C	Urban Area, Buenos Aires	1.1605	0.0001	2.4378	0.0001	18.141	0.002	15.631	0.003	38.104	0.007	0.511946	0.000009	-13.5
112C	Urban Area, Buenos Aires	1.1567	0.0001	2.4373	0.0001	18.084	0.001	15.633	0.001	38.100	0.005	0.511633	0.000009	-19.6
3D	Urban Area, Buenos Aires	1.1615	0.0001	2.4394	0.0001	18.154	0.001	15.629	0.001	38.126	0.003	0.511704	0.000010	-18.2
9D	Urban Area, Buenos Aires	1.1630	0.0001	2.4425	0.0001	18.190	0.002	15.640	0.002	38.200	0.007	0.511660	0.000009	-19.1

Table 2.6. *continued*.

Sample ID	Sample Location	$^{206}Pb/^{207}Pb$	2SE	$^{208}Pb/^{207}Pb$	2SE	$^{206}Pb/^{204}Pb$	2SE	$^{207}Pb/^{204}Pb$	2SE	$^{208}Pb/^{204}Pb$	2SE	$^{144}Nd/^{143}Nd$	2SE	εNd
Urban – Aerosols (<10µm)														
110D	Urban Area, Buenos Aires	1.1629	0.0001	2.4448	0.0001	18.187	0.002	15.639	0.002	38.233	0.007	0.511785	0.000017	-16.6
112D	Urban Area, Buenos Aires	1.1636	0.0001	2.4430	0.0001	18.186	0.001	15.629	0.002	38.182	0.005	0.511940	0.000015	-13.6
624	Urban Area, São Paulo	1.1887	0.0001	2.4472	0.0002	18.634	0.003	15.676	0.002	38.364	0.008	0.511852	0.000017	-15.3
648	Urban Area, São Paulo	1.1645	0.0002	2.4299	0.0003	18.192	0.012	15.621	0.012	37.959	0.032	n.d.	n.d.	n.d.
649	Urban Area, São Paulo	1.1592	0.0002	2.4265	0.0004	18.096	0.004	15.615	0.014	37.879	0.008	n.d.	n.d.	n.d.
650	Urban Area, São Paulo	1.1646	0.0001	2.4354	0.0002	18.189	0.006	15.618	0.003	38.036	0.009	n.d.	n.d.	n.d.
681	Urban Area, São Paulo	1.1829	0.0002	2.4333	0.0003	18.518	0.012	15.655	0.012	38.092	0.032	0.511915	0.000019	-14.1
Southern Africa														
Rural – Aerosols, shelf sediment (bulk)														
PICA	Rural Area, Johannesburg	1.1380	0.0001	2.4043	0.0002	17.773	0.002	15.617	0.003	37.547	0.007	0.511610	0.000015	-20.1
ST0	Sea-shelf off Cape Town	1.2405	0.0002	2.5216	0.0003	19.493	0.006	15.714	0.007	39.625	0.023	0.512255	0.000020	-7.5
ST1	Sea-shelf off Cape Town	1.2082	0.0002	2.4929	0.0004	18.961	0.007	15.694	0.008	39.123	0.025	0.512079	0.000024	-10.9
ST3	Sea-shelf off Cape Town	1.2014	0.0003	2.4966	0.0005	18.832	0.008	15.674	0.010	39.133	0.033	0.512148	0.000015	-9.6
ST6	Sea-shelf off Cape Town	1.2040	0.0002	2.4830	0.0004	18.876	0.005	15.677	0.006	38.927	0.020	0.512162	0.000019	-9.3
ST8	Sea-shelf off Cape Town	1.1885	0.0001	2.4613	0.0002	18.615	0.001	15.663	0.001	38.552	0.004	0.512167	0.000020	-9.2
ST11	Sea-shelf off Cape Town	1.2044	0.0001	2.4839	0.0005	18.895	0.007	15.688	0.007	38.968	0.024	0.512128	0.000019	-9.9
ST13	Sea-shelf off Cape Town	1.1978	0.0002	2.4794	0.0004	18.776	0.006	15.676	0.008	38.867	0.025	0.512130	0.000017	-9.9
Urban – Aerosols (bulk)														
RIVER	Urban Area, Johannesburg	1.0936	0.0001	2.3573	0.0001	17.002	0.003	15.547	0.003	36.650	0.009	0.511527	0.000014	-21.7
DELTA	Urban Area, Johannesburg	1.0926	0.0001	2.3574	0.0001	16.968	0.002	15.531	0.002	36.613	0.007	0.511596	0.000012	-20.3
CMG	Urban Area, Johannesburg	1.1162	0.0001	2.3568	0.0004	17.394	0.005	15.583	0.007	36.727	0.021	0.511585	0.000017	-20.5
EMMER	Urban Area, Johannesburg	1.0956	0.0001	2.3596	0.0002	17.019	0.002	15.534	0.003	36.653	0.009	0.511564	0.000013	-21.0
HUDD	Urban Area, Johannesburg	1.1058	0.0001	2.3692	0.0003	17.191	0.004	15.546	0.005	36.833	0.015	0.511646	0.000017	-19.4
BOT2	Urban Area, Johannesburg	1.0939	0.0017	2.3590	0.0004	16.984	0.066	15.526	0.037	36.679	0.107	0.511565	0.000015	-20.9
Mine – Aerosols (bulk)														
DRD	Mine Dump Site, Johannesburg	1.3133	0.0002	2.2866	0.0003	21.186	0.007	16.132	0.007	36.886	0.022	0.511306	0.000018	-26.0

Table 2.6. *continued*.

Sample ID	Sample Location	$^{206}Pb/^{207}Pb$	2SE	$^{208}Pb/^{207}Pb$	2SE	$^{206}Pb/^{204}Pb$	2SE	$^{207}Pb/^{204}Pb$	2SE	$^{208}Pb/^{204}Pb$	2SE	$^{144}Nd/^{143}Nd$	2SE	εNd
South America – rural and volcanic sediment, <5 µm														
4		1.1946	0.0001	2.4695	0.0001	18.683	0.001	15.639	0.001	38.619	0.003	0.512672	0.000018	0.7
32		1.1942	0.0001	2.4739	0.0001	18.699	0.001	15.658	0.001	38.736	0.003	0.512616	0.000015	-0.4
42		1.1965	0.0001	2.4702	0.0001	18.709	0.001	15.637	0.001	38.627	0.003	0.512548	0.000023	-1.8
CH		1.2031	0.0001	2.4781	0.0002	18.816	0.003	15.640	0.003	38.758	0.011	0.512618	0.000013	-0.4
PU2		1.1892	0.0001	2.4653	0.0001	18.577	0.001	15.621	0.001	38.510	0.003	0.512868	0.000014	4.5
Reference Material														
USGS G-2	**This study (n=22)**	1.1764	0.0001	2.4873	0.0003	18.399	0.005	15.640	0.006	38.902	0.021	0.512230	0.000026	-8.0
USGS G-2	**Weis (2004)**	1.1765	0.0002	2.4878	0.0002	18.396	0.002	15.636	0.005	38.900	0.019	0.512230	0.000013	-8.0

Results for certified reference material USGS G-2 Granite are reported and compared to the recommended literature value (Gladney et al., 1992; Govindaraju, 1989, 1994).

Measured precision is given at the 2σ level (n = 22). n.d. = not determined.

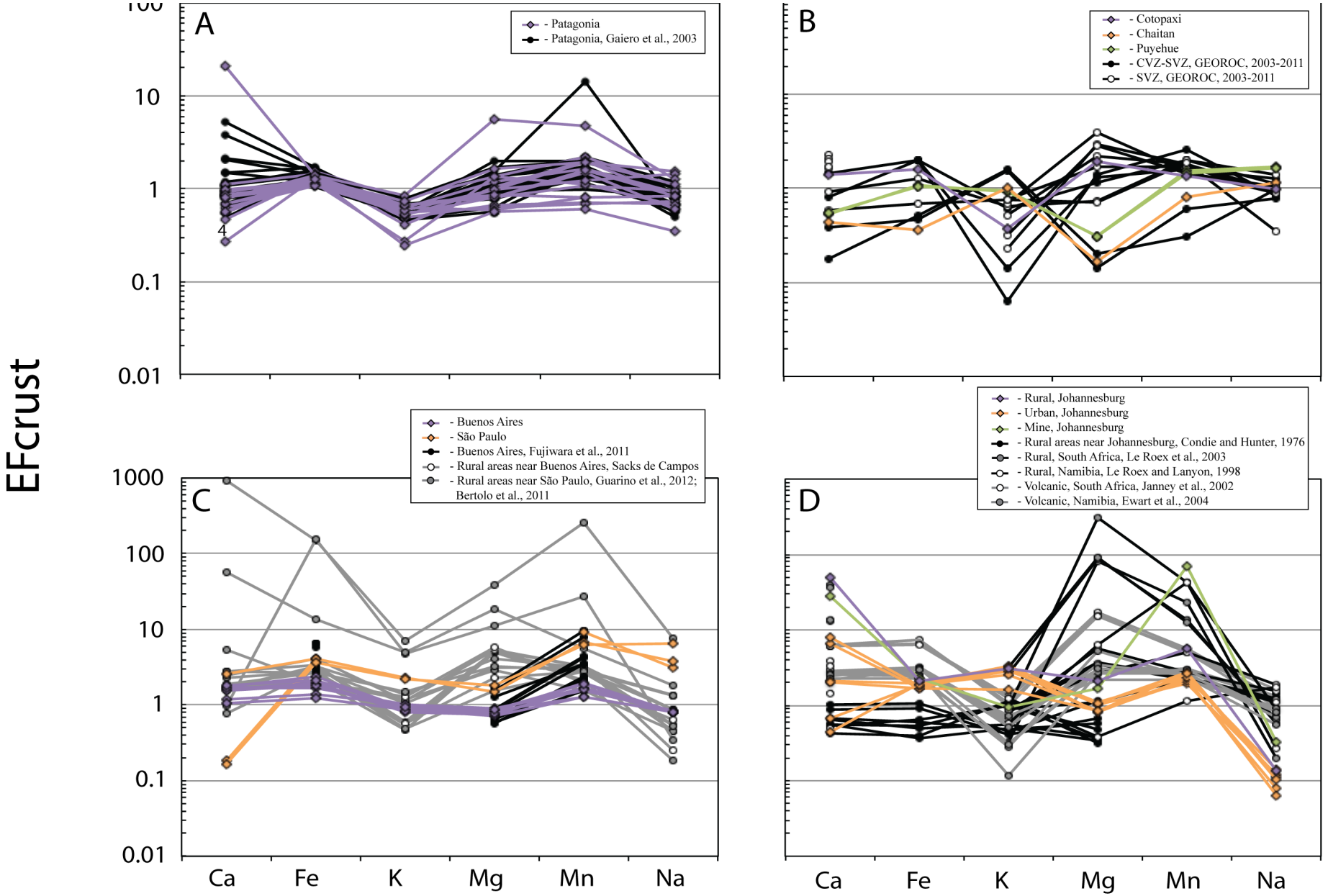

Figure 2.2. Enrichment Factor of select major elements with respect to upper continental crust for major bulk aerosol sources from South American natural sources - rural (A), volcanic (B); South American anthropogenic sources - urban (C); and Southern African natural and anthropogenic sources - rural, urban and mine (D). Literature data are included where available. Errors are shown as 2σ, and are smaller than the symbols used.

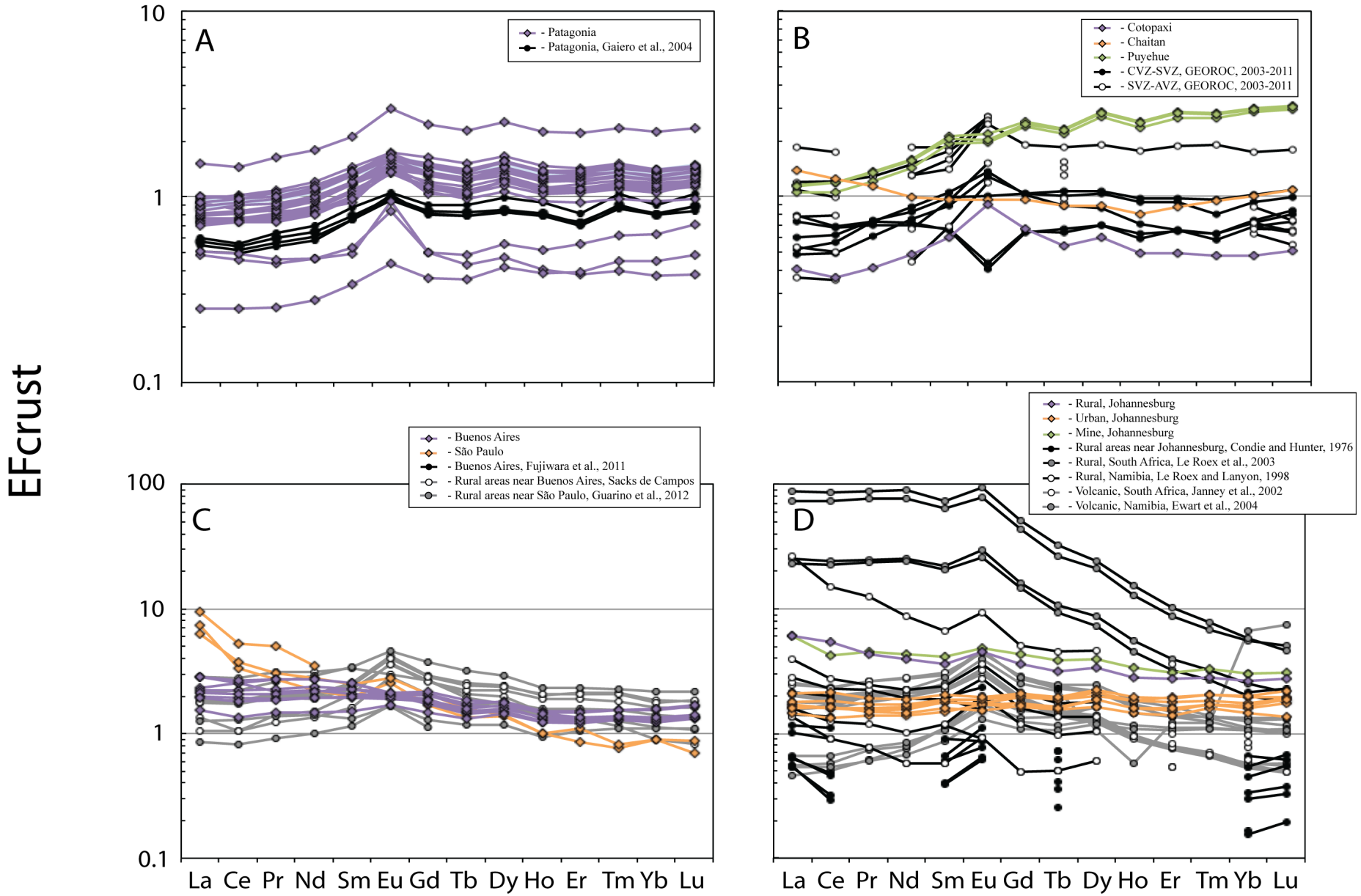

Figure 2.3. Enrichment Factor of REEs with respect to upper continental crust for major bulk aerosol sources from South American natural sources - rural (A), volcanic (B); South American anthropogenic sources - urban (C); and Southern African natural and anthropogenic sources - rural, urban and mine (D). Literature data are included where available. Errors are shown as 2σ, and are smaller than the symbols used.

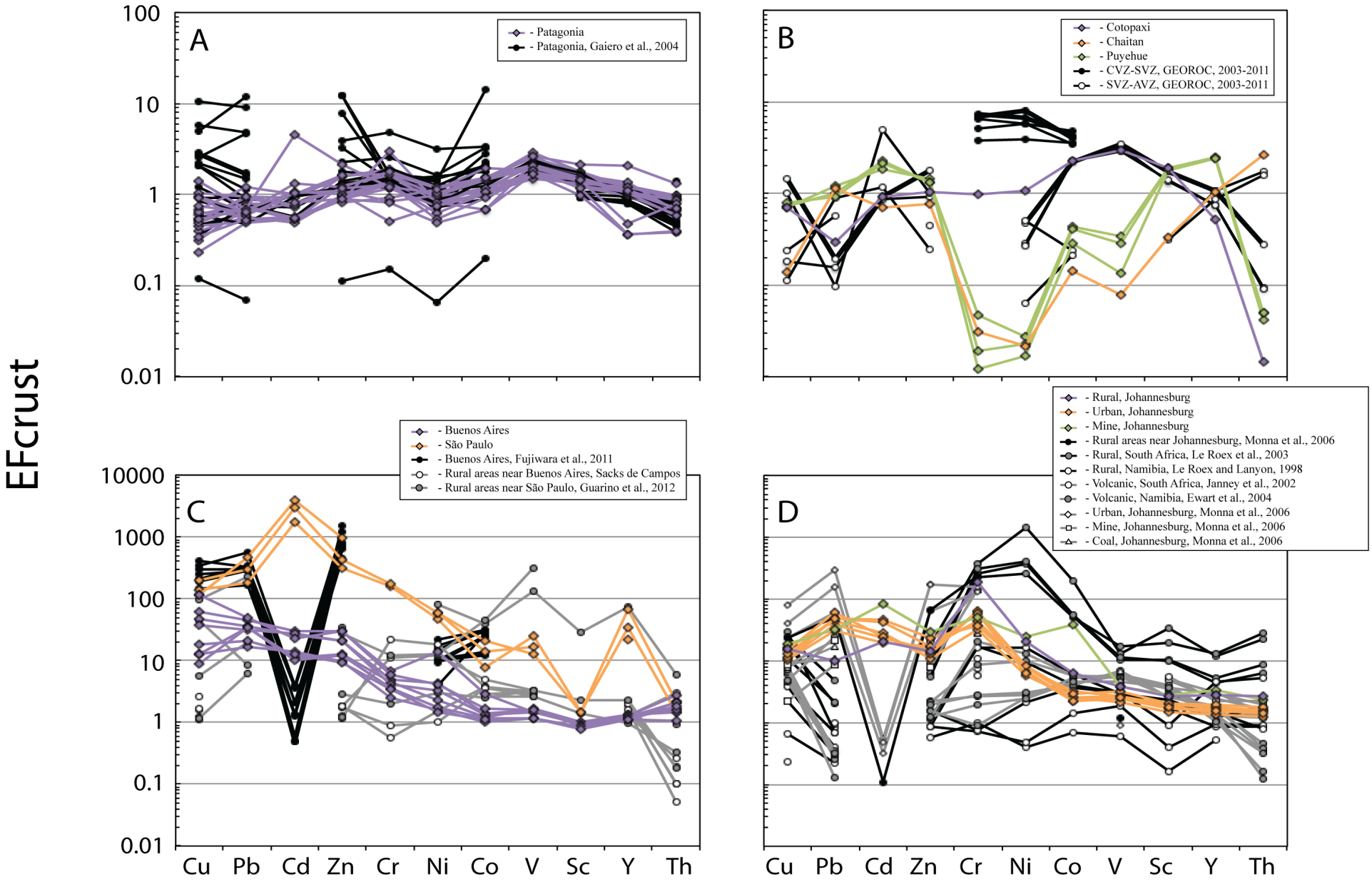

Figure 2.4. Enrichment Factor of select trace elements with respect to upper continental crust for major bulk aerosol sources from South American natural sources - rural (A), volcanic (B); South American anthropogenic sources - urban (C); and Southern African natural and anthropogenic sources - rural, urban and mine (D). Literature data are included where available. Errors are shown as 2σ, and are smaller than the symbols used.

2.3.5. Lead isotopic compositions of aerosol sources

The Pb isotopic compositions are listed in Table 2.6 and illustrated in Figure 2.5 and 2.6. Figure 2.7 demonstrates a map of the spatial distribution of the Pb isotopic composition across South America and Southern Africa. Anthropogenic emissions of Pb were found to overwhelm any natural dust that is typically enriched in ^{208}Pb, unless sampling in pristine environments (e.g. Rosman et al., 1997). Therefore natural and anthropogenic sources were commonly distinguished using Pb isotope ratios involving ^{208}Pb, and to a lesser extent ^{207}Pb and ^{206}Pb (e.g. Bollhofer and Rosman, 2000; Monna et al., 2006). This was true here as natural and anthropogenic sources from South America and Southern Africa were best characterised by their $^{208}Pb/^{207}Pb$ and $^{206}Pb/^{207}Pb$ ratios (Fig. 2.5A). Cross plots of $^{208}Pb/^{204}Pb$ vs. $^{206}Pb/^{204}Pb$ ratios were less indicative (Fig. 2.5B) as the urban, rural and volcanic sources in South America showed overlapping $^{208}Pb/^{204}Pb$ ($^{206}Pb/^{204}Pb$) ratios of 36.114-39.385 (16.560-21.575).

The rural (top soils and riverbed sediment from Patagonia) and volcanic (deposits from Chaiten, Puyehue and Cotopaxi) sources in South America revealed comparable radiogenic Pb isotopic compositions ranging from 1.1733 to 1.2027 in $^{206}Pb/^{207}Pb$ (2.4464-2.4783 in $^{208}Pb/^{207}Pb$). This was due to the similar mineralogy in rural and volcanic sources, and owing to the dispersed volcanic deposits and volcanic rock (basalts, rhyolites and andesites) that cover Patagonia (de Almeida et al., 2000). The radiogenic Pb isotopic signal of these volcanic sources were similar to the Pb isotopic composition of previously analysed volcanic sources within Patagonia and the Andean volcanic belt, which showed 1.1191 to 1.2124 in $^{206}Pb/^{207}Pb$ (2.4555-2.4962 in $^{208}Pb/^{207}Pb$) (GEOROC, 2003-2011; Fig. 2.5A). This also suggested that Pb isotopic compositions were little affected by the analysis of weathered sediment or bedrock for characterising natural aerosol sources.

There was some overlay in rural and urban South American sources (road dust from Buenos Aires and aerosols from São Paulo); generally urban sources in South America exhibited a lower Pb isotopic ratio ranging from 1.1566 to 1.1831 in $^{206}Pb/^{207}Pb$ (2.4296-2.4474 in $^{208}Pb/^{207}Pb$, Fig. 2.5A). Bollhofer and Rosman (2000) published results for aerosol samples from Buenos Aires and São Paulo (1.1190-1.2040 and 2.3940-2.4520, collectively), which were in agreement with results from this study. They suggested that the Pb isotopic compositions in São Paulo and Buenos Aires most likely reflected Pb emissions from industrial sources, as leaded petrol was totally phased out in Brazil by 1991 (Lovei, 1998). However Bollhofer and Rosman's (2000) study indicated that the actual Pb isotopic compositions of South American urban sources extended to a much lower $^{206}Pb/^{207}Pb$ and $^{208}Pb/^{207}Pb$ ratio (i.e., ~1.050-1.200 and ~2.320-2.450). Looking into detail at where the different samples in this study and in the study by Bollhofer and Rosman (2000) were derived from revealed a geographical trend (Fig. 2.7). Lowest Pb isotope ratios were found in urban areas of the southern most areas of South America such as Punta Arenas ($^{208}Pb/^{207}Pb$ ratios of ~2.320-2.350), and higher ratios towards the north ($^{208}Pb/^{207}Pb$ ratios of ~2.410 to 2.450) (Bollhofer and Rosman, 2000, Fig. 2.5A). Bollhofer and Rosman (2000) suggested the low values derived from leaded fuels with a typical Australian Broken Hill signature of $^{206}Pb/^{207}Pb$ ratio of ~1.040-1.066 ($^{208}Pb/^{207}Pb$ ratios of ~2.320-2.335; Cooper et al., 1969; Cummings and Richards, 1975)

distributed globally by Associated Octel (Veron et al., 1999). The use of leaded fuel was not phased out in Chile until the late 2000's. It is likely that Pb isotope measurements of aerosols in southern South American urban sources taken at present day would have reflected a higher Pb isotopic ratio due to a return to a natural radiogenic ^{208}Pb signal exhibited from South America (Fig. 2.5A). However, Bollhofer and Rosman (2000) further proposed that the major atmospheric particulate sources from urban sources from South America derived from regions north of ~45°S, in line with regions analysed in this study (Fig. 2.5, 2.7).

The Pb isotopic composition in the sample from the Southern African rural source (1.1380 ±0.0001 in $^{206}Pb/^{207}Pb$ and 2.4043 ±0.0002 in $^{208}Pb/^{207}Pb$) was similar to published Pb isotope results from mineral dust from the Namib Desert (1.141 ±0.001 in $^{206}Pb/^{207}Pb$; 2.421 ±0.002 in $^{208}Pb/^{207}Pb$; Bollhofer and Rosman, 2000, Fig. 2.5A). Results from this study and the literature suggest that rural sources in Southern Africa have a similar Pb isotopic composition to urban sources in South America (Fig. 2.5A). This reflected the Archean to Neoproterozoic shield formations that cover most of Southern Africa and underlie the urban areas in South America analysed in this study (de Almeida et al., 2000; de Britos Neves et al., 2013, Fig 2.1, Fig. 2.7).

Volcanic sources from Southern Africa were not analysed, but previously published results showed similar Pb isotopic signatures to South American rural and volcanic sources ($^{206}Pb/^{207}Pb$ 1.1245-1.3149; $^{208}Pb/^{207}Pb$ 2.4390-2.5493; Western Cape Province, Janney et al., 2002, Fig. 2.5A), and were most likely due to the similar geological age of these regions (Begg et al., 2009).

The samples representing Southern African urban sources showed $^{206}Pb/^{207}Pb$ ratios of 1.0925-1.1163 and $^{208}Pb/^{207}Pb$ ratios of 2.3564-2.3695 (Fig. 2.5A) and were in line with published results for aerosols from urban sources in Southern Africa (~1.050-1.120 and ~2.330-2.370, Johannesburg, Monna et al., 2006; Namibia, and southeast South Africa, Bollhofer and Rosman, 2000; Fig. 2.5A). However these previous studies suggested that the Pb isotopic signals from urban sources reflected the use of leaded gasoline before the ban in 2006, as the Pb isotopic signals from the urban sources were in line with gasoline brands used in Johannesburg before 2006 (Monna et al., 2006; Fig. 2.5A), showing $^{206}Pb/^{207}Pb$ ratios ~1.050-1.120 ($^{208}Pb/^{207}Pb$ ratios ~2.320-2.370). This was in line with the Pb element enrichment in the urban sources from Southern Africa, which revealed that natural sources did not account for the Pb element enrichments observed in aerosols from these urban areas (Fig. 2.4D). The Pb isotopic ratios from Southern African urban sources and Bollhofer and Rosman's (2000) southern South American urban sources were indistinguishable as they overlap (Fig. 2.5A). This highlighted the use of same leaded fuels in southern South American urban source areas and Southern African urban source areas pre-2006, as acknowledged by Bollhofer and Rosman (2000).

It is likely that the current day Pb isotopic signal of urban sources from Southern Africa may differ to the determined signal from this study. Bollhofer and Rosman (2000) suggested that aside from leaded fuel, mining and coal combustion were the main sources of anthropogenic aerosols from Southern Africa. A detailed look at the mine and coal Pb isotopic signals showed that the mine source from

Southern Africa from this study was isotopically very different to the Southern African urban sources as it was characterised by a very high $^{206}Pb/^{207}Pb$ ratio of 1.3133 ±0.0002 and a rather low $^{208}Pb/^{207}Pb$ ratio of 2.2866 ±0.0003 (Fig. 2.5A). This showed some agreement with previously published results for mine dump sites in Johannesburg which exhibited a $^{208}Pb/^{207}Pb$ ratio <2.250, but was quite different to the $^{206}Pb/^{207}Pb$ which was between ~2.200-2.900 (Monna et al., 2006). As acknowledged by Monna et al. (2006), this most likely reflected the high uranium levels in the Witwatersrand goldfields 5 km west of Johannesburg (Cole, 1998; Poujol et al., 1999). These mine sites in Johannesburg were however different to Pb ore carbonate-hosted sulphide deposits in Kabwe, Tsumeb and Kipushi, Namibia ($^{206}Pb/^{207}Pb$ ~1.100-1.160 and $^{208}Pb/^{207}Pb$ ~2.390-2.450; Kamona et al., 1999) and Pb ore deposits from Rosh Pinah Mine, Namibia ($^{206}Pb/^{207}Pb$ ~1.09-1.15 and $^{208}Pb/^{207}Pb$ ~2.39-2.41; Frimmel et al., 2004). Samples of coal, taken from Johannesburg in 2003 (Monna et al., 2006), exhibited $^{206}Pb/^{207}Pb$ ratios of ~1.205-1.219 and $^{208}Pb/^{207}Pb$ ratios of ~2.469-2.485. Results from this study and previous studies for mine source areas suggested that the range in Pb isotopic composition of mine sites was rather large. The previous studies also implied that a current day Pb signal from urban sources from Southern Africa would be difficult to distinguish from the rural sources from Southern Africa and urban sources from South America as the signal would most likely fall between $^{206}Pb/^{207}Pb$ ~1.090-1.220 ($^{208}Pb/^{207}Pb$ <2.250-2.490), overlapping the Pb compositions of these sources. Lead isotopic ratios of the coal samples were also in line with the volcanic sources from Southern Africa as described above and thus were also undistinguishable (Fig. 2.5A).

2.3.6. Neodymium isotopic compositions of aerosol sources

The Nd isotopic compositions can be expressed as epsilon neodymium (εNd), which correlates to the $^{143}Nd/^{144}Nd$ ratio. Younger, radiogenic rocks are characterised by more positive εNd values, and older, less radiogenic rock are characterised by lower, more negative εNd values (Jacobson and Wassenburg, 1980). The Nd isotopic compositions were listed in Table 2.6 and εNd values were illustrated in Figure 2.6. Literature data are shown where available, as shaded areas.

The εNd values of South American rural and volcanic sources ranged within -3.7 to +3.4, and -1.0 to +4.0, respectively (Fig. 2.6). These data suggested that South American volcanics were characterised by significantly more radiogenic Nd isotopic compositions than most of the rural areas in Patagonia, with 4 out of 5 samples showing a narrow data cluster around +3.7 ±0.3 (Fig. 2.6). These observations agreed with published Nd isotopic compositions in Patagonian topsoils, aeolian dust and glacier sediments (Delmonte et al., 2004; Gaiero et al., 2007; Sugden et al., 2009, Fig. 2.6), which exhibit a range in εNd of –8.9 to 2.7, and results for basaltic to andesitic volcanic rocks from across the CVZ to the AVZ which exhibit higher εNd values of -4.2 to 6.1 (GEOROC; 2003-2011; Gaiero et al., 2007, Fig. 2.6). The radiogenic εNd values in the rural and volcanic sources in South America reflected the

predominantly Mesozoic to present-day volcanic deposits that cover much of Patagonia and the Andes (de Almeida et al., 2000; de Britos Neves et al., 2013).

Southern African rural, urban, and mine, and South American urban sources were distinguishable from rural and volcanic sources from South America due to their less radiogenic εNd values (εNd of -22, -23 to -18, -26, and -22 to -13, respectively, Fig. 2.6). The rural, urban and mine sources from Southern Africa and urban sources from South America could not be discriminated from each other however, due to their similar εNd values (Fig. 2.6). The Nd isotopic compositions of the Southern African rural source was within the range of published results of εNd values from Southern African rural sources (-24 to -8.4, desert sands from Namibia, Delmonte et al., 2004; Fig. 2.6). The wide range in εNd values in rural sources from across Southern Africa most likely reflected the range of geological age of rocks that rural areas in Southern Africa overlie, as acknowledged by Delmonte et al. (2004). This suggested that Nd isotopic compositions was not affected by anthropogenic activities in Southern Africa, and the Nd isotopic compositions in rural, urban and mine sources in Southern Africa and urban sources from South America most likely reflected the similar ages (Archean to Neoproterozoic) of the geology underlying these regions in Southern Africa and South American.

Southern African volcanic sources were not analysed for Nd isotopes in this study. Published data for volcanic sources within the Western Cape (Janney et al, 2002) and along the Northern Etendeka Province in Namibia (Ewart et al., 2004) showed εNd values of +2.4 to +4.7 similar to the natural sources from South America (Fig. 2.6). This was most likely due to similar volcanic ages of the volcanic regions in South America and Southern Africa, which controls the Nd isotopic compositions and also indicated that the assessment of loess or volcanic rock did not affect the Nd isotopic compositions of a source area. This suggested that Southern African volcanic sources from the Phanerozoic covers along the southern region of South Africa were distinguishable from rural, urban and mine sources in Southern Africa and urban sources from South America that overlie the Archean to Neoproterozoic shield, by Nd isotopic compositions.

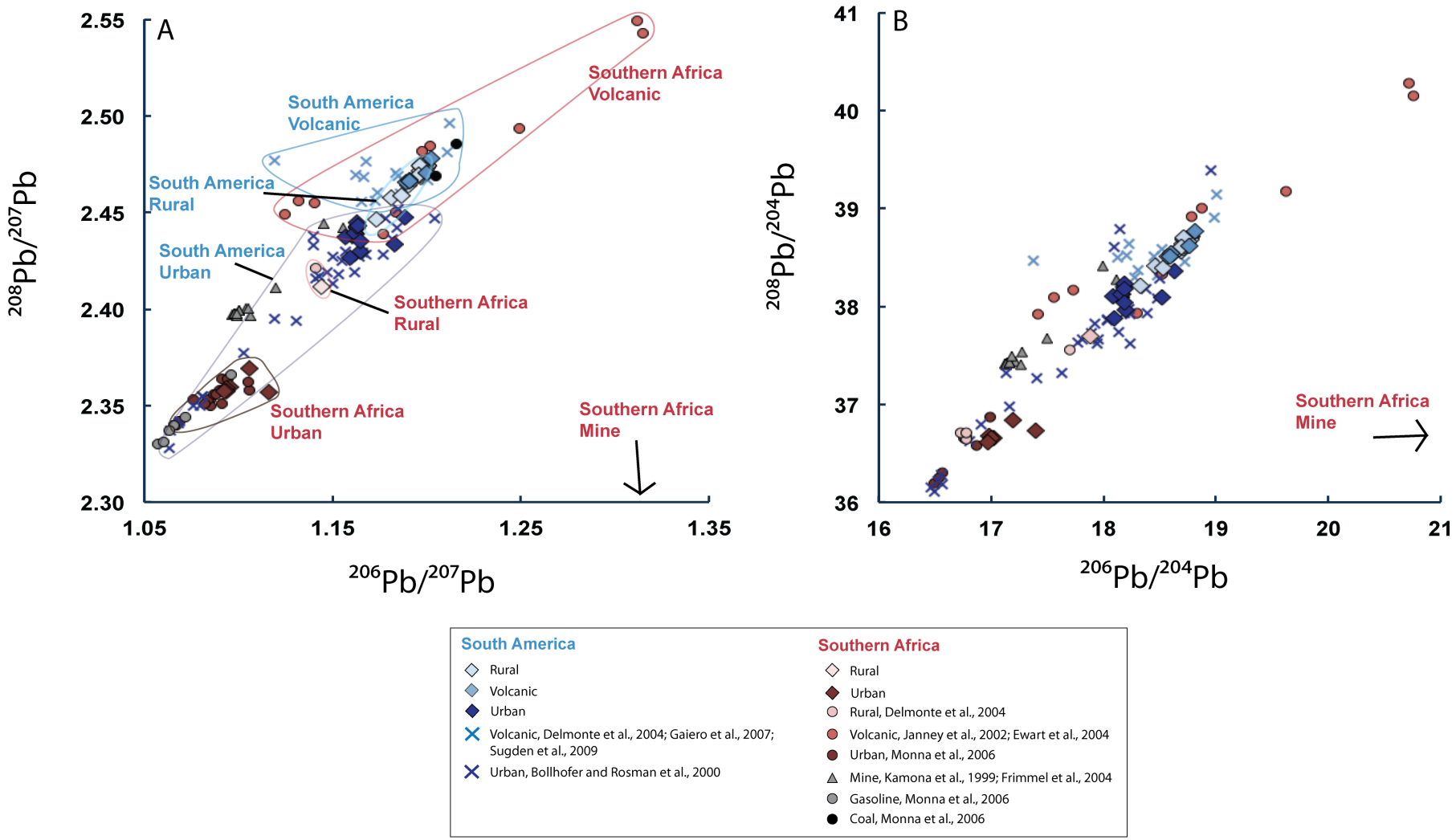

Figure 2.5. Lead isotopic compositions of major bulk aerosol sources from South America and Southern Africa: (A) $^{208}Pb/^{207}Pb$ vs. $^{206}Pb/^{207}Pb$; (B) $^{208}Pb/^{204}Pb$ vs. $^{206}Pb/^{204}Pb$. Literature data are shown where available and are denoted by symbols. Outlined datasets denote data for a source from this study and literature. Errors are to 2σ and are smaller than the symbols used.

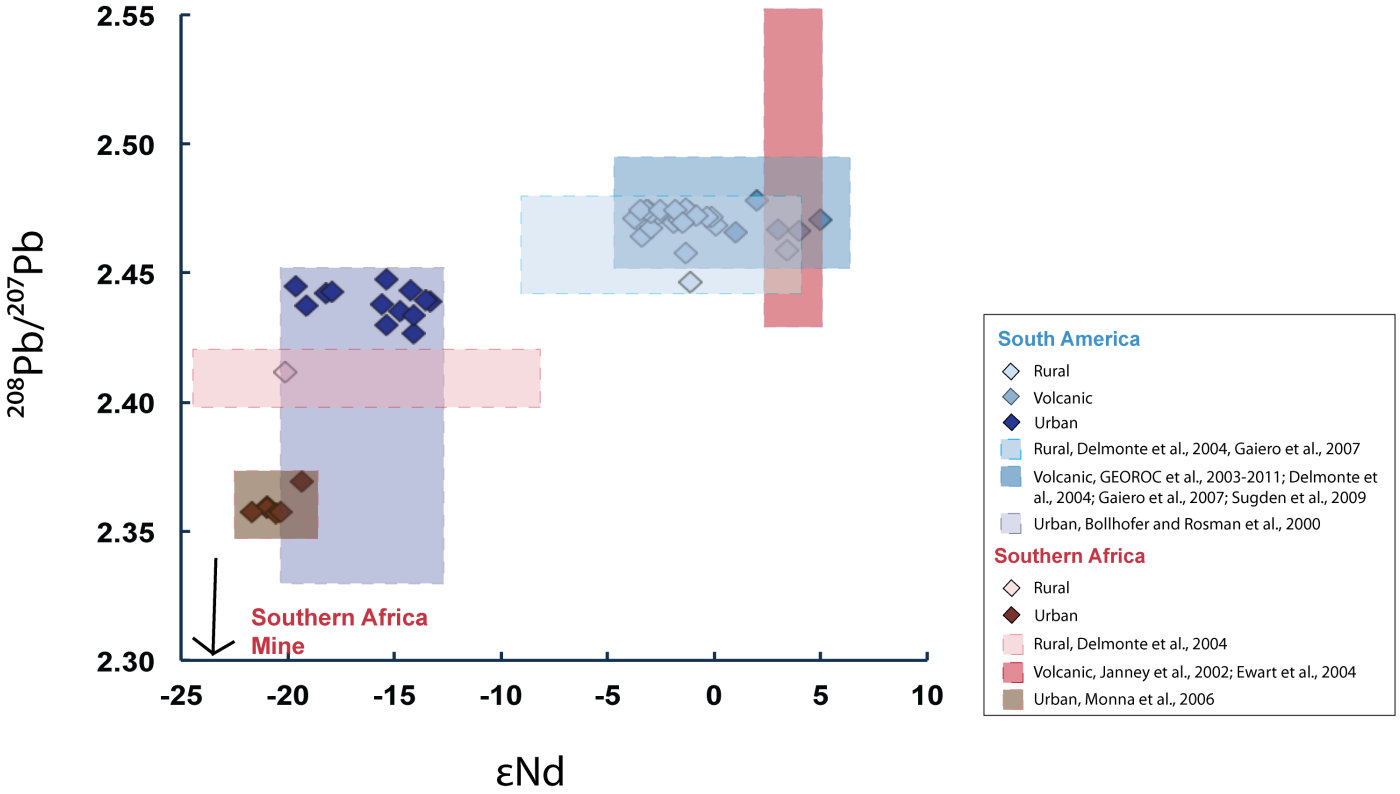

Figure 2.6. $^{208}Pb/^{207}Pb$ vs. εNd compositions of major bulk aerosol sources from South America and Southern Africa. Shaded areas denote quantitative geochemical characterisation per source, which were determined from literature data and data from this study for each proxy. Errors are shown as 2σ, and are smaller than the symbols used. Errors are to 2σ and are smaller than the symbols used.

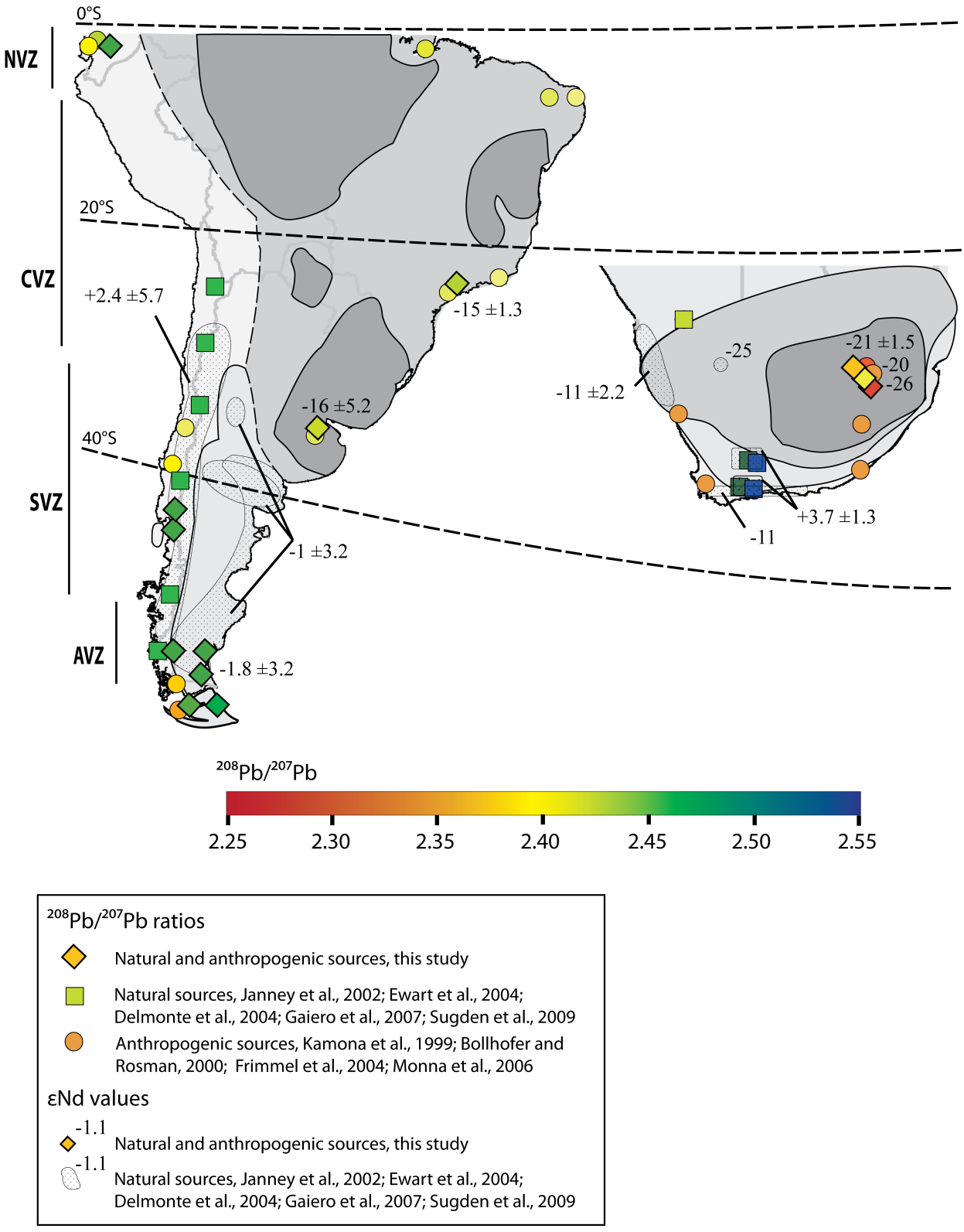

Figure 2.7. Geographical distribution of $^{208}Pb/^{207}Pb$ and εNd values of major bulk natural and anthropogenic aerosol sources from South America and Southern Africa from this study and literature data where available.

2.3.7. Shelf sediments and their geochemical constrain on natural sources from Southern Africa

Seven bulk sediment samples from the continental shelf SW off the coast of Cape Town, South Africa were analysed for major, REE and trace element enrichments, and Pb and Nd isotopic compositions, and were reported in Table 2.4 to 2.6, and except major elements were illustrated in Figure 2.7. Major element enrichment profiles were not shown in Fig. 2.7 because they were not useful for distinguishing between natural and anthropogenic sources from Southern Africa when assessing continental sediments in Section 2.3.2.

Rare earth element enrichment factors relative to the continental crust in the sediments ranged between 1 and 3, with the exception of one sample that showed enrichment between 5 and 10 (Fig. 2.7A). Enrichment factors in trace elements ranged between 0.5 and 10, with the exception of one sample that showed Cr enrichment of 30 and Y enrichment of 20 relative to the crust (Fig. 2.7B). Lead isotopic ratios in the shelf sediments were between 1.19-1.24 in $^{206}Pb/^{207}Pb$ and 2.46-2.52 in $^{208}Pb/^{207}Pb$, and -11 to -7.5 in εNd, with six out of seven samples ranging between -9.2 and -10.9 in εNd (Fig. 2.7C-D).

The rare earth and trace element enrichments relative to the crust in shelf sediments overlay those of the rural sources from Southern Africa (this study) and rural and volcanic sources from previous studies (Condie and Hunter, 1976; Le Roex and Lanyon, 1998; Janney et al., 2002; Le Roex et al., 2003; Ewart et al., 2004; Monna et al., 2006), which were represented by grey shaded areas in Fig. 2.7A and B). The high Pb isotopic compositions were in line with volcanic sources across the western and southern regions of Southern Africa (2.44-2.55 in $^{208}Pb/^{207}Pb$ ratios, Janney et al., 2002; Ewart et al., 2004). Lastly, the εNd values were between the volcanic and rural sources from Southern Africa (+2.5 to +4.7 and -24 to -8.4, respectively, Janney et al., 2002; Ewart et al., 2004; Delmonte et al., 2004). These characteristics showed that the shelf sediment SW off the coast of Southern Africa most likely represented volcanic sources from Southern Africa. Thus the element enrichment and Nd isotopic compositions of the characterised volcanic sources in Section 2.3.3 to 2.3.5 have been expanded. For example, with the exception of Eu, Sm to Lu enrichment factor constrains have been expanded from 0.4 to 0.8, to 0.4 to 10 (Fig. 2.3D and 2.7A), Zn enrichments have been expanded from 1 to 6, to 1 to 10 (Fig. 2.4D and 2.7B), and εNd compositions have been expanded from +2.5 to +4.7 to -11 to +4.7 (Fig. 2.5C and 2.7D). There were no previous data for Cd enrichment composition in volcanic sources. The shelf sediment suggested that Cd enrichment factors ranged between 1 and 6 in volcanic sources from Southern Africa (Fig. 2.7B). These effects on the geochemical constrain of the volcanic sources from Southern Africa were shown in Fig. 2.9 and from here on.

2.3.8. The effect of particle size on the geochemical constrain on natural and anthropogenic sources from South America and Southern Africa

Five fine fraction (<5 μm) sediment samples of topsoil samples from Patagonia (n=3) and volcanic tephra from Chaiten and Puyehue volcanoes along the Andean volcanic belt (n=2) were analysed for major, REE and trace element enrichments, and Pb and Nd isotopic compositions, and were reported in Table 2.4 to

2.6, and except major elements were illustrated in Figure 2.8. Major element enrichment profiles were not shown in Fig. 2.8 because they were not as useful as REE and trace elements for distinguishing between natural and anthropogenic sources when assessing continental sediments and anthropogenic aerosols in Section 2.3.2.

Rare earth element enrichment factors relative to the crust ranged between 0.1 and 3 (Fig. 2.8A). Trace element enrichment factors ranged between 0.5 and 10 in rural samples (samples 4 <5, 32 <5 and 42 <5) and between 0.01 and 2 in volcanic samples (samples CH <5 and PU2 <5) (Fig. 2.8B). Lead and Nd isotopic compositions were between 2.458-2.478 in $^{208}Pb/^{207}Pb$ and 1.181-1.203 in $^{206}Pb/^{207}Pb$ ratios (Fig. 2.8C), and from -1.8 to 4.0 in εNd (Fig. 2.8D).

Figure 2.8 showed that there were some differences between the elemental and isotopic composition of the fine (circle data points) and bulk (square data points) fractions. Two out of five samples (rural samples 32 and 42) showed REE enrichments relative to the crust were lower in the fine fraction than the bulk by an enrichment factor of 0.1 (Fig. 2.8A). One volcanic sample (CH) revealed an enrichment factor relative to the crust lower in the fine fraction than bulk by an enrichment factor of <0.1 (Fig. 2.8A). The enrichment factor of Th in the volcanic sample from Puyehue was >10 times enriched in the fine fraction than the bulk (Fig. 2.8B). The two rural samples, 32 and 42, also showed markedly higher Pb isotope ratios in the fine fraction than in the bulk (negative shifts up to 0.002 in $^{206}Pb/^{207}Pb$ and $^{208}Pb/^{207}Pb$ ratios, and positive shifts of up to 0.013 in $^{206}Pb/^{207}Pb$ and 0.016 in $^{208}Pb/^{207}Pb$ ratios), and shifts in εNd up to +/-5.0 epsilon units (Fig. 2.8C and D). This showed that particle size did impact element and isotopic composition between fine and bulk fractions from the same sediment samples. However the trace element enrichment and isotopic compositions of both the fine and bulk fractions were in line with previously determined compositions of <63 μm fraction and bulk topsoils, riverbed sediment and dust samples from rural and volcanic source areas from Patagonia and the Andean belt in South America (1.12-1.21 in $^{206}Pb/^{207}Pb$ ratios and 2.44-2.50 in $^{208}Pb/^{207}Pb$ ratios, Gaiero et al., 2003, 2004; Delmonte et al., 2004; GEOROC, 2003-2011). This showed that the trace element and Pb and Nd isotopic constrain of rural and volcanic sources were not affected by particle size in source samples. One fine fraction sample showed a lower REE enrichment relative to the crust than that exhibited in published data, thus the REE enrichment constrain of the rural sources from South America were expanded from 0.2 to 2, to 0.1 to 2 (La enrichment factor, Fig. 2.3A and Fig. 2.8A). The negligible affect that particle size showed on element and isotopic constrains of rural and volcanic sources from South America suggested that particle size may have not affected the compositions of anthropogenic sources from South America and natural and anthropogenic sources from Southern African. The effects on the geochemical constrain of the rural sources from South America were shown in Fig. 2.9 and from here on.

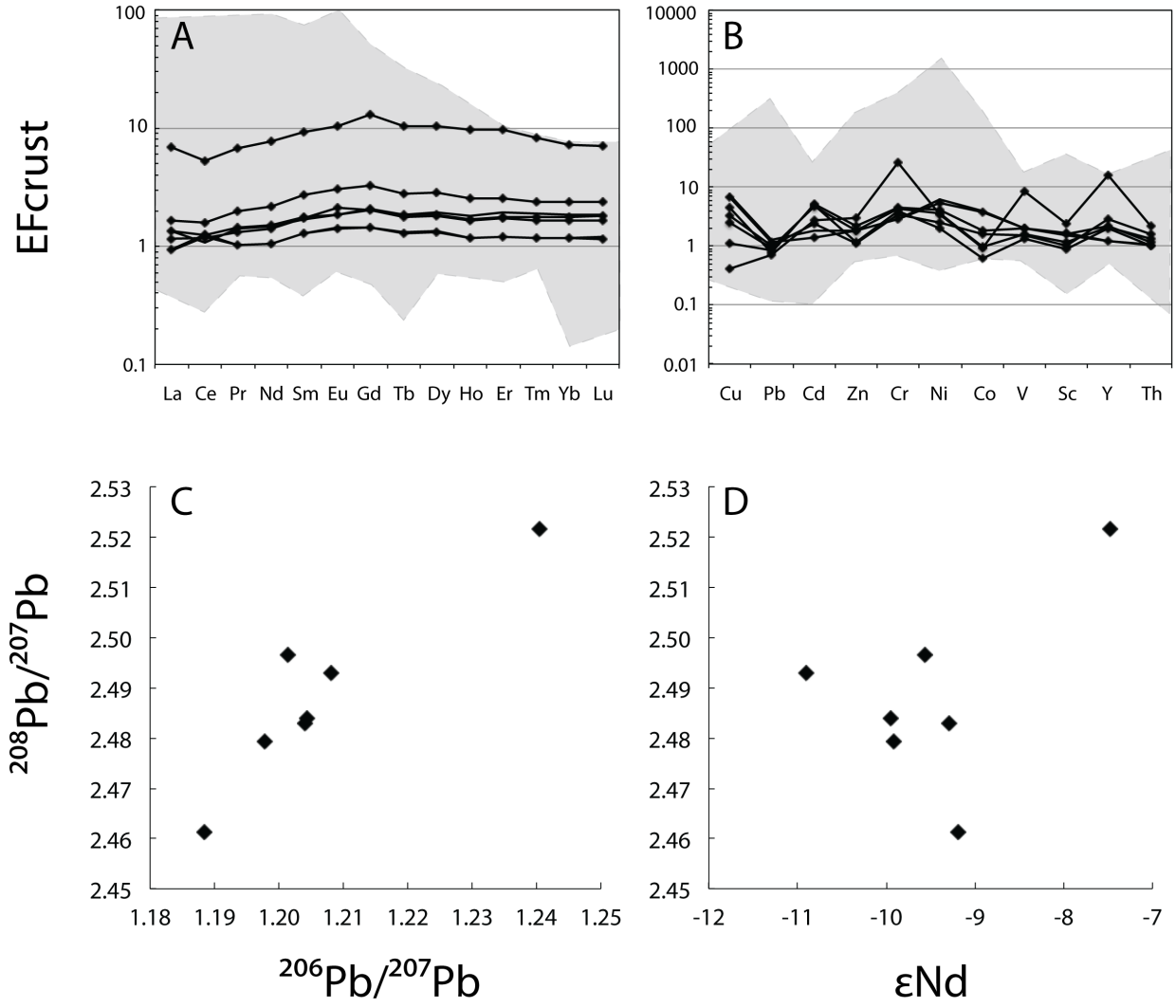

Figure 2.8. Element and isotopic characterisation of bulk shelf sediments – (A) rare earth element and (B) trace element enrichment factors relative to the continental crust, (C) $^{208}Pb/^{207}Pb$ – $^{206}Pb/^{207}Pb$; and (D) $^{208}Pb/^{207}Pb$ – εNd. Literature data for rural and volcanic sources from Southern Africa are shown as light grey shading in panels A and B (rural, urban, mine and coal from Johannesburg; this study; Monna et al., 2006; Le Roex and Lanyon, 1998; Condie and Hunter, 1976; Le Roex et al., 2003; Ewart et al., 2004; volcanic mafic lavas from the Cape Province, Janney et al., 2002). Errors are shown as 2σ, and are smaller than the symbols used.

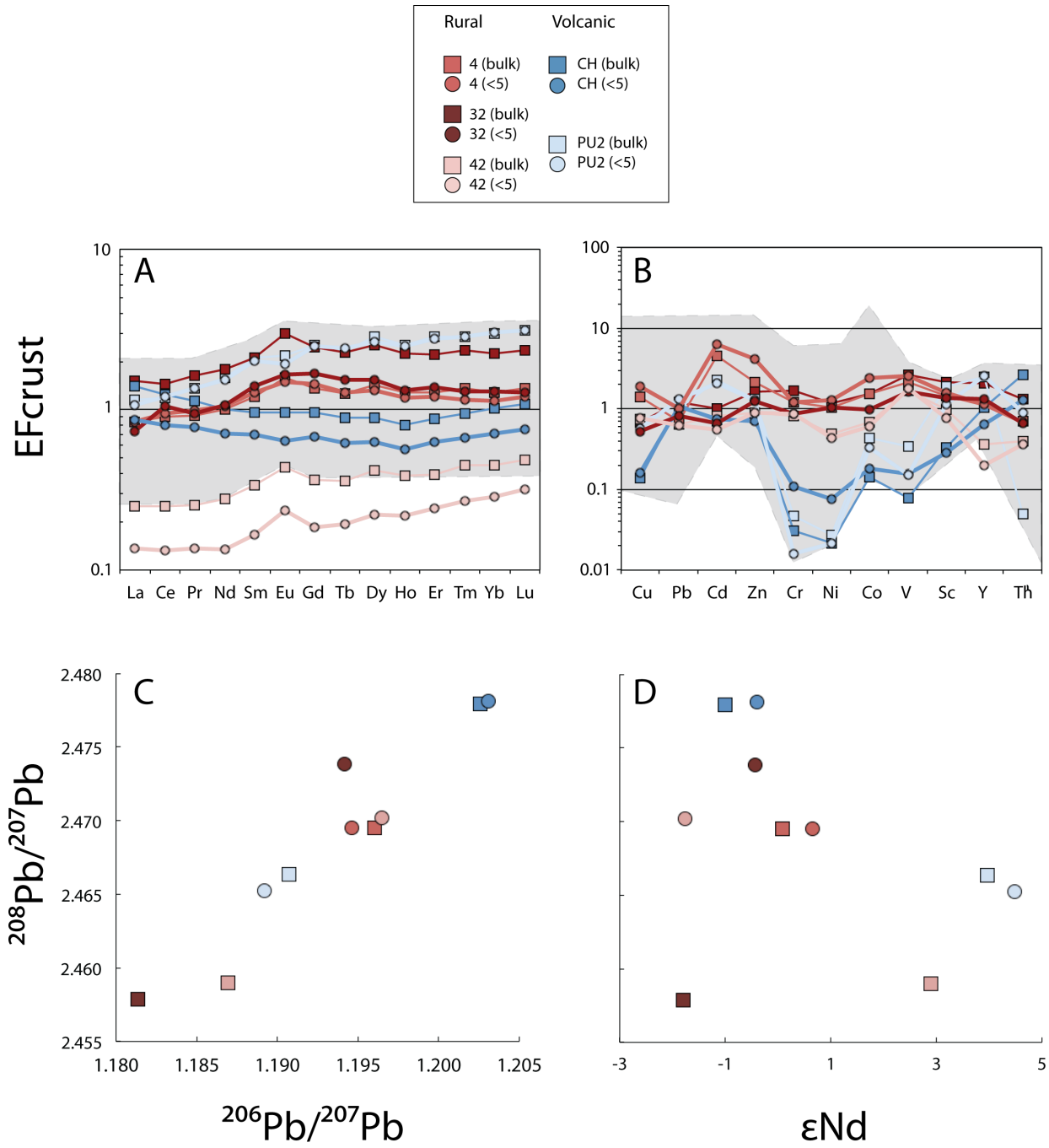

Figure 2.9. Element and isotopic compositions of fine fraction (<5 μm, circle symbols) and bulk fraction (square symbols) of sediments from South American rural and volcanic sources: (A) rare earth element and (B) trace element enrichment factors relative to the continental crust, (C) $^{208}Pb/^{207}Pb$ vs. $^{206}Pb/^{207}Pb$, and (D) $^{208}Pb/^{207}Pb$ vs. εNd. Literature data for rural and volcanic sources from South America were shown as light grey shading in panels A and B (topsoil, dust, river bed sediment and glacier deposits; bulk data from this study; Gaiero et al., 2003, 2004; Delmonte et al., 2004; and volcanic tephra from Andean Volcanic Belt within Patagonia, bulk data from this study; and volcanic rock; GEOROC, 2003-2011). Errors are shown as 2σ, and are smaller than the symbols used.

2.3.9. Provenance tracers of aerosol sources using select element ratios

The use of bivariate plots of major, REE and trace element ratios were assessed for discriminating between South American and Southern African sources, natural and anthropogenic sources, or distinguish differences within sources. The most useful plots were shown in Figure 2.9 and literature data were shown where available.

Fig. 2.9A-C showed that the most useful ratios to discriminate between the major natural sources from the major anthropogenic sources in South America, were Pb/Al, Cd/Al, Zn/Al, and Cu/Al. This was because the trace element was plotted relative to a conservative element in continental crust (Al) which characterised lower trace element/Al ratios in natural sources than anthropogenic sources. The linear correlation between Pb, Cd and Zn, and to a lesser extent Cu further suggested that these elements derived from similar anthropogenic sources (R^2 = 0.790 for Pb/Al and Zn/Al, 0.63 for Pb/Al and Cu/Al, and 0.93 for Cd/Al and Zn/Al, Fig. 2.9A-C). Fig. 2.9B highlighted the significantly higher Cd content in aerosols from São Paulo (Cd/Al×1000 ratio of 2 to 8; this study) compared to the road dusts from Buenos Aires (Cd/Al×1000 ratio of 0.01 to 0.6; this study and data from Fujiwara et al., 2011) showing that Cd/Al ratios were useful for discriminating between different urban sources from South America.

Bivariate plots of Pb/Al, Cd/Al, Zn/Al, and Cu/Al were also useful to distinguish between Southern African natural sources (this study; Le Roex and Lanyon, 1998; Janney et al., 2002; Le Roex et al., 2003; Ewart et al., 2004), and from anthropogenic sources (this study). Natural sources showed lower ratios than the anthropogenic sources (e.g. Pb/Al×1000 ratios in natural sources ranged from 0.03 to 8, and 7 to 20 in anthropogenic sources, Fig. 2.9A and C). The one rural sample from Johannesburg may have represented the transition point between natural and anthropogenic signals in Southern Africa, as this sample plotted between the natural and anthropogenic signals but close to the anthropogenic signal of Pb/Al, Cd/Al, Zn/Al and Cu/Al ratios (e.g. Pb/Al×1000 ratio of 4, Fig. 2.9A-C).

To assess the use of the different Cr enrichment factors and the different LREE enrichment factors in different sources, Cr/Al was plotted against one of the natural vs. anthropogenic proxies identified above (Fig 2.9D). Chromium, as already suggested in Section 2.3.4, showed variations in enrichment factors between different volcanic sources due to different silicic to mafic compositions, as well as different urban areas due to different natural sources or enrichment from human activities. As different REE patterns were also useful for distinguishing between different natural source types, particularly differences in volcanic sources, La/Cr plots were assessed (Fig. 2.9E). The Pb/Al vs. Cr/Al, and Pb/Al vs. La/Cr plots showed no linear correlation and highlighted that anthropogenic sources were not the only controlling factor of Cr content in the sources from South America and Southern Africa. Cr/Al plots showed that the highest ratios were found in mafic to ultramafic sources or urban sources overlying mafic to ultramafic sources (aerosols from São Paulo, Johannesburg and kimberlitic formations from South Africa showed Cr/Al×1000 ratios of ~20 to 200, Fig. 2.9D). Lower ratios were exhibited in silicic to mafic sources or urban sources overlying silicic to mafic sources (natural sources from western and southern Africa and Buenos Aires showed Cr/Al×1000 ratios of 0.6 to ~20, Fig. 2.9D). The lowest

ratios were exhibited in silicic volcanic sources (e.g. silicic volcanics from the Andes from this study showed Cr/Al×1000 ratios of 0.003 to 0.05, Fig. 2.9D). The reverse can be stated for La/Cr with the exception that the most mafic to ultramafic sources from Southern Africa (kimberlitic formations SW of Johannesburg, Le Roex et al., 2003) and silicic/mafic sources from South America (Patagonia and Andean data, this study; GEOROC, 2003-2011) showed similar La/Cr compositions (Fig. 2.9E). Cr/Al and La/Cr plots were useful for discriminating between the urban sources São Paulo and Johannesburg from Buenos Aires (Fig. 2.9D-E). The Cr/Al and La/Cr plots further highlighted that the urban sources (São Paulo and Johannesburg) consisted of Cr that did not derive from the kimberlitic formations SW of Johannesburg. These plots were useful to distinguish between different volcanic sources, between South American rural and volcanic sources that show different mineral compositions, and discriminate between natural and anthropogenic sources and between South American and Southern African urban sources.

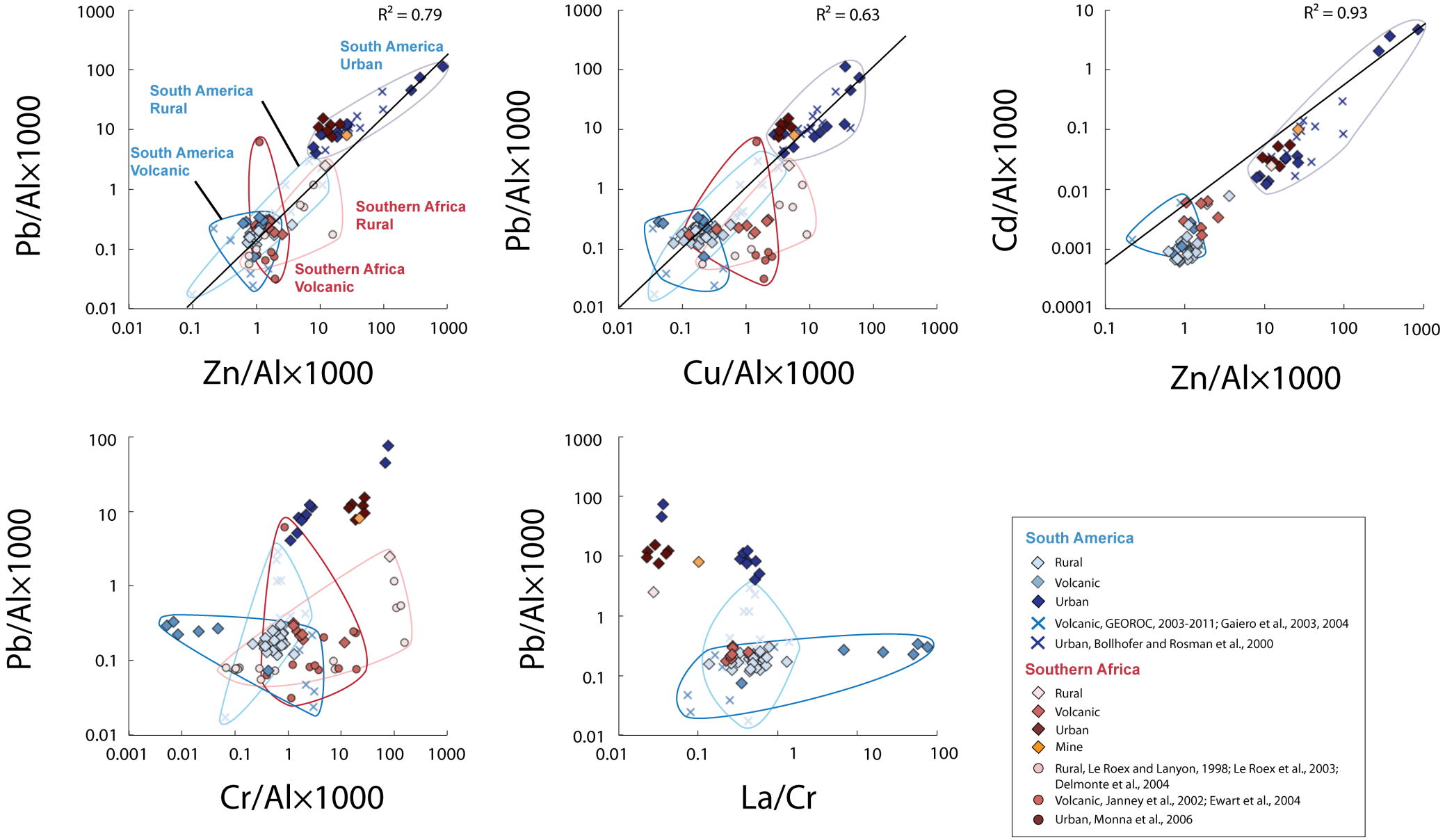

Figure 2.10. Bivariate plots of: (A) Pb/Al×1000 versus Zn/Al×1000; (B) Pb/Al×1000 versus Cu/Al×1000; (C) Cd/Al×1000 versus Zn/Al×1000; (D) Pb/Al×1000 verses Cr/Al×1000; (E) and Pb/Al×1000 verses La/Cr in major aerosol sources from South America and Southern Africa. Literature data were added where available denoted by cross symbols for South American sources and circle symbols for Southern African sources. Correlation (R^2, where 0 =no correlation and 1=direct correlation between two ratios) is shown in Pb/Al, Zn/Al, Cu/Al and Cd/Al (A-C). Errors are shown as 2σ, and are smaller than the symbols used.

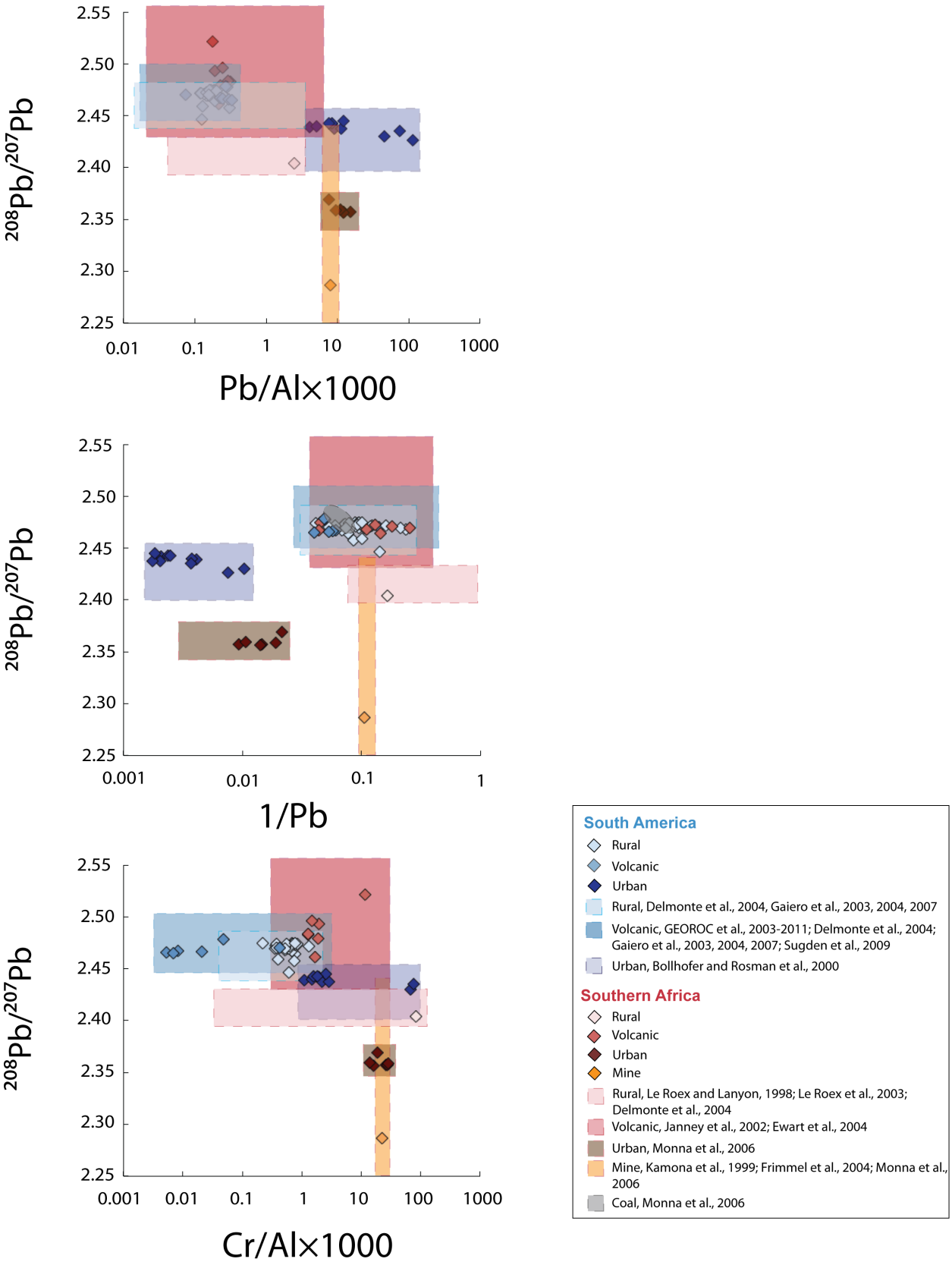

Figure 2.11. $^{208}Pb/^{207}Pb$ versus elemental ratios of: (A) Pb/Al×1000; (B) 1/[Pb]; (C) Cr/Al×1000; and εNd versus elemental ratios of (D) Pb/Al×1000; (E) 1/[Nd]; and (F) Cr/Al×1000 for all source areas. Shaded areas denote quantitative geochemical characterisation per source, which were determined from literature data and data from this study for each proxy. Errors are shown as 2σ, and are smaller than the symbols used.

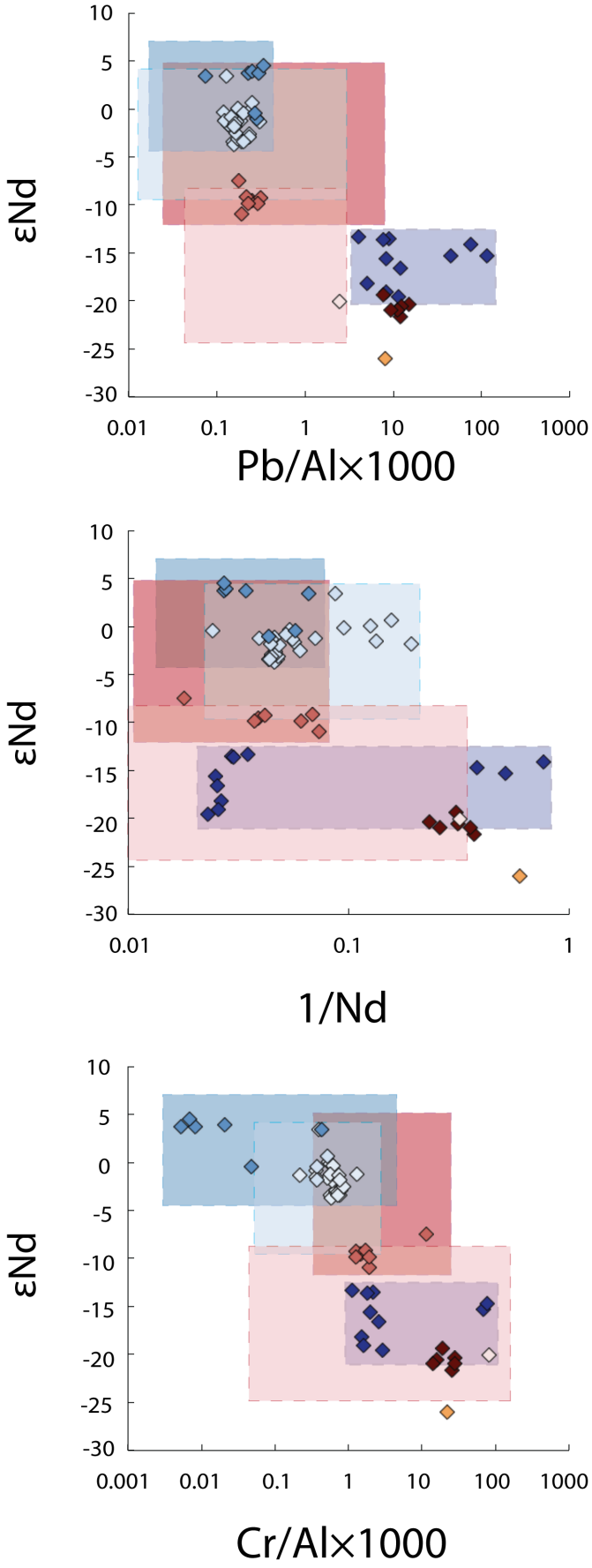

Figure 2.11. *continued*.

Table 2.7. Characteristic mineralogy, element and isotopic composition of major aerosol sources from South America and Southern Africa

Proxy	**South America**		**Southern *Africa***	
	Natural	***Anthropogenic***	***Natural***	***Anthropogenic***
Mineralogy			Mafic to ultramafic minerals, carbonates, evaporates (rural)[*1]	
	Clays, carbonates, plagioclase (rural)			
	Amphiboles and chlorite (volcanic)	Sulfates, calcites, iron-oxides (urban)	Mafic to ultramafic minerals (volcanic)[*1]	
EF_{crust}				
REE	0.1-3, Flat to enriched HREE profile (rural, volcanic)	0.7-10, Flat to enriched LREE profile (urban)	0.1-100, Flat to enriched LREE profile (rural)	1-2, Flat profile (urban)
			0.4-8, Flat to enriched LREE profile (volcanic)	3-6, enriched LREE profile (mine)
Trace element	0.07-15 (rural)	10-5000 in Cu, Pb, Cd, Zn,	0.1-80, with exception of Cr, Ni and Co which reach EF of 2000 (rural)	0.3-300 (urban)
	0.1-10, with exception of Cr, Ni and Th which reach EF of 0.01 (volcanic)	1-10 in Cr, Ni, Co, V, Sc, Y, Th (urban)	0.1-30 (volcanic)	10-100 in Cu, Pb, Cd, Zn Cr, Ni, Co, 3-8 in V, Sc, Y, Th (mine
Element ratio				
Pb/Al×1000	0.015-4 (rural)	4-150 (urban)	0.06-4 (rural)	7-20 (urban)
	0.02-0.5 (volcanic)		0.03-8 (volcanic)	9-10 (mine)
Cd/Al×1000	0.0007-0.01 (rural)	0.01-8 (urban)	0.03-0.04 (rural)	0.02-0.08 (urban)
	0.0008-0.01 (volcanic)		0.001-0.009 (volcanic)	0.09-0.1 (mine)
Zn/Al×1000	0.8-6 (rural)	8-1000 (urban)	10-20 (rural)	9-30 (urban)
	0.2-2 (volcanic)		1-4 (volcanic)	40-50 (mine)
Cr/Al×1000	0.08-4 (rural)	0.9-100 (urban)	0.06-200 (rural)	10-70 (urban)
	0.003-5 (volcanic)		0.6-4 (volcanic)	20-40 (mine)
La/Cr	0.1-2 (rural)	0.05-0.8 (urban)	0.03-0.04 (rural)	0.02-0.06 (urban)
	0.07-100 (volcanic)		0.2-0.6 (volcanic)	
Element concentration (µg/g)				
1/[Pb]	0.035-4 (rural)	0.002-0.015 (urban)	0.08-0.9 (rural)	0.004-0.03 (urban)
	0.03-6 (volcanic)		0.06-0.55 (volcanic)	0.1-0.15 (mine)
				0.07-0.1 (coal)*
1/[Nd]	0.03-0.3 (rural)	0.03-0.8 (urban)	0.01-0.5 (rural)	0.3-0.6 (urban)
	0.015-0.08 (volcanic)		0.01-0.08 (volcanic)	0.7-0.8 (mine)
Isotope composition				
$^{208}Pb/^{207}Pb$	2.447-2.474 (rural)	2.394-2.452 (urban)	2.404-2.421 (rural)	2.330-2.370 (urban)
	2.455-2.446 (volcanic)		2.439-2.549 (volcanic)	<2.250-2.450 (mine)
				2.469-2.485 (coal)[*2]
$^{206}Pb/^{207}Pb$	1.173-1.210 (rural)	1.119-1.204 (urban)	1.138-1.141 (rural)	1.050-1.120 (urban)
	1.119-1.212 (volcanic)		1.125-1.315 (volcanic)	1.100-2.900 (mine)
				1.205-1.219 (coal)[*2]
εNd	-8.9 to +3.4 (rural)	-22 to -13 (urban)	-24 to -8.4 (rural)	-23 to -18 (urban)
	-4.2 to +6.1 (volcanic)		-11 to +4.7 (volcanic)	-26 ±0.3 (mine)

* Data taken solely from literature - [1] Tovher et al., 2009, Begg et al., 2009; [2] Monna et al., 2006

2.3.10. Provenance tracers of atmospheric particulate sources using select element vs. isotopic signatures

Table 2.7 summarises the geochemical proxies identified for characterising and distinguishing the aerosol sources from one another. The most useful of which are illustrated in Figure 2.11 where symbols denote data from this study and shaded areas denote the quantitative geochemical constrain of a proxy for each source (using data from this study and the literature discussed in 2.3.3 to 2.3.6). As described in Section 2.3.5, the major urban sources from South America derived from urban regions north of ~45°S. These sources were illustrated in Fig. 2.11 to represent the most likely urban sources of aerosols from South America to reach the South Atlantic Ocean.

The $^{208}Pb/^{207}Pb$ vs. Pb/Al and 1/[Pb] plots were suitable proxies for distinguishing between natural (rural and volcanic) and anthropogenic (urban) sources in South America. There were no Pb/Al data for coal sources from Southern Africa, however $^{208}Pb/^{207}Pb$ ratios for coal sources from Southern Africa (Monna et al., 2006; shown in Fig. 2.7) overlap with $^{208}Pb/^{207}Pb$ ratios of volcanic sources from Southern Africa. This suggested that $^{208}Pb/^{207}Pb$ vs. Pb/Al were useful to discriminate between natural and specific anthropogenic sources (rural, volcanic and coal) from other anthropogenic sources (urban and mine) from Southern Africa (Fig. 2.11A). The $^{208}Pb/^{207}Pb$ vs. Pb/Al and 1/[Pb] plots were useful to discriminate between the major South American urban sources from Southern Africa urban sources (Fig. 2.11A and B). The $^{208}Pb/^{207}Pb$ vs. Pb/Al plot was also useful to distinguish between the natural sources from South America and Southern African from the anthropogenic sources from South America and Southern Africa, most likely with the exception of coal sources from Southern Africa (Fig. 2.11A). The $^{208}Pb/^{207}Pb$ vs. 1/[Pb] plots were suitable for characterising volcanic and coal sources from rural and mine sources from urban sources from Southern Africa (Fig. 2.11B). This plot also separated the Southern African rural, volcanic, mine and coal sources, from the urban sources from South America (Fig. 2.11B).

The ratios Zn/Al, Cu/Al, Cd/Al, and La/Cr, were omitted from Fig. 2.11 but each showed similar characteristics to $^{208}Pb/^{207}Pb$ vs. Pb/Al, and $^{208}Pb/^{207}Pb$ vs. Cr/Al (for La/Cr only). The $^{208}Pb/^{207}Pb$ vs. Cr/Al plot was useful to discriminate between urban sources from Southern Africa and natural and anthropogenic sources from South America (Fig. 2.10C).

The εNd vs. Pb/Al, 1/[Nd] and Cr/Al plots (Fig. 2.11D-F) were suitable for distinguishing between natural (rural and volcanic) and anthropogenic (urban) sources in South America. They were also useful for discriminating volcanic from urban and mine sources from Southern Africa (Fig. 2.11D-E). The εNd vs. Pb/Al plot was useful for distinguishing rural from urban and mine sources from Southern Africa (Fig. 2.11D-F). The 1/[Nd] ratios were useful to distinguish between the urban sources from South America and showed lower values in road dusts from Buenos Aires (0.03 to 0.05) than from São Paulo (0.5 to 1) (Fig. 2.10E). Lastly the $^{208}Pb/^{207}Pb$ and εNd vs. Cr/Al, similar to the Pb/Al vs. Cr/Al plot in Fig. 2.10 was useful to discriminate within sources dependent on the silicic to ultramafic composition of the source (Fig. 2.11C and F).

2.4. Conclusions

Samples from major aerosol sources in South America and Southern Africa were analysed for their mineralogical, elemental and Pb and Nd isotopic composition. The goal of this study was to provide a geochemical framework of elemental and isotopic characteristics and provenance indicators for the accurate provenance tracing of aerosols from these different sources, with a particular emphasis on the tracing of aerosols transported to the South Atlantic Ocean. The main conclusions are:

1. The element and isotopic composition of shelf sediment were similar to the volcanic sources from Southern Africa and were used to represent these volcanic sources. These data were particularly useful where there was limited literature data for element composition for volcanic sources from Southern Africa.

2. The element and isotopic composition of select natural (rural and volcanic) source samples from South America showed some variation between the bulk and fine fraction. A clear example; the εNd values showed a maximum range of ±5.0 epsilon units, which is large on a geological scale. However these differences were within or similar to the element and isotopic compositions of previously analysed natural sources from South America (Gaiero et al. 2003, 2004, 2007; GEOROC et al., 2003-2011; Delmonte et al., 2004; Sugden et al., 2009). Thus, particle size had negligible effect on the element and isotopic characterisation of natural sources from South America and most likely has negligible effect on the characterisation of anthropogenic sources from South America and natural and anthropogenic sources from Southern Africa. The following element and isotopic geochemical constrains represent fine and bulk data analyses for natural and anthropogenic sources from South America and Southern Africa which are summarised in Table 2.7.

3. Minerals characteristic to natural (amphiboles, chlorites and carbonates, rural sources-Patagonia, and volcanic sources-Andean volcanic belt) and anthropogenic sources (sulfates, calcites and iron-oxides, urban sources north of ~45°S in Brazil and Argentina, including São Paulo and Buenos Aires) from South America were useful to distinguish these sources. Although mineralogy was not analysed in samples from Southern Africa, underlying geology revealed that Southern African sources were distinguishable from South American sources by mafic to ultramafic mineralogy as well as meta-sedimentary mineralogy such as olivine, pyroxenes and carbonates (volcanic, plutonic and sedimentary basin geology, Condie and Hunter, 1976; Le Roex and Lanyon, 1998; Janney et al., 2002; Le Roex et al., 2003; Ewart et al., 2004; Tovher et al. 2006; Begg et al. 2009).

4. Major element enrichment compositions of sources reflected their mineralogy. Despite the differences in mineralogy between different sources, the major element enrichment profiles were similar between all sources, generally ranging between an enrichment factor of 0.1 and 10, relative to the upper continental crust (Taylor and McLennan, 1985), and thus were not useful for distinguishing between different sources. It was worth noting that K_2O enrichment is an indication of biomass burning. The absence of K_2O enrichment in all samples suggested that biomass burning was not a main anthropogenic aerosol source from South America and Southern Africa, as proposed by Chin et al. (2009).

5. Natural and anthropogenic sources from South America were discriminable by REE enrichment profiles relative to the upper continental crust by flat to HREE enrichment (La/Yb ratio of 5.1 to 28.7, enrichment factor between 0.2 and 3) and a range of Eu anomalies (Eu* 0.49 to 3.22) in natural sources compared to flat to LREE enrichment patterns (La/Yb ratio of 10.8 to 112, La enrichment up to 10) in the anthropogenic sources. There were different REE enrichment profile patterns within the rural and volcanic sources from Southern Africa ranging from compositions similar to the continental crust to very high LREE enrichment (La/Yb ratio of 9.1 to 206, La enrichment up to 200). However it was not possible to discriminate between the natural (rural, volcanic) and anthropogenic (urban, coal and mine) sources from Southern Africa by REE enrichment patterns due to overlapping enrichment profiles.

6. Volcanic sources could be characterised from rural sources due to variable Cr and Ni enrichments relative to the crust ranging between 0.01 and 10. These variations were dependent on the silicic to mafic composition of the volcanic sources. The anthropogenic sources from South America were most discriminable from the natural sources from South America by high enrichments in select trace elements (between ~ 1 and 1000 in Cu, Pb, Zn, ~1 and 5000 in Cd, and ~ 1 and 100 in Cr, Ni Co and V). The high trace element enrichments were most likely due to anthropogenic sources such as industrial processes, traffic emissions and oil combustion. The urban sources from Southern Africa revealed a similar trace element enrichment composition to aerosols from one South American anthropogenic source (Buenos Aires), except for high Cr enrichment, which was similar to another South American anthropogenic source (aerosols from São Paulo). Generally trace element enrichment relative to the continental crust overlapped between natural and anthropogenic (rural, volcanic, urban and mine) sources from Southern Africa, however select element enrichment compositions were characteristic of sources. Lead and Cr were enriched in anthropogenic sources (between 20-80) compared to select natural sources (0.1-10). These comparisons showed that Pb and Cr were useful to discriminate between natural and anthropogenic sources in Southern Africa.

7. The natural sources from South America showed radiogenic $^{208}Pb/^{207}Pb$ and εNd isotopic compositions (2.447-2.555, and -8.9 to +6.1, respectively), which were discriminable from less radiogenic anthropogenic sources from South America (2.394-2.452 and -22 to -13, respectively). $^{208}Pb/^{207}Pb$ and εNd compositions were useful to distinguish between the volcanic sources from Southern Africa (2.439-2.549 and -11 to +4.7, respectively) and the less radiogenic rural source from Southern Africa (2.404-2.421 and -24 to -8.4, respectively). The natural sources from Southern Africa were distinguishable from less radiogenic Pb isotopes in urban sources from Southern Africa ($^{208}Pb/^{207}Pb$ of 2.330-2.370). Previously determined Pb isotope ratios from coal and mine sources from Southern Africa (Kamona et al., 1999; Frimmel et al., 2004; Monna et al., 2006) were in line with volcanic and rural sources from Southern Africa, respectively. This suggested that $^{208}Pb/^{207}Pb$ and εNd isotopic compositions were useful to distinguish between different natural (rural from volcanic) and some anthropogenic (urban, mining from coal) sources within Southern Africa. It was difficult to discriminate natural and anthropogenic sources within Southern Africa, and between South America and Southern Africa, due to overlapping Pb isotopic ratios in aerosol sources. It is worth noting that the characterised urban source areas reflected the leaded gasoline element and isotopic signal at the time of sample collection, before the ban of leaded fuel in Southern Africa. Bollhofer and Rosman (2000) suggested mine and coal sources were the dominant anthropogenic aerosol sources after leaded gasoline was phased out. This implies that the isotopic signal of the urban source areas, at present day, would most likely fall between the isotopic compositions of the mine and coal sources from Southern Africa.

8. The major natural and anthropogenic sources in South America were well distinguished in $^{208}Pb/^{207}Pb$, Pb/Al, 1/[Pb], Zn/Al, Cd/Al, Cu/Al, Cr/Al, La/Cr, and $^{208}Pb/^{207}Pb$ vs. εNd, εNd vs. Pb/Al, 1/[Nd], Cr/Al and La/Cr plots. The volcanic sources were well discriminated from the rural, urban and mine source areas from Southern Africa by the same proxies except in 1/[Pb] plots. The $^{208}Pb/^{207}Pb$ vs. 1/[Pb] plot enabled the discrimination of volcanic and coal from rural and mine, and from urban source areas in Southern Africa. This plot also distinguished between the major South American urban sources from natural sources from Southern Africa. The ratios $^{208}Pb/^{207}Pb$ vs. Pb/Al and 1/[Pb] were also useful to distinguish between South American and Southern African major urban source areas. Lastly, Cr/Al and La/Cr ratios highlighted differences in element composition within rural, volcanic and urban sources from South America and Southern Africa, and the 1/[Nd] ratio were useful to discriminate between the urban sources from South America.

9. Due to the similar geologies found in South America and Southern Africa (de Almeida et al., 2000; Bertolo et al., 2011; de Campos, 2012; Guarino et al., 2012; de Brito Neves et al., 2013), this study revealed that the elemental and isotopic compositions of natural or anthropogenic sources that overlie similar geologies often showed similar compositions, which limited the use of geochemical

proxies for provenance tracing of aerosols from South America and Southern Africa. This study did not identify proxies that could discriminate all South American sources from all Southern African sources. More up-to-date data of aerosol sources is required to further improve the geochemical constrains of the most important natural and anthropogenic aerosol sources from South America, and particularly Southern Africa.

CHAPTER 3

Spatial distribution and sources of major, trace and rare earth elements in aerosols along the GEOTRACES South Atlantic transect GA10 at 40°S

3.1. Introduction

Atmospheric deposition has been proven to be a crucial source of essential elements for high nitrate low chlorophyll (HNLC) ocean regions (Martin and Fitswater, 1988; Coale et al., 1991; Boyd et al., 2000). HNLC regions make up ~30% of the Earth's oceans and suggests that atmospheric inputs to the ocean can play a major role in regulating primary productivity and in turn atmospheric the carbon cycle and climate (Martin et al. 1990; Zhuang et al., 1992; Galloway et al., 2004; Jickells et al., 2005). The southern South Atlantic region, along and south of ~40°S, is one of three main HNLC regions and is suggested to be the largest region where marine productivity is limited by the micronutrient iron (Fe) (Martin et al., 1990; Boyd et al., 2000; Mahowald et al., 2005).

Many studies of atmospheric deposition to the oceans have focused on Fe removal from dust, due to iron's main role as a fertiliser (Martin et al., 1990). However the addition of aerosols of differing origin and composition can vary elemental chemistry and consequently element solubility (Baker et al., 2006; Paytan et al., 2009). This can result in phytoplankton responses ranging from fertilisation to unfavorable toxic effects (Paytan et al., 2009). Recent studies showed higher levels of Fe solubility into seawater from anthropogenic aerosols (up to 80%) than from mineral dust from the Saharan desert (up to a few %) (Mahowald et al., 2005; Sholkovitz et al., 2009). With ever growing megacities in the Southern Hemisphere, anthropogenic sources may be more important than natural sources of aerosols that reach the South Atlantic Ocean (Mahowald et al., 2005).

Despite the large implications that aerosols over the remote South Atlantic (along ~40°S) may have for the marine micronutrient budget, in particular anthropogenic contributions, little is known of the geochemical characteristics of these aerosols. This is due to difficulties with obtaining field measurements from remote regions of the South Atlantic Ocean and difficulties with measuring low element concentrations in aerosol samples. For example, aerosols collected over remote regions of the South Atlantic and Indian Ocean showed element concentrations similar to the blank filters used for aerosol collection or close to limit of detection of analytical procedures (Baker et al., 2006, 2013; Witt et al., 2006, 2010). In comparison, there are numerous studies of aerosol provenance and aerosol geochemical characterisation for the North Atlantic Ocean (Radlein and Heumann, 1992; Greaves et al., 1994; Mahowald et al., 2005; Baker et al., 2006, 2010, 2013; Witt et al., 2006; 2010; Sholkovitz et al., 2009; Jimenez-Velez et al., 2009; Buck et al., 2010) and other neighbouring oceans such as the Indian Ocean and Pacific Ocean (Arimoto et al., 1987; Chester et al., 1991) where atmospheric circulation patterns are better understood or aerosol deposition is more abundant.

The major element enrichment relative to the upper continental crust have been analysed in aerosols collected over the South Atlantic between 2001-2005 (Witt et al., 2006; Evangelista et al., 2010; Baker et al., 2013). These were similar to the continental crust in most studies (Witt et al., 2006; Baker et al., 2013). Where air mass back trajectory analysis had been conducted, these suggested aerosols derived

from Patagonian dust sources and reached the east coast of South America between 40-60°S within 5 days (Witt et al., 2006), and reached the open ocean at ~25°S, 36°W within 8 days (Baker et al., 2006). One study showed Fe enrichment above the upper continental crust in aerosols collected close to South American cities (between 25-38°S) (Evangelista et al., 2010) but air mass back trajectories that passed northwards over southern South America implied that enriched dusts from Patagonia accounted for these elevated Fe levels rather than anthropogenic sources from South American cities (Evangelista et al., 2010).

Aerosols collected between 2001-2002 showed enriched levels of trace metals close to anthropogenic regions along the west and east margins of the South Atlantic, but not over the open ocean (Witt et al., 2006). Air mass back trajectories suggested air masses passed over major anthropogenic regions of South America (cities from Brazil and Argentina, as acknowledged by Bollhofer and Rosman, 2000), and implied that aerosols collected between 30-45°S derived from anthropogenic origins (Witt et al., 2006).

Lead (Pb) isotopic ratios have been measured in aerosols from across the South Atlantic and were more varied in open ocean areas of the South Atlantic, which were attributed to a number of different regions contributing to the lead signal (Witt et al., 2006). Lead isotopic ratios of the aerosols collected along the South American coast between 30-45°S (Alleman et al., 2001; Witt et al., 2006) tended to cluster more closely together and were similar to those reported for South American cities (Bollhofer and Rosman, 2000). Aerosols between the equator and ~15°S and 15°W along the western coast of Africa received air masses from southwest Africa (Witt et al. 2006). Lead isotopic ratios, which were similar in the aerosols and mining and coal sources from Southern Africa, suggested mining and coal burning were the main anthropogenic sources of lead (Witt et al., 2006).

The above previous studies on element and Pb isotopic ratios in aerosols highlighted that element enrichment relative to the crust, Pb isotopic composition, and air mass back-trajectory analysis were useful tracers of sources of aerosols. One other method for provenance tracing of aerosols is the use of neodymium (Nd) isotopes. As described in Chapter 2, neodymium is a valuable tracer of different natural sources due to the correlation of the $^{144}Nd/^{143}Nd$ isotope with age of geological formations (Jacobsen and Wassenburg, 1980).

Identifying the sources of aerosols over the South Atlantic Ocean, with particular interest in the HNLC region of the ocean, provides scientists with a better understanding of the controls of natural and anthropogenic contributions on aerosol compositions, and determining sources by geographical location. This information is valuable for understanding the implications aerosols over the South Atlantic may have on air quality over the continent and the ocean, atmospheric transport pathways of aerosols over the ocean, and the potential impact aerosols may have on the element budget in the surface waters of the South Atlantic Ocean.

This study aimed to determine the provenance of aerosols along 40°S of the South Atlantic Ocean and assess the relative importance of natural vs. anthropogenic sources of aerosols from South America and Southern Africa to the South Atlantic. These aims were addressed by: i) determining the major (Al, Ca, Fe, K, Mg, Mn), trace (Cd, Co, Cr, Cu, Ni, Pb, Sc, Th, V, Y, Zn), and rare earth elements (REE), as well as Pb and Nd isotopic compositions of aerosols collected on two cruises along 40°S in the South Atlantic (D357/GA10E and JC068/GA10W) in 2010 and 2011/12 respectively; ii) calculating the enrichment relative to the upper continental crust (UCC) of aerosols and comparing them to air mass back-trajectories of the aerosol sampling locations, potential source areas (as identified in Chapter 2), and previous literature data of aerosols determined across the South Atlantic and neighbouring oceans, to determine the provenance of aerosols, iv) where possible, calculating contributions of elements in aerosols across the transect, and v) assessing the temporal changes if any in aerosol composition over the South Atlantic to suggest implications aerosol sources may have on air quality and atmospheric transport of aerosols to the South Atlantic Ocean.

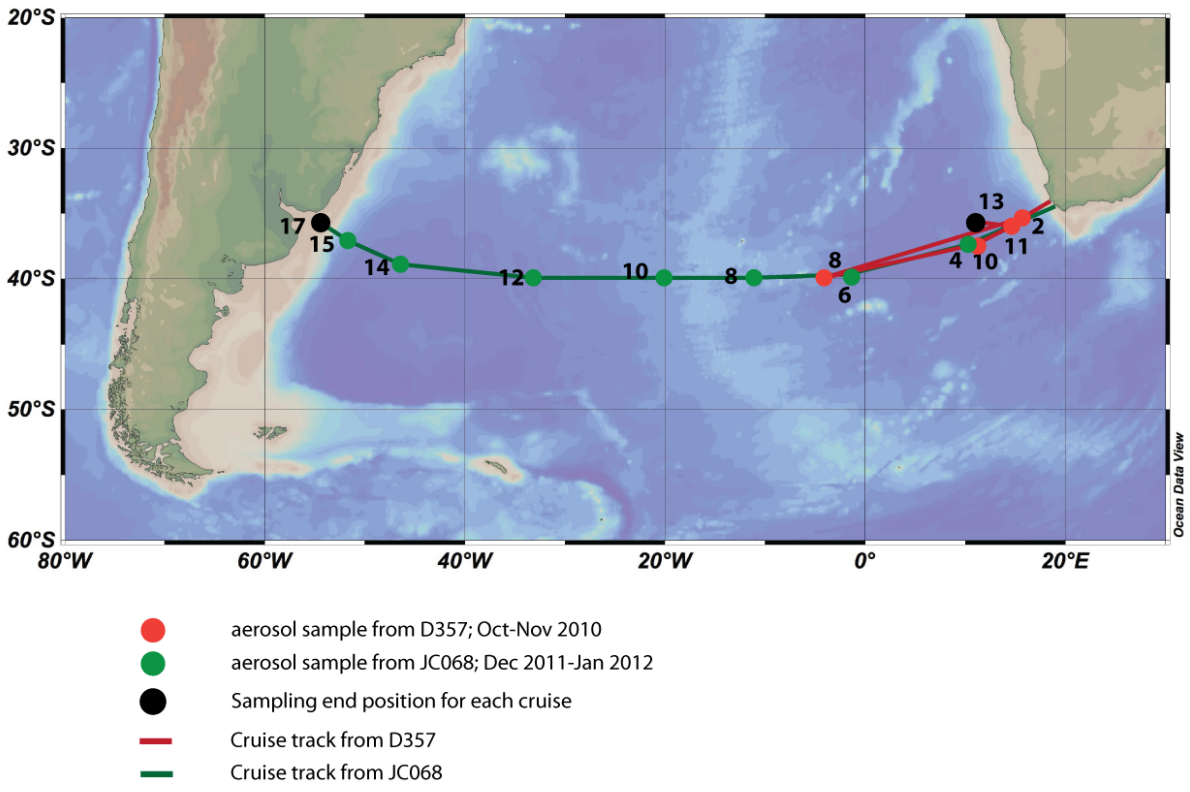

Figure 3.1. Aerosol sampling locations for cruises D357 (red symbols) and JC068 (green symbols). Aerosol sample numbers correlate to sample ID numbers in Table 3.1 and 3.2. Map provided by Schlitzer, R., Ocean Data View, http://odv.awi.de, 2013.

3.2. Sampling and Methods

3.2.1. Aerosol sampling

Aerosol sampling was conducted between 18th October and 22nd November 2010 during cruise D357 on the RRS Discovery, and between 27th December 2011 and 27th January 2012 during cruise JC068 on the RRS James Cook. Cruise tracks and aerosol sampling locations are shown in Figure 3.1 and listed in Tables 3.1 and 2. In brief, the D357 cruise departed from Cape Town (South Africa) and sailed westward up to ~5°W along 40°S before returning back to Cape Town. JC068 also departed from Cape Town but sailed along 40°S across the South Atlantic to Montevideo (Uruguay).

Aerosol collection methods, including preparation of filters, followed the routine procedures previously described in detail (Baker et al., 2003, 2006a; Jickells et al., 2003; Sarthou et al., 2003). In brief, aerosols were typically collected over a ~4 day period onto cellulose Whatman 41 filters (A4-sized) using a high-volume sampler (Graseby Anderson, at $1 m^3 min^{-1}$) mounted on the top deck of the ship in-front of the ships funnel. Samples were collected onto a single filter; thus aerosol samples consist of bulk (coarse and fine) fractions. Coarse particles are generally derived from physical processes (e.g. sea spray generation or desert dust re-suspension), while fine mode particulates are formed from gas-particle conversion processes (e.g. aerosol formation from combustion gases) (Baker et al., 2006). Filters were acid-washed before use on the ship (Baker et al., 2006b; Sarthou et al., 2003), rinsed with liberal amounts of ultrapure water after each soak, and dried overnight under a laminar flow bench before being sealed in zip-lock plastic bags. Aboard the ship all filter handling was carried out using a laminar flow bench. Exposed filters were transferred to individual zip-lock plastic bags immediately after collection, and stored frozen until analysis at Imperial College London. Ships' crew and scientific party continuously monitored sample collection, and the collectors were switched off during ship exhaust checks and under unfavourable wind conditions so that the risk of sample contamination from sources on the ship was minimised (Baker et al., 2003, 2006b; Jickells et al., 2003; Sarthou et al., 2003).

Table 3.1. Location of aerosol sample collection from UK GEOTRACES transect GA10 (D357 cruise; eastern South Atlantic)

	Start position			End position			
Sample ID	**Start date**	**Latitude (° ' ")**	**Longitude (° ' ")**	**End date**	**Latitude (° ' ")**	**Longitude (° ' ")**	**Air volume (m^3)**
D357-2	18/10/2010	34 20.40 S	17 38.45 E	22/10/2010	36 30.79 S	13 10.27 E	5173
D357-8	27/10/2010	40 02.02 S	05 31.69 E	31/10/2010	40 00.01 S	02 30.73 E	4743
D357-10	03/11/2010	37 43.59 S	3 45.29 E	06/11/2010	34 03.85 S	18 04.36 E	1633
D357-11	09/11/2010	34 25.01 S	17 30.21 E	13/11/2010	37 25.45 S	11 20.54 E	5282
D357-13	13/11/2010	37 43.54 S	10 45.17 E	17/11/2010	37 26.45 S	11 36.89 E	5422

Table 3.2. Location of aerosol sample collection from UK GEOTRACES transect GA10 (JC068 cruise; South Atlantic along 40°S)

	Start position			End position			
Sample ID	**Start date**	**Latitude (° ' ")**	**Longitude (° ' ")**	**End date**	**Latitude (° ' ")**	**Longitude (° ' ")**	**Air volume (m^3)**
JC068-4	28/12/2011	35 08.69 S	15 47.25 E	01/01/2012	40 00.03 S	4 50.64 E	5162
JC068-6	01/01/2012	39 59.96 S	4 39.84 E	05/01/2012	39 57.59 S	6 18.87 W	5377
JC068-8	05/01/2012	39 56.25 S	6 33.63 W	09/01/2012	39 59.49 S	15 23.67 W	5534
JC068-10	09/01/2012	40 00.03 S	16 03.14 W	13/01/2012	39 59.99 S	24 19.52 W	5471
JC068-12	13/01/2012	40 00.00 S	24 47.55 W	18/01/2012	39 59.90 S	41 54.76 W	4918
JC068-14	18/01/2012	39 5986 S	42 01.89 W	22/01/2012	38 02.53 S	50 59.56 W	5267
JC068-15	22/01/2012	38 00.10 S	50 59.95 W	25/01/2012	36 31.33 S	52 29.48 W	2437
JC068-17	26/01/2012	36 31.33 S	52 29.48 W	28/01/2012	36 S	55 W	1219

3.2.2. Total digestion of aerosols and separation of lead and neodymium for isotopic analysis

Sample treatment in the laboratory was carried out under uniform light conditions in a laminar flow hood. Ultrapure acids and ultraclean (MQ) water were used throughout all sample preparation stages. Filters were cut into quarters using acid-cleaned ceramic-bladed scissors, after visual inspection to guarantee sample homogeneity. One quarter of the filter was subsequently placed into pre-cleaned 14.7 ml screw top Savillex PTFE vessels and treated with a mixture of 3 ml concentrated $HClO_4$ (11 M) and 1.5 ml concentrated HNO_3 (15.6 M) on a hotplate for 1 to 3 hours at 90°C, and 1 hour each at 110°C, 140°C, 180°C and 220°C in order to remove organics. The Savillex vials were uncapped throughout this procedure. The samples were then digested on a hotplate for 48 hours in a mixture of 2 ml concentrated HF 30 M and 0.5 ml 15.6 M HNO_3 at 120°C with daily ultrasonic treatment according to the digestion method described by Yu et al. (2001). Samples were then evaporated to dryness and re-fluxed twice in 0.5 ml 15.6 M HNO_3 to dissolve any fluorides that may have formed due to excess HF, as insoluble fluorides will affect REE recovery. After digestion, all samples were dissolved into 2.5 ml ca 0.8 M HNO_3. One and a half millilitre were reserved for Pb and Nd isotope work and 1 ml was further diluted to 2 ml ca 0.8 M HNO_3 for elemental concentration analysis.

Lead was separated from the sample matrix by ion exchange chromatography using Eichrom Sr spec resin following the procedure outlined by Weiss et al. (2004). Neodymium was isolated using a two-step column procedure. First, a REE fraction was separated from the sample matrix using Eichrom TRU spec resin, followed by isolation of the Nd fraction from the other REE using Eichrom LN spec resin on volumetrically calibrated Teflon columns following the procedures outlined by Pin and Zalduegui (1997).

3.2.3. Element and isotopic analysis

Major element concentrations as well as REE, Cd, Co, Cr, Cu, Ni, Pb, Zn, V, Sc, Th, and Y concentrations were determined by quadrupole inductively coupled plasma mass spectrometry (Q-ICP-MS) using an Agilent 7700x located at the Natural History Museum (NHM) in London.

Using the same procedures as followed in Chapter 2, quantitative dissolution and data quality was monitored with the certified USGS reference material G-2 granite (n=12) and listed in Tables 3.3 to 3.5. Lead and neodymium isotopic compositions were analysed on a Nu Plasma (Nu Instruments Limited, UK) multiple collector inductively coupled plasma mass spectrometer (MC-ICP-MS). The samples were introduced with a Nu Instruments DSN-100 Desolvation Nebulizer System and PTFE nebulizer.

3.2.4. Determining filter blanks of elements

The aerosol sampling collection method introduces a significant procedural blank, and determining concentrations and isotopic compositions of the blank introduced by high-volume collector aerosol samplers is challenging (Baker et al., 2006a).

There were different types of blank filters, (i) an acid cleaned filter stored in a plastic bag, taken to sea, but never opened at sea, (ii) a cleaned filter placed in the cassette holder of the sample collector, without however exposing it to the atmosphere, (iii) a cleaned filter fitted into the sampler, exposed to the atmosphere for ~4 days, without switching on the motor of the collection unit, and (iv) a cleaned filter fitted into the sampler, exposed to the atmosphere for ~1 minute while the motor was switched on. The average blank contribution of each element in aerosol samples was determined by subtracting the mean of different types of filter blanks ($A_{B,}$ in g per filter) from the instrument measured aerosol sample ($A_{M,}$ in g per filter) to give the element mass in the aerosol sample (A_S, in g per filter) (1).

$$A_S = A_M - A_B \quad (1)$$

For the blank filter for the D357 cruise, these blank values in µg per filter were 8.1 ±7.1 (Al), 4.5 ±3.1 (Fe), 0.8 ±0.6 (Ca), 2 (K), 3.1 ±2.0 (Mg), 0.1 ±0.1 (Mn), 36 (Na), 0.1 ±0.1 (Ni, Cu), 0.01 ±0.03 (V), 1 ±1 (Zn, Cr), <0.01 ±0.006 (Pb, Y), 0.003 (Co), 0.001 ±0.0003 (Cd), and <0.005 ±0.006 (Sc, Th, REE). For the blank filter for the JC068 cruise, these blank values in µg per filter were 4.2 ±1.7 (Al), 7.1 ±3.9 (Fe), 0.8 ±0.4 (Ca), 2 (K), 1.1 ±0.4 (Mg), 0.1 ±0.1 (Mn), 25 ±3.5 (Na), 0.1 ±0.08 (Ni, Cu), 0.1 ±0.009 (V), 0.5 ±0.03 (Zn), 1 ±0.2 (Cr), 0.02 ±0.01 (Pb), 0.01 ±0.002 (Y), 0.008 ±0.009 (Co), 0.001 (Cd), and <0.006 ±0.001 (Sc, Th, REE).

3.2.5. Calculating atmospheric concentrations

Element mass in the aerosol per filter was converted into an atmospheric concentration (X_S, in g per m^3) by dividing by the volume of air (V, in m^3) that was filtered for each sample (2), as previously described by Baker et al. (2006a).

$$X_S = A_S / V \quad (2)$$

The major element atmospheric concentrations (X_S) were further corrected for sea spray contribution of major elements in the aerosol sample, to give (X_{Scorr}, in g per m^3) by equation (3). The component's sea spray-derived atmospheric concentration was calculated by multiplying the sodium concentration in the aerosol (Na^+_S, in g per m^3) with the ratio of the component relative to sodium in seawater (X_{sea}/Na^+_{sea}, in ppm/ppm, taken from Turekian, 1968). This was then subtracted from the non-corrected components' atmospheric concentration (X_S) from equation (2).

$$X_{Scorr} = X_S - (Na^+_S \times (X_{sea}/Na^+_{sea})) \quad (3)$$

Sea spray contributed <1 w/w% in Ca, Mg and K in aerosols, and <0.001 w/w% in Al, Fe and Mn in aerosols. Trace and rare earth element concentrations were not corrected due to the negligible contribution (<0.0001 w/w%) from sea spray in aerosols.

The uncertainty in atmospheric concentration due to the range in blank contribution per element was used to represent the uncertainty in atmospheric concentration. This uncertainty is expressed in Table 3.3 to 3.5. This uncertainty was combined with the uncertainty introduced by the digestion procedure (represented by the element concentration uncertainty in G2 samples) and analytical method (uncertainty introduced by ICP-AES or Q-ICP-MS analysis) to give the analytical uncertainty in atmospheric concentration, and was expressed in Tables 3.3 to 3.5.

3.2.6. Calculating enrichment factors

Element enrichment factor relative to the continental crust are calculated by normalising the sea spray-corrected atmospheric concentrations by the element composition in the upper continental crust (UCC, values taken from Taylor and McLennan). Similarly to Chapter 2, aluminium was used as the reference element for major, REE and trace elements, assuming Al in aerosols is derived largely from continental

dust (Loring et al. 1991). The ratio of the element to Al in the aerosol (taken from atmospheric concentration (g m^{-3}) was divided by the ratio of the element to Al in the UCC (in μg g^{-1}).

The uncertainty in enrichment factors was calculated from combining the uncertainty in atmospheric concentration for the element of interest and Al with the uncertainty introduced by the digestion procedure. This uncertainty is expressed in Figures 3.3 to 3.5.

3.2.7. Correcting lead and neodymium isotope ratios in aerosols

Lead and Nd isotopic ratios of measured aerosol samples (R_M) were blank corrected, to give (R_S), by subtracting the fraction (*f*) of element contribution from blank (mass per filter, i.e. for Pb, Nd) multiplied by the isotopic composition of the element in the blank (R_B) divided by the fraction of sample contribution of element (1-*f*) (4). The fraction of the element contribution from the blank was calculated by diving the mean of different types of filter blanks ($A_{B,}$ in mass per filter) by the instrument measured aerosol sample ($A_{M,}$ in mass per filter) from equation (1).

$$R_S = (R_M - (f(R_B)) / (1-f) \quad (4)$$

The observed maximum absolute uncertainties in the isotopic ratios were based on uncertainties in the isotopic ratios in the soluble fraction due to filter blanks combined with the uncertainties introduced by the instrument and are expressed in Table 3.6 and Figure 3.6. The observed maximum absolute uncertainty in Pb isotopic ratio were 0.006 in $^{208}Pb/^{207}Pb$, 0.009 in $^{206}Pb/^{207}Pb$, 0.1 in $^{206}Pb/^{204}Pb$ and $^{208}Pb/^{204}Pb$, and 0.04 in $^{207}Pb/^{204}Pb$, and was 0.5 in εNd.

Table 3.3. Major element composition of total aerosols collected across the South Atlantic

Sample ID	Al	Ca	Fe	K	Mg	Mn
South Atlantic – aerosols, bulk (ng m^{-3})						
D357-2	5.10 ±1.38	n.d	n.d	n.d	n.d	n.d.
D357-8	5.84 ±1.50		11.0 ±0.7	79.9		0.248 ±0.026
D357-10	7.28 ±4.36		13.4 ±1.9	2.05		0.079 ±0.076
D357-11	4.77 ±1.35		7.32 ±0.58	13.9		0.170 ±0.024
D357-13	6.11 ±1.31		12.8 ±0.6			0.232 ±0.023
JC068-4	16.0 ±0.3		9.56 ±0.76			0.444 ±0.020
JC068-6	50.0 ±0.3		27.0 ±0.7	11.3		0.938 ±0.019
JC068-8	12.0 ±0.3		38.5 ±0.7			0.817 ±0.019
JC068-10	199 ±0.3	6.77 ±0.08	113 ±0.7	64.0		3.61 ±0.02
JC068-12	54.4 ±0.4	24.6 ±0.1	89.6 ±0.8	55.3	50.9 ±0.1	2.00 ±0.02
JC068-14	11.3 ±0.3	19.5 ±0.1	98.1 ±0.7	59.2	93.7 ±0.1	1.73 ±0.02
JC068-15	48.0 ±0.7	5.75 ±0.2	30.4 ±1.6	35.1		0.855 ±0.042
JC068-17	9.17 ±1.43		0.576 ±3.22	5.47		0 ±0.121
Reference Material (% w/w)						
USGS G2, this study (n = 12)	13.65	1.88	2.55	4.41	0.72	0.03
RSD (2σ, %)	6.1	9.8	2.5	7.3	8.4	9.3
USGS G2, cert.	15.39	1.96	2.66	4.48	0.75	0.03
RSD (2σ, %)	0.3	0.08	0.17	0.13	0.03	0.01

Blank spaces indicate sample concentrations below blank filter or seawater contribution limit

Reported element concentrations are calculated from the subtraction of the average blank concentration from the measured sample concentration for each element, ± errors represent the range of element concentrations due to the highest and lowest blank concentrations for each element

Element concentrations with no ± errors represent no upper or lower limit in the element concentration in the blank. This is because measured element concentrations in the blank were below limit of detection, and limit of detection for that element was subtracted from the measured sample concentration.

n.d – not determined

Results for certified USGS reference material G-2 Granite are taken from Gladney et al. (1992) and Govindaraju (1989, 1994). Precision is given as the relative standard deviation (RSD) at the 2σ level (n = 12).

Table 3.4. Rare earth element composition of total aerosols collected across the South Atlantic

Sample ID	La	Ce	Pr	Nd	Sm	Eu	Gd	Tb	Dy	Ho	Er	Tm	Yb	Lu
South Atlantic – aerosols, bulk (pg m^{-3})														
D357-2	1.32 ±0.249	1.59 ±1.13	0.257 ±0.109	0.541 ±0.942	1.33 ±0.079	0.219 ±0.022	n.d	n.d	n.d	n.d	n.d	n.d	0.110 ±0.071	0.149 ±0.015
D357-8	2.12 ±0.272	3.46 ±1.23	0.379 ±0.119	1.28 ±1.01	0.360 ±0.086	0.094 ±0.024	0.336 ±0.095	0.063 ±0.017	0.475 ±0.008	0.093 ±0.031	0.300 ±0.102	0.041 ±0.016	0.323 ±0.077	0.067 ±0.017
D357-10	1.62 ±0.790	1.33 ±3.58	0.067 ±0.345	1.15 ±2.93	0.072 ±0.251		0.019 ±0.276	0.002 ±0.048	0.074 ±0.023	0 ±0.090	0 ±0.006	0 ±0.005	0 ±0.044	0 ±0.003
D357-11	2.39 ±0.244	3.88 ±1.11	0.471 ±0.107	1.59 ±0.905	0.393 ±0.078	0.052 ±0.021	0.364 ±0.085	0.044 ±0.015	0.300 ±0.007	0.065 ±0.028	0.167 ±0.091	0.019 ±0.014	0.106 ±0.069	0.015 ±0.015
D357-13	3.21 ±0.238	6.10 ±1.08	0.741 ±0.104	2.48 ±0.882	0.562 ±0.076	0.104 ±0.021	0.473 ±0.083	0.059 ±0.015	0.392 ±0.007	0 ±0.027	0.218 ±0.089	0.035 ±0.014	0.274 ±0.068	0.043 ±0.014
JC068-4	12.8 ±0.115	22.7 ±0.255	1.79 ±0.033	6.72 ±0.447	0.817 ±0.019	0.196	1.12 ±0.089	0.165 ±0.015	1.05 ±0.013	0.191 ±0.005	0.603 ±0.026	0.093 ±0.005	0.542 ±0.025	0.098 ±0.006
JC068-6	14.1 ±0.111	29.8 ±0.245	3.53 ±0.031	13.6 ±0.429	3.03 ±0.018	0.612	2.73 ±0.086	0.422 ±0.014	2.63 ±0.013	0.535 ±0.005	1.55 ±0.025	0.227 ±0.005	1.44 ±0.024	0.237 ±0.006
JC068-8	3.95 ±0.107	7.92 ±0.238	0.899 ±0.030	7.29 ±0.417	0.734 ±0.017	0.168	0.722 ±0.083	0.119 ±0.014	0.779 ±0.012	0.136 ±0.005	0.440 ±0.025	0.058 ±0.005	0.377 ±0.023	0.084 ±0.006
JC068-10	99.3 ±0.109	219 ±0.241	25.7 ±0.031	106 ±0.421	23.7 ±0.018	4.65	23.0 ±0.084	3.79 ±0.014	24.1 ±0.012	5.07 ±0.005	15.5 ±0.025	2.31 ±0.005	15.5 ±0.024	2.43 ±0.006
JC068-12	30.5 ±0.121	63.9 ±0.268	7.45 ±0.034	30.1 ±0.469	6.29 ±0.020	1.34	5.69 ±0.094	0.855 ±0.015	5.93 ±0.014	0.878 ±0.005	2.79 ±0.028	0.374 ±0.005	2.49 ±0.026	0.394 ±0.006
JC068-14	6.43 ±0.113	11.7 ±0.250	1.12 ±0.032	4.75 ±0.438	0.874 ±0.018	0.180	0.774 ±0.087	0.114 ±0.014	0.637 ±0.013	0.098 ±0.005	0.289 ±0.026	0.042 ±0.005	0.260 ±0.024	0.038 ±0.006
JC068-15	51.7 ±0.244	68.1 ±0.540	7.52 ±0.069	29.2 ±0.946	5.71 ±0.040	1.124	5.29 ±0.189	0.753 ±0.031	4.58 ±0.028	0.919 ±0.0.10	2.65 ±0.056	0.380 ±0.010	2.45 ±0.053	0.362 ±0.012
JC068-17	1.90 ±0.488	4.00 ±1.08	0.570 ±0.138	1.40 ±1.89	0.342 ±0.079	0.052	0.103 ±0.378	0.020 ±0.062	0.070 ±0.055	0 ±0.021	0 ±0.149	0 ±0.007	0 ±0.178	0 ±0.005
Reference Material (μg g^{-1})														
USGS G2, this study (n = 12)	87	158	16	52	7.2	1.3	4.0	0.46	2.2	0.35	0.85	0.1	0.7	0.1
RSD (2σ, %)	1.3	1.2	3.1	2.1	2.5	3.5	4.3	4.0	5.4	4.9	3.8	5.5	4.1	4.4
USGS G2, cert.	89	160	18	55	7.2	1.4	4.3	0.48	2.4	0.4	0.92	0.18	0.8	0.11
RSD (2σ, %)	18	13		22	19	17			25				50	

Reported element concentrations are calculated from the subtraction of the average blank concentration from the measured sample concentration for each element, ± errors represent the range of element concentrations due to the highest and lowest blank concentrations for each element. Element concentrations with no ± errors represent no upper or lower limit in the element concentration in the blank. This is because measured element concentrations in the blank were below limit of detection, and limit of detection for that element was subtracted from the measured sample concentration. Blank spaces indicate sample concentrations below blank filter contribution. n.d. – not determined, n.a. – not available. Results for certified reference material USGS G-2 Granite are taken from Gladney et al. (1992) and Govindaraju (1989, 1994). Precision is given as the relative standard deviation (RSD) at the 2σ level (n = 12).

Table 3.5. Trace element Cu, Pb, Cd, Zn, Cr, Ni, Co, Y, Th, V, and Sc composition of total aerosols collected across the South Atlantic

Sample ID	Cu	Pb	Cd	Zn	Cr	Ni	Co	V	Sc	Y	Th
South Atlantic – aerosols, bulk (pg m^{-3})											
D357-2	317 ±20.4	102 ±1.11	8.70 ±0.063	1495 ±233	n.d.	110 ±21.5	2.48	107 ±5.73	22.7 ±0.102	11.0 ±0.233	0.878
D357-8	178 ±22.3	45.2 ±1.21	4.87 ±0.069	342 ±254	2082 ±289	1144 ±23.4	25.9	229 ±6.25	1.05 ±0.111	3.59 ±0.254	0.639
D357-10	275 ±64.7	132 ±3.53	1.70 ±0.200	4497 ±739	219 ±840	68.1 ±68.1	3.76	131 ±18.2	1.08 ±0.323	4.03 ±0.738	
D357-11	93.0 ±20.0	35.0 ±1.09	2.00 ±0.062	625 ±228	1219 ±260	647 ±21.0	16.3	104 ±5.61	0.351 ±0.100	0.52 ±0.228	0.642
D357-13	88.6 ±19.5	16.4 ±1.06	1.13 ±0.060	229 ±222	3089 ±253	1618 ±20.5	39.6	63.7 ±5.47	1.91 ±0.097	4.02 ±0.222	0.421
JC068-4	300 ±16.0	62.2 ±2.24	10.9	3851 ±5.38	820 ±49.7	411 ±14.8	9.33 ±1.66	91.5 ±1.73	3.13 ±0.090	7.60 ±0.306	1.34 ±0.054
JC068-6	326 ±15.3	73.8 ±2.15	9.33	1113 ±5.17	1736 ±47.7	2103 ±14.2	50.4 ±1.59	147 ±1.66	9.05 ±0.087	19.5 ±0.294	4.25 ±0.052
JC068-8	155 ±14.9	26.4 ±2.09	10.8	417 ±5.02	7535 ±46.3	4865 ±3.8	117 ±1.54	80.0 ±1.61	2.47 ±0.084	5.71 ±0.285	1.02 ±0.050
JC068-10	219 ±15.1	102 ±2.11	4.26	601 ±5.08	4551 ± 46.9	8460 ±13.9	161 ±1.56	178 ±1.63	57.2 ±0.085	149 ±0.289	27.8 ±0.051
JC068-12	239 ±16.8	57.8 ±2.35	14.6	699 ±5.65	14130 ±52.1	7066 ±15.5	180 ±1.74	176 ±1.81	15.1 ±0.095	26.7 ±0.321	7.89 ±0.057
JC068-14	538 ±15.7	64.4 ±2.20	10.8	983 ±5.27	26408 ±48.7	14800 ±14.5	290 ±1.62	174 ±1.69	2.40 ±0.088	3.45 ±0.300	1.36 ±0.053
JC068-15	344 ±33.8	333 ±4.74	25.1	2661 ±11.4	201 ±105	159 ±31.3	12.5 ±3.51	421 ±3.66	15.4 ±0.191	37.6 ±0.648	10.0 ±0.114
JC068-17	643 ±67.7	344 ±9.49	2.34	4054 ±22.8	58.7 ±210	0 ±137	0 ±5.66	0 ±11.4			1.22 ±0.228
Reference Material (µg g^{-1})											
USGS G2, this study (n=12)	9.1	32	0.02	86	7.6	2.2	24	4.5	9.1	35	4.7
RSD (2σ, %)	1.1	1.0	0.01	7.4	1.2	0.4	0.6	0.2	0.3	1.6	0.4
USGS G2, cert.	11	30	n.a.	86	n.a.	n.a.	25	4.6	11	36	3.5
RSD (2σ, %)	73	n.a.	n.a.	19	n.a.	n.a.	16	30	36	22	23

Reported element concentrations are calculated from the subtraction of the average blank concentration from the measured sample concentration for each element, ± errors represent the range of element concentrations due to the highest and lowest blank concentrations for each element. Element concentrations with no ± errors represent no upper or lower limit in the element concentration in the blank. This is because measured element concentrations in the blank were below limit of detection, and limit of detection for that element was subtracted from the measured sample concentration. Blank spaces indicate sample concentrations below blank filter contribution. n.d. – not determined, n.a. – not available. Results for certified reference material USGS G-2 Granite are taken from Gladney et al. (1992) and Govindaraju (1989, 1994). Precision is given as the relative standard deviation (RSD) at the 2σ level (n = 12).

Table 3.6. Lead and Nd isotope ratios and εNd values for total aerosols collected across the South Atlantic

Sample ID	Blank corrected $^{206}Pb/^{207}Pb$	±	$^{208}Pb/^{207}Pb$	±	$^{206}Pb/^{204}Pb$	±	$^{207}Pb/^{204}Pb$	±	$^{208}Pb/^{204}Pb$	±	$^{144}Nd/^{143}Nd$	±	εNd	±
South Atlantic – aerosols, bulk														
D357-2	n.d		n.d		n.d		n.d		n.d		n.d			
D357-8	1.1462	0.0032	2.4092	0.0017	17.818	0.058	15.554	0.012	37.47	0.05	.			
D357-10	1.1546	0.0075	2.4211	0.0041	17.983	0.138	15.598	0.028	37.76	0.13	0.512337$^{(T)}$	0.000028	-5.3	0.5
D357-11	1.1357	0.0038	2.3980	0.0021	17.687	0.077	15.574	0.015	37.35	0.07				
D357-13	1.1460	0.0035	2.4072	0.0019	17.789	0.064	15.533	0.013	37.39	0.06				
JC068-4	1.1569	0.0010	2.4211	0.0005	18.048	0.027	15.601	0.010	37.77	0.03	0.512405$^{(T)}$	0.000015	-4.0	0.3
JC068-6	1.1710	0.0007	2.4358	0.0003	18.297	0.018	15.626	0.007	38.06	0.02	0.512574	0.000022	-1.0	0.2
JC068-8	1.1476	0.0058	2.4141	0.0027	17.806	0.156	15.519	0.059	37.46	0.19	0.512578$^{(T)}$	0.000020	-0.8	0.4
JC068-10	1.1814	0.0005	2.4549	0.0002	18.453	0.013	15.620	0.005	38.35	0.02	0.512778	0.000012	2.8	
JC068-12	1.1714	0.0009	2.4434	0.0004	18.284	0.025	15.609	0.009	38.14	0.03				
JC068-14	1.1607	0.0008	2.4237	0.0004	18.098	0.021	15.592	0.008	37.79	0.03				
JC068-15	1.1789	0.0003	2.4312	0.0002	18.445	0.009	15.645	0.003	38.04	0.01	0.512218	0.000016	-8.1	0.1
JC068-17	1.1497	0.0006	2.4186	0.0003	17.917	0.017	15.584	0.006	37.69	0.02				
Reference Material														
USGS G2, this study (n=22)	1.1764	0.0001	2.4873	0.0003	18.399	0.005	15.640	0.006	38.902	0.021	0.512230	0.000026	-8.0	0.5
USGS G2, Weis (2006)	1.1765	0.0002	2.4878	0.0002	18.396	0.002	15.636	0.005	38.900	0.019	0.512230	0.000013	-8.0	

Blank spaces indicate samples where concentrations were too low for precise isotope analysis. n.d. = not determined

Results for measured and certified reference material USGS G-2 Granite are also shown for comparison. Precision is given as the relative standard deviation (RSD) at the 2σ level (n = 22). All samples were analysed by MC-ICP-MS, except for selected low Nd abundance samples, which were measured by TIMS and are denoted by $^{(T)}$.

$^{143}Nd/^{144}Nd$ ratios are corrected relative to a JNdi ratio of 0.512115 (Tanaka et al., 2000). Epsilon Nd values were calculated using a CHUR value of 0.512638.

Table 3.7. Element and isotopic composition of sources taken from Chapter 2

Proxy	**South America**		**Southern *Africa***	
	Natural	***Anthropogenic***	***Natural***	***Anthropogenic***
Element ratio				
Pb/Al×1000	0.015-4 (rural) 0.02-0.5 (volcanic)	4-150 (urban)	0.06-4 (rural) 0.03-8 (volcanic)	7-20 (urban) 9-10 (mine)
Cd/Al×1000	0.0007-0.01 (rural) 0.0008-0.01 (volcanic)	0.01-8 (urban)	0.03-0.04 (rural) 0.001-0.009 (volcanic)	0.02-0.08 (urban) 0.09-0.1 (mine)
Zn/Al×1000	0.8-6 (rural) 0.2-2 (volcanic)	8-1000 (urban)	10-20 (rural) 1-4 (volcanic)	9-30 (urban) 40-50 (mine)
La/Cr	0.1-2 (rural) 0.07-100 (volcanic)	0.05-0.8 (urban)	0.03-0.04 (rural) 0.2-0.6 (volcanic)	0.02-0.06 (urban)
Element concentration (µg/g)				
1/[Pb]	0.035-4 (rural) 0.03-6 (volcanic)	0.002-0.015 (urban)	0.08-0.9 (rural) 0.06-0.55 (volcanic)	0.004-0.03 (urban) 0.1-0.15 (mine) 0.07-0.1 (coal)*
1/[Nd]	0.03-0.3 (rural) 0.015-0.08 (volcanic)	0.03-0.8 (urban)	0.01-0.5 (rural) 0.01-0.08 (volcanic)	0.3-0.6 (urban) 0.7-0.8 (mine)
Isotope composition				
$^{208}Pb/^{207}Pb$	2.447-2.474 (rural) 2.455-2.446 (volcanic)	2.394-2.452 (urban)	2.404-2.421 (rural) 2.439-2.549 (volcanic)	2.330-2.370 (urban) <2.250-2.450 (mine) 2.469-2.485 (coal)*
$^{206}Pb/^{207}Pb$	1.173-1.210 (rural) 1.119-1.212 (volcanic)	1.119-1.204 (urban)	1.138-1.141 (rural) 1.125-1.315 (volcanic)	1.050-1.120 (urban) 1.100-2.900 (mine) 1.205-1.219 (coal)*
εNd	-8.9 to +3.4 (rural) -4.2 to +6.1 (volcanic)	-22 to -13 (urban)	-24 to -8.4 (rural) -11 to +4.7 (volcanic)	-23 to -18 (urban) -26 ±0.3 (mine)

EF_{crust} denotes enrichment factor relative to the continental crust

* Data taken solely from literature, Monna et al., 2006

Table 3.7. *continued*.

Element or Isotopic Composition	South America Natural	Anthropogenic	Southern Africa Natural	Anthropogenic
EF_{crust}				
Pb	0.07-10 (rural) 0.1-1 (volcanic)	10-1000	0.2-80 (rural) 0.1-80 (volcanic)	10-200 (urban) 10-30 (mine) 10-20 (coal)*
Zn	0.1-20 (rural) 0.2-2 (volcanic)	20-10000	0.6-80 (rural) 1-3 (volcanic)	10-200 (urban) 10-30 (mine)
Cu	0.1-10 (rural) 0.1-2 (volcanic)	10-500	0.2-20 (rural) 0.5-9 (volcanic)	10-100 (urban) 2-20 (mine) 8-20 (coal)*
V	1-3 (rural) 0.08-4 (volcanic)	1-50	0.7-2 (rural) 1-10 (volcanic)	1-10 (urban) 5-6 (mine) 8-10 (coal)*
Cr	0.2-5 (rural) 0.01-8 (volcanic)	1-200	0.8-400 (rural) 1-100 (volcanic)	50-200 (urban) 60-70 (mine)
Ni	0.7-3 (rural) 0.02-9 (volcanic)	1-100	0.5-200 (rural) 2-20 (volcanic)	20-100 (urban) 30-40 (mine)
Co	0.2-20 (rural) 0.1-6 (volcanic)	1-30	0.8-200 (rural) 0.7-7 (volcanic)	2-3 (urban) 40-50 (mine)
Cd	0.5-5 (rural, volcanic)	0.1-4000	0.1-20 (rural) 1-8 (volcanic)	0.1-40 (urban) 80-100 (mine)
REE	0.1-3 (rural, volcanic)	1-10	0.1-100 (rural) 0.4-15 (volcanic)	1-2 (urban) 3-6 (mine)
Sc, Y, Th	0.01-2 (rural, volcanic)	1-100	1-3 (rural) 1-20 (volcanic)	1-4 (urban, mine)
Al, Ca, Fe, K, Mg, Mn	0.2-20 (rural) 0.06-5 (volcanic)	0.1-10	0.1-400 (rural) 0.1-20 (volcanic)	0.07-8 (urban) 0.4-80 (mine)

3.3. Results

3.3.1. Air mass trajectories over the South Atlantic Ocean

Five-day air mass back-trajectories for arrival heights of 10, 500 and 1000m above the ship's position were examined across the South Atlantic to assist deciphering aerosol sample provenance (calculated using HYSPLIT (Draxler and Rolph, 2013; Rolph, 2013). Examples of the air mass back-trajectories are shown in Figure 3.2. The temporal ranges were selected based on the short residence times of aerosols in the atmosphere, typically hours to days (e.g. Raes et al., 2000). Most natural and anthropogenic aerosols are injected into the atmosphere within the planetary boundary between ~ 300 to 1500 m above sea level (Hasse, 1983), although volcanic emissions and large-scale dust storms can reach above this layer (Carlson and Prospero, 1972; Jickells et al., 2005).

The five day back-trajectories for all sampling locations during the two cruises showed three patterns (Fig. 3.2): (i) prevailing winds from the southwest, potentially tapping into South American sources (JC068-12 and 10; Fig. 3.2C, D), (ii) prevailing winds from the southwest, potentially tapping into Antarctic sources (JC068-17 and 15, represented by Fig. 3.2A; JC068-10, Fig. 3.2D; JC068-8, Fig. 3.2E; and D357-10; Fig. 3.2G), and (iii) prevailing winds that originated to the east, west or south away from any continental land masses (i.e. open ocean; JC068-14, Fig. 3.2.B; JC068-6, 4, and D357-8, represented by Fig. 3.2F, and D357-11, 13, 2; represented by Fig. 3.2H).

The most prevalent pattern is that the eastern part of the transect between ~5°W-20°E during both cruises (early January 2012 and October/November 2010), received air masses that had spent the majority of the five days over the open ocean (Fig. 3.2E-H). Different arrival heights (10, 500 and 1000 m) revealed different prevailing wind directions (Fig. 3.2F-H). However, these air mass back trajectories were extended to 10 days (not shown here; Draxler and Rolph, 2013) and revealed contact with central to southern South America, Antarctica, and Southern Africa. Aerosol samples collected from the more central part of the South Atlantic (10-35°W, 8 to 15 January 2012; Fig. 3.2C-E) received air masses from southwesterly directions, which passed over southern South America and the Antarctic Peninsula before reaching the middle of the South Atlantic. They were mainly influenced by high-level (> 4000m) air masses (Fig 3.2C-E).

Aerosol samples collected from the two westernmost locations in the South Atlantic (west of ~50°W, between 18 and 29 January 2012; Fig. 3.2A) received air masses from southwesterly directions and the five-day back-trajectories did not indicate pathways crossing the continents. This region received high-level (> 3000m) and lower level (< 1000m) contributions of air masses.

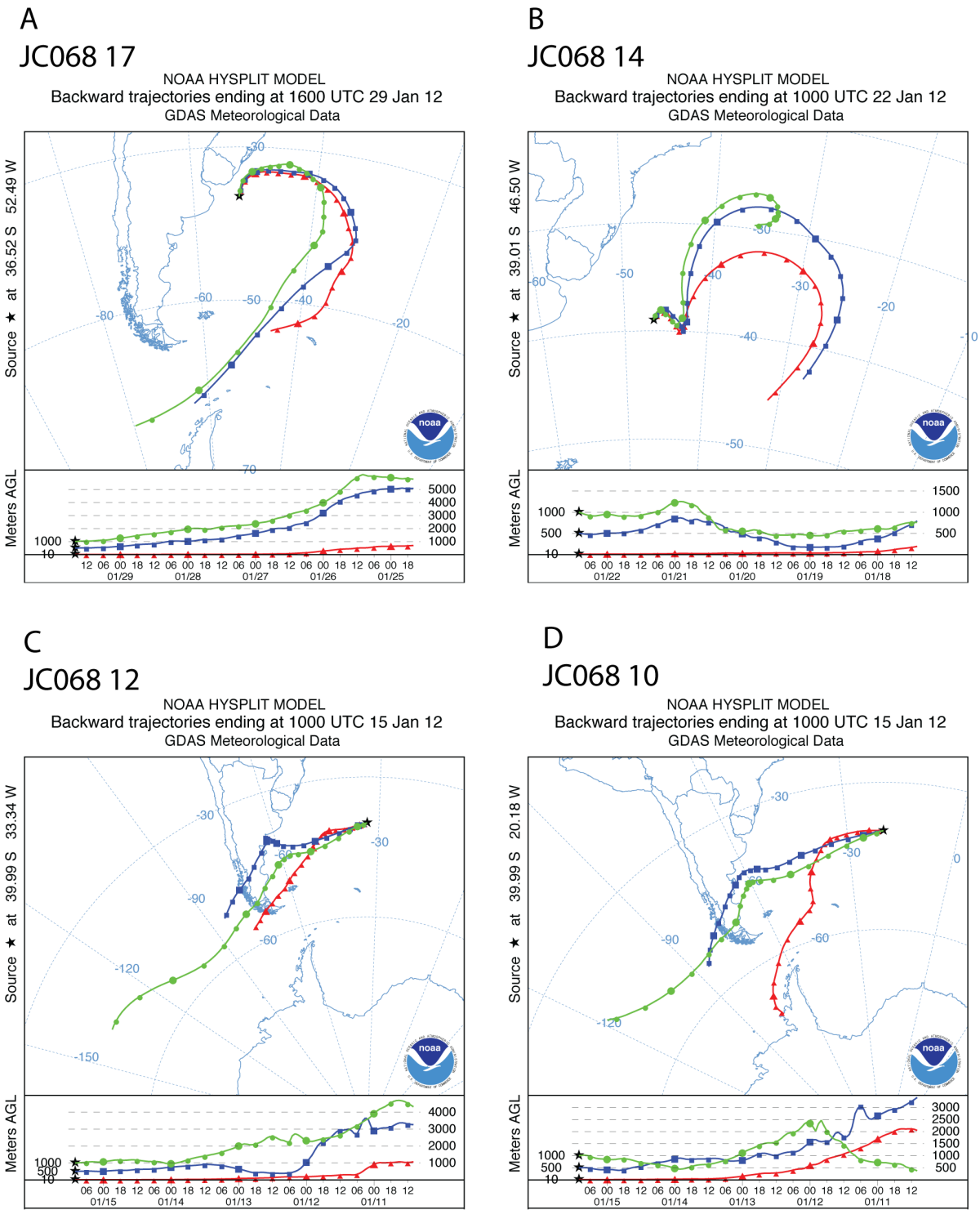

Figure 3.2. Examples of five-day air mass back-trajectories for aerosol samples for cruise D357 and JC068. Arrival heights of 10, 500 and 1000 m above the ship's positions are shown. Maps provided by Draxler and Rolph, 2003.

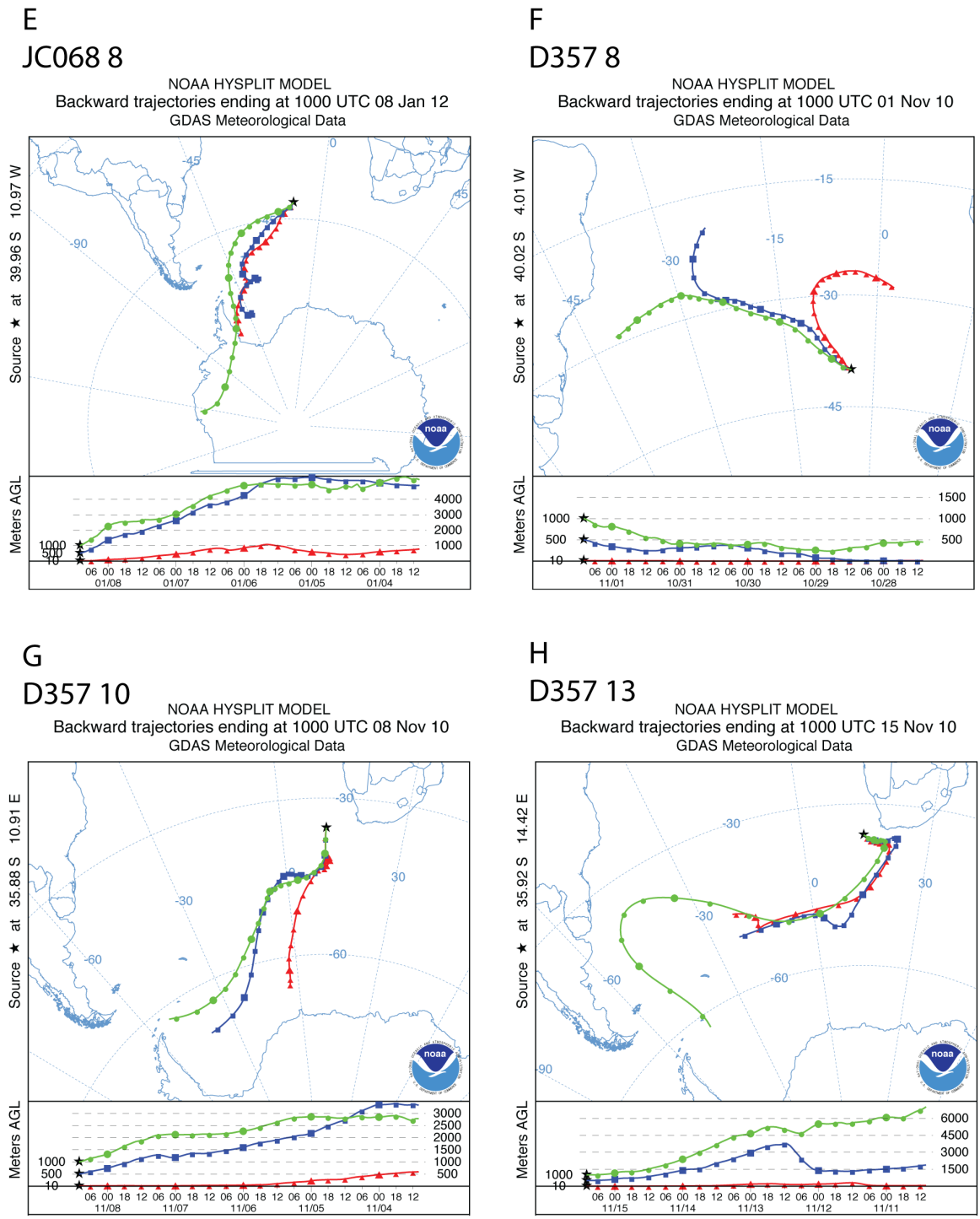

Figure 3.2. *continued.*

3.3.2. Element enrichment composition in aerosol samples

Low particulate matter content on filters collected along the 40°S transect in the South Atlantic did not enable the determination of the mineralogy of aerosol samples. However, masses were sufficient in most cases to determine major, rare earth and trace element atmospheric concentrations. These are listed in Table 3.3 to 3.5. Element enrichment factors of aerosols against longitude across the South Atlantic are illustrated in Figures 3.3 to 3.5. Natural and anthropogenic sources of aerosols from South America and Southern Africa are listed for comparison in Table 3.7.

The uncertainties in element atmospheric concentrations (Table 3.3 to 3.5) and enrichment factors were large (Fig. 3.5 to 3.5). This was due to the low element mass in the soluble fraction of aerosol samples close to limit of detection of the analytical instruments, or due to over correction of element contribution in the soluble fraction of the multiple filter blanks. Although large, similar uncertainties were reported in element composition of aerosols over remote oceans (Baker et al., 2006; Witt et al, 2006; 2010). For calculated enrichment factors that showed uncertainty ≤0%, the upper limit of the enrichment factor were reported and these are denoted as symbols outlined in red with a red error bar down to zero in the figures.

Highest enrichments relative to the upper continental crust of Zn, Pb, Cu and to a lesser extent V, were observed at the westernmost (west of ~45°W, sample JC068-14) and easternmost (east of ~5°E, sample JC068-4) margins of the South Atlantic in the order of Zn>Pb>Cu>>V (enrichment factor up to 1000 in Zn, up to 200 in Pb and Cu, and up to 20 in the west and up to 50 in the east in V; Fig. 3.3). Enrichment factors relative to the crust of Zinc, Pb, Cu and V in aerosols decreased to the central ocean to an enrichment factor ranging between 1 and 4 (sample JC068-10) at ~20°W and to an enrichment factor ranging between 5 and 20 (sample JC068-12) at ~35°W (Fig. 3.3). Enrichment patterns of Zn, Pb, Cu, and V suggested the South Atlantic can be divided into a western and eastern section either side of ~20°W (Fig. 3.3).

High enrichments relative to the crust in Cr, Ni, and Co were observed in the west at ~45°W and decreased to the eastern margin of the South Atlantic showing a general decrease in enrichment from 6000 in the west to up to 1000 in the east in Cr and Ni, and from 200 in the west to up to 80 in the east in Co (Fig. 3.3). Exceptional to this trend, lower Cr, Ni and Co enrichment factors relative to the crust were observed in the two westernmost samples west of ~45°W (enrichment factor of 10 in Cr and Ni, and between 2 and 5 in Co, JC068-15, and -17; Fig. 3.3). Cadmium enrichments were consistently high, ranging between 100 and 2000, except at ~20°W Cd enrichment was much lower (enrichment factor of 20, Fig. 3.3).

REE, and Sc, Y and Th of enrichment factors ranged between 0.5 and 5 across the open ocean, however east of ~10°E larger enrichment in Lu and Y (10), and Sc (40) were observed (Fig. 3.4). Of the REE, Fig. 3.4 shows only La and Nd, as the REE enrichment patterns were particularly homogenous in the aerosols across the South Atlantic Ocean.

Iron and Mn enrichment factors ranged between 1 and 10, except at the westernmost samples Fe enrichment factors were 0.15 at sample JC068-17 and Fe and Mn showed enrichment of 20 at sample JC068-14 (Fig. 3.5). Enrichment data for Mg were limited (n=2) and ranged from a factor of 5 at samples JC068-12 to 50 at sample JC068-14 (Fig. 3.5). Figure 3.5 showed large variations in K enrichments relative to the crust ranging between 0.6 and 30 across the ocean. Enrichment data for Ca were also limited (n=4) and ranged between 0.3 and 5 between sample JC068-12 and -15 (Fig. 3.5).

3.3.3. Lead and neodymium isotopic compositions of aerosol samples

Lead and Nd isotopic compositions of aerosols are listed in Table 3.6 and are shown in Figure 3.6. All samples were analysed except sample D357-2 for their Pb isotopic composition. There were low concentrations of Nd in most aerosol samples necessary for isotopic analysis (<15ng), thus Nd isotopic compositions were only realized in six aerosol samples.

Aerosol samples collected across the South Atlantic showed a range in $^{206}Pb/^{207}Pb$ ($^{208}Pb/^{207}Pb$) ratios of 1.13-1.18 (2.39-2.46) (Fig. 3.6). $^{208}Pb/^{207}Pb$ ratios were <2.43 at the westernmost and easternmost margins and the highest $^{208}Pb/^{207}Pb$ ratio was observed at ~20°W (Fig. 3.6). The highest $^{208}Pb/^{207}Pb$ ratios were coupled with the highest εNd value (2.8; sample JC068-10), while the lowest εNd values were coupled with the lowest $^{208}Pb/^{207}Pb$ ratios at the westernmost and easternmost margins (εNd values of -8.1 ±0.1 in the west, sample JC068-15, and εNd of -4 ±0.3 to -5.3 ±0.5 in the east, samples D357-13 and JC068-4, Fig. 3.6).

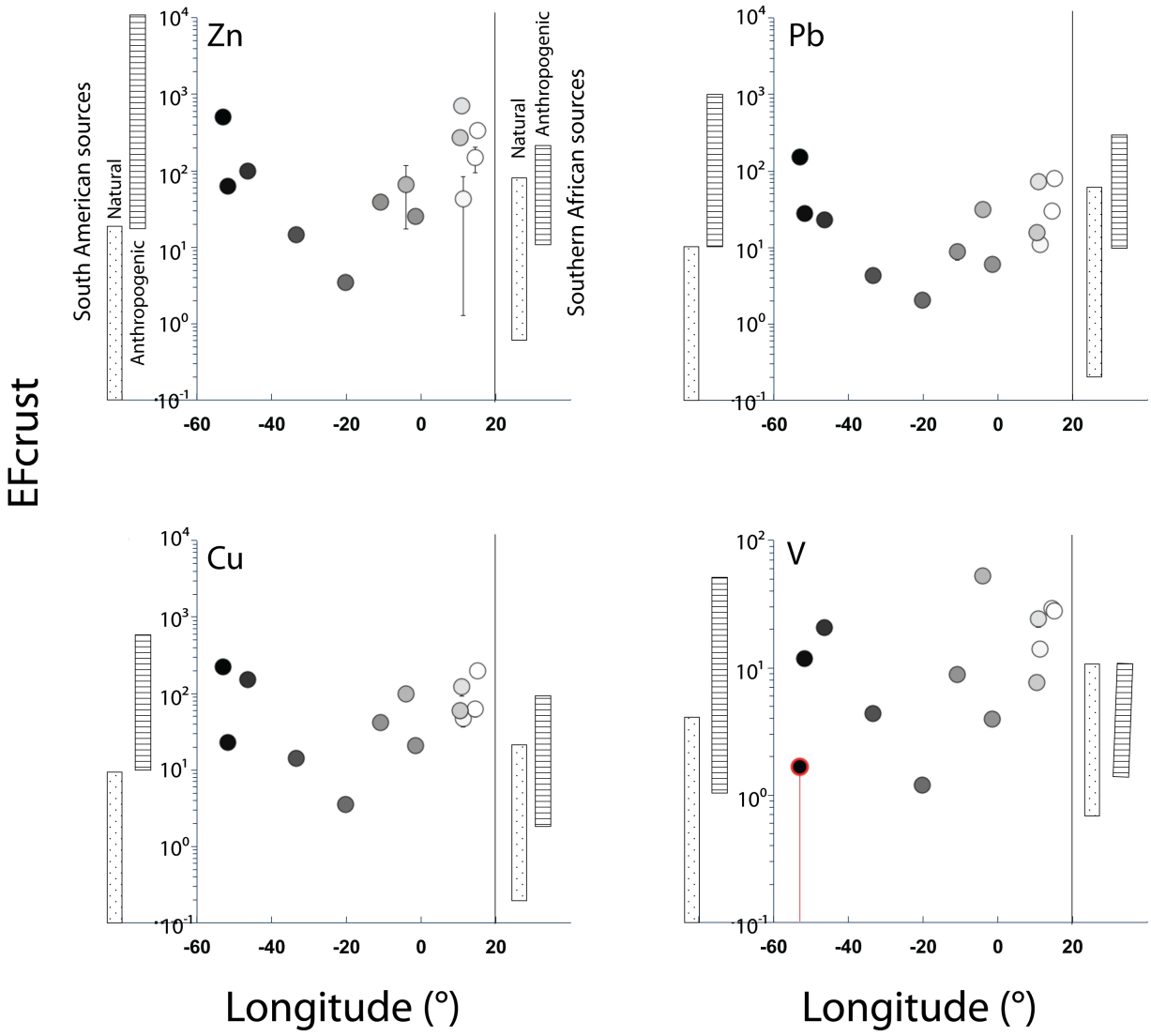

Figure 3.3. Enrichment factors relative to the upper continental crust of select trace metals in aerosol samples from across the South Atlantic Ocean. Aerosols west to east are denoted by black to white shading. Trace element enrichment factors that were reported as characteristic of natural (dotted bar) and anthropogenic (lined bar) sources from South America and Southern Africa are shown (as characterised in Chapter 2, taken from Table 3.3). Where average enrichment factors were zero, calculated using the average blank atmospheric concentration for an element, the enrichment factor calculated using the smallest blank atmospheric concentration for an element were presented; these data are denoted by a red outline with a red error bar that reaches zero. Errors were based on analytical uncertainties to 2σ.

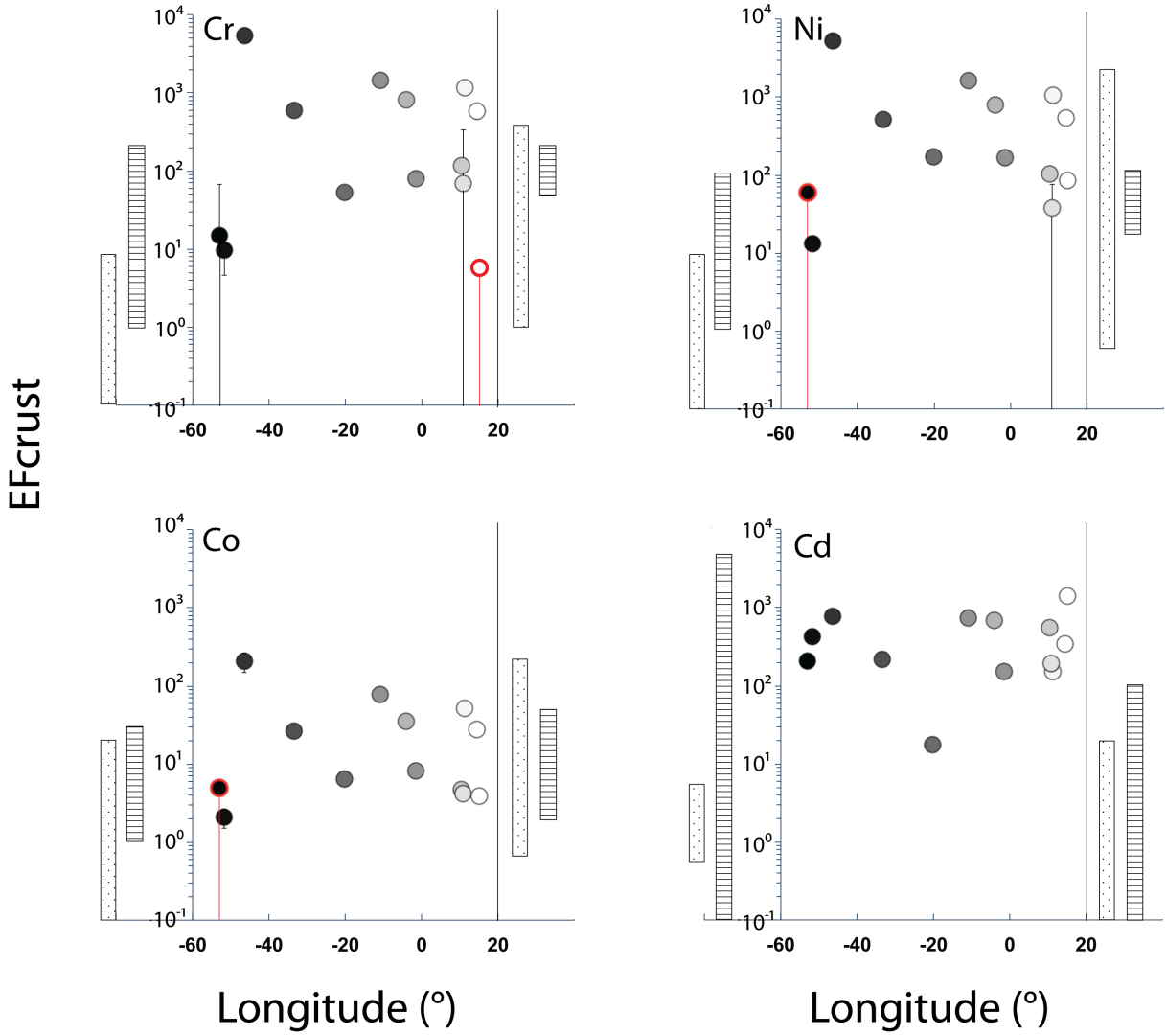

Figure 3.3. *continued*.

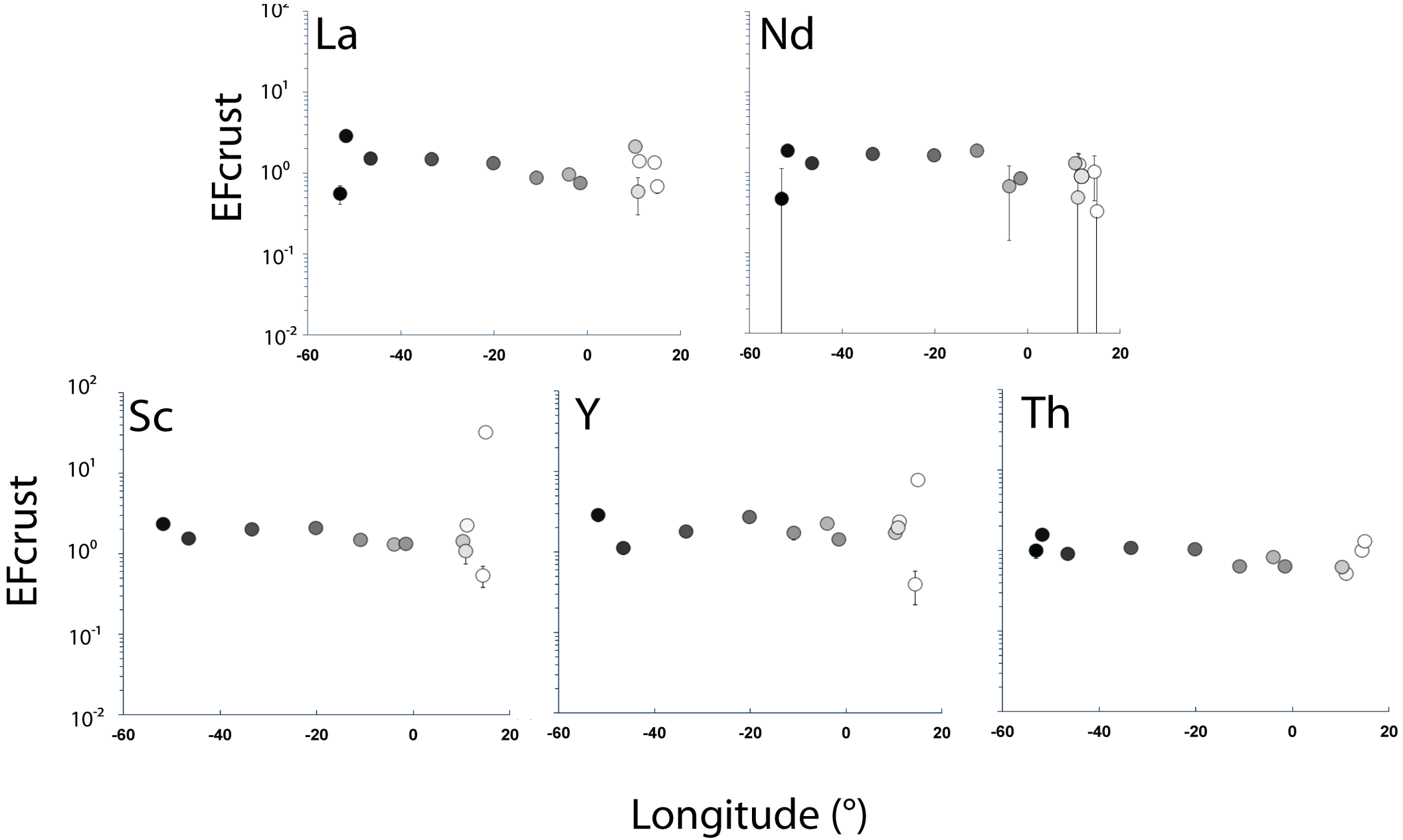

Figure 3.4. Enrichment factors relative to the upper continental crust of rare earth elements (La, Nd), Sc, Y and Th in aerosol samples across the South Atlantic Ocean. Aerosols west to east are denoted by black to white shading. Errors were based on analytical uncertainties to 2σ.

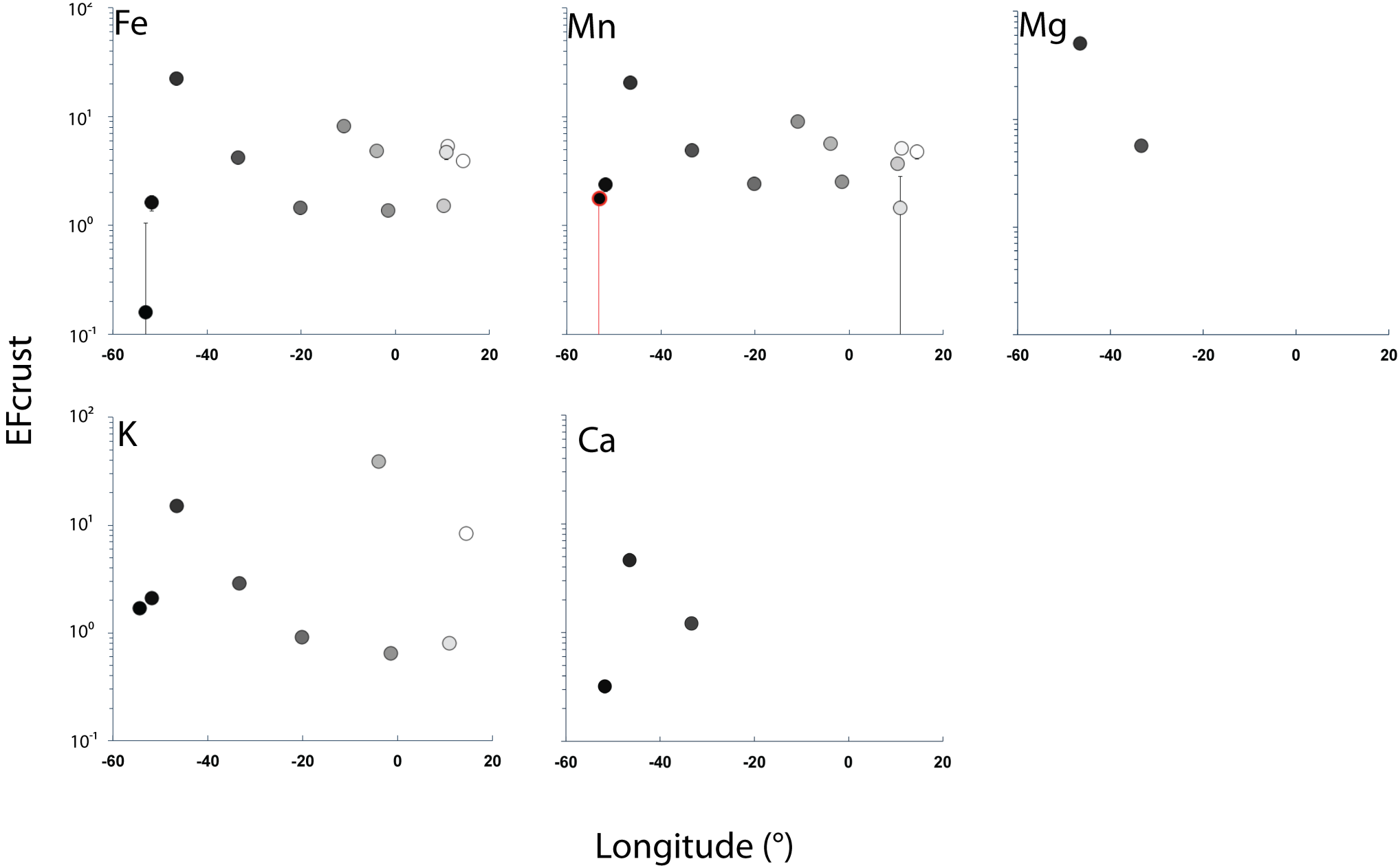

Figure 3.5. Enrichment factors relative to the upper continental crust of major elements in aerosol samples across the South Atlantic Ocean. Aerosols west to east are denoted by black to white shading. Where enrichment factors are below zero (calculated using the average blank concentration for an element), the enrichment factor calculated using the smallest blank concentration for an element is presented; data denoted by a red outline with a red error bar. Errors were based on analytical uncertainties to 2σ.

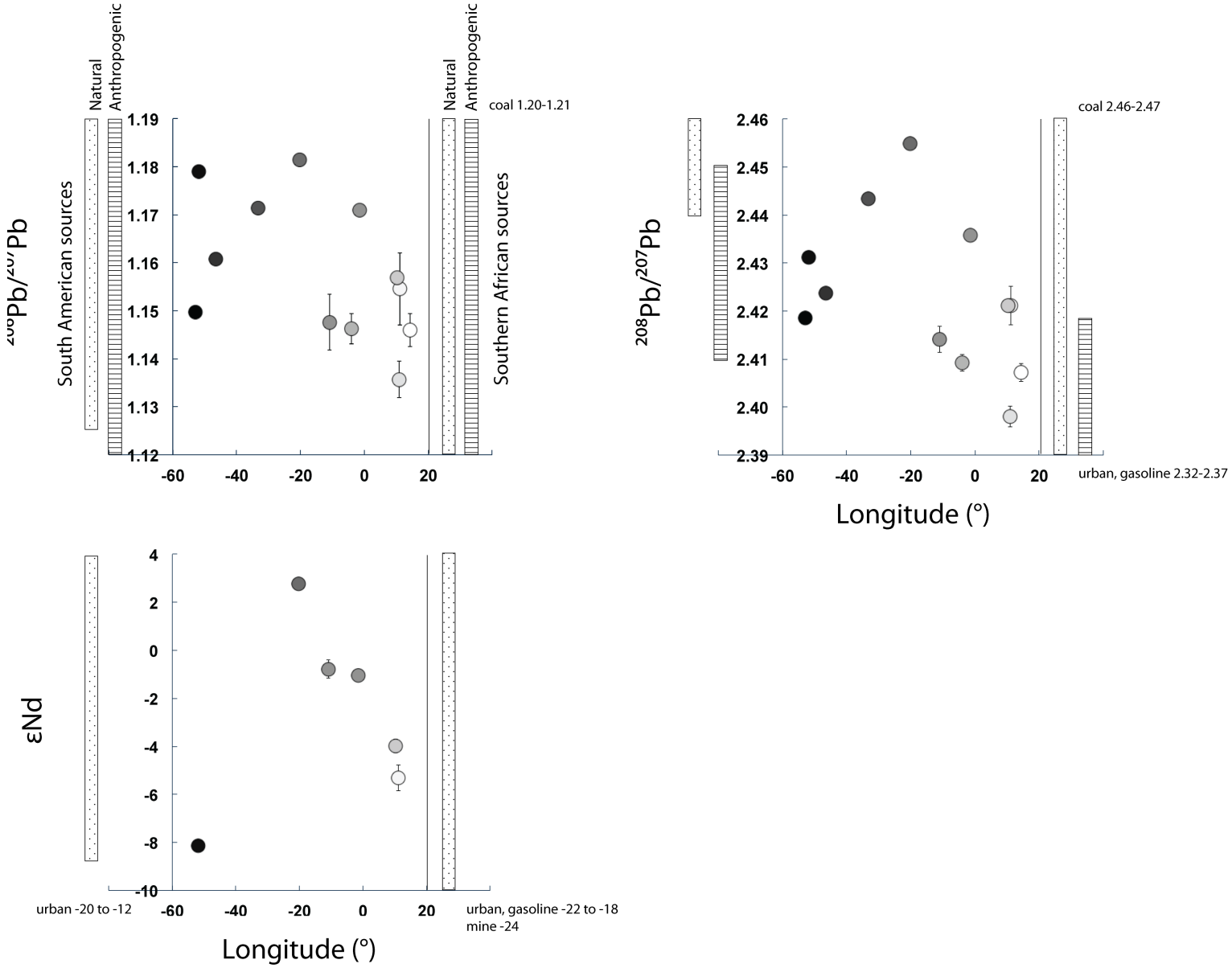

Figure 3.6. Lead and neodymium isotopic composition in aerosol samples across the South Atlantic Ocean. Aerosols west to east are denoted by black to white shading. Lead and neodymium isotopic compositions that were reported as characteristic of natural (dotted bar) and anthropogenic (lined bar) sources from South America and Southern Africa are shown (as characterised in Chapter 2, taken from Table 3.3). Errors were based on analytical uncertainties to 2σ.

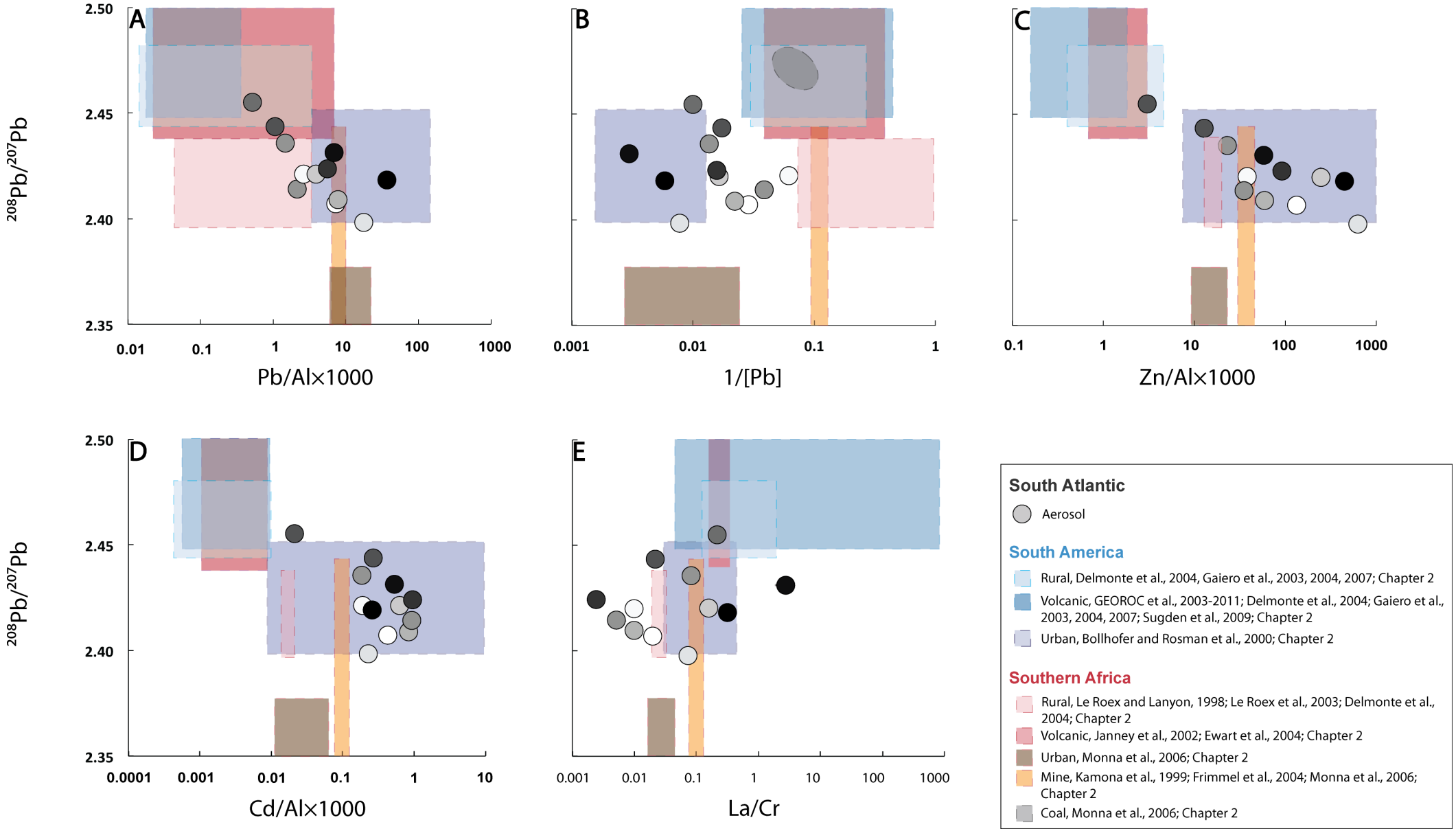

Figure 3.7. $^{208}Pb/^{207}Pb$ versus: (A) Pb/Al×1000, (B) 1/[Pb], (C) Zn/Al×1000, (D) Cd/Al×1000; and (E) La/Cr for aerosols (circle symbols) from across the South Atlantic Ocean. Aerosols west to east are denoted by black to white shading. Source regions from literature are shown where available (shaded areas), taken from Table 3.3. Errors were based on analytical uncertainties to 2σ and are smaller than the symbols plotted.

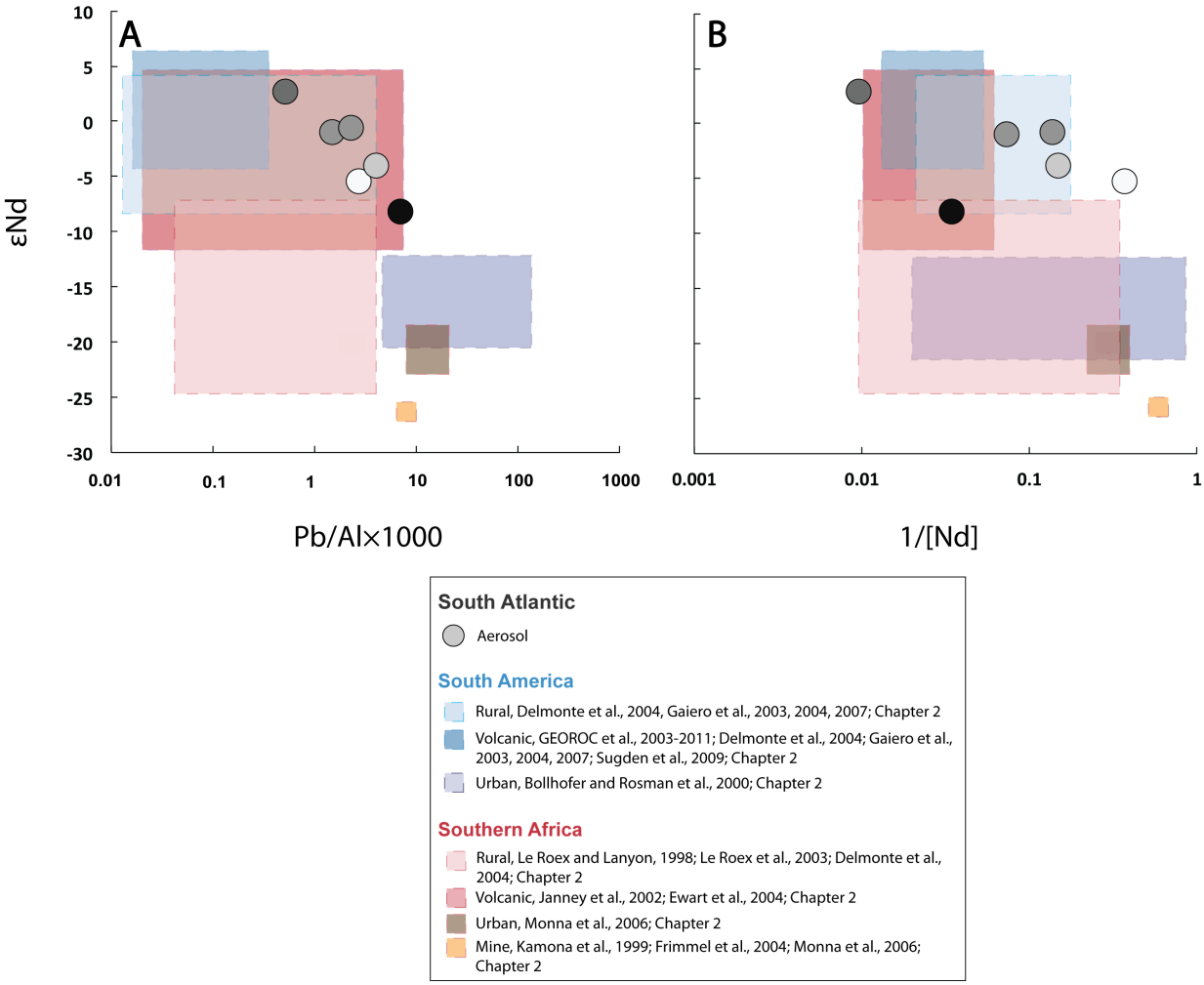

Figure 3.8. εNd vs. (A) Pb/Al×1000 and (B) 1/[Nd] for aerosols (circle symbols) from across the South Atlantic Ocean. Aerosols west to east are denoted by black to white shading. Errors were based on analytical uncertainties to 2σ and are smaller than the symbols plotted. Source regions from literature are shown where available (shaded areas), taken from Table 3.3.

3.4. Discussion

Natural and anthropogenic sources from South America and Southern Africa were compared to the element enrichment values and Pb and Nd isotopic composition in the aerosols in Figures 3.3 and 3.6. Bivariate plots of element ratios and Pb and Nd isotopic compositions of aerosols collected across the South Atlantic are illustrated in Figure 3.7 and 3.8 and were compared to major natural and anthropogenic sources from South America and Southern Africa (as reported in Chapter 2). Element and isotopic compositions of aerosols from this study and previous studies of aerosols over the South Atlantic and neighbouring oceans are listed in Table 3.6 and were referred to, to compare aerosol compositions over spatial and temporal regions.

3.4.1. Trace metal sources in the aerosols collected in the western section of the South Atlantic

3.4.1.1. Zinc, Lead, Copper, Cadmium

Low enrichments of Zn, Pb, and Cu at ~20°W and to a lesser extent at ~35°W, and lowest enrichment in Cd at ~20°W (Fig. 3.3) coincided with the air mass back trajectories that showed contact with southern South America and Antarctica (Fig. 3.2C and D, respectively). $^{208}Pb/^{207}Pb$, Pb/Al, 1/[Pb], Zn/Al, and Cd/Al ratios were in line with natural aerosol sources from South America (Gaiero et al., 2003; GEOROC, 2003-2011; Delmonte et al., 2004; as reported in Chapter 2; Table 3.6, light blue shading, Figure 3.7). These previous studies suggested that volcanics and meta-sediments of acid to mafic composition from Patagonia and the Andes were the main natural dust sources from South America. This study emphasised that dusts from these sources travelled west across the ocean and were the dominant contributing sources of Zn, Pb, Cu and Cd in aerosols between ~20-35°W.

The high enrichments in Zn and Cd, and similar trends in enrichments of Pb, and Cu suggested that these elements derived from similar sources. High enrichments in trace metals, Zn, Pb, Cu, Cd, and to a lesser extent V, closer to land than over the remote ocean suggested anthropogenic sources of these trace metals in the western margin of the South Atlantic, although air mass back-trajectories in the western section of the South Atlantic (west of ~20°W) showed no contact with land or limited contact with South America (at ~20-35°W) or Antarctica (at ~10°W). This trend was in line with previous studies in provenance of trace metals in aerosols over global oceans (e.g. Arimoto et al., 1987; Pacyna, 1989; Chester et al., 1991; Chester, 2000; Pacyna and Pacyna, 2001; Kim and Church, 2002; Witt et al., 2010). The Pb/Al, 1/[Pb], Zn/Al and Cd/Al signals in aerosols collected over the western section were consistent with those from anthropogenic sources from South America (Bollhofer and Rosman, 2000; Fujiwara et al., 2011; as reported in Chapter 2, Table 3.6, dark blue shading, Fig. 3.7). Bollhofer and Rosman (2000) suggested that the most important anthropogenic sources of aerosols from South America were from

north of ~45S from Argentina and Brazil. The $^{208}Pb/^{207}Pb$ ratios in the aerosols were in line with anthropogenic sources north of 45°S from South America (Bollhofer and Rosman, 2000; Gioia et al., 2010; dark blue shading, Fig. 3.7). This implied that these were important anthropogenic sources of aerosols from South America to reach the South Atlantic. Previous studies of global sources of anthropogenic elements suggested that the anthropogenic sources from South America north of 45°W were mainly from industrial processes, non-ferrous metal processing, smelting, biomass burning, coal burning and oil combustion, and mining (Nriagu et al., 1988; Bollhofer and Rosman, 2000; Pacyna et al., 2001; Mirlean et al., 2005). Lead isotopic compositions of aerosols also agreed with previous studies of aerosols from the western margin of the South Atlantic between 30-45°S (1.142-1.163 in $^{206}Pb/^{207}Pb$ ratios and 2.400-2.432 in $^{208}Pb/^{207}Pb$ ratios, Alleman et al., 2001; Witt et al., 2006). These previous studies also reported that industrial processes and metal processing of Pb, and most likely other trace metals such as Zn, Cu and Cd, were the dominant non-crustal supply of these elements to the South Atlantic Ocean at ~30-45°S at the western margin between 2001-2005 (Alleman et al., 2001; Witt et al., 2006). These previous studies also reflected diminishing impacts of anthropogenic Pb from leaded gasoline in aerosols collected over the South Atlantic since the ban across South America before the 2000s.

3.4.1.2. Vanadium

Vanadium enrichment values in aerosols in the western margin were in line with natural and anthropogenic sources from South America (Fig. 3.3). There was only slight enrichment in V relative to the continental crust in one aerosol in the western section. As V is a tracer for oil combustion (Kowalczyk et al., 1978; Pacyna et al., 2001; Okuda et al., 2007), this implied that oil combustion was not an important anthropogenic source in comparison to other potential anthropogenic sources of V, such as industrial and metal processes. The low enrichment values in V however suggested that the natural sources of V (Patagonian and Andean dusts, Gaiero et al., 2003; as reported in Chapter 2) were more important than anthropogenic sources of V in aerosols in the western margin. This also reflected a reduction in impact of fuel emissions to total anthropogenic emissions from South America, since the ban of leaded fuel.

3.4.1.3 Chromium, Nickel, Cobalt

The similar trends in Cr, Ni and Co enrichment factors in aerosols across the South Atlantic suggested that these elements derived from similar sources, dissimilar to the sources of Zn, Pb, Cu and Cd. The enrichment factors of Cr, Ni and Co in the two westernmost aerosols (sample JC068-15 and -17, west of ~55°W) were similar to natural sources from South America (Patagonian and Andean dusts, Gaiero et al., 2003; as reported in Chapter 2; Table 3.7, Fig. 3.3) and anthropogenic sources from South America

(industrial and combustion emissions from urban areas north of ~45S, Chapter 2, Table 3.7, Fig. 3.3). Air mass pathways passing close to southern South America (Fig. 3.2A) and La/Cr plots (Cr, Ni and Co element composition was represented by La/Cr in Fig. 3.7) revealed that these two aerosols most likely received Cr, Ni and Co from natural sources from South America. It was likely that Cr, Ni and Co derived from mafic geology where these elements are typically associated (e.g. Agnieszka and Barbara, 2012), in line with the mafic volcanic and plutonic geology across Patagonia and the Andes (de Almeida et al., 2000) which shows La/Cr ratios of ~0.05 to ~1 (as reported in Chapter 2).

This study could not rule out that anthropogenic sources could have played a part in the Cr, Ni and Co contribution in the two westernmost aerosols as these aerosols had received anthropogenic sources of Zn, Pb, Cu and Cd. Anthropogenic sources of Cr were most likely from coal combustion and atmospheric emissions from metal processing (Pacyna, 2001). The relationship between Cr, Ni and Co was in contrast to Pacyna's (2001) study, which found that V and Ni were associated with oil combustion. It was likely that Ni and Co were associated with Cr from these anthropogenic sources due to the use of mafic materials where these elements are typically associated, as mentioned above.

The Cr and Ni enrichments in the aerosols east of ~55°W in the western section (Fig. 3.3) were more enriched than previously characterised sources from South America (Table 3.6, Fig. 3.3 and represented as La/Cr in Fig. 3.7). There were difficulties in determining the exact cause of this occurrence, as there may have been a number of possibilities. These include unknown source characterisation, longer residence times of Cr and Ni in the atmosphere, and Cr and Ni enriched natural sources such as volcanic emissions.

The potential anthropogenic sources from South America were limited to studies of urban regions pre-dating 2000, and limited to up-to-date data (collected in 2010, Chapter 2) for only two urban regions that were collected during the summer while the aerosols over the Atlantic were collected during the winter. Recent studies suggested that anthropogenic contribution to aerosols is greater during the winter than the summer due to lower mineral dust contributions during the wetter and colder seasons (e.g. Ramanathan et al., 2001, 2002; Srivastava et al., 2014), and thus have implied that the characterised sources did not account for potentially higher trace element enrichments attainable during the winter season. This further suggested that the aerosols collected during the D357 and JC068 cruises may represent the elemental composition of aerosols during the winter season but not during the summer season.

There are mobile and immobile forms of Cr and Ni that may cause these elements to remain in the atmosphere for long periods of time (between 7 to 10 days) and allow Cr and Ni bearing particulates to travel over long distances (Kimbrough et al., 1999). For example lower pH environments, such as acidic conditions in cloud formations, results in oxidised Cr (VI), which is more soluble and mobile than Cr (III). Chromium (VI) is typically more abundant than Cr (III) in atmospheric emissions from industrial processes (Johnson et al., 2006), and may result in the retention of Cr (VI) in gases and liquids in clouds.

Lastly, it could not be ruled out that enriched natural sources such as volcanic emissions may have caused high Cr and Ni enrichment. Chromium and Ni predominantly occur in the fraction bound with Fe and Mn oxides (Agnieszka and Barbara, 2012), which result in mobile forms of Cr and Ni (Jickells and Spokes, 2001; Desboeufs et al., 2001). Fig. 3.3 and 3.5 showed some correlation in Cr, Ni and Fe, Mn enrichment patterns across the ocean. Furthermore, low pH conditions in the atmosphere may have caused the release of mobile Cr and Ni.

3.4.2. Trace metal sources in the aerosols collected in the eastern section of the South Atlantic

3.4.2.1. Zinc, Lead, Copper, Vanadium

High enrichments in trace metals observed in aerosols that had seen contact with central South America (samples JC068-6 at ~1°W and D357-8 at ~3°E) within ~10° in longitude to the only aerosol sample that had seen contact with Antarctica (JC068-8 at ~10°W) suggested that Antarctica was not a major source of dust to the South Atlantic (Fig. 3.2 and 3.3). Enrichments of Zn, Pb, Cu, and V (Fig. 3.5), and $^{208}Pb/^{207}Pb$ and 1/[Pb] ratios (Fig. 3.7) suggested Southern Africa played a major role in their aerosol sources in the eastern section of the South Atlantic, as well as sources from South America. The increase in Zn, Pb, Cu and to a lesser extent V enrichments from the remote ocean, from ~20°W, to high enrichments at the coast of Southern Africa was a strong indication of continental influence in their enrichments, most likely from anthropogenic sources (Fig. 3.3). The relatively lower $^{208}Pb/^{207}Pb$ ratios in the aerosols over the eastern section, except at ~1°W (sample JC068-6), compared to aerosols at the western margin suggested different sources of Pb were observed in the aerosols in the eastern and western sections (Fig. 3.6). Bollhofer and Rosman (2000) suggested gasoline contributed 40% while mining and coal burning contributed 60% of anthropogenic aerosols from Southern Africa. Since the ban of Pb in 2006 in South Africa, Bollhofer and Rosman's study (2000) suggested that mining and coal contributed to the majority (>60%) of anthropogenic emissions that impact aerosol composition in urban sources in Southern Africa. Taking all the above into consideration the Pb isotopic compositions in aerosols east of ~20°W were most likely in line with the compositions of mine sources (~1.09-1.33 in $^{206}Pb/^{207}Pb$ and <2.25-2.42 in $^{208}Pb/^{207}Pb$; Johannesburg, Monna et al., 2006, and as determined in Chapter 2; Rosh Pinah, Namibia, Frimmel et al., 2004; Kabwe and Tsumeb, Namibia, Kamona et al., 1999; Table 3.7, Fig. 3.6 and 3.7) than coal (~1.20-1.21 in $^{206}Pb/^{207}Pb$ and ~2.46-2.47 in $^{208}Pb/^{207}Pb$; Monna et al., 2006, Table 3.7, Fig.3.6 and 3.7). This strongly suggested that mine sources played a more important role in atmospheric Pb contributions, and most likely associated elements Zn, Cu and V, over the eastern section of the South Atlantic, than emissions from coal burning from Southern Africa. The 1/[Pb] ratios in aerosols were similar to signals from anthropogenic sources from South America, and anthropogenic and natural

sources from Southern Africa. This further illustrated the major influence that Southern African sources may have on Pb compositions in aerosols east of ~20°W (Fig. 3.7).

3.4.2.2. Chromium, Nickel, Cobalt, Cadmium

Lowest Cr and Ni enrichments in aerosols in the eastern section were in line with air mass back trajectories that passed over Southern Africa up to 10 days prior to aerosol deposition and were in line with enrichments from previously characterised natural dust sources from Southern Africa (Table 3.7, Fig. 3.3). This suggested that Cr and Ni enrichments in aerosols over the eastern section could have received contributions from sources from Southern Africa. Previously determined natural dust sources from Southern Africa such as desert dust from Namibia and the Kalahari were likely sources of aerosols at the eastern margin of the South Atlantic (Delmonte et al., 2004; Bollhofer and Rosman, 2000; as reported in Chapter 2; Table 3.6).

Enrichment relative to the continental crust of Co at the eastern part of the South Atlantic were in line with rural and mine sources from Southern Africa (enrichment of <10 and >10 in rural and mine source areas, respectively, from Johannesburg, Monna et al., 2006; as reported in Chapter 2; Fig. 3.7). This suggested that Co may have derived from rural sources where Co enrichments were <10, and from mining activities from Southern Africa where Co enrichments were >10.

At the same time, the consistently high enrichment in Cr, Ni, Cd and to a lesser extent Co west and east of ~20°W (Fig. 3.3) coupled with air mass circulation that dominantly travelled west to east (Fig. 3.2.) suggested that aerosols dominantly from anthropogenic sources from South America were delivered to the eastern section of the South Atlantic. As discussed in Section 3.4.2, high enrichments in Cr, Ni and Co may have also been attributed to enriched natural sources from South America.

All the above occurrences were a strong indication that aerosols originated from South America and reached the coast of Southern Africa due to west to east long-range atmospheric transportation, while also receiving aerosols from Southern Africa. This was a useful indication that experimental data were in line with models of atmospheric circulation across the South Atlantic as reported in previous works (Prospero et al., 2002; Meskhidze et al., 2007; Johnson et al., 2011), and that air pathways carried atmospheric particulates from Africa to the South Atlantic (as suggested by atmospheric models from Piketh et al., 2002). These studies focused on the transportation of natural dusts, however it was highlighted in this study that anthropogenic aerosols were also important in long-range transportation of particulates from South America to across the South Atlantic. This is similar to the North Atlantic where long-range transport of anthropogenic and natural atmospheric particulates across the ocean have been reported (e.g. Jickells and Spokes, 2001; Sholkovitz et al., 2009).

3.4.3. Major element sources

Iron and Mn enrichments relative to the crust were in line with previous studies of Fe and Mn in aerosols over the South Atlantic between the 1980s-2002 (between ~0.1-10; Witt et al., 2006; Radlein and Heumann, 1992; Murphy et al., 1985; Table 3.8) aside from Fe and Mn enrichments at sample JC068-14. Iron and Mn enrichments were also similar to those reported over regions of the North Atlantic (<10; Baker et al., 2013; Kim and Church, 2002; Sholkovitz et al., 2009; Jimenez-Velez et al., 2009; Buck et al., 2010) and South Atlantic (<10; Evangelista et al., 2012). This suggested that Fe and Mn similar to the North Atlantic, derived from natural dust sources. The similarly enriched level in Mg to Fe and Mn at sample JC068-14 may have suggested that Mg shows similar trends to Fe and Mn in enrichment factor across the ocean. This may be due to shared sources as Fe, Mn and Mg are typically associated in mafic rock. There were no trends in K enrichment factor across the ocean and there was not enough enrichment data for Ca to deduce more than Ca enrichment factors below 10 suggested that Ca derived from natural sources.

The major element enrichments in aerosols were in line with natural sources from South America and Southern Africa (0.1-400, Condie and Hunter et al., 1976; Le Roex and Lanyon, 1998; GEOROC et al., 2003-2011; Gaiero et al., 2003; Le Roex et al., 2003; as reported in Chapter 2, Table 3.7). There was not enough evidence to suggest that non-crustal sources impact major element enrichments. The enriched levels of Fe and Mn at sample JC068-14 (Fig. 3.5) may have been due to enriched natural dusts from South America. The variable enrichments in major elements may have also been a result of variable wind patterns, and different transient sources coupled with variable residence times of elements in the atmosphere (Moore et al., 1973; Turekian et al., 1977; Talbot and Andren, 1983).

3.4.4. Mineral dust

The rare earth elements, and Y, Th and to a lesser extent Sc enrichments relative to the crust (Fig. 3.4) suggested that they were of continental origin and were not affected by anthropogenic sources of trace metals. These findings were in agreement with one previous study of Saharan dust fluxes to the North Atlantic (enrichment factor of 0.8-1, Greaves et al., 1994) and were in line with enrichments from natural sources from Patagonia and the Andean volcanic belt in South America (0.01-10, Gaiero et al., 2004; as reported in Chapter 2; Table 3.7). The εNd and 1/[Nd] ratios in aerosols at ~20°W implied that volcanic dusts were more important natural sources of aerosols than mineral dust from South America (-8.9 to +3.4 in εNd in mineral dust and -4.2 to +6.1 in volcanic sources, GEOROC et al., 2003-2011; Delmonte et al., 2004; Gaiero et al., 2007; Sugden et all., 2009; as reported in Chapter 2, Table 3.7, Fig. 3.6 and 3.8). The εNd and 1/[Nd] ratios in the aerosols in the western margin and aerosols between ~10-20°W in the eastern section agreed with the less radiogenic Nd isotopic signals of the natural sources from South America (GEOROC, 2003-20011; Delmonte et al., 2004; Gaiero et al., 2007; Sugden et al., 2009; as

reported in Chapter 2, Fig. 3.8). Similarly to the trace elements, Cd, Cr, Ni and Co, this suggested that lithogenic particulates from South America were delivered to across the 40°S transect of the South Atlantic through long-range atmospheric transportation.

The slight enrichments in Sc above REE, Y and Th at the eastern margin may have been due to anthropogenic source inputs (Fig. 3.4). Scandium is particularly associated with uranium mining (e.g. Rose, 1960) and Southern Africa was host to one of the largest open pit uranium mines in the world (Rio Tinto, 2014). Furthermore, as indicated by enrichment trends in other trace metals in aerosols over the eastern margin of the South Atlantic (as discussed in Section 3.4.2), mining sources from Southern Africa were most likely the major anthropogenic source of Sc in aerosols over the eastern margin (Table 3.7).

Table 3.8. Examples of select element enrichment factors and lead and neodymium isotopic compositions of aerosols from literature

Element or isotopic composition	Sample date	$^{208}Pb/^{207}Pb$	$^{206}Pb/^{207}Pb$	Pb	Zn	Cu	V	Cr	Ni	Co	Cd	REE	Majors
This study	**2010 and**	**2.395-2.455**	**1.130-1.180**	**2-200**	**1-1000**	**3-300**	**1-60**	**1-5000**	**1-5000**	**2-200**	**1-2000**	**1**	**1-100 (Ca,Mn,K)**
S Atlantic (~20°E-60°W, ~40°S)	**2011/12**											**-8.1 to +2.8 (εNd)**	**0.1-30 (Fe)** **0.3-100 (Mg)**
(1) S Atlantic (~40-60°W, ~30-50°S)	2002	2.400-2.432	1.142-1.163	>90-1300	>90-1300	>90-1300					>90-1300		0.1-10 (Fe, Mn)
(1) S Atlantic (~20-40°W, ~20-30°S)	2002	2.336-2.429	1.056-1.188										
(2) S Atlantic	<2001	2.400-2.432	1.142-1.163										
(3) Equatorial and S Atlantic (0°N-35°S)	<2002			<10	<10	<10		<10	<10		<100		0.1-10 (Fe, Mn)
(4) S Atlantic	<2013												0.1-10 (Fe, Mn)
(5) S Atlantic	1989			215	200	50		50	100		23000		
(6) S Atlantic	<1985			2364	784	161							
(4) N Atlantic	<2013												1-10 (Fe, Mn)
(7) N Atlantic	2003/4						<10		15				<10 (Fe)
(8) N Atlantic	2003			<10			20						<10 (Mn)
(3) N Atlantic (31°N)	<2002			<100	<1000	<10		<10	<10		<1000		<10 (Mn)
(1) N Atlantic	2002	2.415-2.454	1.142-1.166			<10					<10		
(9) N Atlantic (Saharan dust)	2004			<10			<10		<10		<10		<10 (Fe)
(10) N Atlantic (Saharan dust)	<1994											0.8-1	
(6) N Atlantic	<1985			9.1	3.8	1.2					9.4		
(1) W Indian Ocean	2002	2.415-2.445	1.150-1.183	>90-1300	>90-1300	>90-1300							
(11) W Indian Ocean	2007			<10	~100	<100	<10	~10	<100	<10	<100		
(12) Indian Ocean	1987			158	13	10							
(13) Tropical S Pacific Ocean	1979			146	114	27							

(1) Witt et al., 2006; (2) Alleman et al., 2001; (3) Kim and Church, 2002; (4) Baker et al., 2013; (5) Radlein and Heumann, 1992; (6) Murphy et al., 1985; (7) Sholkovitz et al., 2009; (8) Buck et al., 2010; (9) Jimenez-Velez et al., 2009; (10) Greaves et al., 1994; (11) Witt et al., 2010; (12) Chester et al., 1991; (13) Arimoto et al., 1987

Table 3.9 Select anthropogenic source contributions of elements from South America over the South Atlantic Ocean

Element	Longitude		
	West of ~45°W	Between ~20-35°W	East of 20°W
Pb	55-75%	30-40%	
Zn	60-65%	30-40%	
Cu	55-75%	30-50%	
Cd	70-90%	50%	70-90%

3.4.5. Calculating source contributions of select elements to aerosols across the South Atlantic Ocean

Air mass back trajectories and element enrichments for aerosols, and provenance proxies identified in Chapter 2, showed strong indications that South America was the most important source of both natural and anthropogenic sources of Zn, Pb, Cu and V to the western section of the South Atlantic. The difference in enrichment factor of an element in an aerosol (X) and the lower limit enrichment factor of the natural source area from South America (X_N) was calculated, and then divided by the difference in the upper end-limit of the anthropogenic source area (X_A) and lower-limit enrichment of the natural source area from South America (from Table 3.7 and Fig. 3.3). This value was then multiplied by 100 to present the anthropogenic contribution in percentage (A, in %) (5), and the results are shown in Table 3.9. These calculations showed similar results when conducted with Pb isotopic ratios and highlighted that enrichment factors relative to the upper continental crust can be used to assess element contributions in aerosols. By combining the assessment of provenance tracing aerosols over the South Atlantic Ocean by elemental and isotopic compositions, air mass back trajectories and calculating source contributions of elements over the South Atlantic, a simplified diagrammatic of qualitative source contributions and how they vary across the South Atlantic Ocean were summarised in Figure 3.9. The contributions for V were not calculated as the natural and anthropogenic source compositions were quite similar (Fig. 3.5).

$$A = ((X-X_N) / (X_A-X_N)) \times 100 \quad (5)$$

Anthropogenic sources contributed 55-75% of total Pb west of ~45°W, and 30-40% (and thus 60-70% natural dust) at ~20-35°W. The anthropogenic Zn and Cu contributions were also high on the western margin ranging between 60-65% and 55-75%, respectively, and 30-40% for total Zn and 30-50% for total Cu at ~20-35°W. Anthropogenic Pb contributions were lower than over parts of the North Atlantic where anthropogenic Pb was estimated to account for up to 80% total atmospheric Pb deposition

(Jickells and Spokes, 2001; Mahowald et al., 2005). This was in line with studies that suggested aerosol fluxes are lower over the South Atlantic Ocean than the North Atlantic Ocean. Assuming that long-range transportation of Cd across the South Atlantic originated from South America, anthropogenic sources contributed between 70-90% of the total Cd in aerosols distributed across the ocean, except at ~20°W where anthropogenic contribution of total Cd in aerosols is 50%.

It was difficult to determine Pb, Zn, Cu or V source contributions, except Cd, over the eastern section of the South Atlantic due to the overlapping elemental and isotopic compositions of South American and Southern African sources. It was also difficult to quantify Cr, Ni and Co source contributions across the ocean due to undetermined upper-limits in element composition of anthropogenic sources from South America.

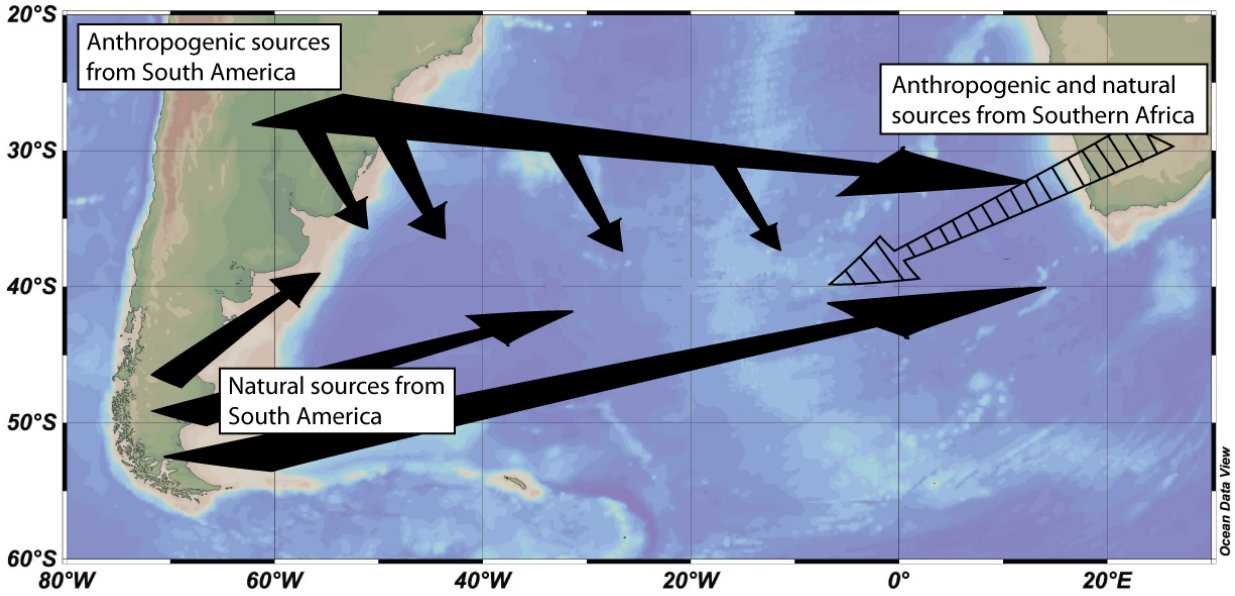

Figure 3.9 Simplified diagrammatic of qualitative source contributions across the South Atlantic Ocean. The arrows indicate general source regions and atmospheric pathways of aerosols from the source to the ocean from South America (black arrows) and South Africa (dashed arrow).

3.4.6. Implications on temporal variation in sources of aerosols to the South Atlantic Ocean and air quality

The trends in enrichments of trace metals and provenance proxies across the South Atlantic revealed implications of the nature of the anthropogenic sources and the behaviour of elements in the atmosphere. The higher enrichments of Zn and Cd relative to Cu, Pb and V at the ocean margins suggested that Zn and Cd were the most common and dominant component of the five elements to derive from anthropogenic sources from South America (Fig. 3.3). The enrichments of Zn and Cd in aerosols were in line with

previously determined aerosol compositions over the western margin of the South Atlantic between ~40-60°W and ~30-50°S (>90-1300 in Zn and Cd, Witt et al., 2006, Table 3.8). Zinc enrichments were also similar in aerosols determined pre-1989 while Cd was lower (200 to 784 in Zn determined by Radlein and Heumann, 1992, and Murphy et al., 1985; and ~23000 in Cd; Murphy et al., 1985, Table 3.8). This suggested that anthropogenic sources of Zn over the South Atlantic remain as important today as in the 1980s while Cd may have decreased since the 1980s but remains consistent since Witt's 2006 study (2002, Table 3.8). Lead and Cu enrichments were similar to aerosols reported in 2003 (>90-1300 in Pb and Cu; Witt et al., 2006, Table 3.8) and in 1989 (215 in Pb and 50 in Cu; Radlein and Heumann, 1992, Table 3.8). Copper enrichments reported in this study were also in line with Cu enrichments before 1985 while Pb enrichments were lower than before 1985 (161 in Cu, 2364 in Pb; Murphy et al., 1985). Previous studies of Pb and Cu enrichments in aerosols over the western margin of the South Atlantic suggested that anthropogenic Pb emissions from South America may have reduced since the 1980s and would reflect the fall in Pb-enriched combustion emissions, or showed large temporal fluctuations, while anthropogenic sources of Cu, similar to Zn, remain as important today as in the 1980s. The possible change in Pb emissions would mean that there was a reduced Pb toxicity in the air and thus better air quality over major urban areas in South America at the time of this study than in the 1980s.

There were limited studies of Cr and Ni composition in aerosols over the South Atlantic, however these implied that the South Atlantic received higher Cr and Ni enrichment relative to the continental crust during this study than prior to in the 2000s (<10 in the 2000s, Alleman et al., 2001; up to 100 pre-1989 (Radlein and Heumann, 1992). Chromium and Ni enrichment in aerosols were also higher than in aerosols over the North Atlantic (<15 in the 2000s, Kim and Church, 2002; Sholkovitz et al., 2009; Jimenez-Velez et al., 2009) and over the Indian Ocean in 2007 (<10 and <100, respectively, Witt et al., 2010). This study implied that unlike other neighbouring oceans, the South Atlantic received higher enrichments in Cr and Ni than other common anthropogenic elements, Zn, Pb, Cu, Cd, and V (Fig. 3.3, Table 3.7 and 3.8) and the particularly high enrichments in Cr and Ni may pose concerns for air quality over source regions from South America and Southern Africa, and element exchange behaviours between air and water.

3.5. Conclusions

A set of 13 were aerosols collected across the 40°S transect of the South Atlantic Ocean from two cruises (D357 during Oct 2010 and JC068 during Dec 2011 to Jan 2012). These were analysed for major, trace and REE compositions and Pb and Nd isotopic compositions to determine provenance of selected elements and some implications to atmospheric transport over the South Atlantic.

Four of the metals considered (Zn, Pb, Cu and to a lesser extent V) showed high enrichments relative to the continental crust at the west (west of ~45°W) and east margins (east of ~5°W) of the South Atlantic and all declined in enrichments to the remote ocean, to ~20-35°W. Despite air mass back trajectories that showed pathways passing close to southern South America at the western margin and pathways passing over South America, Antarctica and Southern Africa, these trends in enrichment suggested that Zn, Pb, Cu and V distributions over the South Atlantic were controlled by anthropogenic sources from South America and Southern Africa.

In contrast, Cr, Ni and to a lesser extent Co showed high enrichments relative to continental crust at the west margin (between ~45°W to 20°W) and declined in enrichment to the east margin which coincided with air mass pathways dominantly prevailing west to east over the South Atlantic Ocean, and suggested that anthropogenic sources from South America most likely dominated their distribution over the South Atlantic. It however could not be ruled out that enriched natural sources such as volcanic dusts or long-residence times (between 7-10 days) may have contributed to the high enrichments in Cr, Ni and Co exhibited across the ocean. This further revealed that Cr, Ni and Co underwent long-distance transportation west to east across the ocean. The two westernmost aerosols, west of ~50°W were the exception to this trend and showed Cr, Ni and Co enrichments typical of crustal and anthropogenic origin. Cadmium was highly enriched relative to the continental crust across the ocean, except at ~20°W and suggested anthropogenic sources governed Cd supply across the South Atlantic.

Major, REE, Sc, Y and Th enrichments were typical of continental crust. Enrichments in major elements (enrichment factor up to 80) over the South Atlantic were not enough evidence to suggest anthropogenic origin and may have rather been explained by variable wind patterns and variable residence times in the atmosphere. Slight enrichments relative to continental crust of Sc (enrichment factor up to 30) in aerosols east of ~10°E may have been due to anthropogenic sources from Southern Africa.

Lead isotopic ratios (^{208}Pb, ^{207}Pb and ^{206}Pb) and trace element ratios (Pb/Al, 1/[Pb], Zn/Al and Cd/Al) showed distinct signals consistent with major anthropogenic sources from South America most typical of industrial and metal processes, and coal combustion. Vanadium is a tracer for oil combustion and low V enrichments relative to other trace metal enrichments suggested oil combustion sources were not as important as industrial and metal processes, and coal combustion sources, for atmospheric particulates that reach the South Atlantic. The La/Cr ratio, εNd and 1/[Nd] signals west of ~50°W and

between ~20-35°W were consistent with natural sources of Cr, Ni, Co, major and REEs from Patagonia and the Andean volcanic belt from southern South America. Higher Pb isotopic ratios between ~20-35°W than west of ~50°W indicated that volcanic dust sources dominated over mineral dust sources between ~20-35°W and to a lesser extent west of ~50°W. Over the eastern section of the South Atlantic, east of ~20°W, Pb isotopic ratios, Pb/Al and 1/[Pb] showed signals consistent with a mixture of South American and Southern African sources. High enrichments in trace metals relative to continental crust at the eastern margin and Pb isotopic ratios were particularly useful at showing that anthropogenic aerosol sources from Southern Africa, predominantly from mine sources, played a major role on trace metal contributions at the eastern margin.

Taking into account that natural and anthropogenic sources from South America appeared to be the main sources of aerosols west of ~20°W, anthropogenic source contributions were calculated from enrichment factors. Anthropogenic sources contributed ~55-75% of total Pb and Cu, and ~60-65% of total Zn in aerosol masses west of ~45°W, and ~30-40% of total Pb and ~30-50% of total Zn and Cu between ~20-35°W. As Cd appeared to be delivered to the South Atlantic from South America, anthropogenic Cd contributions were ~70-90% of total Cd delivered across the ocean, except at ~20°W where anthropogenic Cd contributions were ~50%.

The high enrichments in Zn, Pb, Cu, and Cd in aerosols in the western margin were in line with recent studies of trace metal composition in aerosols along 40°S (Radlein and Heumann, 1992; Alleman et al., 2001; Kim and Church, 2002; Witt et al., 2006; Baker et al., 2010) and Pb was below enrichments in aerosols over the South Atlantic pre-1985 (Murphy et al., 1985) These studies also implied that there has been little change in Zn, Cd, Cu and V emission concentrations from anthropogenic sources from South America over the last few decades, and potential decreases in Pb concentrations would reflect the fall in Pb-enriched combustion emissions.

Relatively higher enrichments in Cr and Ni than Zn, Pb, Cu and Cd across the ocean suggested that anthropogenic emissions of Cr and Ni were greater than anthropogenic sources of Zn, Pb, Cu and Cd. This further implied that Cr and Ni may have derived from additional sources than Pb, Zn, Cu and Cd, or higher ion mobility resulted in a longer residence time of Cr and Ni in the atmosphere. Such enrichments in Cr and Ni have not been reported in aerosols over the South Atlantic and neighbouring oceans such as the North Atlantic and Indian Ocean, and implied that the particularly high enrichments in Cr and Ni may pose concerns for air quality over source regions from South America and Southern Africa, and element exchange behaviours between air and water.

This study showed that Pb and Nd isotopic compositions in aerosols were useful tracers of anthropogenic and natural sources, respectively, and the combination with elemental data provided further details of the distribution and provenance of elements across the South Atlantic, particularly those that did not appear to be associated with Pb or Nd. For instance Pb crustal enrichment trends across the South Atlantic appeared to be associated with Zn, Cu and V but were not well associated with Cr, Ni and

Co in aerosols and suggested different major sources and possibly Cr and Ni phases were more mobile and susceptible to remaining in the atmosphere than Pb, Zn, Cu and V.

This study has provided detail of the sources of elements in aerosols that reach the South Atlantic Ocean along a transect; however caution should be taken with aspects of the provenance assessment. Natural dust sources were reported to contribute greater dust emissions during the summer due to the arid and hotter conditions, while anthropogenic sources contributed greater aerosol emissions during the wetter and cooler periods of winter due to lower natural dust contributions (e.g. Ramanathan et al., 2001, 2002; Srivastava et al., 2014). The aerosol dataset in this study was restricted to the winter. Provenance assessments using sources from South America were conducted using data gathered during the summer (Fujiwara et al., 2011; Chapter 2). This may have affected the provenance assessment of trace elements from South America. For example, Cr and Ni enrichments were higher in the aerosol than in the characterised anthropogenic sources. A number of reasons were suggested to account for this outcome, two of which were limited data for source characterisation, and seasonal variation in aerosol composition. There were 13 aerosol samples, 7 of which were collected over the eastern section of the South Atlantic. This resulted in fewer data points for the western margin and limited the assessment of element and isotopic trends across the transect. The low element mass in aerosol samples presented large uncertainties (up to >95%). This largely affected the lowest element concentration in samples closest to the west and east margins of the ocean. With limited data points, this further restricted the assessment of element and isotopic trends across the transect.

CHAPTER 4

Major, trace and rare earth element solubility in aerosols along the South Atlantic GEOTRACES GA10 (40°S) transect

4.1. Introduction

The South Atlantic Ocean is reportedly depleted in elements essential to biological activity (Prospero et al., 2002), most likely due to low inputs of atmospheric particulates across the South Atlantic (e.g. Duce et al. 1991; Li, 2008). However, biogeochemical models suggest that a region of high primary productivity and active sedimentation exists along ~40°S across the South Atlantic Ocean (Mahowald et al., 2005). Iron in the surface water is a main limiting factor of primary productivity in this region because of its low solubility in seawater and rapid uptake in biological reactions (Mahowald et al., 2005). Due to the short residence time of Fe in the ocean (0.6yrs, Bruland and Lohan, 2003), major atmospheric deposition or higher solubility of elements in the aerosols deposited along ~40°S than the rest of the ocean were thought to be the most likely supply of Fe to this region (Mahowald et al., 2005), but this idea has not been well constrained by atmospheric modeling and geochemical data.

Particulate matter can undergo significant chemical processes in the cloud during transport resulting in photochemical reactions and organic complexation, this process can increase solubility (e.g. Losno, 1989; Zhuang et al., 1992; Kieber et al., 2003; Hand et al., 2004; Paris et al., 2011; Shi et al., 2012). In clouds, acidic gases such as HNO_3, SO_2 and NH_3 are present and modify the pH of the cloud droplets, which can increase the soluble fraction of mineral particles (Heimburger et al., 2013). Decreases in mineral size with distance due to weathering and settling of larger particles increases the proportion of their volume exposed to surface processes available for dissolution (Baker and Jickells, 2006). Subsequently, the smaller the aerosol and the longer the distance travelled, the more soluble they become (Baker and Jickells, 2006). Higher element solubility has been reported from anthropogenic particulate matter than natural mineral dust (e.g. Colin et al., 1990; Jickells et al., 1992; Spokes et al., 1994; Ebert and Baechmann, 1998; Desboeufs et al., 2001). Most recent findings have suggested that aerosol sources and aerosol types have greater influence on the aerosol solubility than these other factors due to acidification of finer particles in anthropogenic than natural mineral dust (Colin et al., 1990; Jickells et al., 1992; Spokes et al., 1994; Ebert and Baechmann, 1998; Baker et al., 2006, 2013; Sholkovitz et al., 2009). Anthropogenic particulates, in particular from combustion emissions, were found to contain smaller particle size fractions than continental dusts and displayed higher solubility (as much as ~80% of Fe) upon entering the ocean than continental dusts (1-2% of Fe; Sholkovitz et al., 2009). As much as 80% of the annual dry deposition of soluble iron from aerosols to the surface ocean of the North Atlantic was derived from anthropogenic sources (Jickells and Spokes, 2001; and Mahowald et al., 2005, respectively). Solubility of Fe, Mn and Al in flyash (38%, 97%, 43% respectively) is higher than for natural dusts (0.04%, 2%, 0.1% respectively) (Desboeufs et al., 2001).

There is a lot of solubility data for major elements Fe, Mn, and Al from aerosols over oceans (Jickells and Spokes, 2001; Baker et al., 2006; Sartou et al., 2007, 2003; Baker et al., 2010; Witt et al., 2010; Buck et al., 2013; Heimburger et al., 2013; Baker et al., 2013). This is due to their importance in

biological processes such as photosynthesis and nitrogen fixation (Boyd and Ellwood, 2010), and the use of Al to estimate mineral dust inputs to the ocean (Measures and Vink, 2000). There is little data on the solubility of trace and rare earth elements in aerosols over the global oceans (e.g. Greaves et al., 1994; Witt et al., 2010; Heimberger et al., 2013). A number of the first-row transition metals are essential for marine organisms (Bruland et al., 1991; Coale, 1991; Butler, 1998) and iron may be co-limited by other transition metals, such as manganese (Mn; Middag et al., 2011), copper (Cu; Annett et al., 2008), cobalt (Co, Saito et al., 2002), zinc (Zn, Morel et al., 1991) and nickel (Ni, Price and Morel, 1991). These elements are typically more enriched relative to the continental crust in anthropogenic aerosols than natural mineral dusts (e.g. Chester and Jickells, 2012). Therefore it is important to understand, in particular the major and trace metal solubility from aerosols, as this may increase or inhibit marine primary productivity.

With growing concerns in the implications that anthropogenic aerosols may have on the element availability to surface seawater and potentially crucial supply of elements to the ocean surface waters of the South Atlantic via the atmosphere, it is essential to improve the understanding of the affect anthropogenic sources have on the distribution and solubility of elements that may impact the supply of elements important to marine biogeochemical processes in the South Atlantic Ocean. Assessing the lead (Pb) isotopic composition in the soluble phase will also give indications of the importance of anthropogenic verses natural sources of lead (and associated elements) in the element supply to the ocean as Pb is a useful provenance indicator of different natural and anthropogenic sources of Pb (e.g. Bollhofer and Rosman et al., 2000; Witt et al., 2006; Monna et al., 2006; Gioia et al., 2010).

Based on the previous Chapters, 2 and 3, and the studies discussed above, this study hypothesized that higher solubility would be observed for elements that exhibit higher enrichment relative to the upper continental crust, assuming that higher enrichment is due to anthropogenic sources. This should be linked to the spatial variation in enrichment across the South Atlantic. This study aimed to investigate the importance of natural vs. anthropogenic aerosol sources on the availability of elements to the surface seawater of the South Atlantic Ocean. This was accomplished by i) determining major, trace and REE compositions and Pb isotopic ratios in the soluble fraction from aerosols collected along 40°S of the South Atlantic Ocean using an ammonium acetate buffer solution to conduct a weak acid extraction at pH 4.7. This extraction can represent wet deposition of aerosols from the atmosphere (particle dropout from the atmosphere in liquid or gaseous form due to rainfall or atmospheric cloud processes) (Bruland et al., 2001) and therefore element supply to seawater. The soluble fraction of aerosol elements were then compared to the total aerosol element and isotopic composition (taken from Chapter 3), potential aerosol sources (taken from Chapter 2), and element enrichment relative to the continental crust in total aerosols (taken from Chapter 3) to assess ii) the solubility of elements from aerosols over the South Atlantic, iii) the importance of natural vs. anthropogenic sources on element solubility and iv) the implications these solubility estimates have for element availability to the marine environment.

4.2. Sampling and Methods

4.2.1. Aerosol sampling

Aerosol sampling was conducted between 18th October and 22nd November 2010 during cruise D357/GA10E on the RRS Discovery, and between 27th December 2011 and 27th January 2012 during cruise JC068/GA10W on the RRS James Cook. Cruise tracks and aerosol sampling locations are shown in Chapter 3. The aerosol sampling and preparation methods have been previously described in Chapter 3 and followed previously conducted routine procedures (Baker et al., 2003, 2006a; Jickells et al., 2003; Sarthou et al., 2003). In brief, bulk aerosol (collected on a single filter) were collected over a ~4 day period onto cellulose Whatman 41 filters (A4-sized; Sarthou et al., 2003) by a high-volume sampler (Graseby Anderson, at $1m^3$ min^{-1}) mounted on the top deck (monkey island) of the ship in-front of the ships funnel. Filters were acid-washed before use on the ship (Sarthou et al., 2003; Baker et al., 2006b). Aboard the ship all filter handling was carried out using a laminar flow bench.

4.2.2. Aerosol leaching procedure

Sample treatment in the laboratory was carried out in a laminar flow bench housed laboratory with pre-filtered air. Ultrapure acids and ultraclean (MQ) water were used throughout all sample preparation stages. Soluble trace elements were extracted from aerosol samples with ultrapure ammonium acetate buffer solution (pH4.7) as a model for element release from aerosols in rainwater. This procedure is similar to the method employed by Bruland et al. (2001) to indicate the presence of bioavailable Fe in upwelling particulate matter off the coast of California and has been used multiple times thereafter (Desboeufs et al., 2001; Baker et al., 2006a, 2006b, 2013; Witt et al., 2006, 2010) to determine the bio(geo)availability of elements (e.g. Fe, P, Mn, Al, Zn, Pb, Cu, Ba) from aerosols over an ocean for seawater dissolution. Half of the aerosol filter was cut into small pieces with acid-cleaned ceramic-bladed scissors and suspended in 50 ml of buffer solution for 1-2 hrs at room temperature. The supernatant was subsequently filtered (0.2 mm, cellulose acetate filter), dried and then acidified with concentrated (15.6 M) HNO_3. The samples were then evaporated twice and then re-dissolved in 2.5 ml ca 0.8M HNO_3. One and a half millilitre were reserved for Pb isotope work and 1 ml was further diluted to 2 ml ca 0.8M HNO_3 for elemental concentration analysis.

4.2.3. Elemental and isotopic analysis

Major element (Ca, Na, K, Mg, Fe) concentrations and REE, Cd, Co, Cr, Cu, Ni, Pb, Zn, V, Sc, Th, and Y concentrations were determined by inductively coupled plasma quadrupole mass spectrometry (ICP-QMS) using an Agilent 7700x located at the Natural History Museum (NHM) in London. Using the same procedures as followed in Chapter 2 and 3, lead was separated from the sample matrix by ion

exchange chromatography using Eichrom Sr spec resin following the procedure outlined by Weiss et al. (2004). Neodymium was isolated using a two-step column procedure using TRU.Spec to separate REE from other elements followed by LN.Spec resin to separate the LREE from one another (Pin and Zalduegui, 1997). Lead and neodymium isotopic compositions were analysed on a Nu Plasma (Nu Instruments Limited, UK) multiple collector inductively coupled plasma mass spectrometer (MC-ICP-MS). The samples were introduced with a Nu Instruments DSN-100 Desolvation Nebulizer System and PTFE nebulizer. Simiarly, using the same procedures as followed in Chapter 2 and 3; quantitative dissolution and data quality was monitored with the certified USGS reference material G-2 granite (n=12) and listed in Tables 4.1, 4.2 and 4.4.

4.2.4. Filter blank corrections of elements in the soluble fraction of aerosols

The aerosol sampling on the ship using a high-volume collector aerosol sampler has a significant procedural blank (Baker et al., 2006a, and as described in Chapter 3). The same leaching procedure was carried out for aerosol samples and filter blanks to quantify the blank contributions to element and isotopic compositions in the soluble fraction of aerosols.

For the soluble filter blank from the D357 cruise, these blank values (in µg per filter, n=3) were 0.6 ±0.3 (Al), 0.2 ±0.2 (Fe), 13 ±41 (K), 3.4 ±1.6 (Mg), 0.05 ±0.03 (Mn), and 22 ±10 (Na), 0.4 ±0.1 (Zn), 0.01 ±0.004 (Pb), 0.07 ±0.02 (Cu), 0.1 ±0.02 (Cr), 0.02 ±0.1 (Ni), 0.002 ±0.003 (Cd, Co, Y), 0.006 ±0.01 (V), <0.0004 ±0.0003 (Sc, Th, REE). For the soluble filter blank from the JC068 cruise, these blank values (in µg per filter, n=3) were 0.2 ±0.1 (Al), 0.2 ±0.2 (Fe), 1 (K), 2.4 ±3.1 (Mg), 0.01 ±0.003 (Mn), and 17 ±17 (Na), 0.4 ±0.02 (Zn), 0.02 ±0.004 (Pb), 0.1 ±0.1 (Cu), 0.1 ±0.009 (Cr), 0.02 ±0.1 (Ni), 0.008 ±0.02 (Cd), 0.002 ±0.001 (Co, Y), 0.003 ±0.004 (V), <0.0001 ±0.00003 (Sc, Th, REE). The soluble filter blank (in µg per filter) was subtracted from the measured aerosol mass (in µg per filter) to give the aerosol sample mass (X_S, in µg per filter) as described in detail in Chapter 3.

4.2.5. Sea spray corrections of elements in the soluble fraction of aerosols

The aerosol sample mass (X_S, in µg per filter) was further corrected for sea spray contributions following equation (1). The component's sea spray-derived mass (in µg per filter) was calculated by multiplying the Na^+ in the aerosol (Na^+_S, in µg per filter) with the ratio of the component relative to Na+ in seawater (X_{sea}/Na^+_{sea}, in ppm/ppm, taken from Turekian, 1968). The component's sea spray-derived mass was subtracted from the aerosol sample mass to give the sea spray corrected aerosol sample (X_{Scorr}, in µg per filter).

$$X_{Scorr} = X_S - (Na^+_S \times (X_{sea}/Na^+_{sea})) \quad (1)$$

The blank and sea spray corrected aerosol data (X_{Scorr}) are expressed in Table 4.1 and 4.2. The uncertainty of the blank measurement in the soluble fraction (in µg per filter) quantified in Section 4.2.4 was used to express the uncertainty in X_{Scorr}.

4.2.6. Solubility calculations

The solubility (in %) of each element was calculated by dividing the soluble fraction of an element (X_S in µg per filter) by the total element in an aerosol (taken from Chapter 3 and expressed here as X_T, in µg per filter), and then multiplied by 100 (2).

$$\text{Solubility} = (X_S / X_T) \times 100 \quad (2)$$

The uncertainties (in %) were combined for the soluble fraction of element in the aerosol, for the total element in the aerosol (taken from Chapter 3), and the uncertainty introduced by the digestion procedure and instrument (ICP-QMS) to estimate the analytical uncertainties in element solubilities. These are expressed in Table 4.3 and shown in Figures 4.1 to 4.4.

4.2.7. Correcting lead isotope ratios in the soluble fraction of aerosols

The Pb isotopic ratios of the soluble fraction of aerosol samples (R_M) were blank corrected to give (R_S) by equation (3). First the fraction (*f*) of blank contribution of Pb in the soluble fraction (µg in soluble fraction per filter for Pb) was multiplied by the Pb isotopic ratio in the soluble fraction of the filter blank (R_B) to give $f(R_B)$. This was subtracted from the Pb isotopic ratio in the soluble fraction of the aerosol sample (R_M), followed by a division of the fraction of sample contribution of Pb in the soluble fraction (1-*f*). The fraction of Pb contribution in the soluble fraction from the blank was calculated by the mean blank mass (µg in soluble fraction per filter) divided by the measured Pb mass in soluble fraction of the aerosol sample (µg in soluble fraction per filter) as quantified in Section 4.2.4.

$$R_S = (R_M - f(R_B)) / (1-f) \quad (3)$$

The observed maximum absolute uncertainties in the isotopic ratios are reported in Table 4.4 and Figure 4.5.

Table 4.1. Major and trace element composition in the soluble fraction of aerosols over the South Atlantic from the D357 and JC068 cruise, in μg per filter, except Sc, Y and Th which are in ng per filter

Sample ID	Al	Fe	K	Mg	Mn	Cu	Pb	Cd	Zn	Cr	Ni	Co	V	Sc	Y	Th
D357-2	3.33	2.89			0.726	1.13	0.343	0.046	6.83	0.807	4.21	0.096	0.455		0.352	0.818
D357-8	8.14	9.74		10.3	0.794	0.669	0.167	0.013	1.37	1.25	3.73	0.090	0.957		2.74	
D357-10	1.50	0.205			0.006	0.315	0.133	0.001	5.44	0.014	0.046	0.000	0.140		0.154	
D357-11	2.43	2.34			0.338	0.329	0.143	0.004	2.64	0.009	0.761	0.019	0.373		3.87	
D357-13	1.53	3.54			0.655	0.403	0.056	0.011	1.57	0.730	2.78	0.070	0.230		8.09	
JC068-4	8.69	11.6			0.582	1.15	0.830	0.083	16.1	0.906	2.13	0.051	0.255		7.71	
JC068-6	15.1	10.4			2.14	0.758	0.174	0.004	2.36	1.61	6.68	0.166	0.394	1.74	23.1	1.45
JC068-8	7.92	46.0			3.46	0.696	0.097	0.039	2.20	6.13	22.0	0.576	0.109		4.49	
JC068-10	19.0	135			9.02	0.895	0.208	0.025	1.80	25.5	41.5	1.07	0.317	9.99	53.8	3.54
JC068-12	7.78	51.4			4.90	0.502	0.091	0.031	2.10	2.85	12.4	0.515	0.122	4.40	32.2	2.96
JC068-14	8.38	159	0.743		10.0	2.47	0.299	0.010	5.51	31.8	63.7	1.53	0.323		8.35	1.11
JC068-15	9.61	3.59	42.5		1.04	0.517	0.569	0.025	7.11	0.043	0.593	0.023	0.759	2.27	11.9	1.52
JC068-17	1.67	0.143			0.042	0.253	0.082	0.030	3.53	0.005	0.065	0.001	0.002		1.16	
Reference Material (% w/w major elements, μg/g trace elements)																
USGS G2, this study (n = 12)	13.65	2.55	4.41	0.72	0.03	9.1	32	0.02	86	7.6	2.2	4.5	35	4.7	9.1	24
RSD (2σ, %)	6.1	2.5	7.3	8.4	9.3	12	3.3	45.62	8.6	15.1	18.8	3.6	4.7	9.6	3.3	2.5
USGS G2, cert.	15.39	2.66	4.48	0.75	0.03	11	30	n.a.	86	n.a.	n.a.	4.6	36	3.5	11	25
RSD (2σ, %)	0.3	0.17	0.13	0.03	0.01	n.a.	53	n.a.	9.3	n.a.	n.a.	15	11	11	18	8

Blank space indicates sample concentration below range of uncertainty for filter blank and seawater contribution

n.a – not available

Results for certified USGS reference material G-2 Granite are taken from Gladney et al. (1992) and Govindaraju (1989, 1994).

Precision is given as the relative standard deviation (RSD) at the 2σ level (n = 12).

Table 4.2. Rare earth element composition in the soluble fraction of aerosols over the South Atlantic from the D357 and JC068 cruise, in ng per filter

Sample ID	La	Ce	Pr	Nd	Sm	Eu	Gd	Tb	Dy	Ho	Er	Tm	Yb	Lu
D357-2	2.27	2.13	0.205	1.27	0.228	0.078	0.205	0.030	0.210	0.026	0.062			
D357-8	3.25	3.83	0.370	1.60	0.206	0.000	0.375	0.056	0.324	0.076	0.194		0.111	
D357-10	0.23	0.185	0.132	0.46	0.035	0.000	0.004	0.008	0.016					
D357-11	4.29	7.33	0.946	3.94	0.781	0.167	0.833	0.144	0.734	0.113	0.254	0.051	0.340	0.042
D357-13	3.82	7.16	0.888	3.73	0.650	0.121	0.805	0.092	0.602	0.142	0.323		0.235	
JC068-4	4.68	7.72	1.05	4.55	0.588	0.113	1.08	0.147	0.595	0.144	0.445	0.051	0.337	0.057
JC068-6	14.2	29.5	3.81	16.2	3.33	0.780	3.73	0.473	3.05	0.536	1.79	0.219	1.21	0.218
JC068-8	3.62	6.58	0.841	3.75	0.806	0.135	0.972	0.150	0.706	0.127	0.535	0.041	0.249	0.057
JC068-10	37.4	72.5	10.2	44.1	9.15	2.16	10.4	1.58	8.62	1.53	4.66	0.620	3.63	0.573
JC068-12	23.7	46.2	6.61	29.1	6.47	1.38	6.70	0.889	5.31	1.03	2.97	0.346	2.41	0.351
JC068-14	9.19	15.6	2.08	9.67	1.74	0.341	1.96	0.222	1.41	0.275	0.911	0.091	0.648	0.093
JC068-15	19.9	25.6	3.20	13.9	3.53	0.527	2.61	0.335	1.84	0.369	0.972	0.115	0.767	0.105
JC068-17	2.27	2.13	0.205	1.27	0.228	0.078	0.205	0.030	0.210	0.026	0.062			
Reference Material (% w/w major elements, μg/g trace elements)														
USGS G2, this study (n = 12)	87	158	16	52	7.2	1.3	4.0	0.46	2.2	0.35	0.85	0.1	0.7	0.1
RSD (2σ, %)	1.3	1.2	3.1	2.1	2.5	3.5	4.3	4.0	5.4	4.9	3.8	5.5	4.1	4.4
USGS G2, cert.	89	160	18	55	7.2	1.4	4.3	0.48	2.4	0.4	0.92	0.18	0.8	0.11
RSD (2σ, %)	9.0	6.3	n.a.	10.9	9.7	1.0	n.a.	n.a.	12.5	n.a.	n.a.	n.a.	25	n.a..

Blank space indicates sample concentration below range of uncertainty for filter blank and seawater contribution

n.a – not available

Results for certified USGS reference material G-2 Granite are taken from Gladney et al. (1992) and Govindaraju (1989, 1994).

Precision is given as the relative standard deviation (RSD) at the 2σ level (n = 12).

Table 4.3. Solubility (in %) of major, trace and rare earth elements from aerosols over the South Atlantic Ocean from the D357 and JC068 cruise

Solubility (%)	Longitude	Al	Fe	K	Mn	Cu	Pb	Cd	Zn	Cr	Ni	Co	V	Sc	Y	Th
D357-2	15.0	13	n.a.	n.a.	n.a.	69	65	103	88	n.a.	74	744	83		0.62	18
D357-8	-4.0	29	19		68	79	78	56	84	13	69	73	88		16	
D357-10	10.9	13	0.94		4.7	70	62	22	74	3.8	42	6.4	65		2.3	
D357-11	14.4	9.7	6.1		38	67	77	39	80	0.14	22	22	68		140	
D357-13	11.2	4.6	5.1		52	84	63	178	126	4.4	32	33	66		37	
JC068-4	10.3	11	24		25	74	258	147	81	21	100	106	54		20	
JC068-6	-1.5	5.6	7.2		43	43	44	7.5	394	17	59	61	50	3.4	22	6.3
JC068-8	-11.0	12	22		77	81	66	65	95	15	82	89	25		14	
JC068-10	-20.2	1.8	22		46	75	37	108	55	103	90	122	33	3.2	6.6	2.3
JC068-12	-33.3	2.9	12		50	43	32	43	61	4.1	36	58	14	5.9	25	7.6
JC068-14	-46.5	14	31	0.24	110	87	88	18	106	23	82	100	35		46	16
JC068-15	-51.7	8.2	4.9	50	50	62	70	41	110	8.7	153	76	74	6.1	13	6.3
JC068-17	-54.3	15	20		14	32	20	1054	72	7.7	99	18	31			

Blank spaces indicate sample concentrations below filter blank and sea spray contribution outside uncertainties

n.a. – not available due to undetermined total concentration (µg/filter)

Red outlined data with red error bar denote upper limit of element solubility where uncertainty is ≤0%

Blue outlined data denote element solubility where uncertainty is below and ≥100%

Shaded data refer to solubility >100% and outside blank and sea spray uncertainties

Longitude denotes the mean point between the beginning and end position of each aerosol sample collection, calculated from Chapter 3.

Table 4.3. *continued*.

Solubility (%)	Longitude	La	Ce	Pr	Nd	Sm	Eu	Gd	Tb	Dy	Ho	Er	Tm	Yb	Lu
D357-2	15.0	33	26	15	45	3.3	6.8								
D357-8	-4.0	32	23	21	26	12		24	19	14	17	14	0	7.3	0
D357-10	10.9	8.7	8.5	121	24	30		13	3.6	13					
D357-11	14.4	34	36	38	47	38	61	43	62	46	33	29	51	61	52
D357-13	11.2	22	22	22	28	21	21	31	29	28	37	27	0.0	16	0.0
JC068-4	10.3	7.1	6.6	11	13	14	11	19	17	11	15	14	11	12	11
JC068-6	-1.5	19	18	20	22	20	24	25	21	22	19	21	18	16	17
JC068-8	-11.0	17	15	17	9.3	20	15	24	23	16	17	22	13	12	12
JC068-10	-20.2	6.9	6.1	7.3	7.6	7.1	8.5	8.3	7.6	6.5	6	5.5	4.9	4.3	4.3
JC068-12	-33.3	16	15	18	20	21	21	24	21	18	24	22	19	20	18
JC068-14	-46.5	27	25	35	39	38	36	48	37	42	53	60	41	47	46
JC068-15	-51.7	16	15	17	20	25	19	20	18	16	16	15	12	13	12
JC068-17	-54.3	11	9.4	6.3	24			17	7.9	36	0.1	0.4	0.2	0.5	0.1

Table 4.4. Lead isotope ratios in the soluble fraction of aerosols over the South Atlantic Ocean from the D357 and JC068 cruise

Sample ID	Blank corrected $^{206}Pb/^{207}Pb$	±	$^{208}Pb/^{207}Pb$	±	$^{206}Pb/^{204}Pb$	±	$^{207}Pb/^{204}Pb$	±	$^{208}Pb/^{204}Pb$	±
South Atlantic – soluble aerosol										
D357-2	1.1391	0.0003	2.4069	0.0005	17.769	0.005	15.5987	0.0003	37.544	0.008
D357-8	1.1399	0.0007	2.4088	0.0011	17.785	0.010	15.6014	0.0006	37.580	0.016
D357-10	1.1359	0.0009	2.4018	0.0014	17.714	0.013	15.5946	0.0007	37.456	0.019
D357-11	1.1336	0.0008	2.4010	0.0013	17.662	0.012	15.5806	0.0007	37.409	0.018
D357-13	1.1496	0.0021	2.4145	0.0032	17.899	0.031	15.5700	0.0017	37.593	0.046
JC068-4	1.1610	0.0012	2.4369	0.0003	18.098	0.020	15.5881	0.0013	37.987	0.008
JC068-6	1.1637	0.0055	2.4306	0.0016	18.183	0.093	15.6263	0.0064	37.982	0.040
JC068-8	1.1569	0.0099	2.4218	0.0028	18.053	0.168	15.6050	0.0116	37.793	0.072
JC068-10	1.1669	0.0046	2.4353	0.0013	18.229	0.078	15.6221	0.0054	38.044	0.034
JC068-12	1.1623	0.0106	2.4310	0.0030	18.135	0.180	15.6027	0.0123	37.930	0.077
JC068-14	1.1510	0.0032	2.4142	0.0009	17.949	0.054	15.5939	0.0037	37.646	0.023
JC068-15	1.1802	0.0017	2.4300	0.0005	18.492	0.029	15.6684	0.0020	38.075	0.012
JC068-17	1.1555	0.0116	2.4220	0.0033	18.017	0.197	15.5918	0.0136	37.763	0.085
Reference Material										
USGS G-2, this study (n=22)	1.1764	0.0001	2.4873	0.0003	18.399	0.005	15.640	0.006	38.902	0.021
USGS G-2, Weis	1.1765	0.0002	2.4878	0.0002	18.396	0.002	15.636	0.005	38.900	0.019

Results for certified reference material USGS G-2 Granite are taken from Gladney et al. (1992) and Govindaraju (1989, 1994). Precision is given as the relative standard deviation (RSD) at the 2σ level (n = 12).

All samples were analysed by MC-ICP-MS.

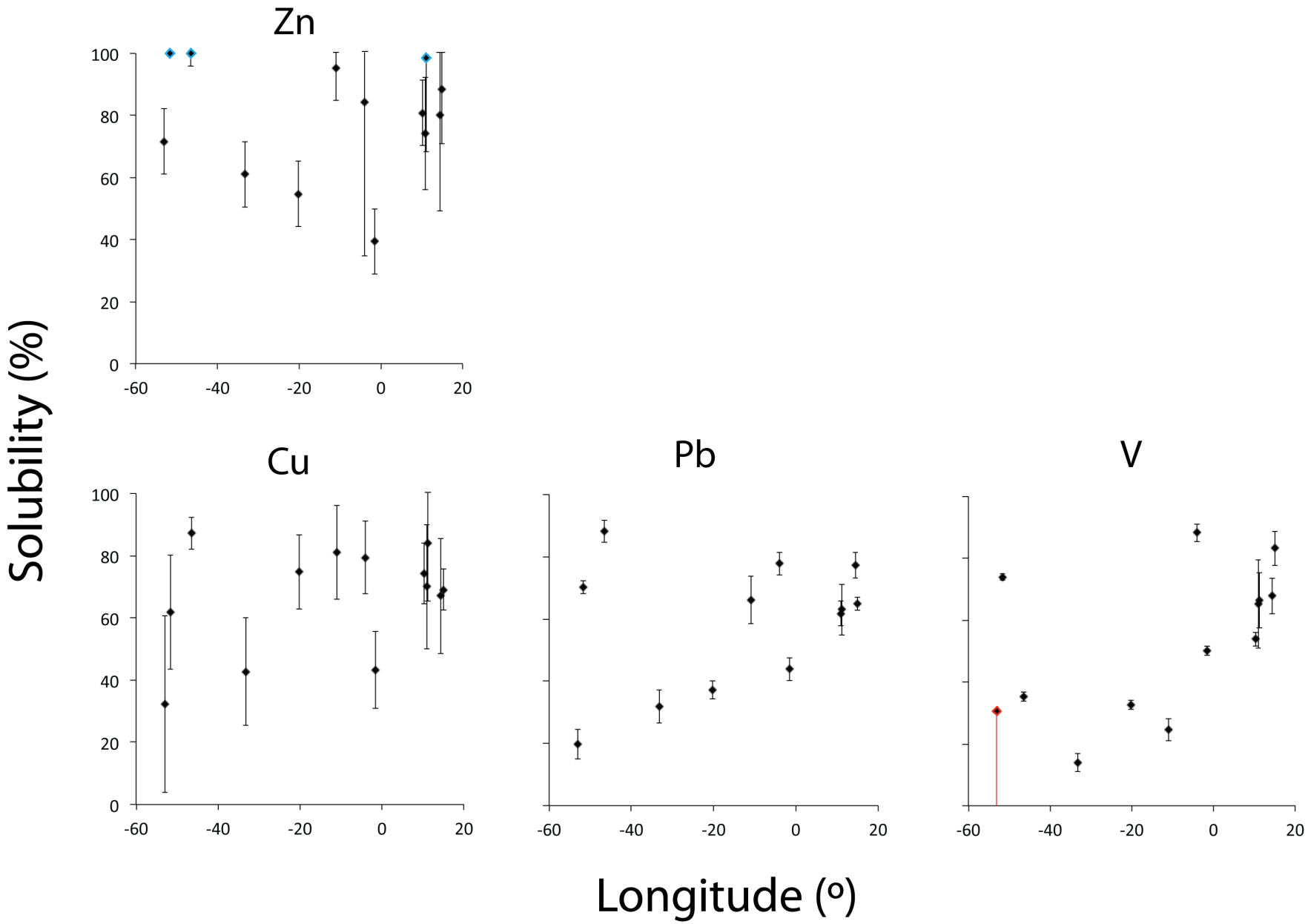

Figure 4.1. Solubility (in %) of trace elements and K and Mn from aerosols from cruise D357 and JC068 across the South Atlantic Ocean. Red outlined data with red error bar denote upper limit of element solubility where uncertainty is ≤0%. Blue outlined data denote element solubility where uncertainty is below and ≥100%. Errors were based on analytical uncertainties to 2σ.

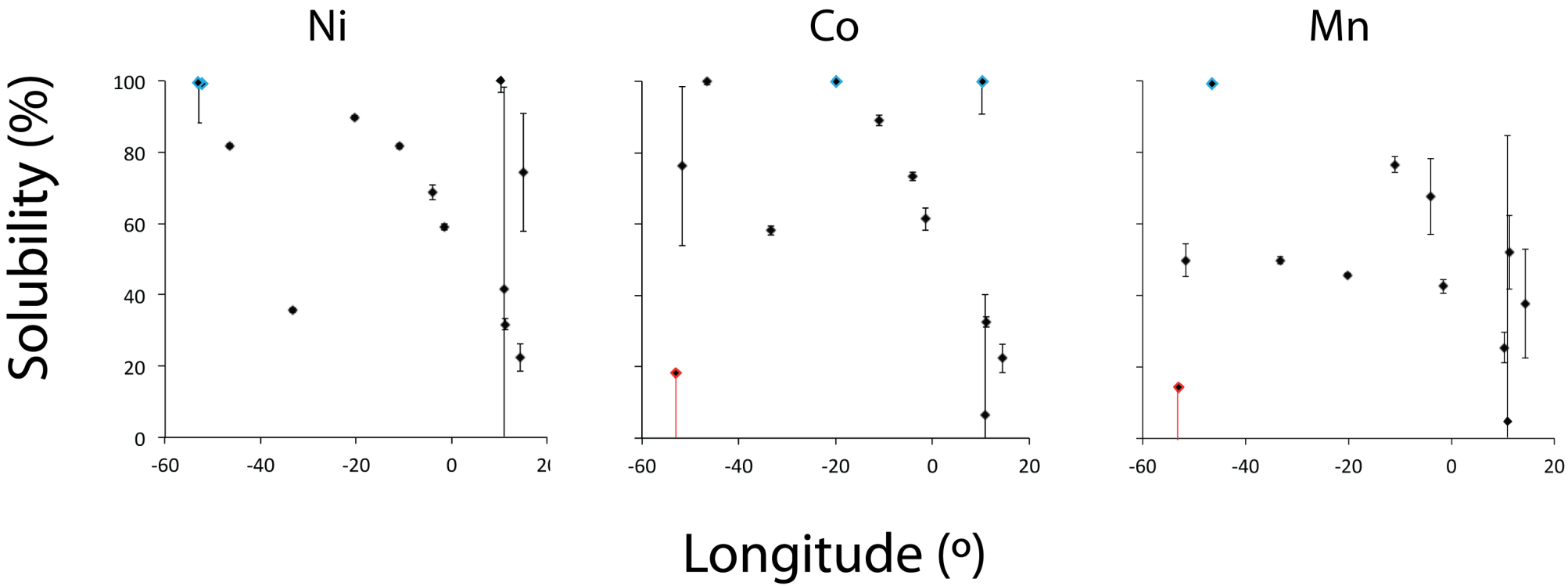

Figure 4.1. *continued*.

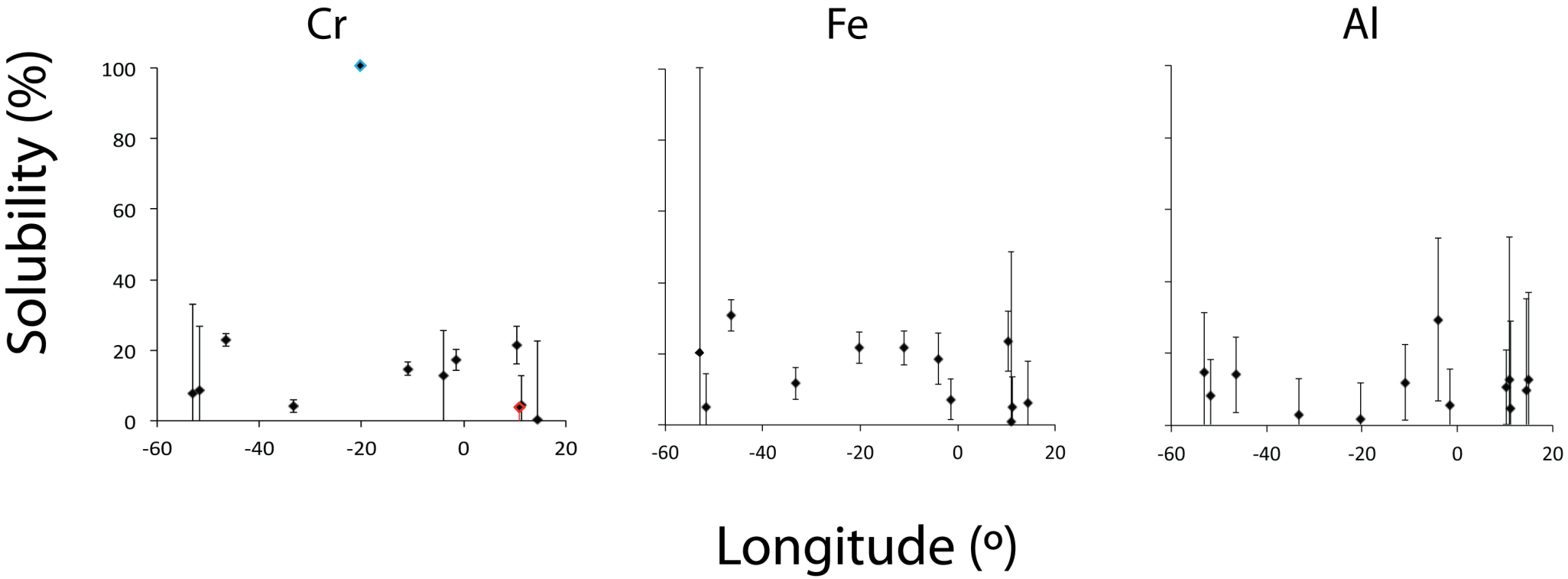

Figure 4.2. Solubility (in %) of Cr, Fe and Al from aerosols from cruise D357 and JC068 across the South Atlantic Ocean. Red outlined data with red error bar denote upper limit of element solubility where uncertainty is ≤0%. Blue outlined data denote element solubility where uncertainty is below and ≥100%. Errors were based on analytical uncertainties to 2σ.

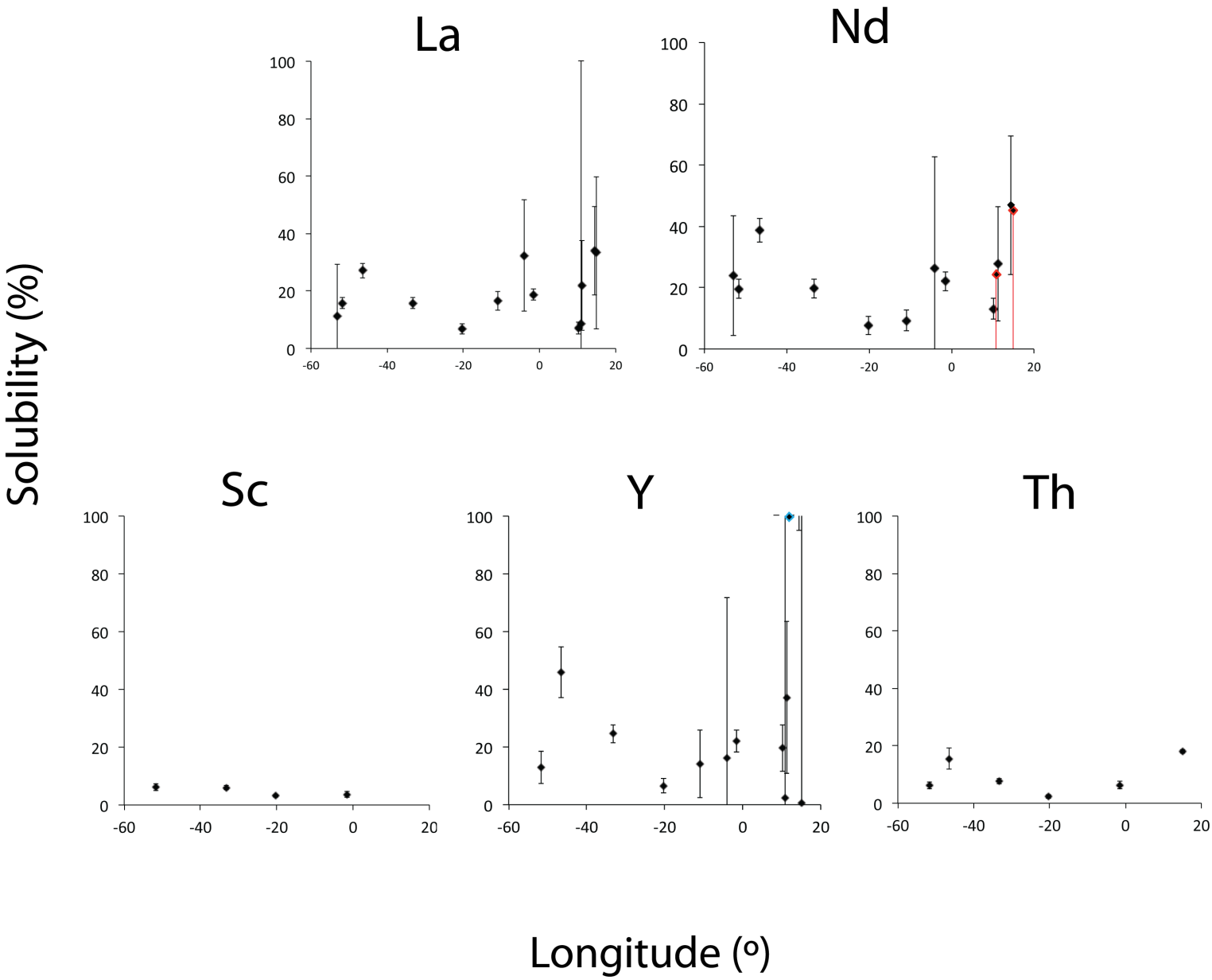

Figure 4.3. Solubility (in %) of rare earth elements and Sc, Y and Th from aerosols from cruise JC068 and D357 across the South Atlantic Ocean. Red outlined data with red error bar denote upper limit of element solubility where uncertainty is ≤0%. Blue outlined data denote element solubility where uncertainty is below and ≥100%. Errors were based on analytical uncertainties to 2σ.

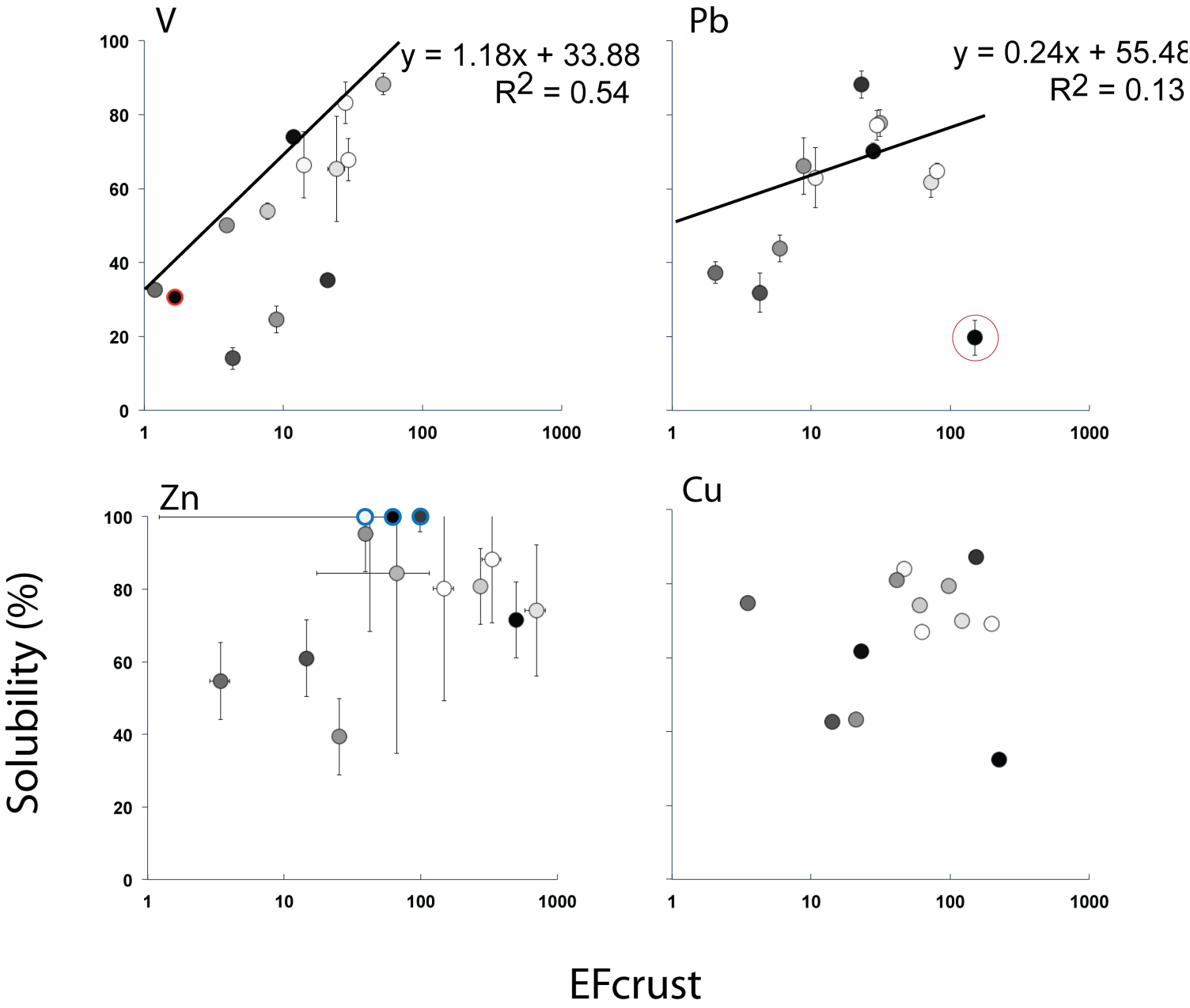

Figure 4.4. Solubility (in %) vs. enrichment factor relative to the continental crust in total bulk aerosols for select elements. Enrichment factors are taken from Chapter 3. R^2 denotes (regression) correlation between solubility and enrichment factor (0 =no correlation and 1 =direct correlation between solubility and enrichment factor). Aerosol west to east across the South Atlantic denoted by black to white coloured symbols. Anomalous data were circled with a red circle. Red outlined data with red error bar denote upper limit of element solubility where uncertainty is ≤0%. Blue outlined data denote element solubility where uncertainty is below and ≥100%. Errors were based on analytical uncertainties to 2σ.

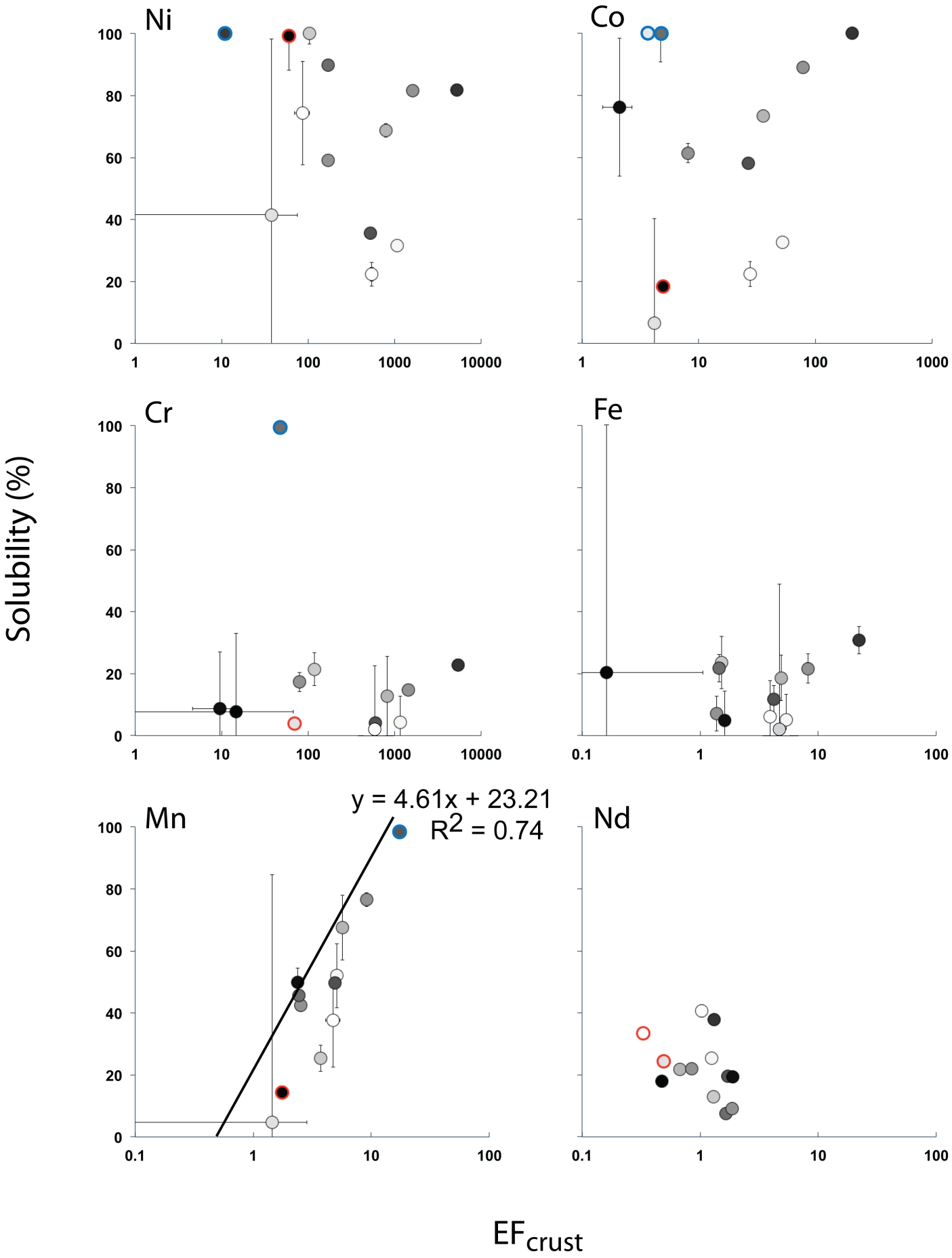

Figure 4.4. *continued*.

4.3. Results and Discussion

4.3.1. Uncertainties in aerosol solubility

The major, trace and REE concentrations of the soluble fraction of aerosols over 40°S transect of the South Atlantic are shown in Table 4.1 and 4.2. Calculated solubility using the total aerosol element composition data from Chapter 3 are listed in Table 4.3 and illustrated in Figures 4.1 to 4.4. Examples of previously published solubility of aerosols over the South Atlantic, North Atlantic, Indian Ocean, Pacific and laboratory experiments of solubility of natural and anthropogenic aerosols are expressed in Table 4.5.

The uncertainties in element composition in the soluble fraction (Table 4.1 and 4.2) and in solubility were large (Fig. 4.1 to 4.4). This was due to the low element mass in the soluble fraction of aerosol samples close to limit of detection of the analytical instruments, or due to over correction of element contribution in the soluble fraction of the multiple filter blanks. For calculated solubilities that showed uncertainty ≤0%, the upper limit of the solubility were reported and these are marked in red in Table 4.3. For calculated solubilities that showed uncertainty ≥100% solubility data were reported as >95% soluble and these are marked in blue in Table 4.3 and Fig. 4.1 to 4.4. Calculated solubilities that fell outside limits of solubility (<0% and >100%) were omitted from the figures but are listed in Table 4.3 (highlighted as grey shading) and were most likely due to inhomogeneous deposition of aerosol sample across the total filter paper, or contamination. Cadmium and Mg solubilities are omitted from the tables and figures, and K solubilities are omitted from the figures. This was due to large uncertainties in Ca solubility and limited Mg and K data.

4.3.2. Spatial variation in aerosol solubility to the South Atlantic Ocean

The leaching protocol aimed to represent wet deposition (Bruland et al., 2001). Upon wet deposition of aerosols elements from aerosols are in a soluble form and may enter straight into the microlayer on the surface of the seawater (Buck et al., 2006). This suggested that during wet deposition the leaching protocol represents the solubilities of elements directly into the ocean, directly affecting the marine element budget.

The solubility of Zn ranged between 30 and >95%. Although Zn exhibited large uncertainties, the highest solubilities in Zn (>60%) were observed at the stations between ~45°W and 51°W at the westernmost part (western margin) and at the stations east of ~10°W at the easternmost part (eastern margin) of the South Atlantic (Fig. 4.1). The solubility of Cu ranged between <5 and >95% west of ~45°W and between 20 and >95% across the rest of the South Atlantic (Fig. 4.1). Solubilities of Pb and V ranged between 10 and 40%, and were <40%, respectively. They showed highest solubility, between 50 and 90%, at the western and eastern margins (Fig. 4.1). High solubilities of Zn, Cu, Pb and V were in line with previous work in urban areas even though the extraction procedures were conducted with pH8-8.3 solutions (~20-60% using a seawater extraction procedure at pH 8 in China; Jiang et al., 2014; and ~30-

80% also at pH 8.3 in Taiwan, Hsu et al., 2010). They were also in line with aerosols from the western Indian Ocean using the rainwater extraction procedure at pH 4.7 (~30-100%, Witt et al., 2010). This study suggested that these solubilities in trace elements were due to anthropogenic aerosol sources from South Africa (Witt et al., 2010).

Nickel, Co, and Mn showed a wide range of solubilities between <5 and >95% for Ni and Co and between <5 and 80% for Mn for the westernmost aerosol and at the eastern margin, and were above 40% solubility elsewhere across the South Atlantic (Fig. 4.1). Such ranges in solubility of Ni have been reported in aerosols from urban areas (Ni ~20-60% at pH 8, Jiang et al., 2014) and of Ni, Co and Mn in aerosols collected over oceans (Ni ~20-80%, Co ~10-73%, and Mn ~22-95% over the Indian Ocean, Witt et al., 2010, all at pH 4.7; and Mn ~61-70% and 54-78% over the North and South Atlantic, respectively, Baker et al., 2013, Baker et al., 2006). Although higher solubility of Co were observed from urban samples (Co 0.78% at pH 8, Thuroczy et al., 2010) than mineral dust samples (Co of 0.14% at pH 8) in Thuroczy et al. (2010), both range at the lower range of solubility of Co reported in this study.

The solubility of Cr, Fe and Al in contrast were consistently low across the South Atlantic, <30%, except at ~20°W (sample JC068-10) with >95% solubility for Cr, and east of ~5°W large uncertainties suggested Fe and Al solubility were as high as 50% (Fig. 4.2). West of ~51°W, Fe solubility was >95% (Fig. 4.2). Low solubility of Cr was in line with aerosols from urban areas (<20% at pH 8; Jiang et al., 2014) and dominantly anthropogenic aerosols that reached the Indian Ocean (~3-30% at pH 4.7, Witt et al., 2010). The solubility of Fe and Al in aerosols over the South Atlantic showed some agreement with previous studies for the South Atlantic using the same extraction procedure as this study (Fe ~2.4-20%, 35-50°S, ~20-50°W Baker et al., 2013, Fe ~5-20% at 30°S, Baker et al., 2010) and Indian Ocean (Fe ~1-45% and Al ~7-21%, Witt et al., 2010; Fe ~10%, Buck et al., 2010). They also fell within the range of Fe and Al solubility from anthropogenic material (Fe ~0.001-80%; Jickells and Spokes, 2001; Al ~43%, Desboeufs et al., 2001). Iron and Al solubility in this study ranged higher than those from the North Atlantic Ocean for Saharan dust (Al ~0.1-10% and Fe ~1-10%; e.g. Jickells and Spokes, 2001; Bonnet et al., 2004; Baker et al., 2006; Sartou et al., 2007; Baker et al., 2013), and were within the range of solubility of anthropogenic material (Fe ~0.001-80%; Jickells and Spokes, 2001; Al ~43%, Desboeufs et al., 2001).

The solubility of REE (represented by La and Nd in Fig. 4.3) was in general <30% but uncertainties were large in the west and east margins of the South Atlantic (Fig. 4.3). Yttrium exhibited solubility across the 40°S transect up to 30% except between 40 and 60% at ~45°W and large uncertainties in the east margin suggested as much as >95% solubility (Fig. 4.3). Scandium and Th solubility for aerosols was <10% and <20%, respectively, across the South Atlantic (Fig. 4.3). These ranges in REE solubility are in agreement with reports that revealed high variability in REE solubility from aerosols over the ocean (Greaves et al., 1994; Tachikawa et al., 1999); in one case reaching more than 70% for aerosols over the ocean during wet deposition (rainwater samples of pH 5.2-5.6, Heimburger et al., 2013).

4.3.3. Correlation of solubility and element enrichment factors with air mass back trajectories and the effect on element supply to the ocean

Anthropogenic aerosol sources may have contributed to the high element solubility of aerosols observed in select major and trace elements in this study. The percentage solubility of select major, trace and REE were compared to the total aerosol enrichment relative to the continental crust (enrichment factors taken from Chapter 3) and air mass back trajectories (computed from a Hybrid Single Particle Langrangian Intergrated trajectory from the NOAA Air Resource Laboratory (HYSPLIT) model (Draxler and Rolph, 2013, Rolph, 2013) to assess the importance of natural vs. anthropogenic aerosol sources on the solubility. The air mass back trajectories were described in detail in Chapter 3. In brief, air mass back trajectories within 5 days suggested predominantly anthropogenic trace metal sources from South America contributed to the western part of the South Atlantic, natural sources of Zn, Pb, Cu, V and possibly Cr, Ni and Co and predominantly anthropogenic sources of Cr and Ni from South America contributed to the remote ocean (between ~20-35°W), and air masses received over the eastern part of the ocean within 10 days passed over South America, Antarctica and Southern Africa. Aerosols received over the eastern part of the ocean were believed to have received anthropogenic and natural contributions from South America and mainly anthropogenic sources from Southern Africa (as reported in Chapter 3).

Figure 4.4 plots the solubility vs. total aerosol enrichment factor for selected elements. Aerosols west to east across the South Atlantic are denoted by black to white coloured data (Fig. 4.4). There was a positive correlation between V solubility and enrichments relative to the crust (R^2 = 0.54, n = 13; regressive correlation expresses that 0 =no correlation and a large scatter of data between two components and 1 =direct correlation between two components). The lowest values were observed across the west and central parts of the South Atlantic, and the highest values were observed on the eastern margin as well as at ~51°W in the western margin. Lead solubility and enrichments also showed a positive correlation (R^2 = 0.13, n = 11, Fig. 4.5). The lowest solubility and enrichment were in samples towards the middle of the ocean (between 20-35°W at samples JC068-10 and -12, and 1°W at JC068-6) while the highest in aerosols at the western and eastern margin (Fig. 4.4). The exception to this is the low solubility of Pb west of ~51°W (circled in red, Fig. 4.5), which has been omitted from the determination of correlation calculation. There was a clear correlation between Mn solubility and enrichment in Mn relative to the crust (R^2 = 0.74, y = 4.61x + 23.21, n = 12, Fig. 4.4). However enrichment in Mn did not exceed 10 except in one case, and the highest solubilities and enrichments did not correlate with aerosols collected from the margins of the ocean, as suggested by V and Pb patterns in solubility vs. enrichment (Fig. 4.4). Instead the highest solubilities were towards the middle of the ocean (Fig. 4.4). For all other major (K, Fe) and trace elements (Zn, Cd, Ni, Co, Cr), there were no clear trends in solubility and enrichments relative to the continental crust (Fig. 4.4). Figure 4.4 further showed Nd solubility vs. enrichment factor for aerosols as an example of REE, Sc, Y and Th, and also exhibited no clear trends.

The high solubility of elements was linked with high enrichments relative to the upper continental crust and air mass back trajectories adjacent to continental regions suggesting anthropogenic sources, for V and Pb only. This was in line with conclusions reported in Chapter 3 that V and Pb in aerosols are controlled by anthropogenic sources where V and Pb were more enriched relative to the continental crust in anthropogenic sources than natural sources. The solubilities of Mn were in line with air mass back trajectories and enrichment of Mn that correlated with dust inputs from the continents. This agreed with conclusions in Chapter 3 that revealed that higher enrichments in Mn may be due to natural aerosol sources and volcanic dust was more important than mineral dust contribution in aerosols, in particular for Mn. This suggested that Mn solubility and enrichment relative to the crust may be a useful indicator for volcanic dust.

Since the leaching protocol represents the solubilities of elements directly into the ocean, directly affecting the marine element budget, the correlation between V and Pb solubility and enrichment has implied that higher anthropogenic V and Pb contributions in aerosols will mean higher V and Pb delivered to the South Atlantic Ocean and consequently a higher V and Pb surface seawater budget. The same is suggested for higher contributions of Mn due to increased volcanic dust deposition. Apart from V and Pb, the above findings are in contrast to the expected positive correlation between element solubility and anthropogenic aerosols reported for major and trace elements (e.g. Colin et al., 1990; Jickells et al., 1992; Spokes et al., 1994; Ebert and Baechmann, 1998; Desboeufs et al., 2001). This study has suggested that the relationship between solubility and anthropogenic sources is not as simple as was first suggested and that natural and anthropogenic aerosols in the Southern Hemisphere do not behave in the same way as in aerosols elsewhere that have shown a direct correlation between solubility and anthropogenic aerosols (e.g. dust and anthropogenic aerosols from the North Atlantic, China, Taiwan, Jickells and Spokes, 2001; Desboeufs et al., 2001; Hsu et al., 2010; Chiang et al., 2014). For example, higher Fe solubility in aerosols over the South Atlantic than the North Atlantic (Jickells and Spokes, 2001; Bonnet et al., 2004; Baker et al., 2006; Sartou et al., 2007; Baker et al., 2013) suggested that Fe from natural dust sources in the Southern Hemisphere, i.e. Patagonian dust delivered to the South Atlantic (as determined in Chapter 3), behave differently than the Fe from natural dust sources over the Northern Hemisphere, i.e. Saharan dust delivered to the North Atlantic. This may have been due to differences in mineralogy in these sources or differences in particle size, atmospheric processes, and atmospheric transport patterns over the different oceans.

4.3.4. Lead isotopic composition of the soluble fraction of aerosols

Lead isotope compositions of the soluble fraction of aerosols are listed in Table 4.4 and are shown in Figure 4.5. All aerosol samples were analysed for Pb isotopic compositions.

$^{206}Pb/^{207}Pb$ ratios showed more radiogenic values in the west (1.1802 ±0.0017, at ~51°W), lowest values at the east (1.1328-1.1517, ~10-20°W), and elsewhere an overall range between ~1.1500-1.1700

(Fig. 4.5). The lowest $^{206}Pb/^{207}Pb$ values at the eastern margin were from the D357 cruise and suggested that there may have been a difference in Pb sources in the soluble fraction of aerosols between the D357 and JC068 cruise (Fig. 4.5). The $^{208}Pb/^{207}Pb$ ratios also suggested that there were different trends in the aerosols between the two cruises. Aerosols from the JC068 cruise showed more radiogenic $^{208}Pb/^{207}Pb$ ratios on the west that increased to the east (2.4220 ±0.0033 rising to 2.4353 ±0.0013), while all aerosols from the D357 were less radiogenic (2.3997-2.4177) (Fig. 4.5).

The $^{208}Pb/^{207}Pb$ ratios of the soluble Pb in the JC068 samples were in line with major anthropogenic sources from South America typical of industrial sources, metal processing, smelting, waste incineration, coal burning and fuel combustion, as characterised in previous studies of urban areas of South America (~2.420-2.450; Bollhofer and Rosman, 2000; Gioia et al., 2010; Chapter 2). The $^{208}Pb/^{207}Pb$ ratios of the soluble Pb in the D357 samples were consistent with Pb isotopic ratios typical of mining sources from Namibia and South Africa (<2.250-2.420; Kamona et al., 1999; Bollhofer and Rosman, 2000; Frimmel et al., 2004; Monna et al., 2006, Chapter 2). Coal burning was another major anthropogenic source of aerosols from Southern Africa since the ban of leaded fuel (Bollhofer and Rosman, 2000; Monna et al., 2006; Witt et al., 2010). Lead isotopic ratios in the soluble fraction however suggested coal burning was not an important anthropogenic source that impacts the soluble Pb from aerosols in the eastern margin of the South Atlantic, which exhibited $^{208}Pb/^{207}Pb$ ratios between ~2.460-2.470 (Monna et al., 2006). Figure 4.5 further suggested that the Pb isotopic compositions in the soluble fraction of the aerosols differed to their compositions in the total bulk aerosol (data taken from Chapter 3), whereby lower Pb isotopic ratios were generally observed in the soluble fraction than the total aerosol. This suggested that the anthropogenic aerosol were more susceptible to dissolution. Anthropogenic sources were typical of lower Pb isotopic ratios than natural source areas from South America ($^{208}Pb/^{207}Pb$ ratios of ~2.440-2.500; GEOROC, 2003-2011; Chapter 2) and Southern Africa ($^{208}Pb/^{207}Pb$ ratios of ~2.400-2.550, Monna et al., 2006; Chapter 2). This was in line with the correlation between solubility and enrichment values of Pb in aerosols (Fig. 4.4). This highlighted that the soluble Pb derives from fine particulates or Pb in gaseous phases. Differences in Pb isotopic signals in the soluble fraction and total aerosol also revealed that Pb isotopic signals in total aerosols are useful for provenance tracing of aerosols, while Pb isotopic signals in the soluble fraction are useful for deciphering element supply to the seawater.

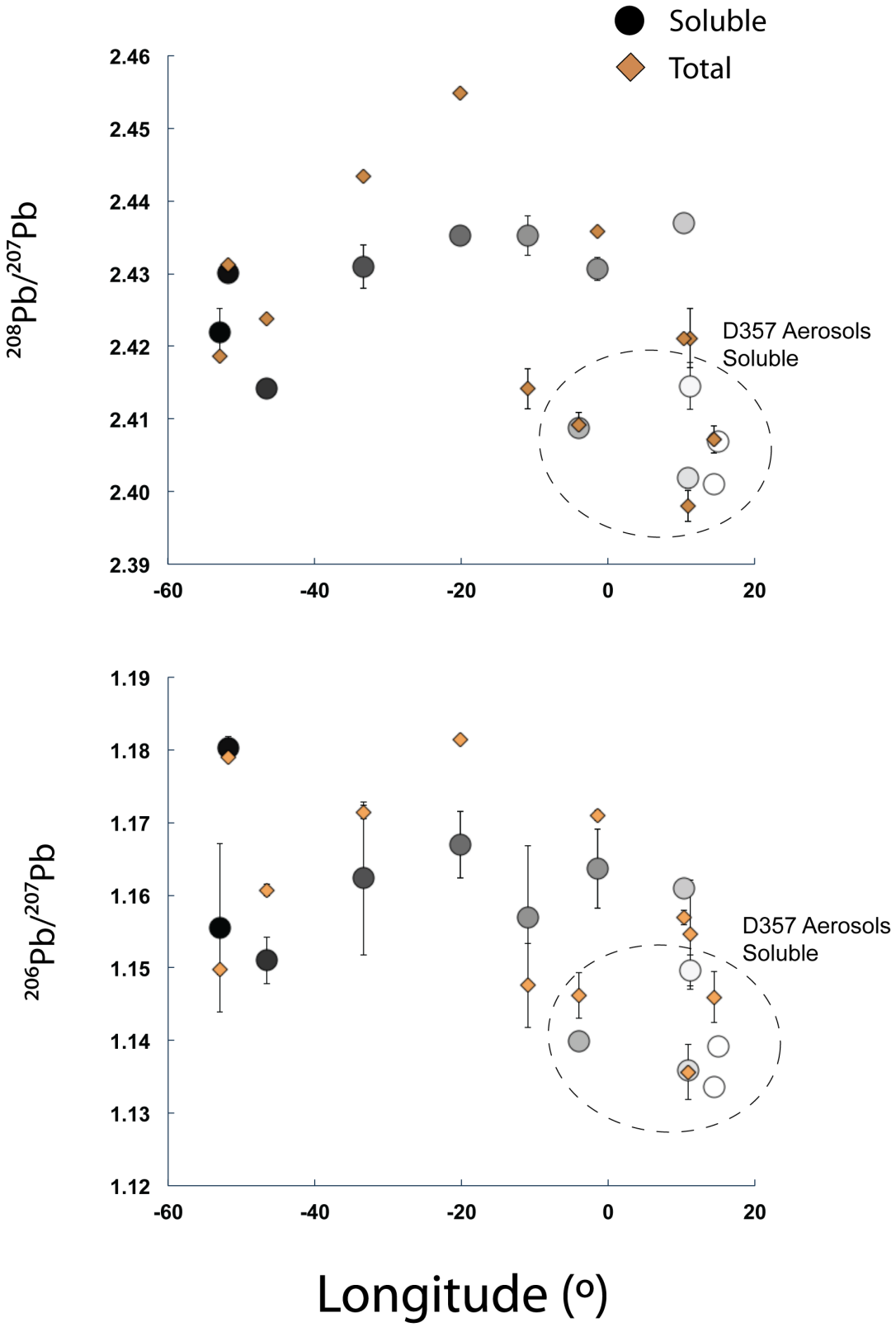

Figure 4.5. $^{206}Pb/^{207}Pb$ and $^{208}Pb/^{207}Pb$ isotopic ratios of soluble fraction of aerosols (circle symbols) and total aerosols (diamond symbols) across the South Atlantic Ocean. The Pb isotopic ratios of the soluble fraction of aerosols from the D357 cruise are encircled in a dash-lined circle. Aerosols west to east across the South Atlantic denoted by black to white coloured symbols. Errors were based on analytical uncertainties to 2σ.

Table 4.5. Examples of solubility of elements from aerosols over oceans and select natural and anthropogenic aerosols taken from literature

Element or isotopic composition	Sample date	Pb	Zn	Cu	V	Cr	Ni	Co	Cd	REE, Sc, Y, Th	Majors
This study	**2010 and**									**<5->95% REE** **<10% Sc** **<5->95% Y**	**<5->95% Fe** **<50% Al** **<5-80% Mn**
S Atlantic (~20°E-60°W, ~40°S), pH 4.7	**2011/12**	**10-90%**	**30->95%**	**<5->95%**	**<5-90%**	**<5->95%**	**<5->95%**	**<5->95%**	**n/a**	**<20% Th**	**20-80% K**
(1) S Atlantic (0-50°S), pH 4.7	2013										2.4-20% Fe 6.8-18% Al 54-78% Mn
(2) Atlantic, pH 4.7	2010										0.09-6.48% Al
(3) N Atlantic, pH 4.7	2007, 2004, 2003										0.1-10% Al 1-10% Fe 3-4% Al
(4) N Atlantic, pH 4.7	2006										>90% Mn
(5) N Atlantic, pH 4.7 –natural dust, anthropogenic aerosol, pH 4.7	2001										1-2% Fe, 0.001-80% Fe
(6) N Atlantic (Saharan dust), pH 8	1994									1-3%	7-21% Al 1-45% Fe
(7) W Indian Ocean, pH 4.7	2010	30->95%	70->95%	50-91%	50-62%	3-30%	20-80%	10-73%	70->95%		22-95% Mn
(8) Indian Ocean, pH 5.6	2013										10% Fe >70% Al, Mn
(9) S Indian Ocean, pH 5.2-5.6	2013									>70% La, Ce, Nd	>51% Fe <20% Al
(10) China, anthropogenic aerosols coal burning, pH 8	2014	20-60%	>60%	>60%	>60%	<20%	20-60%		>60%		20-60% Fe, Mn
(11) Leachate experiments –natural dust, anthropogenic aerosol, pH 8	2010		16%, 5.2%					0.14%, 0.78%			0.1%, 43% Al 0.04%, 38% Fe
(12) Leachate experiments –natural dust, flyash, pH 5	2001										2%, 97% Mn 0.9% Al
(5) Leachate experiments, pH5.5	2001										50% Mn
(13) Taiwan, anthropogenic aerosols, pH 8.3	2010	30-80%	30-80%	30-80%					30-80%	10% Y	10-50% Mn

(1) Baker et al., 2013; (2) Baker et al., 2010; (3) Sartou et al., 2007, 2003; Croot et al., 2004b; (4) Baker et al., 2006; (5) Jickells and Spokes, 2001; (6) Greaves et al., 1994; (7) Witt et al., 2010; (8) Buck et al., 2013; (9) Heimburger et al., 2013; (10) Jiang et al., 2014; (11) Thuroczy et al., 2010; (12) Desboeufs et al., 2001; (13) Hsu et al., 2010

n/a - denotes uncertainties in element solubility are too high

blank spaces denote no available data

4.3.5. Influence of element supply from aerosols to the ocean surface waters

Detecting the aerosol impact on the marine element budget is a challenging task because the ocean is a dynamic system. Upon entry to the ocean surface waters, biogeochemical uptake of elements, ocean circulation, residence time of elements, and other element sources affects the element budget in the surface water (Chester and Jickells, 2012). However the unique aspect of this study is that aerosol samples across the GEOTRACES GA10 40°S transect across the South Atlantic were collected alongside water samples. The impact of the transient dynamics of the ocean are assumed to be omitted in such data collections, permitting a direct assessment of the impact of element supply from aerosols on the marine element budget.

One study of element composition in the surface water (10-25 m) from water samples that were simultaneously collected as the aerosols from along the GEOTRACES GA10 40°S transect has been published (Wyatt et al., 2014) and have been compared to the Zn solubility from aerosols across the transect. Wyatt et al. (2014) reported concentrations of Zn that averaged 0.13 ±0.09 nM in the upper surface layer (10-25 m) across the remote ocean except at stations closest to the South American and South African continents where Zn concentrations were higher, 1.25 and 0.39 ±0.01 nM, respectively. The residence time of Zn in the ocean is ~1000 years (Bruland and Lohan, 2003) and suggested that the heterogeneous Zn composition across the ocean most likely reflected external supply most noticeable at the continental margins of the South Atlantic (Wyatt et al., 2014). The high solubilities of Zn from aerosols across the South Atlantic except at some most central samples (JC068-6, 10 and 12, Fig. 4.1) revealed that there was some correlation to the highest Zn concentrations exhibited at the continental margins. The absence of high concentrations of Zn in the ocean towards the middle of the South Atlantic however suggested that atmospheric Zn may have contributed to the Zn in surface waters of the South Atlantic, but the atmosphere was not the governing control in distribution of Zn concentration across the ocean.

Iron composition of seawater along the 40°S transect was not available at the time of this study and there are limited studies that have determined the Fe solubility in aerosols north and south of the 40°S transect (Witt et al., 2006; Baker et al., 2013). Both implied that at present there was not enough information to infer if there is a correlation between the Fe supply from aerosols to the ocean on the marine Fe budget and the high primary productivity expected along the 40°S transect. Although there was not enough evidence to determine the impact of trace elements on primary production along the transect, the high solubility in trace elements from aerosols may have an important role in controlling the biological activity in the surface waters of the South Atlantic.

4.4. Conclusions

The soluble major, trace, and rare earth element concentrations and Pb isotopic ratios were determined in aerosols collected in two cruises (D357 during Oct-Nov, 2010 and JC068 during Dec 2011-Jan 2012) along the GEOTRACES GA10 transect 40°S across the South Atlantic Ocean.

Zinc, Cu, Pb, Ni, Mn, and Co solubility ranged between 30 and >95% for Zn, between <5 and >95% for Cu, between 10 and 90% for Pb, between <5 and 90% for V, <5 and >95% for Ni and Co, and between <5 and >80% for Mn. Low solubility for Cr, Fe and Al was generally observed, <30%, except at ~20°W Cr exhibits >95% solubility. Rare earth element showed in general solubilities <30% except in the west (~45°W) and east (~15°E) regions of the South Atlantic which showed solubilities of up to >95%. Yttrium exhibited solubility up to 30% across the 40°S transect, except at ~45°W between 40 and 60% and in the east margin as much as >95% solubility. Scandium and Th solubility for aerosols was <10% and <20%, respectively, across the South Atlantic. As the leach protocol represented the wet deposition and therefore element solubility directly into the seawater when soluble aerosols come into direct contact with the ocean surface, the above determined solubilities presented the highest solubilities of elements from aerosols that may enter the ocean surface waters of the South Atlantic during wet deposition.

The high solubility of elements was linked with enrichments relative to the upper continental crust, where highest enrichments were exhibited adjacent to the continental margins, suggesting anthropogenic source control on solubility, for V and Pb only. High solubilities correlated well with element enrichment for Mn but showed highest enrichments over the open ocean than by the continental margins which correlated with natural dust sources, in particular, greater volcanic rather than mineral dust contributions in aerosols at the open ocean. This suggested that volcanic dusts governed Mn solubility and that Mn may be a useful tracer of volcanic sources in aerosols over the South Atlantic. This study revealed that aside for V and Pb, solubility did not correlate with anthropogenic aerosol sources, which is in contrast to other studies and suggested that aerosols over the South Atlantic behave differently to aerosols elsewhere (e.g. over the North Atlantic, China, Taiwan, Jickell and Spokes, 2001; Desboeufs et al., 2001; Hsu et al., 2010; Chiang et al., 2014). For other elements such as Fe, other processes may control element solubility over the South Atlantic, such as fine particulate size control on solubility, cloud processing during long-range transport over the South Atlantic, and chemical properties of elements in the aerosols.

Lead isotopic signals differed in the soluble fraction to the total aerosol. Lead isotopic signals in the soluble fraction of the aerosols were consistent with anthropogenic sources from South America and Southern Africa, while Pb isotopic signals in the total aerosols were consistent with mixing of natural and anthropogenic sources from South America and Southern Africa. This implied that anthropogenic Pb particulates are more susceptible to weak acid leaching than natural Pb particulates, which is in line with

the correlation between solubility and enrichment values in Pb in aerosols. These findings also revealed that leaching most likely releases anthropogenic Pb that were confined to fine particulate or gaseous phases. This further highlighted that Pb isotopic signals in total aerosols are useful for provenance tracing of aerosols, while Pb isotopic signals in the soluble fraction of aerosols are useful for deciphering element supply to the seawater.

Tracing the impact of aerosols delivered to the ocean is a complicated task due to a number of aspects that effect element budget in the ocean. This includes ocean water circulation, biogeochemical reactions, residence time, and sources of elements to the ocean. Simultaneously collected aerosol and seawater samples from the same localities were assumed to cancel out the transient dynamics of the ocean and suggested that these datasets can be compared to assess the direct impact of element supply in aerosols on element budget in the ocean. Thus far there is one published study of element composition (of Zn) in the surface waters that were simultaneously collected as the aerosols from along the GEOTRACES GA10 40°S transect across the South Atlantic (Wyatt et al., 2014). High solubilities of Zn from aerosols across the South Atlantic except at some most central samples revealed some correlation to the highest Zn concentrations in the ocean exhibited at the continental margins. The absence of high concentrations of Zn in the ocean towards the middle of the South Atlantic however suggested that atmospheric Zn may have contributed to the Zn in surface waters of the South Atlantic, but the atmosphere was not the governing control in distribution of Zn across the ocean.

At the time of this study Fe concentrations of seawater from along the transect were not available and there was limited data to compare Fe in aerosols from this study with aerosols collected north and south of 40°S (Witt et al., 2006; Baker et al., 2013) to assess the impact of Fe from aerosols on the marine element budget and therefore high primary productivity that is expected along the transect. To develop a better understanding of the impact of atmospheric deposits over the 40°S transect may have on primary productivity in this region, additional data are required that include surface water Fe concentrations, atmosphere and ocean circulation modeling along the 40°S transect, and further aerosol sampling campaigns north and south of the 40°S transect. Although there was not enough evidence to determine the impact of trace elements on primary production along the transect, the high solubility in trace elements from aerosols may have an important role in controlling the biological activity in the surface waters of the South Atlantic.

This study provided a wide range of elemental data and Pb isotopic data useful in studies that assess element solubility from aerosols in the atmosphere to the ocean, determining source control on element deposition from aerosols to ocean, how humans will impact the transport of the bio(geo)available fraction of iron and other important elements to the ocean, and thus which sources will respond or control climate change.

CHAPTER 5

Conclusions

The main aims and objectives of this thesis were met. The mineralogy, element and Pb and Nd isotopic compositions were realised in natural and anthropogenic sources from South America and Southern Africa. The element and Pb and Nd isotopic compositions were realised in 13 aerosols along the 40°S transect of the South Atlantic Ocean from two cruises (D357 during Oct 2010 and JC068 during Dec 2011 to Jan 2012), and the element and Pb isotopic composition, and element solubility by atmospheric dissolution were determined from the aerosols collected over the South Atlantic. The main novel data determined in this thesis are summarised below followed by a discussion of the implications these novel data may have in the wider scientific community of source characterisation, aerosol provenance tracing and element supply to the ocean via the atmosphere. This thesis concludes with a discussion of some of the main limitations of this thesis and further works to advance the studies carried out during this thesis.

5.1 Main findings

5.1.1. Source characterisation by geochemical proxies

In Chapter 2, an up to date element and Pb and Nd isotopic characterisation of major natural and anthropogenic aerosol sources from South America and Southern Africa was presented, and are summarised in Table 2.7 and Table 3.3.

Mineralogy and element enrichment relative to the continental crust profiles showed some variations between sources and within sources but the most successful proxies identified in this study for distinguishing aerosol sources was through the use of Pb and Nd isotopes and element ratios. The South American natural and anthropogenic sources in South America were well distinguished by $^{208}Pb/^{207}Pb$, and in $^{208}Pb/^{207}Pb$ vs. Pb/Al, 1/[Pb], Zn/Al, Cd/Al, Cr/Al, and εNd plots, and εNd vs. Pb/Al, 1/[Nd] and Cr/Al plots. The volcanic sources were well discriminated from the rural, urban and mine sources from Southern Africa by the same proxies except 1/[Pb]. The $^{208}Pb/^{207}Pb$ vs. 1/[Pb] plot enables the discrimination of volcanic and coal from rural and mine from urban sources in Southern Africa as well as South American urban sources from natural sources from Southern Africa. The $^{208}Pb/^{207}Pb$ vs. Pb/Al and 1/[Pb] plots were also useful to distinguish between South American urban sources north of 45°S from urban sources from Southern Africa. Lastly, the La/Cr ratio and REE profile patterns highlighted differences in element composition within rural and volcanic sources in South America and the 1/[Nd] ratio enabled the discrimination between the urban source regions from South America.

This study produced an up to date quantitative characterisation of geochemical constraints of select natural and anthropogenic sources from South America and Southern Africa. These quantified proxies may be particularly useful for calculating the natural verses anthropogenic contributions to aerosols in aerosol provenance studies.

5.1.2. Geochemical characterisation of aerosols and sources of aerosols across the South Atlantic

In Chapter 3, element and isotopic compositions of bulk aerosols revealed that natural and anthropogenic sources from South America and Southern Africa contributed to aerosols over the South Atlantic, with varying importance across the 40°S transect.

Four of the metals considered (Zn, Pb, Cu and to a lesser extent V) showed high enrichments relative to the continental crust at the west (west of ~45°W) and east margins (east of ~5°W) of the South Atlantic and all declined in enrichments to the remote ocean, to ~20-35°W. Despite air mass back trajectories that showed pathways passing close to southern South America at the western margin and pathways passing over South America, Antarctica and Southern Africa, these trends in enrichment suggested that Zn, Pb, Cu and V distributions over the South Atlantic were controlled by anthropogenic sources from South America and Southern Africa.

In contrast, Cr, Ni and to a lesser extent Co showed high enrichments relative to continental crust at the west margin (between ~45°W to 20°W) and declined in enrichment to the east margin which coincided with air mass pathways dominantly prevailing west to east over the South Atlantic Ocean, and suggested that anthropogenic sources from South America most likely dominated their distribution over the South Atlantic. It however could not be ruled out that enriched natural sources such as volcanic dusts or long-residence times (between 7-10 days) may have contributed to the high enrichments in Cr, Ni and Co exhibited across the ocean. This further revealed that Cr, Ni and Co underwent long-distance transportation west to east across the ocean. The two westernmost aerosols, west of ~50°W were the exception to this trend and showed Cr, Ni and Co enrichments typical of crustal and anthropogenic origin. Cadmium was highly enriched relative to the continental crust across the ocean, except at ~20°W and suggested anthropogenic sources governed Cd supply across the South Atlantic.

Major, REE, Sc, Y and Th enrichments were typical of continental crust. Enrichments in major elements (enrichment factor up to 80) over the South Atlantic were not enough evidence to suggest anthropogenic origin and may have rather been explained by variable wind patterns and variable residence times in the atmosphere. Slight enrichments relative to continental crust of Sc (enrichment factor up to 30) in aerosols east of ~10°E may have been due to anthropogenic sources from Southern Africa.

The natural and anthropogenic source contributions to the South Atlantic were identified with the geochemical proxies reported in Chapter 2. Lead isotopic ratios (^{208}Pb, ^{207}Pb and ^{206}Pb) and trace element ratios (Pb/Al, 1/[Pb], Zn/Al and Cd/Al) showed distinct signals consistent with major anthropogenic sources from South America most typical of industrial and metal processes, and coal combustion. Vanadium is a tracer for oil combustion and low V enrichments relative to other trace metal enrichments suggested oil combustion sources were not as important as industrial and metal processes, and coal combustion sources, for atmospheric particulates that reach the South Atlantic. The La/Cr ratio, εNd and 1/[Nd] signals west of ~50°W and between ~20-35°W were consistent with natural sources of Cr, Ni, Co, major and REEs from Patagonia and the Andean volcanic belt from southern South America. Higher Pb

isotopic ratios between ~20-35°W than west of ~50°W indicated that volcanic dust sources dominated over mineral dust sources between ~20-35°W and to a lesser extent west of ~50°W. Over the eastern section of the South Atlantic, east of ~20°W, Pb isotopic ratios, Pb/Al and 1/[Pb] showed signals consistent with a mixture of South American and Southern African sources. High enrichments in trace metals relative to continental crust at the eastern margin and Pb isotopic ratios were particularly useful at showing that anthropogenic aerosol sources from Southern Africa, predominantly from mine sources, played a major role on trace metal contributions at the eastern margin.

Anthropogenic source contributions were calculated from enrichment factors. Anthropogenic sources contributed ~55-75% of total Pb and Cu, and ~60-65% of total Zn in aerosol masses west of ~45°W, and ~30-40% of total Pb and ~30-50% of total Zn and Cu between ~20-35°W. As Cd appeared to be delivered to the South Atlantic from South America, anthropogenic Cd contributions were ~70-90% of total Cd delivered across the ocean, except at ~20°W where anthropogenic Cd contributions were ~50%.

5.1.3. Solubility of aerosols over the South Atlantic Ocean and Pb isotope composition of soluble fraction of aerosols

In Chapter 4, the determined solubilities of elements in aerosols under wet deposition conditions were presented. Zinc, Cu, Pb, Ni, Mn, and Co solubility ranged between 30 and >95% for Zn, between <5 and >95% for Cu, between 10 and 90% for Pb, between <5 and 90% for V, <5 and >95% for Ni and Co, and between <5 and >80% for Mn. Low solubility for Cr, Fe and Al was generally observed, <30%, except at ~20°W Cr exhibits >95% solubility. Rare earth element showed in general solubilities <30% except in the west (~45°W) and east (~15°E) regions of the South Atlantic which showed solubilities of up to >95%. Yttrium exhibited solubility up to 30% across the 40°S transect, except at ~45°W between 40 and 60% and in the east margin as much as >95% solubility. Scandium and Th solubility for aerosols was <10% and <20%, respectively, across the South Atlantic. As the leach protocol represented the wet deposition and therefore element solubility directly into the seawater when soluble aerosols come into direct contact with the ocean surface, the above determined solubilities presented the highest solubilities of elements from aerosols that may enter the ocean surface waters of the South Atlantic during wet deposition.

The high solubility of elements was linked with enrichments relative to the upper continental crust, where highest enrichments were exhibited adjacent to the continental margins, suggesting anthropogenic source control on solubility, for V and Pb only. High solubilities correlated well with element enrichment for Mn but showed highest enrichments over the open ocean than by the continental margins which correlated with natural dust sources, in particular, greater volcanic rather than mineral dust contributions in aerosols at the open ocean. This suggested that volcanic dusts governed Mn solubility and that Mn may be a useful tracer of volcanic sources in aerosols over the South Atlantic. This study revealed that aside for V and Pb, solubility did not correlate with anthropogenic aerosol sources, which is in contrast to other studies and suggested that aerosols over the South Atlantic behave differently to

aerosols elsewhere (e.g. over the North Atlantic, China, Taiwan, Jickell and Spokes, 2001; Desboeufs et al., 2001; Hsu et al., 2010; Chiang et al., 2014). For other elements such as Fe, other processes may control element solubility over the South Atlantic, such as fine particulate size control on solubility, cloud processing during long-range transport over the South Atlantic, and chemical properties of elements in the aerosols.

Lead isotopic signals differed in the soluble fraction to the total aerosol. Lead isotopic signals in the soluble fraction of the aerosols were consistent with anthropogenic sources from South America and Southern Africa, while Pb isotopic signals in the total aerosols were consistent with mixing of natural and anthropogenic sources from South America and Southern Africa. This implied that anthropogenic Pb particulates are more susceptible to weak acid leaching than natural Pb particulates, which is in line with the correlation between solubility and enrichment values in Pb in aerosols. These findings also revealed that leaching most likely releases anthropogenic Pb that were confined to fine particulate or gaseous phases.

5.1.4. The use of provenance indicators for tracing aerosol sources

At a time where the power to provenance trace using only Pb isotope ratios is reducing due to the removal of the typically low radiogenic Pb isotopic signal of gasoline (which is lower than other anthropogenic sources), this study showed that Pb isotopic compositions in aerosols still retained some use as a tracer of anthropogenic and natural sources. The combination with Nd isotopic and elemental data however provided further details of the distribution and provenance of elements across the South Atlantic, particularly those that did not appear to be associated with Pb or Nd isotopes. This may be a useful approach for future provenance tracing studies. For instance, Pb crustal enrichment trends across the South Atlantic appeared to be associated with Zn, Cu and V but were not well associated with Cr, Ni and Co in aerosols. This suggested different major sources and that possibly Cr and Ni phases were more mobile and susceptible to remaining in the atmosphere than Pb, Zn, Cu and V.

The assessment of Pb isotopic signals in total and soluble aerosols were useful to suggest that Pb isotopic ratios in total aerosols are useful for provenance tracing of aerosols, while Pb isotopic signals in the soluble fraction of aerosols are useful for deciphering element supply to the seawater.

5.1.5. Air quality and temporal changes

Relatively higher enrichments in Cr and Ni than Zn, Pb, Cu and Cd in total aerosols across the ocean suggested that anthropogenic emissions of Cr and Ni were greater than anthropogenic sources of Zn, Pb, Cu and Cd from South America. This implied that Cr and Ni may have derived from additional sources than Pb, Zn, Cu and Cd, or higher ion mobility resulted in a longer residence time of Cr and Ni in the atmosphere. Such enrichments in Cr and Ni have not been reported in aerosols over the South Atlantic and neighbouring oceans such as the North Atlantic and Indian Ocean prior to this study, and implied that

the particularly high enrichments in Cr and Ni may pose concerns for air quality over source regions from South America and Southern Africa.

The high enrichments in Zn, Pb, Cu, and Cd in total aerosols in the western margin (Chapter 3) were in line with recent studies of trace metal composition in aerosols along 40°S (Radlein and Heumann, 1992; Alleman et al., 2001; Kim and Church, 2002; Witt et al., 2006; Baker et al., 2010) while Pb was below enrichments in aerosols over the South Atlantic pre-1985 (Murphy et al., 1985). These studies implied that Zn, Cd, Cu and V emission concentrations from anthropogenic sources from South America have not altered air quality at source regions and the South Atlantic over the last few decades, but there may have been a decrease in Pb concentrations which would reflect the fall in Pb-enriched combustion emissions.

The future of aerosol sources and air quality depends on human activities because anthropogenic sources emit such high levels of trace elements into the atmosphere, which are detrimental to human health. Let alone specific negative effects of elements, the fine particulate fractions of anthropogenic aerosols result in increased adsorption into the body than larger natural particulates. If these emission concentrations increase then anthropogenic contribution will increase, reducing air quality and increasing the concentration of anthropogenic aerosols transported from anthropogenic sources to the ocean. Furthermore, although outside the scope of this thesis, higher anthropogenic aerosols would most likely have a direct effect on climate. This is due to reflection of sunlight by particulates in the atmosphere (e.g. Eby, 2004).

5.1.6. Atmospheric transport

This thesis has suggested that air masses travel west to east by westerly winds across the entire South Atlantic Ocean. Air masses may pass over southern South America, the east coast of central and northern South America, or Antarctica. In the eastern section of the South Atlantic air masses passed from the west, south and the east and showed contact with South America, Antarctica or Southern Africa. Anthropogenic sources have generally played a larger role than natural sources in trace element contributions to aerosols reaching across the South Atlantic Ocean. This is similarly reported across the Northern Hemisphere and highlights the impact that anthropogenic aerosols are having on the aerosols transported over the Southern Hemisphere most likely due to growing cities and human activities in the Southern Hemiphere (e.g. Jickells and Spokes, 2005; Sholkovitz et al., 2009).

5.1.7. Implications of aerosol source impact on ocean chemistry and marine processes

This study provided a wide range of elemental data and Pb isotopic data useful in studies that assess element solubility from aerosols in the atmosphere to the ocean, determining sources control on element deposition from aerosols to ocean, how humans will impact the transport of the bio(geo)available fraction

of iron and other important elements to the ocean, and thus which sources will respond or control climate change.

In Chapter 4, higher enrichments in anthropogenic trace elements did not result in a higher solubility, except for V and Pb. Since the leaching protocol represents the solubilities of elements directly into the ocean, directly affecting the marine element budget, the correlation between V and Pb solubility and enrichment implied that higher anthropogenic V and Pb contributions in aerosols will mean higher V and Pb delivered to the South Atlantic Ocean and consequently a higher V and Pb surface seawater budget. This in contrast to all previous studies that have suggested a positive correlation in element solubility and anthropogenic materials (e.g. Colin et al., 1990; Jickells et al., 1992; Spokes et al., 1994; Ebert and Baechmann, 1998; Desboeufs et al., 2001). These findings have suggested that the relationship between solubility and anthropogenic sources is not as simple as was first suggested and that natural and anthropogenic aerosols in the Southern Hemisphere do not behave in the same way as in aerosols elsewhere that have shown a direct correlation between solubility and anthropogenic aerosols (e.g. dust and anthropogenic aerosols from the North Atlantic, China, Taiwan, Jickells and Spokes, 2001; Desboeufs et al., 2001; Hsu et al., 2010; Chiang et al., 2014). The correlation between Mn solubility and enrichment has implied that higher volcanic Mn contributions in aerosols will mean higher Mn delivered to the South Atlantic Ocean and consequently a higher Mn surface seawater budget. This may result in increased biological activity as Mn acts as a nutrient in the ocean surface waters. For other elements, other processes could be dominant over the South Atlantic, such as fine particulate size control on solubility, cloud processing during long-range transport over the South Atlantic and chemical properties of elements in the aerosol.

Tracing the impact of aerosols delivered to the ocean is a complicated task due to a number of aspects that effect element budget in the ocean. This includes ocean water circulation, biogeochemical reactions, residence time, and sources of elements to the ocean. Simultaneously collected aerosol and seawater samples from the same localities were assumed to cancel out the transient dynamics of the ocean and suggested that these datasets can be compared to assess the direct impact of element supply in aerosols on element budget in the ocean. Thus far there is one published study of element composition (of Zn) in the surface waters that were simultaneously collected as the aerosols from along the GEOTRACES GA10 40°S transect across the South Atlantic (Wyatt et al., 2014). High solubilities of Zn from aerosols across the South Atlantic except at some most central samples revealed some correlation to the highest Zn concentrations in the ocean exhibited at the continental margins. The absence of high concentrations of Zn in the ocean towards the middle of the South Atlantic however suggested that atmospheric Zn may have contributed to the Zn in surface waters of the South Atlantic, but the atmosphere was not the governing control in distribution of Zn across the ocean. A continued aim of the GEOTRACES project will be to assess the impact that aerosol solubility may have on the ocean element budget by comparing the element solubility data from this thesis and element concentration data for seawater collected during the GEOTRACES cruises yet to be determined.

Chapter 3 revealed that Fe in aerosols over the South Atlantic derived from natural, predominantly volcanic sources from South America. Although the photochemical controls on Fe solubility from aerosols over the South Atlantic Ocean have not been constrained in Chapter 4, this thesis highlighted the natural sources from South America are responsible for the Fe supply via the atmosphere to the South Atlantic and must play a major role in controlling climate. At the same time, an increased climate temperature will increase arid conditions and further increase dust emissions over the ocean. Thus dust release from large arid sources from South America may have a positive feedback relationship with climate change.

5.2. Limitations and Further Work

5.2.1 Limitations and improvements in source characterisation

In Chapter 2, an up-to-date source characterisation was limited to one anthropogenic source type from South America, urban samples. The source characterisation was also limited in natural loess and anthropogenic aerosol sources from Southern Africa by low sample batches (n=1 for rural, and n=1 for mine samples from Johannesburg) and no anthropogenic source samples younger than 2006 (post-lead ban in South Africa). The potential effect the latter may have had on the geochemical constrain of Pb isotopes in anthropogenic sources was taken into account in the isotopic characterisation of anthropogenic sources from Southern Africa. Nonetheless, source samples from select anthropogenic sources such as industrial plant emissions and waste incineration plants from South America and a larger number of natural and anthropogenic aerosol sources from Southern Africa post-2006 may improve source characterisation in Chapter 2 and aerosol provenance tracing in Chapter 3.

Furthermore, anthropogenic aerosol contribution is reportedly higher during the winter periods (e.g. Ramanathan et al., 2001; Srivastava et al., 2014). The source samples from South America were gathered during the summer (Fujiwara et al., 2011; as reported in Chapter 2) while the aerosol samples were collected during the winter. This may have explained the higher Cr and Ni enrichments in aerosols than in the characterised anthropogenic sources. Consequently, this highlighted that it is important to sample both source material and aerosols during the same seasons of a year, particularly in the interest of accurately assessing the anthropogenic source contributions to aerosols.

5.2.2. Limitations of isotope ratios

This thesis revealed that Nd was too low in low atmospheric input environments such as the South Atlantic to analyse for Nd isotopes in total and soluble fraction of aerosols and was thus not as useful a tracer as Pb for low aerosol input regions. An alternative natural tracer than REE may be ideal such as hafnium (Hf) (e.g. Vervoort and Patchett, 1996; van de Flierdt et al., 2007;Yang et al., 2009; Liu et al.,

2014). However the use of Hf as a tracer requires a more robust method for sample digestion, as hafnium-containing zircon is not fully digested by the acid digestion methods described throughout this thesis (e.g. Liu et al., 2014).

5.2.3. Aerosol collection method and improving the assessment of controls on aerosol solubility

This study highlighted that sampling of aerosols in low input environments is limited by sampling procedures that are non-sensitive to low trace metal concentrations, particularly of Cd. Possible inhomogeneity of aerosol deposition on filters, contamination introduced to filters during the sampling procedure, and significant element contribution from the filters themselves resulted in large uncertainties in atmospheric concentrations and aerosol solubility (often >50%). These aspects affected the lowest element concentrations in samples closest to the west and east margins of the ocean and limited interpretations in Chapters 3 and 4.

It may be useful to alter the way representative filter blanks are measured. For instance, ensure the sampling equipment has been cleaned and switched on for an amount of time, e.g. a few hours to a day, before taking a motor blank or exposure blank. Alternatively, for studies interested in trace metal analysis on aerosols of low concentration environments, a sampling procedure that introduces a smaller blank contribution or contamination may be more suitable than the procedure used for this study. For instance, exchange components of the sampling device to non-metal and non-rubber components that do not introduce trace metal contamination, e.g. Teflon. Alternatively, use a non-metal adhesive layer to trap the aerosol sample rather than filters, although this may introduce another difficulty of separating the aerosol sample from the adhesive layer.

In Chapter 4, the suggestion that element solubility from aerosols did not correlate with anthropogenic sources of aerosols, except for V and Pb, implied that other factors such as particle size and chemical processing may have played larger roles than natural vs. anthropogenic sources on element solubility. To answer what sort of chemical behaviour are important to increase solubility includes information such as aerosol particle sizes and mineralogy, and particle imaging. This was not achievable in this thesis due to difficulties with extracting particles from the filters. A collaborated aerosol group at University of Norwich (Chance, R; Baker, A) within the GEOTRACES project will be assessing the element composition of aerosols of different particle sizes collected simultaneously as the aerosols analysed during this thesis. The assessment may be able to provide some detail to the particle size control on element solubility across the transect. A method that results in a larger aerosol mass collection that is relatively easy to separate from the sampling medium (e.g. the filter) without destroying the particulates may permit mineralogical analysis and grain imaging. A longer exposure time for each aerosol sample should be an adequate means to improve aerosol mass collection, although this would require longer days at sea. Furthermore, total and soluble atmospheric concentrations and element solubilities from this thesis and studies from University of Norwich may assess the precision of the aerosol collection method.

5.2.4 Limitations and improving aerosol and ocean chemistry data

The aerosol dataset represented a snapshot in aerosol composition across the ocean. Potential differences in atmospheric composition during the winter to summer seasons suggests that conducting an aerosol collection during the summer season may present a different geochemical characterisation of the aerosols, that were conducted during the winter. For example, an expected higher natural source contribution of dust during the summer than winter may result in a higher Fe enrichment in aerosols relative to the continental crust during the summer.

Comparing the aerosol data to seawater data to assess the impact of aerosol solubility on the high primary productivity region of the South Atlantic is restricted. At the time of this study Fe concentrations of seawater from along the transect were not available. A geochemical assessment of the impact that the atmosphere has on the high primary productivity region along ~40°S was hindered by limited data for comparing Fe in aerosols and seawater north and south of 40°S (Witt et al., 2006; Baker et al., 2013). There was also not enough evidence at present to determine the impact of trace elements on primary production along the transect. The high solubility in trace elements from aerosols may also have an important role in controlling the biological activity in the surface waters of the South Atlantic. To address this issue, additional data are required that include surface water element concentrations, atmosphere and ocean circulation modeling along the 40°S transect, and further aerosol sampling campaigns are required. An aerosol and seawater sampling campaign along the 40°S transect with sampling also north and south of 40°S every ~10-20° longitude during the summer would provide the minimum data to geochemically assess the impact of the atmosphere on the high primary productivity region along ~40°S. Conducting the same sampling campaigns during the winter may enhance the assessment of seasonal variation in aerosol composition over the South Atlantic, aerosol solubility, and seasonal variation in the impact of the atmosphere on marine processes.

REFERENCES

Agnieszka, J., & Barbara, G. (2012). Chromium, nickel and vanadium mobility in soils derived from fluvioglacial sands. *Journal of Hazardous Materials, 237*, 315-322. doi: 10.1016/j.jhazmat.2012.08.048

Albarede, F., & Beard, B. (2004). Analytical methods for non-traditional isotopes. In C. M. Johnson, B. L. Beard & F. Albarede (Eds.), *Geochemistry of Non-Traditional Stable Isotopes* (Vol. 55, pp. 113-152).

Alkmim, F. F., Marshak, S., & Fonseca, M. A. (2001). Assembling West Gondwana in the Neoproterozoic: Clues from the Sao Francisco craton region, Brazil. *Geology, 29*(4), 319-322. doi: 10.1130/0091-7613(2001)029<0319:awgitn>2.0.co;2

Alleman, L. Y., Church, T. M., Veron, A. J., Kim, G., Hamelin, B., & Flegal, A. R. (2001). Isotopic evidence of contaminant lead in the South Atlantic troposphere and surface waters. *Deep-Sea Research Part Ii-Topical Studies in Oceanography, 48*(13), 2811-2827. doi: 10.1016/s0967-0645(01)00019-4

Andrade, F., Orsini, C., & Maenhaut, W. (1994). RELATION BETWEEN AEROSOL SOURCES AND METEOROLOGICAL PARAMETERS FOR INHALABLE ATMOSPHERIC PARTICLES IN SAO-PAULO CITY, BRAZIL. *Atmospheric Environment, 28*(14), 2307-2315. doi: 10.1016/1352-2310(94)90484-7

Annett, A. L., Lapi, S., Ruth, T. J., & Maldonado, M. T. (2008). The effects of Cu and Fe availability on the growth and Cu : C ratios of marine diatoms. *Limnology and Oceanography, 53*(6), 2451-2461. doi: 10.4319/lo.2008.53.6.2451

Arimoto, R., Duce, R. A., Ray, B. J., Hewitt, A. D., & Williams, J. (1987). TRACE-ELEMENTS IN THE ATMOSPHERE OF AMERICAN-SAMOA - CONCENTRATIONS AND DEPOSITION TO THE TROPICAL SOUTH-PACIFIC. *Journal of Geophysical Research-Atmospheres, 92*(D7), 8465-8479. doi: 10.1029/JD092iD07p08465

Associated Octel (1995). Worldwide gasoline survey 1992-1993, OPP No. 4 (4/95)

Baker, A. R., Kelly, S. D., Biswas, K. F., Witt, M., & Jickells, T. D. (2003). Atmospheric deposition of nutrients to the Atlantic Ocean. *Geophysical Research Letters, 30*(24). doi: 10.1029/2003gl018518

Baker, A. R., Jickells, T. D., Biswas, K. F., Weston, K., & French, M. (2006). Nutrients in atmospheric aerosol particles along the Atlantic Meridional Transect. *Deep-Sea Research Part Ii-Topical Studies in Oceanography, 53*(14-16), 1706-1719. doi: 10.1016/j.dsr2.2006.05.012

Baker, A. R., Jickells, T. D., Witt, M., & Linge, K. L. (2006a). Trends in the solubility of iron, aluminium, manganese and phosphorus in aerosol collected over the Atlantic Ocean. *Marine Chemistry, 98*(1), 43-58. doi: 10.1016/j.marchem.2005.06.004

Baker, A. R., French, M., & Linge, K. L. (2006b). Trends in aerosol nutrient solubility along a west-east transect of the Saharan dust plume. *Geophysical Research Letters, 33*(7). doi: 10.1029/2005gl024764

Baker, A. R., & Croot, P. L. (2010). Atmospheric and marine controls on aerosol iron solubility in seawater. *Marine Chemistry, 120*(1-4), 4-13. doi: 10.1016/j.marchem.2008.09.003

Baker, A. R., Adams, C., Bell, T. G., Jickells, T. D., & Ganzeveld, L. (2013). Estimation of atmospheric nutrient inputs to the Atlantic Ocean from 50 degrees N to 50 degrees S based on large-scale field sampling: Iron and other dust-associated elements. *Global Biogeochemical Cycles, 27*(3), 755-767. doi: 10.1002/gbc.20062

Balcaen, L., Moens, L., & Vanhaecke, F. (2010). Determination of isotope ratios of metals (and metalloids) by means of inductively coupled plasma-mass spectrometry for provenancing purposes - A review. *Spectrochimica Acta Part B-Atomic Spectroscopy, 65*(9-10), 769-786. doi: 10.1016/j.sab.2010.06.005

Barry, R. & Choerley, R. (1987). Atmosphere, weather, climate. Atmospheric physics.

Bechis, F., Encinas, A., Concheyro, A., Litvak, V. D., Aguirre-Urreta, B., & Ramos, V. A. (2014). New age constraints for the Cenozoic marine transgressions of northwestern Patagonia, Argentina (41 degrees-43 degrees S): Paleogeographic and tectonic

implications. *Journal of South American Earth Sciences, 52*, 72-93. doi: 10.1016/j.jsames.2014.02.003

Begg, G. C., Griffin, W. L., Natapov, L. M., O'Reilly, S. Y., Grand, S. P., O'Neill, C. J., Bowden, P. (2009). The lithospheric architecture of Africa: Seismic tomography, mantle petrology, and tectonic evolution. *Geosphere, 5*(1), 23-50. doi: 10.1130/ges00179.1

Berner, E. & Berner, R. (1996). Global Environment: water, air and geochemical cycles, Prentice-Hall.

Bertine K.K. & Goldberg E.D. (1977). History of heavy metal contamination in shallow coastal sediments around Mitelene, Greece. International Journal of Environmental Analytical Chemistry, 68: 281-293.

Bertolo, R., Bourotte, C., Marcolan, L., Oliveira, S., & Hirata, R. (2011). Anomalous content of chromium in a Cretaceous sandstone aquifer of the Bauru Basin, state of Sao Paulo, Brazil. *Journal of South American Earth Sciences, 31*(1), 69-80. doi: 10.1016/j.jsames.2010.10.002

Biscaye, P. (1965). Mineralogy and Sedimentation of Recent Deep-Sea Clay in the Atlantic Ocean and Adjacent Seas and Oceans, *Geological Society of America Bulletin, 76* (7): 803.

Biscaye, P. E., Grousset, F. E., Revel, M., VanderGaast, S., Zielinski, G. A., Vaars, A., & Kukla, G. (1997). Asian provenance of glacial dust (stage 2) in the Greenland Ice Sheet Project 2 Ice Core, Summit, Greenland. *Journal of Geophysical Research-Oceans, 102*(C12), 26765-26781. doi: 10.1029/97jc01249

Bish, DL & Post, JE, editors. (1989). Modern Powder Diffraction. Reviews in Mienralogy. 20. Mineralogical Society of America.

Bollhofer, A., & Rosman, K. J. R. (2000). Isotopic source signatures for atmospheric lead: The Southern Hemisphere. *Geochimica et Cosmochimica Acta, 64*(19), 3251-3262. doi: 10.1016/s0016-7037(00)00436-1

Bollhofer, A., & Rosman, K. J. R. (2001a). Isotopic source signatures for atmospheric lead: The Northern Hemisphere. *Geochimica et Cosmochimica Acta, 65*(11), 1727-1740. doi: 10.1016/s0016-7037(00)00630-x

Bollhofer, A., & Rosman, K. J. R. (2001b). Lead isotopic ratios in European atmospheric aerosols. *Physics and Chemistry of the Earth Part B-Hydrology Oceans and Atmosphere, 26*(10), 835-838. doi: 10.1016/s1464-1909(01)00094-6

Bonnet, S., & Guieu, C. (2004). Dissolution of atmospheric iron in seawater. *Geophysical Research Letters, 31*(3). doi: 10.1029/2003gl018423

Bory, A., & Bout-Roumazeilles, V. (2012). Topsoils and riverbed sediment collected from southern Patagonia.

Boyd, P. W., Watson, A. J., Law, C. S., Abraham, E. R., Trull, T., Murdoch, R., & Zeldis, J. (2000). A mesoscale phytoplankton bloom in the polar Southern Ocean stimulated by iron fertilization. *Nature, 407*(6805), 695-702. doi: 10.1038/35037500

Boyd, P. W., Jickells, T., Law, C. S., Blain, S., Boyle, E. A., Buesseler, K. O., Watson, A. J. (2007). Mesoscale iron enrichment experiments 1993-2005: Synthesis and future directions. *Science, 315*(5812), 612-617. doi: 10.1126/science.1131669

Boyd, P. W., & Ellwood, M. J. (2010). The biogeochemical cycle of iron in the ocean. *Nature Geoscience, 3*(10), 675-682. doi: 10.1038/ngeo964

Bragg, W.H.; Bragg, W.L. (1913). "The Reflexion of X-rays by Crystals". *Proc R. Soc. Lond. A* 88 (605): 428–38. doi:10.1098/rspa.1913.0040. (Free access)

Bremner, J. M., & Willis, J. P. (1993). MINERALOGY AND GEOCHEMISTRY OF THE CLAY FRACTION OF SEDIMENTS FROM THE NAMIBIAN CONTINENTAL-MARGIN AND THE ADJACENT HINTERLAND. *Marine Geology, 115*(1-2), 85-116. doi: 10.1016/0025-3227(93)90076-8

Bruland, K. W., Donat, J. R., & Hutchins, D. A. (1991). INTERACTIVE INFLUENCES OF BIOACTIVE TRACE-METALS ON BIOLOGICAL PRODUCTION IN OCEANIC WATERS. *Limnology and Oceanography, 36*(8), 1555-1577.

Bruland, K. W., Rue, E. L., & Smith, G. J. (2001). Iron and macronutrients in California coastal upwelling regimes: Implications for diatom blooms. *Limnology and Oceanography, 46*(7), 1661-1674.

Bruland, K. W. & Lohan, M., C. (2003). Controls of trace metals in seawater, treatise on geochemistry, Elderfield, H., Elsevier Sciences, Cambridge.

Buck, C. S., Landing, W. M., Resing, J. A., & Measures, C. I. (2010). The solubility and deposition of aerosol Fe and other trace elements in the North Atlantic Ocean: Observations from the A16N CLIVAR/CO2 repeat hydrography section. *Marine Chemistry, 120*(1-4), 57-70. doi: 10.1016/j.marchem.2008.08.003

Butler, A. (1998). Acquisition and utilization of transition metal ions by marine organisms. *Science, 281*(5374), 207-210. doi: 10.1126/science.281.5374.207

Carlson, T., & Prospero, J. (1972). The Large-Scale Movement of Saharan Air Outbreaks over the Northern Equatorial Atlantic, *Journal of Applied Meteorology, 11*, 283-297.

Caroli, S. (2006). Proceedings of the 3rd Nordic Conference on Plasma Spectrochemistry, 40

Castanho, A. D. A., & Artaxo, P. (2001). Wintertime and summertime Sao Paulo aerosol source apportionment study. *Atmospheric Environment, 35*(29), 4889-4902. doi: 10.1016/s1352-2310(01)00357-0

Chang, Q., Mishima, T., Yabuki, S., Takahashi, Y., & Shimizu, H. (2000). Sr and Nd isotope ratios and REE abundances of moraines in the mountain areas surrounding the Taklimakan Desert, NW China. *Geochemical Journal, 34*(6), 407-427.

Chester, R. (2000). *Marine Geochemistry*. Blackwell Science, Oxford.

Chester, R., Berry, A. S., & Murphy, K. J. T. (1991). The distribution of particulate atmospheric trace metals and mineral aerosols over the Indian Ocean. *Marine Chemistry, 34*, 261-290.

Chester, R., & Jickells, T. D. (2012). *Marine Geochemistry,* 3rd Ed, Wiley-Blackwell.

Chin, M. (2009. Dust emission, transport and effects on air quality: A global model simulation and comparison with multi-platform data. NASA Goddard Space Flight.

Chuang, P. Y., Duvall, R. M., Shafer, M. M., & Schauer, J. J. (2005). The origin of water soluble particulate iron in the Asian atmospheric outflow. *Geophysical Research Letters, 32*(7). doi: 10.1029/2004gl021946

Cid-Aguero, D. (2011). Volcanic deposits collected from Chile in Patagonia.

Coale, K. H. (1991). EFFECTS OF IRON, MANGANESE, COPPER, AND ZINC ENRICHMENTS ON PRODUCTIVITY AND BIOMASS IN THE SUB-ARCTIC PACIFIC. *Limnology and Oceanography, 36*(8), 1851-1864.

Cole, D. I. (1998). Uranium. In: Wilson, M. G. C., Anhausser, C. R. (Eds.), The Mineral Resources of South Africa Handbook, vol. 16. Council for Geoscience, 642-652.

Colin, J. L., Jaffrezo, J. L., & Gros, J. M. (1990). SOLUBILITY OF MAJOR SPECIES IN PRECIPITATION - FACTORS OF VARIATION. *Atmospheric Environment Part a-General Topics, 24*(3), 537-544. doi: 10.1016/0960-1686(90)90008-b

Condie, K. & Hunter, D. (1976). Trace element geochemistry of Archean granitic rocks from the Barberton region, South Africa. Earth and Planetary Science Letters, 29(2), 389-400

Cooper, J. A., Reynolds, P. H., & Richards, J. R. (1969). Double-spike calibration of the Broken Hill standard lead. *Earth Planet Science Letters, 6*, 467-478.

Covelli, S., & Fontolan, G. (1997). Application of a normalization procedure in determining regional geochemical baselines. *Environmental Geology, 30*(1-2), 34-45.

Crocket, K. C., Lambelet, M., de Flierdt, T. v., Rehkaemper, M., & Robinson, L. F. (2014). Measurement of fossil deep-sea coral Nd isotopic compositions and concentrations by TIMS as NdO+, with evaluation of cleaning protocols. *Chemical Geology, 374*, 128-140. doi: 10.1016/j.chemgeo.2014.03.011

Cummings, G. L., & Richards, J. R. (1975). Ore lead isotope ratios in a continuously changing earth. Springer Verlag, Berlin, Heidelberg, New York.

de Almeida, F. F. M., Neves, B. B. D., & Carneiro, C. D. (2000). The origin and evolution of the South American Platform. *Earth-Science Reviews, 50*(1-2), 77-111.

de Brito Neves, B. B., & Fuck, R. A. (2013). Neoproterozoic evolution of the basement of the South-American platform. *Journal of South American Earth Sciences, 47*, 72-89. doi: 10.1016/j.jsames.2013.04.005

de Campos, R. S., Philipp, R. P., Massonne, H.-J., & Chemale, F., Jr. (2012). Early post-collisional Brasiliano magmatism in Botuvera region, Santa Catarina, southern Brazil: Evidence from petrology, geochemistry, isotope geology and geochronology of the diabase and lamprophyre dikes. *Journal of South American Earth Sciences, 37*, 266-278. doi: 10.1016/j.jsames.2012.02.005

de Miranda, R. M., Andrade, M. D., Worobiec, A., & Van Grieken, R. (2002). Characterisation of aerosol particles in the Sao Paulo Metropolitan Area. *Atmospheric Environment, 36*(2), 345-352. doi: 10.1016/s1352-2310(01)00363-6

Delmonte, B., Basile-Doelsch, I., Petit, J. R., Maggi, V., Revel-Rolland, M., Michard, A., & Grousset, F. (2004). Comparing the Epica and Vostok dust records during the last 220,000 years: stratigraphical correlation and provenance in glacial periods. *Earth-Science Reviews, 66*(1-2), 63-87. doi: 10.1016/j.earscirev.2003.10.004

Desboeufs, K. V., Losno, R., & Colin, J. L. (2001). Factors influencing aerosol solubility during cloud processes. *Atmospheric Environment, 35*(20), 3529-3537. doi: 10.1016/s1352-2310(00)00472-6

Desboeufs, K. V., Sofikitis, A., Losno, R., Colin, J. L., & Ausset, P. (2005). Dissolution and solubility of trace metals from natural and anthropogenic aerosol particulate matter. *Chemosphere, 58*(2), 195-203. doi: 10.1016/j.chemosphere.2004.02.025

Dickin, A. (1995). Radiogenic Isotope Geochemistry. Cambridge: Cambridge University Press.

Dolgopolova, A., Weiss, D. J., Seltmann, R., Kober, B., Mason, T. F. D., Coles, B., & Stanley, C. J. (2006). Use of isotope ratios to assess sources of Pb and Zn dispersed in the environment during mining and ore processing within the Orlovka-Spokoinoe mining site (Russia). *Applied Geochemistry, 21*(4), 563-579. doi: 10.1016/j.apgeochem.2005.12.014

Dostal, J., Zentilli, M., Caelles, J.C. & Clark, A.h. (1977). Geochemistry and origin of volcanic rocks of the Andes (26-28S). *Contributions Mineral Petrology*. 63:113-128.

Draxler, R.R., & Rolph, G.D. (2013). HYSPLIT (HYbrid Single-Particle Lagrangian Integrated Trajectory) Model access via NOAA ARL READY. Website (http://www.arl.noaa.gov/HYSPLIT.php). NOAA Air Resources Laboratory, College Park, MD.

Ducart, D. F., Crosta, A. P., Souza Filho, C. R., & Coniclio, J. (2006). Alteration mineralogy at the Cerro La Mina epithermal prospect, Patagonia, Argentina: Field mapping, short-wave infrared spectroscopy, and ASTER images. *Economic Geology, 101*(5), 981-996. doi: 10.2113/gsecongeo.101.5.981

Duce, R. A., Liss, P. S., Merrill, J. T., Atlas, E. L., Buat-Menard, P., Hicks, B. B., et al. (1991). THE ATMOSPHERIC INPUT OF TRACE SPECIES TO THE WORLD OCEAN. *Global Biogeochemical Cycles, 5*(3), 193-260. doi: 10.1029/91gb01778

Ebert, P., & Baechmann, K. (1998). Solubility of lead in precipitation as a function of raindrop size. *Atmospheric Environment, 32*(4), 767-771. doi: 10.1016/s1352-2310(97)00344-0

Eby, N. (2004). Principles of Environmental Geochemistry. *Thomson-Brooks/Cole.*

Elderfield, H., Upstillgoddard, R., & Sholkovitz, E. R. (1990). THE RARE-EARTH ELEMENTS IN RIVERS, ESTUARIES, AND COASTAL SEAS AND THEIR SIGNIFICANCE TO THE COMPOSITION OF OCEAN WATERS. *Geochimica et Cosmochimica Acta, 54*(4), 971-991. doi: 10.1016/0016-7037(90)90432-k

Erel, Y., Veron, A., & Halicz, L. (1997). Tracing the transport of anthropogenic lead in the atmosphere and in soils using isotopic ratios. *Geochimica et Cosmochimica Acta, 61*(21), 4495-4505. doi: 10.1016/s0016-7037(97)00353-0

Evan, A. T., Foltz, G. R., & Zhang, D. (2012). Physical Response of the Tropical-Subtropical North Atlantic Ocean to Decadal-Multidecadal Forcing by African Dust. *Journal of Climate, 25*(17), 5817-5829. doi: 10.1175/jcli-d-11-00438.1

Evangelista, H., Maldonado, J., dos Santos, E. A., Godoi, R. H. M., Garcia, C. A. E., Garcia, V. M. T., & Gaiero, D. M. (2010). Inferring episodic atmospheric iron fluxes in the Western South Atlantic. *Atmospheric Environment, 44*(5), 703-712. doi: 10.1016/j.atmosenv.2009.11.018

Ewart, A., Marsh, J. S., Milner, S. C., Duncan, A. R., Kamber, B. S., & Armstrong, R. A. (2004). Petrology and geochemistry of early cretaceous bimodal continental flood volcanism of the NW Etendeka, Namibia. Part 1: Introduction, mafic lavas and re-evaluation of mantle source components. *Journal of Petrology, 45*(1), 59-105. doi: 10.1093/petrology/egg083

Feng, J. L., Hu, Z. G., Cui, J. Y., & Zhu, L. P. (2010). Distributions of lead isotopes with grain size in aeolian deposits. *Terra Nova, 22*(4), 257-263. doi: 10.1111/j.1365-3121.2010.00941.x

Ferrat, M., Weiss, D. J., Strekopytov, S., Dong, S., Chen, H., Najorka, J., Sinha, R. (2011). Improved provenance tracing of Asian dust sources using rare earth elements and selected trace elements for palaeomonsoon studies on the eastern Tibetan Plateau. *Geochimica et Cosmochimica Acta, 75*(21), 6374-6399. doi: 10.1016/j.gca.2011.08.025

Ferrat, M., Weiss, D. J., Spiro, B., & Large, D. (2012). The inorganic geochemistry of a peat deposit on the eastern Qinghai-Tibetan Plateau and insights into changing atmospheric circulation in central Asia during the Holocene. *Geochimica et Cosmochimica Acta, 91*, 7-31. doi: 10.1016/j.gca.2012.05.028

Ferrat, M., Weiss, D. J., & Strekopytov, S. (2012). A single procedure for the accurate and precise quantification of the rare earth elements, Sc, Y, Th and Pb in dust and peat for provenance tracing in climate and environmental studies. *Talanta, 93*, 415-423. doi: 10.1016/j.talanta.2012.01.052

Frimmel, H. E., Jonasson, I. R., & Mubita, P. (2004). An Eburnean base metal source for sediment-hosted zinc-lead deposits in Neoproterozoic units of Namibia: Lead isotopic and geochemical evidence. *Mineralium Deposita, 39*(3), 328-343. doi: 10.1007/s00126-004-0410-7

Fujiwara, F., Rebagliati, R. J., Dawidowski, L., Gómez, D., Polla, G., Pereyra, V., & Smichowski, P. (2011). Spatial and chemical patterns of size fractionated road dust collected in a megacitiy. *Atmospheric Environment, 45*(8), 1497-1505. doi: 10.1016/j.atmosenv.2010.12.053

Gaiero, D. M., Probst, J. L., Depetris, P. J., Bidart, S. M., & Leleyter, L. (2003). Iron and other transition metals in Patagonian riverborne and windborne materials: geochemical control and transport to the southern South Atlantic Ocean. *Geochimica et Cosmochimica Acta, 67*(19), 3603-3623. doi: 10.1016/s0016-7037(03)00211-4

Gaiero, D. M., Depetris P. J., Probst J-L., Bidart S. M., Leleyter L. (2004). The signature of river- and wind-borne material exported from Patagonia to the southern latitudes: a view from REEs and implications for paleoclimatic interpretations. *GCA*.

Gaiero, D. M., Brunet, F., Probst, J.-L., & Depetris, P. J. (2007). A uniform isotopic and chemical signature of dust exported from Patagonia: Rock sources and occurrence in southern environments. *Chemical Geology, 238*(1-2), 107-120. doi: 10.1016/j.chemgeo.2006.11.003

Galer, S. & Abouchami, W. (1998). Practical application of lead triple spiking for correction of instrumental mass discrimination. Mineral Magazine. 62, 491-492.

Gallet, S., Jahn, B. M., & Torii, M. (1996). Geochemical characterization of the Luochuan loess-paleosol sequence, China, and paleoclimatic implications. *Chemical Geology, 133*(1-4), 67-88. doi: 10.1016/s0009-2541(96)00070-8

Galloway, J. N., Dentener, F. J., Capone, D. G., Boyer, E. W., Howarth, R. W., Seitzinger, S. P., Vorosmarty, C. J. (2004). Nitrogen cycles: past, present, and future. *Biogeochemistry, 70*(2), 153-226. doi: 10.1007/s10533-004-0370-0

Gasso, S., & Stein, A. F. (2007). Does dust from Patagonia reach the sub-Antarctic Atlantic ocean? *Geophysical Research Letters, 34*(1). doi: 10.1029/2006gl027693

GEOROC (2003-2011). Geochemistry of Rocks of the Oceans and Continents. Website (http://www.georoc.mpch-mainz.gwdg.de/georoc/)

Getty, S. R., Gutzler, D. S., Asmerom, Y., Shearer, C. K., & Free, S. J. (1999). Chemical signals of epiphytic lichens in southwestern North America; natural versus man-made sources for airborne particulates. *Atmospheric Environment, 33*(30), 5095-5104. doi: 10.1016/s1352-2310(99)00222-8

Gioia, S. M. C. L., Babinski, M., Weiss, D. J., & Kerr, A. A. F. S. (2010). Insights into the dynamics and sources of atmospheric lead and particulate matter in Sao Paulo, Brazil, from high temporal resolution sampling. *Atmospheric Research, 98*(2-4), 478-485. doi: 10.1016/j.atmosres.2010.08.016

Gladney, E.S., Jones, E.A., Nickell, E.J., and Roelandts, I. (1992, 1988). Compilation of elemental concentration data for USGS AGV-1, GSP-1 and G-2: *Geostandards Newsletter, 16*:111-300.

Goldberg, E. D., Koide, M., Schmitt, R. A., & Smith, R. H. (1963). Rare-earth distributions in the marine environment, *Geophysical Research, 68*, 4209-4217.

Gomez, M. B., Gomez, M. M., & Palacios, M. A. (2003). ICP-MS determination of Pt, Pd and Rh in airborne and road dust after tellurium coprecipitation. *Journal of Analytical Atomic Spectrometry, 18*(1), 80-83. doi: 10.1039/b209727n

Goody, R. & Walker, J. (1972). Atmospheres, Foundations of the East Science Series. Prentice-Hall.

Govindaraju, K. (1989, 1989). Compilation of working values and sample description of 272 geostandards: *Geostandards Newsletter, 13*:1-113.

Govindaraju, K. (1994, 1994). Compilation of working values and description for 383 geostandards: *Geostandards Newsletter, 18*:1-158.

Greaves, M. J., Statham, P. J., & Elderfield, H. (1994). RARE-EARTH ELEMENT MOBILIZATION FROM MARINE ATMOSPHERIC DUST INTO SEAWATER. *Marine Chemistry, 46*(3), 255-260. doi: 10.1016/0304-4203(94)90081-7

Grousset, F. E., & Biscaye, P. E. (2005). Tracing dust sources and transport patterns using Sr, Nd and Pb isotopes. *Chemical Geology, 222*(3-4), 149-167. doi: 10.1016/j.chemgeo.2005.05.006

Grunder, A. L. (1987). LOW DELTA-O-18 SILICIC VOLCANIC-ROCKS AT THE CALABOZOS CALDERA COMPLEX, SOUTHERN ANDES - EVIDENCE FOR UPPER-CRUSTAL CONTAMINATION. *Contributions to Mineralogy and Petrology, 95*(1), 71-81. doi: 10.1007/bf00518031

Guarino, V., Azzone, R. G., Brotzu, P., Gomes, C. d. B., Melluso, L., Morbidelli, L., . . . Brilli, M. (2012). Magmatism and fenitization in the Cretaceous potassium-alkaline-carbonatitic complex of Ipanema So Paulo State, Brazil. *Mineralogy and Petrology, 104*(1-2), 43-61. doi: 10.1007/s00710-011-0168-4

Guieu, C., Bonnet, S., Wagener, T., & Loye-Pilot, M. D. (2005). Biomass burning as a source of dissolved iron to the open ocean? *Geophysical Research Letters, 32*(19). doi: 10.1029/2005gl022962

Guveni, D. & Akinci, G. (2011). Comparison of acid digestion techniques to determine heavy metals in sediment and soil samples, Gazi University. Journal of Science. 24(1). 29-34.

Hand, J. L., Mahowald, N. M., Chen, Y., Siefert, R. L., Luo, C., Subramaniam, A., & Fung, I. (2004). Estimates of atmospheric-processed soluble iron from observations and a global mineral aerosol model: Biogeochemical implications. *Journal of Geophysical Research-Atmospheres, 109*(D17). doi: 10.1029/2004jd004574

Hanson, P. J., Evans, D. W., Colby, D. R., & Zdanowicz, V. S. (1993). ASSESSMENT OF ELEMENTAL CONTAMINATION IN ESTUARINE AND COASTAL ENVIRONMENTS BASED ON GEOCHEMICAL AND STATISTICAL MODELING OF SEDIMENTS. *Marine Environmental Research, 36*(4), 237-266. doi: 10.1016/0141-1136(93)90091-d

Hasse, L. (1983). Introductory meteorology and fluid mechanics. In Air-sea exchange of gases and particles. Liss, P. S. and W. G. N. Slinn, Reidel.

Haywood, J., Francis, P., Osborne, S., Glew, M., Loeb, N., Highwood, E., & Hirst, E. (2003). Radiative properties and direct radiative effect of Saharan dust measured by the C-130 aircraft during SHADE: 1. Solar spectrum. *Journal of Geophysical Research-Atmospheres, 108*(D18). doi: 10.1029/2002jd002687

Heimburger, A., Losno, R., & Triquet, S. (2013). Solubility of iron and other trace elements in rainwater collected on the Kerguelen Islands (South Indian Ocean). *Biogeosciences, 10*(10), 6617-6628. doi: 10.5194/bg-10-6617-2013

Hlavay, J., Prohaska, T., Weisz, M., Wenzel, W., & Stingeder, G. (2004). Determination of trace elements bound to soils and sediment fraction. Pure Applied Chemistry. 76(2). 415-442. (IUPAC Tehcnical Report).

Homoky, W. (2010). UK GEOTRACES D357 Cruise Cape Town to Cape Town.

Honda, M., Yabuki, S., & Shimizu, H. (2004). Geochemical and isotopic studies of aeolian sediments in China. *Sedimentology, 51*(2), 211-230. doi: 10.1046/j.1365-3091.2003.00618.x

Hsu, S.-C., Wong, G. T. F., Gong, G.-C., Shiah, F.-K., Huang, Y.-T., Kao, S.-J., & Tseng, C.-M. (2010). Sources, solubility, and dry deposition of aerosol trace elements over the East China Sea. *Marine Chemistry, 120*(1-4), 116-127. doi: 10.1016/j.marchem.2008.10.003

Humphries, M. (2013). Rare earth elements: The global supply chain. CRS Report for Congress

Intergovernmental Panel on Climate Change (IPCC). (2007). In: Solomon, S. D., et al. (Eds.), Climate Change 2007: the Physical Science Basis. Cambridge University Press, New York.

Jacobsen, S. B., & Wasserburg, G. J. (1980). SM-ND ISOTOPIC EVOLUTION OF CHONDRITES. *Earth and Planetary Science Letters, 50*(1), 139-155. doi: 10.1016/0012-821x(80)90125-9

Jakes, P., & White, A. J. R. (1972). HORNBLENDES FROM CALC-ALKALINE VOLCANIC-ROCKS OF ISLAND ARCS AND CONTINENTAL MARGINS. *American Mineralogist, 57*(5-6), 887-&.

Janney, P. E., Le Roex, A. P., Carlson, R. W., & Viljoen, K. S. (2002). A chemical and multi-isotope study of the Western Cape olivine melilitite province, South Africa: Implications for the sources of kimberlites and the origin of the HIMU signature in Africa. *Journal of Petrology, 43*(12), 2339-2370. doi: 10.1093/petrology/43.12.2339

Jiang, S. Y. N., Yang, F., Chan, K. L., & Ning, Z. (2014). Water solubility of metals in coarse PM and PM2.5 in typical urban environment in Hong Kong. *Atmospheric Pollution Research, 5*(2), 236-244. doi: 10.5094/apr.2014.029

Jickells, T. D., Davies, T. D., Tranter, M., Landsberger, S., Jarvis, K., & Abrahams, P. (1992). TRACE-ELEMENTS IN SNOW SAMPLES FROM THE SCOTTISH HIGHLANDS - SOURCES AND DISSOLVED PARTICULATE DISTRIBUTIONS. *Atmospheric Environment Part a-General Topics, 26*(3), 393-401. doi: 10.1016/0960-1686(92)90325-f

Jickells, T.D., & Spokes, L. (2001). Atmospheric iron inputs to the ocean. In: Hunter, K., Turner, D. (Eds.), The Biogeochemistry of Iron in Seawater. John Wiley, New York, 85–122.

Jickells, T. D., Kelly, S. D., Baker, A. R., Biswas, K., Dennis, P. F., Spokes, L. J., & Yeatman, S. G. (2003). Isotopic evidence for a marine ammonia source. *Geophysical Research Letters, 30*(7). doi: 10.1029/2002gl016728

Jickells, T. D., An, Z. S., Andersen, K. K., Baker, A. R., Bergametti, G., Brooks, N., Torres, R. (2005). Global iron connections between desert dust, ocean biogeochemistry, and climate. *Science, 308*(5718), 67-71. doi: 10.1126/science.1105959

Jimenez-Velez, B., Detres, Y., Armstrong, R. A., & Gioda, A. (2009). Characterization of African Dust (PM2.5) across the Atlantic Ocean during AEROSE 2004. *Atmospheric Environment, 43*(16), 2659-2664. doi: 10.1016/j.atmosenv.2009.01.045

Johnson, J., Schewel, L., & Graedel, T. E. (2006). The contemporary anthropogenic chromium cycle. *Environmental Science & Technology, 40*(22), 7060-7069. doi: 10.1021/es060061i

Johnson, M. S., Meskhidze, N., Kiliyanpilakkil, V. P., & Gasso, S. (2011). Understanding the transport of Patagonian dust and its influence on marine biological activity in the South Atlantic Ocean. *Atmospheric Chemistry and Physics, 11*(6), 2487-2502. doi: 10.5194/acp-11-2487-2011

Jones, C. E., Halliday, A. N., Rea, D. K., & Owen, R. M. (2000). Eolian inputs of lead to the North Pacific. *Geochimica et Cosmochimica Acta, 64*(8), 1405-1416. doi: 10.1016/s0016-7037(99)00439-1

Kamber, B.S., Gladu, A.H., Comparison of Pb purification by anion-exchange resin methods and assessment of long-term reproducibility of Th/U/Pb ratio measurements by Q-ICP-MS, Geostandards and Geoanalytical Research, 33, 2, 169-181, 2009

Kamona, A. F., Leveque, J., Friedrich, G., & Haack, U. (1999). Lead isotopes of the carbonate-hosted Kabwe, Tsumeb, and Kipushi Pb-Zn-Cu sulphide deposits in relation to Pan African orogenesis in the Damaran-Lufilian Fold Belt of Central Africa. *Mineralium Deposita, 34*(3), 273-283. doi: 10.1007/s001260050203

Kay, S. M., Ardolino, A. A., Gorring, M. L., & Ramos, V. A. (2006). The Somuncura Large Igneous Province in Patagonia: Interaction of a Transient Mantle Thermal Anomaly with a Subducting Slab. *Journal of Petrology, 48*(1), 43-77. doi: 10.1093/petrology/egl053

Kieber, R. J., Willey, J. D., & Avery, G. B. (2003). Temporal variability of rainwater iron speciation at the Bermuda Atlantic time series station. *Journal of Geophysical Research-Oceans, 108*(C8). doi: 10.1029/2001jc001031

Kim, G., & Church, T. M. (2002). Wet deposition of trace elements and radon daughter systematics in the South and equatorial Atlantic atmosphere. *Global Biogeochemical Cycles, 16*(3). doi: 10.1029/2001gb001407

Kimbrough, D. E., Cohen, Y., Winer, A. M., Creelman, L., & Mabuni, C. (1999). A critical assessment of chromium in the environment. *Critical Reviews in Environmental Science and Technology, 29*(1), 1-46. doi: 10.1080/10643389991259164

Kojima, K., Murakami, M., Yoshimizu, C., Tayasu, I., Nagata, T., & Furumai, H. (2011). Evaluation of surface runoff and road dust as sources of nitrogen using nitrate isotopic composition. *Chemosphere, 84*(11), 1716-1722. doi: 10.1016/j.chemosphere.2011.04.071

Komárek, M., Ettler, V., Chrastny, V. (2008). Lead isotopes in environmental sciences: A review. Environment International. 34. 562-577.

Kowalczyk, G. S., Choquette, C. E., & Gordon, G. E. (1978). CHEMICAL ELEMENT BALANCES AND IDENTIFICATION OF AIR-POLLUTION SOURCES IN WASHINGTON, DC. *Atmospheric Environment, 12*(5), 1143-1153. doi: 10.1016/0004-6981(78)90361-x

Kumar, N., Gamboa, L., & Mascle, J. (1977). Geological history and origin of Sao Paulo Plateau (Southeastern Brazilian Margin). Comparison with the Angolan Margin, and the early evolution of the northern South Atlantic. Report of Deep Sea Drilling Project, Leg 39, 927-945.

Le Roex, A. P., Bell, D. R., & Davis, P. (2003). Petrogenesis of group I kimberlites from Kimberley, South Africa: Evidence from bulk-rock geochemistry. *Journal of Petrology, 44*(12), 2261-2286. doi: 10.1093/petrology/egg077

Le Roex, A. P., & Lanyon, R. (1998). Isotope and trace element geochemistry of Cretaceous Damaraland lamprophyres and carbonatites, northwestern Namibia: Evidence for plume-lithosphere interactions. *Journal of Petrology, 39*(6), 1117-1146.

Lee, S.-H., & Allen, H. C. (2012). Analytical Measurements of Atmospheric Urban Aerosol. *Analytical Chemistry, 84*(3), 1196-1201. doi: 10.1021/ac201338x

Li, F., Ginoux, P., & Ramaswamy, V. (2008). Distribution, transport, and deposition of mineral dust in the Southern Ocean and Antarctica: Contribution of major sources. *Journal of Geophysical Research-Atmospheres, 113*(D10). doi: 10.1029/2007jd009190

Liu, Y. X., Li, Q. X., Ma, N., Sun, X. L., Bai, J. F., & Zhang, Q. (2014). Application of the Zr/Hf Ratio in the Determination of Hafnium in Geochemical Samples by High-Resolution Inductively Coupled Plasma Mass Spectrometry. *Analytical Chemistry, 86*(23), 11570-11577. doi: 10.1021/ac503517f

Loppi, S., & Pirintsos, S. A. (2003). Epiphytic lichens as sentinels for heavy metal pollution at forest ecosystems (central Italy). *Environmental Pollution, 121*(3), 327-332. doi: 10.1016/s0269-7491(02)00269-5

Loring, D. H. (1991). NORMALIZATION OF HEAVY-METAL DATA FROM ESTUARINE AND COASTAL SEDIMENTS. *Ices Journal of Marine Science, 48*(1), 101-115. doi: 10.1093/icesjms/48.1.101

Losno, R. (1989). Chimied'éléments minéraux en trace dans les pluies méditerranéennes, Ph.D. Thesis, Université de Paris 7.

Lovei, M. (1998). Phasing out lead from gasoline: Worldwide experience and policy. World Bank Technical Paper No. 397, Pollution Management Series

Lu, Y.-W., & Sun, Y.-C. (2008). An on-line electrodialyzer-ICP-MS analytical system for direct determination of trace metal impurities in KOH. *Journal of Analytical Atomic Spectrometry, 23*(4), 574-578. doi: 10.1039/b712296a

Luo, C., Mahowald, N., Bond, T., Chuang, P. Y., Artaxo, P., Siefert, R., & Schauer, J. (2008). Combustion iron distribution and deposition. *Global Biogeochemical Cycles, 22*(1). doi: 10.1029/2007gb002964

Luo, G., Yu, F., & Wang, Z. (2009). Impact of aerosol on sea surface temperature over the subtropical Atlantic Ocean: A potential trigger factor of the NAO phase conversion? *Geophysical Research Letters, 36*. doi: 10.1029/2008gl036035

Lutgens, F. & Tarbuck, E. (1992). The atmosphere: an introduction to meteorology. Prentice-Hall

Mahowald, N. M., Baker, A. R., Bergametti, G., Brooks, N., Duce, R. A., Jickells, T. D., & Tegen, I. (2005). Atmospheric global dust cycle and iron inputs to the ocean. *Global Biogeochemical Cycles, 19*(4). doi: 10.1029/2004gb002402

Marfil, S. & Maiza, P (2012). Geochemistry of Hydrothermal Alteration in Volcanic Rocks Silvina Marfil and Pedro Maiza. *INTECH Open Access Publisher.*

Martin, J. H., & Fitzwater, S. E. (1988). IRON-DEFICIENCY LIMITS PHYTOPLANKTON GROWTH IN THE NORTHEAST PACIFIC SUBARCTIC. *Nature, 331*(6154), 341-343. doi: 10.1038/331341a0

Martin, J. H. (1990). GLACIAL-INTERGLACIAL CO2 CHANGE: THE IRON HYPOTHESIS. *Paleoceanography, 5*(1), 1-13. doi: 10.1029/PA005i001p00001

Mason, T. F. D., Weiss, D. J., Horstwood, M., Parrish, R. R., Russell, S. S., Mullane, E., & Coles, B. J. (2004). High-precision Cu and Zn isotope analysis by plasma source mass spectrometry - Part 1. Spectral interferences and their correction. *Journal of Analytical Atomic Spectrometry, 19*(2), 209-217. doi: 10.1039/b306958c

Mason, T.F.D. (2005). Zn and Cu isotopic variability in the Alexandrinka volcanic-hosted massive sulphide (VHMS) ore deposit, Urals, Russia, Chemical Geology, 221, 170-187

McConnell, C. L., Highwood, E. J., Coe, H., Formenti, P., Anderson, B., Osborne, S., & Harrison, M. A. J. (2008). Seasonal variations of the physical and optical characteristics of Saharan dust: Results from the Dust Outflow and Deposition to the Ocean (DODO) experiment. *Journal of Geophysical Research-Atmospheres, 113*(D14). doi: 10.1029/2007jd009606

McMurry, P. H. (2000). A review of atmospheric aerosol measurements. *Atmospheric Environment, 34*(12-14), 1959-1999. doi: 10.1016/s1352-2310(99)00455-0

Measures, C. I., & Vink, S. (2000). On the use of dissolved aluminum in surface waters to estimate dust deposition to the ocean. *Global Biogeochemical Cycles, 14*(1), 317-327. doi: 10.1029/1999gb001188

Meskhidze, N., Nenes, A., Chameides, W. L., Luo, C., & Mahowald, N. (2007). Atlantic Southern Ocean productivity: Fertilization from above or below? *Global Biogeochemical Cycles, 21*(2), n/a-n/a. doi: 10.1029/2006gb002711

Middag, R., de Baar, H. J. W., Laan, P., Cai, P. H., & van Ooijen, J. C. (2011). Dissolved manganese in the Atlantic sector of the Southern Ocean. *Deep-Sea Research Part Ii-Topical Studies in Oceanography, 58*(25-26), 2661-2677. doi: 10.1016/j.dsr2.2010.10.043

Mirlean, N., Robinson, D., Kawashita, K., Vignol, M. L., Conceicao, R., & Chemale, F. (2005). Identification of local sources of lead in atmospheric deposits in an urban area in Southern Brazil using stable lead isotope ratios. *Atmospheric Environment, 39*(33), 6204-6212. doi: 10.1016/j.atmosenv.2005.07.002

Monastra, V., Derry, L. A., & Chadwick, O. A. (2004). Multiple sources of lead in soils from a Hawaiian chronosequence. *Chemical Geology, 209*(3-4), 215-231. doi: 10.1016/j.chemgeo.2004.04.027

Monna, F., Poujol, M., Losno, R., Dominik, J., Annegarn, H., & Coetzee, H. (2006). Origin of atmospheric lead in Johannesburg, South Africa. *Atmospheric Environment, 40*(34), 6554-6566. doi: 10.1016/j.atmosenv.2006.05.064

Moore, H. E., Poet, S. E., & Martell, E. A. (1973). RN-222, PB-210, BI-210, AND PO-210 PROFILES AND AEROSOL RESIDENCE TIMES VERSUS ALTITUDE. *Journal of Geophysical Research, 78*(30), 7065-7075. doi: 10.1029/JC078i030p07065

Morcelli, C. P. R., Figueiredo, A. M. G., Sarkis, J. E. S., Enzweiler, J., Kakazu, M., & Sigolo, J. B. (2005). PGEs and other traffic-related elements in roadside soils from Sao Paulo, Brazil. *Science of the Total Environment, 345*(1-3), 81-91. doi: 10.1016/j.scitotenv.2004.10.018

Morel, F. M. M., Hudson, R. J. M., & Price, N. M. (1991). LIMITATION OF PRODUCTIVITY BY TRACE-METALS IN THE SEA. *Limnology and Oceanography, 36*(8), 1742-1755.

Morel, F. M. M., Milligan, A. J., & Saito, M. A. (2003). Marine bioinorganic chemistry: The role of trace metals in the oceanic cycles of major nutrients. In The Oceans and Marine Geochemistry. Treatise on Geochemistry (ed. H. Elderfield), Oxford: Elsevier.

Morel, F. M. M., & Price, N. M. (2003). The biogeochemical cycles of trace metals in the oceans. *Science, 300*(5621), 944-947. doi: 10.1126/science.1083545

Murphy, K. J. T. (1985). The trace metal chemistry of the Atlantic aerosol. PhD thesis, University of Liverpool.

Nriagu, J. O., & Pacyna, J. M. (1988). QUANTITATIVE ASSESSMENT OF WORLDWIDE CONTAMINATION OF AIR, WATER AND SOILS BY TRACE-METALS. *Nature, 333*(6169), 134-139. doi: 10.1038/333134a0

Nriagu, J. O. (1990). THE RISE AND FALL OF LEADED GASOLINE. *Science of the Total Environment, 92*, 13-28. doi: 10.1016/0048-9697(90)90318-o

Okuda, T., Nakao, S., Katsuno, M., & Tanaka, S. (2007). Source identification of nickel in TSP and PM2.5 in Tokyo, Japan. *Atmospheric Environment, 41*(35), 7642-7648. doi: 10.1016/j.atmosenv.2007.08.050

Pacyna, J. M. (1989). Atmospheric emissions of As, Cd, Pb and Hg from high temperature processes in power generation and industry, and their transport. In: T. C. Hutchinson and K. Mecma (Eds), SCOPE Metals Cycling Workshop. Scientific Committee on Problems of the Environment, Toronto. Wiley Eastern, New Delhi (in press).

Pacyna, J. M., & Pacyna, E. G. (2001). An assessment of global and regional emissions of trace metals to the atmosphere from anthropogenic sources worldwide. *Environmental Reviews, 9*, 269-298.

Papp, J. F. (2007). Chromium - A national mineral commodity perspective, U.S. Geological Survey, Open-file Report 2007-1167, 49, 18

Paris, R., Desboeufs, K. V., & Journet, E. (2011). Variability of dust iron solubility in atmospheric waters: Investigation of the role of oxalate organic complexation. *Atmospheric Environment, 45*(36), 6510-6517. doi: 10.1016/j.atmosenv.2011.08.068

Paytan, A. (2009). Toxicity of atmospheric aerosols on marine phytophlankton. Proceedings of the National Academy of Sciences of the United States of America. 106(12). 4601-4605

Piketh, S. J. (2002). Chemical evidence of long-range atmospheric transport over southern Africa. *Journal of Geophysical Research, 107*(D24). doi: 10.1029/2002jd002056

Pin, C., & Zalduegui, J. F. S. (1997). Sequential separation of light rare-earth elements, thorium and uranium by miniaturized extraction chromatography: Application to isotopic analyses of silicate rocks. *Analytica Chimica Acta, 339*(1-2), 79-89. doi: 10.1016/s0003-2670(96)00499-0

Plunkett, R. (1941). Tetrafluoroethylene polymers.

Pöschl, U. (2005). Atmospheric Aerosols, Composition, Transportation, Climate and Health Effects, Atmospheric Chemistry, 44, 7520-7540

Poujol, M., & Anhaeusser, C. R. (2001). The Johannesburg Dome, South Africa: new single zircon U-Pb isotopic evidence for early Archaean granite-greenstone development within the central Kaapvaal Craton. *Precambrian Research, 108*(1-2), 139-157. doi: 10.1016/s0301-9268(00)00161-3

Prevec, S. A., Anhaeusser, C. R., & Poujol, M. (2004). Evidence for archaean lamprophyre from the Kaapvaal Craton, South Africa. *South African Journal of Science, 100*(11-12), 549-555.

Price, N. M., & Morel, F. M. M. (1991). COLIMITATION OF PHYTOPLANKTON GROWTH BY NICKEL AND NITROGEN. *Limnology and Oceanography, 36*(6), 1071-1077.

Prospero, J. M., Charlson, R. J., Mohnen, V., Jaenicke, R., Delany, A. C., Moyers, J., & Rahn, K. (1983). THE ATMOSPHERIC AEROSOL SYSTEM - AN OVERVIEW. *Reviews of Geophysics, 21*(7), 1607-1629. doi: 10.1029/RG021i007p01607

Prospero, J. M., Ginoux, P., Torres, O., Nicholson, S. E., & Gill, T. E. (2002). Environmental characterization of global sources of atmospheric soil dust identified with the Nimbus 7 Total Ozone Mapping Spectrometer (TOMS) absorbing aerosol product. *Reviews of Geophysics, 40*(1). doi: 10.1029/2000rg000095

Raes, F., Van Dingenen, R., Vignati, E., Wilson, J., Putaud, J. P., Seinfeld, J. H., & Adams, P. (2000). Formation and cycling of aerosols in the global troposphere. *Atmospheric Environment, 34*(25), 4215-4240. doi: 10.1016/s1352-2310(00)00239-9

Ramanathan, V., Crutzen, P. J., Lelieveld, J., Mitra, A. P., Althausen, D., Anderson, J., & Valero, F. P. J. (2001). Indian Ocean Experiment: An integrated analysis of the climate forcing and effects of the great Indo-Asian haze. *Journal of Geophysical Research-Atmospheres, 106*(D22), 28371-28398. doi: 10.1029/2001jd900133

Rapela, C. W., & Kay, S. M. (1988). LATE PALEOZOIC TO RECENT MAGMATIC EVOLUTION OF NORTHERN PATAGONIA. *Episodes, 11*(3), 175-182.

Rehkamper, M., Schonbachler, M., & Stirling, C. H. (2001). Multiple collector ICP-MS: Introduction to instrumentation, measurement techniques and analytical capabilities. *Geostandards Newsletter-the Journal of Geostandards and Geoanalysis, 25*(1), 23-40. doi: 10.1111/j.1751-908X.2001.tb00785.x

Rekacewicz, P. (2003). Strategic Plan for the U. S. Climate Change Science Program

Reynolds, R. & Moore, D. (1997). X-Ray diffraction and the identification and analysis of clay minerals. 2nd Ed. Oxford University Press, New York.

Rio Tinto (2014). Website (httl://www.rossing.com)

Rolph, G.D. (2013). Real-time Environmental Applications and Display sYstem (READY). Website (http://www.ready.noaa.gov). NOAA Air Resources Laboratory, College Park, MD.

Rose, E. R. (1960). Rare earths of the Grenville Sub-Provine Ontatio and Quebec. GSC Report Number 59-10. Ottawa: Geological Survey of Canada Department of Mines and Technical Surveys

Rosello, E., Haring, C., Cardinali, G., Suarez, F., Laffitte, G. & Nevistic, A. (2008). Hydrocarbons and petroleum geology of Tierra del Fuego, Argentina. Geologica Acta, 6(1), 69-83

Rosman, K. J. R., Chisholm, W., Boutron, C. F., Candelone, J. P., & Gorlach, U. (1993). ISOTOPIC EVIDENCE FOR THE SOURCE OF LEAD IN GREENLAND SNOWS SINCE THE LATE 1960S. *Nature, 362*(6418), 333-335. doi: 10.1038/362333a0

Rosman, K. J. R., Chisholm, W., Boutron, C. F., Candelone, J. P., & Hong, S. (1994a). ISOTOPIC EVIDENCE TO ACCOUNT FOR CHANGES IN THE CONCENTRATION OF LEAD IN GREENLAND SNOW BETWEEN 1960 AND 1988. *Geochimica et Cosmochimica Acta, 58*(15), 3265-3269. doi: 10.1016/0016-7037(94)90054-x

Rosman, K. J. R., Chisholm, W., Boutron, C. F., Candelone, J. P., & Patterson, C. C. (1994b). ANTHROPOGENIC LEAD ISOTOPES IN ANTARCTICA. *Geophysical Research Letters, 21*(24), 2669-2672. doi: 10.1029/94gl02603

Rosman, K. J. R., Chisholm, W., Hong, S. M., Candelone, J. P., & Boutron, C. F. (1997). Lead from Carthaginian and Roman Spanish mines isotopically identified in Greenland ice dated from 600 BC to 300 AD. *Environmental Science & Technology, 31*(12), 3413-3416. doi: 10.1021/es970038k

Roundhill, D., Solangi, I., Memon, S., Bhanger, M., & Yilmaz, M. (2009) The liquid-liquid extraction of toxic metals (Cd, Hg and Pb), Review. Journal of Analytical Environmental Chemistry. 10(1-2). 1-13.

Saito, M. A., Moffett, J. W., Chisholm, S. W., & Waterbury, J. B. (2002). Cobalt limitation and uptake in Prochlorococcus. *Limnology and Oceanography, 47*(6), 1629-1636.

Sarthou, G., Baker, A. R., Blain, S., Achterberg, E. P., Boye, M., Bowie, A. R., & Worsfold, P. J. (2003). Atmospheric iron deposition and sea-surface dissolved iron concentrations in the eastern Atlantic Ocean. *Deep-Sea Research Part I-Oceanographic Research Papers, 50*(10-11), 1339-1352. doi: 10.1016/s0967-0637(03)00126-2

Sarthou, G., Baker, A. R., Kramer, J., Laan, P., Laes, A., Ussher, S., & Blain, S. (2007). Influence of atmospheric inputs on the iron distribution in the subtropical North-East Atlantic Ocean. *Marine Chemistry, 104*(3-4), 186-202. doi: 10.1016/j.marchem.2006.11.004

Science Committee on Oceanic Research (SCOR) (2006). GEOTRACES Science Plan. An International study of the marine biogeochemical cycles of trace elements and their isotopes. Report No. 1.

Sedwick, P. N., Sholkovitz, E. R., & Church, T. M. (2007). Impact of anthropogenic combustion emissions on the fractional solubility of aerosol iron: Evidence from the Sargasso Sea. *Geochemistry Geophysics Geosystems, 8*. doi: 10.1029/2007gc001586

Serra, N., Avellaneda, N. M., & Stammer, D. (2014). Large-scale impact of Saharan dust on the North Atlantic Ocean circulation. *Journal of Geophysical Research-Oceans, 119*(2), 704-730. doi: 10.1002/2013jc009274

Shi, Z., Krom, M. D., Jickells, T. D., Bonneville, S., Carslaw, K. S., Mihalopoulos, N., & Benning, L. G. (2012). Impacts on iron solubility in the mineral dust by processes in the source region and the atmosphere: A review. *Aeolian Research, 5*, 21-42. doi: 10.1016/j.aeolia.2012.03.001

Sholkovitz, E. R., Sedwick, P. N., & Church, T. M. (2009). Influence of anthropogenic combustion emissions on the deposition of soluble aerosol iron to the ocean: Empirical estimates for island sites in the North Atlantic. *Geochimica et Cosmochimica Acta, 73*(14), 3981-4003. doi: 10.1016/j.gca.2009.04.029

Spokes, L. J., Jickells, T. D., & Lim, B. (1994). SOLUBILIZATION OF AEROSOL TRACE-METALS BY CLOUD PROCESSING - A LABORATORY STUDY. *Geochimica et Cosmochimica Acta, 58*(15), 3281-3287. doi: 10.1016/0016-7037(94)90056-6

Srivastava, A. K., Singh, S., Tiwari, S., & Bisht, D. S. (2012). Contribution of anthropogenic aerosols in direct radiative forcing and atmospheric heating rate over Delhi in the

Indo-Gangetic Basin. *Environmental Science and Pollution Research, 19*(4), 1144-1158. doi: 10.1007/s11356-011-0633-y

Stefansson, A., Gunnarsson, I., & Giroud, N. (2007). New methods for the direct determination of dissolved inorganic, organic and total carbon in natural waters by Reagent-Free (TM) Ion Chromatography and inductively coupled plasma atomic emission spectrometry. *Analytica Chimica Acta, 582*(1), 69-74. doi: 10.1016/j.aca.2006.09.001

Stern, C. R., & Kilian, R. (1996). Role of the subducted slab, mantle wedge and continental crust in the generation of adakites from the Andean Austral volcanic zone. *Contributions to Mineralogy and Petrology, 123*(3), 263-281. doi: 10.1007/s004100050155

Stumm, W., and Morgan, J. (1996). Aquatic chemistry: chemical equilibria and rates in natural waters, 3rd Ed. Wiley.

Sugden, D. E., McCulloch, R. D., Bory, A. J. M., & Hein, A. S. (2009). Influence of Patagonian glaciers on Antarctic dust deposition during the last glacial period. *Nature Geoscience, 2*(4), 281-285. doi: 10.1038/ngeo474

Tachikawa, K., Jeandel, C., & Roy-Barman, M. (1999). A new approach to the Nd residence time in the ocean: the role of atmospheric inputs. *Earth and Planetary Science Letters, 170*(4), 433-446. doi: 10.1016/s0012-821x(99)00127-2

Talbot, R. W., & Andren, A. W. (1983). RELATIONSHIPS BETWEEN PB AND PB-210 IN AEROSOL AND PRECIPITATION AT A SEMIREMOTE SITE IN NORTHERN WISCONSIN. *Journal of Geophysical Research-Oceans and Atmospheres, 88*(NC11), 6752-6760. doi: 10.1029/JC088iC11p06752

Tanaka, T., Togashi, S., Kamioka, H., Amakawa, H., Kagami, H., Hamamoto, T., Dragusanu, C. (2000). JNdi-1: a neodymium isotopic reference in consistency with LaJolla neodymium. *Chemical Geology, 168*(3-4), 279-281. doi: 10.1016/s0009-2541(00)00198-4

Taylor, S. R., & McLennan, S. M. (1985). The Continental Crust: Its Composition and Evolution. Blackwell, Oxford.

Thomas, D. J., Bralower, T. J., & Jones, C. E. (2003). Neodymium isotopic reconstruction of late Paleocene-early Eocene thermohaline circulation. *Earth and Planetary Science Letters, 209*(3-4), 309-322. doi: 10.1016/s0012-821x(03)00096-7

Thuroczy, C. E., Boye, M., & Losno, R. (2010). Dissolution of cobalt and zinc from natural and anthropogenic dusts in seawater. *Biogeosciences, 7*(6), 1927-1936. doi: 10.5194/bg-7-1927-2010

Tohver, E., D'Agrella-Filho, M. S., & Trindade, R. I. F. (2006). Paleomagnetic record of Africa and South America for the 1200-500 Ma interval, and evaluation of Rodinia and Gondwana assemblies. *Precambrian Research, 147*(3-4), 193-222. doi: 10.1016/j.precamres.2006.01.015

Turekian, K. K., Nozaki, Y., & Benninger, L. K. (1977). GEOCHEMISTRY OF ATMOSPHERIC RADON AND RADON PRODUCTS. *Annual Review of Earth and Planetary Sciences, 5*, 227-255. doi: 10.1146/annurev.ea.05.050177.001303

Turekian, K. (1968). *Oceans*. Prentice-Hall.

Twyman, R. (2005). Wet digestion, In: Sample dissolution for elemental analysis. A.D. Sawant (Ed.). Elsevier.

Ulke, A. G., & Andrade, M. F. (2001). Modeling urban air pollution in Sao Paulo, Brazil: sensitivity of model predicted concentrations to different turbulence parameterizations. *Atmospheric Environment, 35*(10), 1747-1763. doi: 10.1016/s1352-2310(00)00498-2

Usher, C. R., Michel, A. E., Stec, D., & Grassian, V. H. (2003). Laboratory studies of ozone uptake on processed mineral dust. *Atmospheric Environment, 37*(38), 5337-5347. doi: 10.1016/j.atmosenv.2003.09.014

Vaisman, A. G., & Lacerda, L. D. (2003). Estimated heavy metal emissions to the atmosphere due to projected changes in the Brazilian energy generation matrix. *Regional Environmental Change, 3*(4), 140-145. doi: 10.1007/s10113-002-0053-0

Van De Flierdt, T., Goldstein, S. L., Hemming, S. R., Frank, M., & Halliday, A. N. (2007). Global neodymium hafnium isotope systematics - Revisited. *Geochimica et Cosmochimica Acta, 71*(15), A1053-A1053.

Vasconcellos, P. C., Balasubramanian, R., Bruns, R. E., Sanchez-Ccoyllo, O., Andrade, M. F., & Flues, M. (2007). Water-soluble ions and trace metals in airborne particles over urban areas of the state of sauo paulo, Brazil: Influences of local sources and long range transport. *Water Air and Soil Pollution, 186*(1-4), 63-73. doi: 10.1007/s11270-007-9465-2

Veron, A., Flament, P., Bertho, M. L., Alleman, L., Flegal, R., & Hamelin, B. (1999). Isotopic evidence of pollutant lead sources in Northwestern France. *Atmospheric Environment, 33*(20), 3377-3388. doi: 10.1016/s1352-2310(98)00376-8

Vervoort, J. (2012). http://serc.carleton.edu/research_education/geochemsheets/techniques/, Washington State University and Paul Mueller, University of Florida

Walder, A. J., Abell, I. D., Platzner, I., & Freedman, P. A. (1993). LEAD ISOTOPE RATIO MEASUREMENT OF NIST 610 GLASS BY LASER ABLATION INDUCTIVELY COUPLED PLASMA MASS-SPECTROMETRY. *Spectrochimica Acta Part B-Atomic Spectroscopy, 48*(3), 397-402. doi: 10.1016/0584-8547(93)80044-u

Wang, Y. J., Cheng, H., Edwards, R. L., He, Y. Q., Kong, X. G., An, Z. S., & Li, X. D. (2005). The Holocene Asian monsoon: Links to solar changes and North Atlantic climate. *Science, 308*(5723), 854-857. doi: 10.1126/science.1106296

Wang, Y. & Chen, J. (2010). Study of stable isotope model for saturated soil water movement in the condition of evaporation. Journal of Sichuan University: Engineering Science Edition. 42(1). 10-13.

Wang, L., Liang, T., Zhang, Q., & Li, K. (2014). Rare earth element components in atmospheric particulates in the Bayan Obo mine region. *Environmental Research, 131*, 64-70. doi: 10.1016/j.envres.2014.02.006

Weis, D., Kieffer, B., Maerschalk, C., Barling, J., de Jong, J., Williams, G. A., Mahoney, J. B. (2006). High-precision isotopic characterization of USGS reference materials by TIMS and MC-ICP-MS. *Geochemistry Geophysics Geosystems, 7*. doi: 10.1029/2006gc001283

Weiss, D. J., Kober, B., Dalgopolova, A., Gallagher, K., Spiro, B., Le Roux, G., Coles, B. J. (2004). Accurate and precise Pb isotope ratio measurements in environmental samples by MC-ICP-MS. *International Journal of Mass Spectrometry, 232*(3), 205-215. doi: 10.1016/j.ijms.2004.01.005

Wildeman, T. R., & Haskin, L. (1965). Rare-earth elements in ocean sediments, *Geophysical Research, 70* (12), 2905-2910

Witt, M., Baker, A. R., & Jickells, T. D. (2006). Atmospheric trace metals over the Atlantic and South Indian Oceans: Investigation of metal concentrations and lead isotope ratios in coastal and remote marine aerosols. *Atmospheric Environment, 40*(28), 5435-5451. doi: 10.1016/j.atmosenv.2006.04.041

Witt, M. L. I., Mather, T. A., Baker, A. R., De Hoog, J. C. M., & Pyle, D. M. (2010). Atmospheric trace metals over the south-west Indian Ocean: Total gaseous mercury, aerosol trace metal concentrations and lead isotope ratios. *Marine Chemistry, 121*(1-4), 2-16. doi: 10.1016/j.marchem.2010.02.005

Wolf, R. (2005), Crustal Imaging & Characterisation, USGS

Wolff, E. W., & Suttie, E. D. (1994). ANTARCTIC SNOW RECORD OF SOUTHERN-HEMISPHERE LEAD POLLUTION. *Geophysical Research Letters, 21*(9), 781-784. doi: 10.1029/94gl00656

Woodhead, J.D. (2002). A simple method for obtaining highly accurate Pb-isotope data by MC-ICP-MS, J. of Anal. At Spectrom., 17, 1381

Wu J., Rember R. & Cahill C. (2007). Dissolution of aerosol iron in the surface waters of the North Pacific and North Atlantic oceans as determined by a semi continuous flow-through reactor method. Global Biogeochemical Cycles 21, GB4010. doi:10.1029/ 2006GB002851

Wyatt, N. J., Milne, A., Woodward, E. M. S., Rees, A. P., Browning, T. J., Bouman, H. A., & Lohan, M. C. (2014). Biogeochemical cycling of dissolved zinc along the GEOTRACES South Atlantic transect GA10 at 40 S. *Global Biogeochemical Cycles, 28*(1), 44-56. doi: 10.1002/2013gb004637

Yang, J., Gao, S., Chen, C., Tang, Y., Yuan, H., Gong, H., & Wang, J. (2009). Episodic crustal growth of North China as revealed by U-Pb age and Hf isotopes of detrital zircons from modern rivers. *Geochimica et Cosmochimica Acta, 73*(9), 2660-2673. doi: 10.1016/j.gca.2009.02.007

Yu, Z. S., Robinson, P., & McGoldrick, P. (2001). An evaluation of methods for the chemical decomposition of geological materials for trace element determination using ICP-MS. *Geostandards Newsletter-the Journal of Geostandards and Geoanalysis, 25*(2-3), 199-217. doi: 10.1111/j.1751-908X.2001.tb00596.x

Zhuang, G., Yi, Z., Duce, R. A., & Brown, P. R. (1992). CHEMISTRY OF IRON IN MARINE AEROSOLS. *Global Biogeochemical Cycles, 6*(2), 161-173. doi: 10.1029/92gb00756

Appendix

Insights into improved provenance tracing using Pb isotopic ratios of aerosols into the South Atlantic Ocean

R. Khondoker, D.Weiss, T. van de Flierdt, M. Rehkämper

Oral presentation at Geochemistry Group Research in Progress Annual Meeting, Open University, UK, March 2013

Abstract
The atmosphere is an important pathway of delivering nutrients to the ocean surface waters, which play a role in marine bio-geochemical processes. Our understanding of the atmospheric inputs and their influences on marine micronutrient cycles in the South Atlantic Ocean, compared to its well-studied neighbour the North Atlantic Ocean, is limited. The South Atlantic Ocean has a limited seawater micronutrient content in comparison to the North Atlantic Ocean that receives a large proportion of its nutrients from the Saharan Desert. However, along the 40°S transect across the South Atlantic Ocean there is a region of higher algal growth in comparison to the rest of the South Atlantic Ocean.

In addition, in recent years it has become clear that atmospheric emissions from cities and human activities such as road traffic and industrial plant emissions can impact atmospheric inputs into the ocean. This in turn affects the marine micronutrient budget, which in turn affects marine bio-geochemical processes. Although air quality studies have been carried out for some cities that may influence atmospheric inputs into the South Atlantic Ocean, such as São Paulo, Buenos Aires, and Cape Town, the impact of such cities on marine micronutrient budgets has not been studied and may be significant.

In this study, sediment and aerosol samples of potential source regions combined with previous studies of source regions were used to characterise different sources to compare to aerosols collected along the 40°S transect along the South Atlantic Ocean. Pb isotopic ratios were used as a proxy for anthropogenic sources to identify, distinguish and determine the importance between anthropogenic and natural sources of aerosols into the South Atlantic Ocean along the 40°S transect.

Provenance tracing of aerosols in the South Atlantic Ocean using Pb and Nd isotopes and select trace and rare earth elements

R. Khondoker, D. Weiss, T. van De Flierdt, M. Rehkämper, R. Chance, A. Baker, S. Strekopytov, E. Williams, J. Najorka

Poster presentation at Goldschmidt Conference, Florence, Italy, August 25-30, 2013

Abstract
The atmosphere is an important pathway of delivering nutrients to ocean surface waters. These nutrients can play a vital role in marine biogeochemical processes and ultimately the global carbon cycle. However, our understanding of the atmospheric inputs and their influences on marine micronutrient cycles is limited, particularly in the South Atlantic, a region where models predict widely variable fluxes of micronutrients to the ocean from the atmosphere.

Moreover, in recent years it has become clear that atmospheric emissions from cities and human activities, such as road traffic and industrial plant emissions, can significantly impact atmospheric inputs and thus alter micronutrient fluxes to the ocean. Although air quality studies have been carried out for some cities bordering the South Atlantic Ocean, including São Paulo and Buenos Aires, the impact of emissions from such cities on marine micronutrient budgets has not been studied in detail.

Here, we present rare earth and select trace element data as well as results from Pb and Nd isotope analysis of sediments, volcanic ash, road dusts, aerosol filters and lichens from Patagonia, recent Cotopaxi, Chaitén and Puyehue volcanic eruptions, and the cities of São Paulo, Buenos Aires and Johannesburg. All sites are potential atmospheric aerosol sources for the South Atlantic Ocean. The rare earth and trace element concentration data and the isotopic results allow characterisation of the different source sites with adequate resolution to distinguish between South American and Southern African as well as anthropogenic and natural aerosol sources. This provenance information will be applied to interpret the first comprehensive geochemical data set (comprising rare earth, other trace element concentrations, and Pb, Nd isotope compositions) for aerosol filters collected in the South Atlantic Ocean at approximately 40° S during the UK GEOTRACES cruises D357 and JC068.

Assessing the geochemistry of aerosols in the South Atlantic Ocean along the 40° S transect using Pb and Nd isotopes and REE and select trace elements

Roulin Khondoker, Dominik Weiss, Tina van de Flierdt, Mark Rehkämper, Alex Baker, Rosie Chance, Stanislav Strekopytov, Emma Williams, Pedro Cid-Agüero, Patricia Smichowski, Marly Babinski, Rémi Losno, Aloys Bory, Viviane Bout-Roumazeilles

Oral presentation at the 1st International DUST Conference, Castellaneta Marina, Italy, June 1-6, 2014

Abstract

The atmosphere is an important pathway of delivering nutrients and other major and trace elements to ocean surface waters, which can play a vital role in marine biogeochemical processes and ultimately the global carbon cycle. However the dynamics of atmospheric inputs (sources, fluxes) and their solubility in seawater remain little constrained, especially in the South Atlantic Ocean, a region where models predict widely variable atmospheric dust fluxes. Moreover, in recent years it has become clear that anthropogenic sources are potentially more important for certain elements than natural sources. Air quality studies have been carried out for some cities bordering the South Atlantic, including São Paulo and Buenos Aires, but the impact of emissions from such cities on marine elemental budgets has not been studied in detail.

In a first step, we present results on rare earth elements, select trace elements, as well as Pb and Nd isotopic compositions for sediments, volcanic ash, road dusts, aerosol filters and lichens from rural and urban areas in South America and South Africa, which potentially serve as aerosol source regions to the South Atlantic. Using bivariate plots of $^{208}Pb/^{207}Pb$ vs Pb/Al, $^{208}Pb/^{207}Pb$ vs La/Yb, and $^{208}Pb/^{207}Pb$ vs ε_{Nd} we can distinguish between South American and Southern African sources, and also between rural and urban areas on each side of the South Atlantic Ocean.

In a second step, we apply the new provenance information to interpreting the first comprehensive geochemical data set for aerosol filters collected in the South Atlantic along 40° S during the UK GEOTRACES cruises D357 and JC068 (GA10) in 2010 and 2011/2012. Atmospheric processing conditions were experimentally constrained to evaluate their affect on aerosol geochemistry. The results suggest that long-range aerosol transport across the South Atlantic is dominated by the westerlies and comprises a mixture of South American rural and urban sources. Atmospheric processing conditions partially dissolve the aerosols and show a less radiogenic Pb isotopic composition than total digested aerosols, indicating that the urban phase is more susceptible to dissolution than the rural phase.